An investigation into the subcellular localisation of co-factors that stimulate prion protein conversion

James Fionnlagh Graham

Thesis for the degree of Doctor of Philosophy

University of Warwick

Department of Biological Sciences

September 2009

The published papers after page 236 have been excluded at the request of the university

Table of contents

List of tables and figures

Chapter 4

Acknowledgments

I would like to thank first and foremost my supervisors, Dr Andrew Gill and Dr Louise Kirby, for their patience and wisdom in guiding me through my PhD. I am indebted to the wealth of knowledge and insight you both gave me on a daily basis. I would also like to thank my supervisor at the University of Warwick, Dr Teresa Pinheiro, whose valued comments have been greatly appreciated.

I would also particularly like to thank Dr Steve Banner for experimental help, advice, friendship and extensive scientific and non-scientific musings in the laboratory throughout the past ~3 years. Thanks also to Larry Hunt and Dominic Kurian for mass spectrometry work, Ruth Hennion for countless tips and advice on cell culture survival techniques, Sonya Agarwal for doing the fibrilisation experiments, and Dr Sandra McCutcheon, who gave critical but helpful comments on my thesis manuscript, I am very grateful for your input. Finally, I would also like to thank all members, past and present, of the TSE group at Compton who put up with me throughout my studies.

I would like to dedicate my thesis to my parents, who without their unrivalled love and support, nothing would have been achieved.

Declaration of authorship

I, James Fionnlagh Graham declare that the thesis entitled 'an investigation into the subcellular localisation of co-factors that stimulate prion protein conversion' and the work presented in the thesis are both my own, and have been generated by me as the result of my own original research.

Summary

An investigation into the subcellular localisation of co-factors that stimulate prion protein conversion.

Transmissible spongiform encephalopathies are a group of fatal neurodegenerative disorders affecting humans and animals. The prion hypothesis states that the infectious agent is predominantly composed of misfolded prion protein (PrP^{Sc}). One of the challenges to this hypothesis is the existence of prion strains. Different strains of the infectious agent are thought to arise from different conformations of PrP^{Sc}, which can be faithfully passaged onto the native cellular form (PrP^{C}) during conversion. It has also been suggested that strain specific co-factors aid in the refolding process of PrP^{C} during conversion. The preferential targeting of different transmissible spongiform encephalopathy (TSE) strains to specific brain regions, different cell types and even different subcellular localisations, implies the presence of strain specific co-factors in those disease affected areas. The production of prion particles *in vitro*, by amplification either with or without exogenous seed, supports this hypothesis but typically results in particles with infectivity titres less than those isolated *ex vivo*. This project investigated the involvement of accessory molecules and the subcellular localisation of conversion. Potential accessory molecules were sourced from subcellular fractionation of TSE susceptible cell lines and scrapie associated fibrils from TSE infected mouse brains and analysed using a cell free conversion assay and an oligomerisation assay for their strain specific qualities. The cell free conversion assay, previously shown to replicate many aspects of TSE disease, was used to investigate the location of disease-specific co-factors, by use of fractions derived from gradient centrifugation of a scrapie-susceptible cell line. Plasma membrane enriched fractions from the LD9 cell line enhanced the conversion efficiency of ME7 and 79A mouse scrapie in the CFCA. Equivalent fractions from a second scrapie-susceptible cell line also stimulate conversion. I also showed that subcellular fractions that enhance disease-specific prion protein conversion prevent *in vitro* oligomerisation of recombinant prion protein, suggesting the existence of separate, competing mechanisms of specific and non-specific misfolding *in vivo*.

Abbreviations

Asn	asparagine
ATPase	adenosine triphosphate synthase
BASE	bovine amyloidotic spongiform encephalopathy
BSE	bovine spongiform encephalopathy
CamKII	calcium/calmodulin dependent protein kinase
CD	circular dichroism
CFCA	cell free conversion assay
CHO	carbohydrate
CJD	Creutzfeldt-Jacob disease
CNP1	2',3'-cyclic nucleotide 3'-phosphodiesterase
CNS	central nervous system
Cu^{2+}	copper (II) ions
CuZn	copper/zinc
CWD	chronic wasting disease
DGE	density gradient electrophoresis
dH_2O	de-ionized water
DMSO	dimethyl suphoxide
Dmxl2	Dmx-like 2 protein
DNA	deoxyribonucleic acid
DNase	deoxyribonuclease
Dpl	doppel
DTT	dithiothreitol
DY	drowsy strain of TME
E.coli	*Escherichia coli*
ECL	enhanced chemiluminesence
EDTA	ethylenediaminetetra-acetic acid
EMEM	Eagle's modified essential medium
ER	endoplasmic reticulum
ESI	electrospray ionisation
fCJD	familial Creutzfeldt-Jacob disease
FCS	foetal calf serum
FDC	follicular dendritic cell

FFE	free flow electrophoresis
FFI	fatal familial insomnia
FPLC	fast protein liquid chromatography
FSE	feline spongiform encephalopathy
g	gravity
GAGs	glycosaminoglycans
GAPDH	glyceraldehyde 3-phosphate dehydrogenase
GPI	glycosylphatidylinositol
GSS	Gerstmann-Straussler syndrome
HBSS	Hank's buffered salt solution
HCl	hydrochloric acid
HMF	heavy mitochondrial fraction
HPLC	high-pressure liquid chromatography
HRP	horseradish peroxidise
HY	hyper strain of TME
IAA	iodoacetamide
ic	intra-cerebral
ID	identification
IMAC	immobilised metal anion chromatography
Indel	insertion/deletion mutation
IPI	international protein index
IPTG	isopropyl β-D-1-thiogalactopyranoside
kDa	kilo dalton
LB	Luria broth
LDS	Lithium dodecyl sulphate
LMF	light mitochondrial fraction
Lrp1	prolow-density lipoprotein
MBM	meat-bone meal
$MgCl_2$	magnesium chloride
MLSB	modified Laemmeli sample buffer
Mobp	myelin associated oligodendrocyte basic protein
mRNA	messenger RNA
MS	mass spectrometry
MS/MS	tandem mass spectrometry

nAChR	β4 subunit of nicotinic acetycholine
NaCl	sodium chloride
NaOH	sodium hydroxide
NBBS	newborn bovine serum
Ni	nickel
NMR	nuclear magnetic resonance
OD	optical density
ORD	octapeptide repeat deletion
ORI	octapeptide repeat insertion
PBS	phosphate buffered saline
PCR	polymerase chain reaction
PK	proteinase K
PMCA	protein misfolding cyclic amplification
PMSF	phenylmethanesulphonylfluoride
PNS	post nuclear supernatant
Prni	prion incubation time gene
Prnp	mammalian PrP gene
PRNP	human PrP gene
PrP	prion protein
$PrP^{O/O}$	PrP-null knockout mice
PrP^{27-30}	27-30 kDa proteolytic cleavage product of PrP
PrP^{C}	cellular isoform of the prion protein
PrP^{d}	disease-associated prion protein
PrPL	prion protein ligand
PrP^{res}	protease-resistant prion protein
PrP^{Sc}	scrapie-like isoform of the prion protein
PrP^{TSE}	TSE-associated prion protein
PS	pentosan polysulphate
PTFE	polytetrafluoroethylene
PVDF	polyvinylidene fluoride
Q-ToF	quadrupole – time of flight mass spectrometer
QUIC	quaking-induced conversion assay
rER	rough endoplasmic reticulum
rHaPrP	recombinant hamster prion protein

RML	Rocky mountain laboratory
rMoPrP	recombinant mouse prion protein
rMo3F4PrP	recombinant mouse prion protein with 3F4 epitope
RNA	ribonucleic acid
rOvPrP	recombinant ovine prion protein
rOvPrP^{ARR}	recombinant PrP with A136R154R171
rOvPrP^{VRQ}	recombinant PrP with V136R154Q171
RPM	revolutions per minute
rPrP	recombinant prion protein
RT	room temperature
SAF	scrapie associated fibrils
sCJD	sporadic Creutzfeldt-Jacob disease
SDS	sodium dodecyl sulphate
SDS PAGE	sodium dodecyl sulphate polyacrylamide gel electrophoresis
SEC	size exclusion chromatography
SEM	standard error of the mean
SHa	Syrian hamster
Sinc	Scrapie incubation gene
SMB	scrapie mouse brain cell line
SMB-PS	scrapie mouse brain cell line cured with pentosan polysulphate
SSBP/1	scrapie sheep brain pool 1
SSCA	scrapie cell assay
TB	terrific broth
TBS	tris buffered saline
TME	transmissible mink encephalopathy
TSE	transmissible spongiform encephalopathy
UV	ultra-violet
vCJD	variant Creutzfeldt-Jacob disease

1. Introduction

1.1 Introduction to Prions

Prions exist as self propagating proteins that replicates autocatalytically by converting the native host protein into the prion state. In 2004, new data showed that observations on the conformational variations in yeast prions determined strain variation (Chien *et al.*, 2004). The term prion describes the infectious properties of proteinaceous agents that are devoid of nucleic acid and are segregated based on differences in conformation. Critically, prions are infectious and are generally known to cause a fundamental change in the host phenotype.

Mammalian prions are associated with the disease, transmissible spongiform encephalopathy (TSE), a neurodegenerative disorder characterised by the post-translational conversion of the mammalian prion protein (PrP). Mammalian TSEs were the first set of pathological states to be implicated with a self propagating protein. Initially, they were the only known instance of the prion concept, however, a number of different fungal proteins are now known to exhibit prion-like properties (Coustou *et al.*, 1997, Shorter and Lindquist, 2005, Wickner *et al.*, 2007).

1.2 Prion Hypothesis

The identity of the agent which causes transmissible spongiform encephalopathies has been debated for many years. Initial observations of scrapie in sheep, described the infectious agent as a slow virus infection. However, work by Alper and colleagues in the 1960's showed that the transmissible scrapie agent was resistant to treatments such as nucleases and ultraviolet light, with no effect on infectivity (Alper *et al.*, 1966 and 1967). This led to the hypothesis that the scrapie agent was not only devoid of any associated nucleic acid but was composed of an aberrant protein (Griffith, 1967, Bolton *et al.*, 1982). Prusiner described the infectious agent as a novel proteinaceous infectious particle that was devoid of nucleic acid and was responsible for scrapie in sheep (1982). The term prion was coined from *pro*teinaceous *in*fectious particle and Prusiner described the prion to be a novel

pathogen that was neither a virus nor a viroid. The protein associated with the transmissible agent was proposed to be a host encoded sialoglycoprotein that was protease resistant and had a molecular weight of 27-30 kDa (Bolton *et al.*, 1982). The hypothesis that the prion protein was host encoded was inferred by sequencing of hamster mRNA which revealed a partial amino acid sequence for PrP (Oesch *et al.*, 1985). The native cellular isoform of PrP was designated PrP^{C} (*c*ellular) whereas the disease associated isoform was designated PrP^{Sc} (*sc*rapie-like). During disease there is a post-translational modification that causes native PrP^{C} to misfold into the disease associated isoform, PrP^{Sc}.

1.3 Prion Protein

The mammalian prion protein gene (*Prnp*) encodes a protein of between 250 and 260 amino acids, depending on species (Oesch *et al.*, 1985). Mammalian *Prnp* is constitutively expressed and has been well characterised in several eutherian species such as sheep, cattle, rodents and humans (Rheede *et al.*, 2003). The prion protein is synthesised on ribosomes on the rough endoplasmic reticulum (rER) where, like many other plasma membrane bound proteins, it is post-translationally modified. During normal cellular function, PrP undergoes cleavage of its N-terminal signal and C-terminal hydrophobic peptide, the disulphide bridge forms, two N-linked mannose-rich oligosaccharides are added, as well as a glycosyl-phosphatidylinositol (GPI) anchor (Stahl *et al.*, 1987). PrP is trafficked through the Golgi body where the two N-linked oligosaccharides are modified to contain sialic acid. PrP^{C} is then packaged into vesicles and trafficked to the plasma membrane (Harris *et al.*, 2003).

1.3.1 PrP Structure

The first nuclear magnetic resonance (NMR) structure of PrP was of the mouse PrP domain 121-231, which revealed a C-terminal globular structure composed of three α-helices and a short anti-parallel β-sheet (Riek *et al.*, 1996). The α-helices are between residues 144 to 154, 179 to 193 and 200 to 217, and the β-strands between residues 128 to 131 and 161 to 164. The disulphide bridge is located between a

cysteine at residue 179 on the first turn of the second α-helix and a cysteine at residue 214 on the last turn of the third α-helix. In figure 1.1 the schematic diagrams of the primary and secondary structure of PrP^C is shown. Riek and co-workers then published data on the NMR structure of full length murine PrP (1997), which highlighted the structurally disordered nature of the N-terminal region between residues 23-120. NMR structures for recombinant human and bovine PrP molecules were published, revealing structural variations implicated in the species barrier phenomenon, as described in section 1.9 (Zahn *et al.*, 2000, Lopez Garcia *et al.*, 2000). In 2004, the first NMR structure for PrP^C was published (Hornemann *et al.*, 2004). This was achieved through the isolation of PrP^C, in the absence of detergents, from healthy calf brains and demonstrated that the structure was identical to that of recombinant bovine PrP expressed in *E.coli*. This data showed that recombinant proteins, which are deficient in glycosylation, can be utilised in prion protein structural studies. In contrast, X-ray crystallography of PrP^C has been difficult with only two publications to date, which include the crystal structure of the truncated recombinant human PrP in a dimeric form (Knaus *et al.*, 2001) and the globular C-terminus region (123–230) of recombinant ovine PrP (Haire *et al.*, 2001).

The prion protein has two variably occupied sites for glycosylation, at asparagine residues 180 and 196 and generate either di-, mono- or un-glycosylated PrP as shown in figure 1.1 (Stimson *et al.*, 1999). Glycan analysis of PrP reveals a broad range of sugars at the two glycosylation sites with at least 52 different sugars found on Syrian hamster (SHa) PrP (Rudd *et al.*, 2001). The significance of glycoform diversity is not fully understood in terms of the normal function of PrP. However, PrP glycosylation is proposed to be a factor in determining TSE strains and is discussed later (Tuzi *et al.*, 2008).

1.3.2 PrP Function

PrP^C is ubiquitously expressed in most cell types, suggesting that it may be important and functionally significance as PrP-null ($PrP^{0/0}$) transgenic mice appear to develop

A

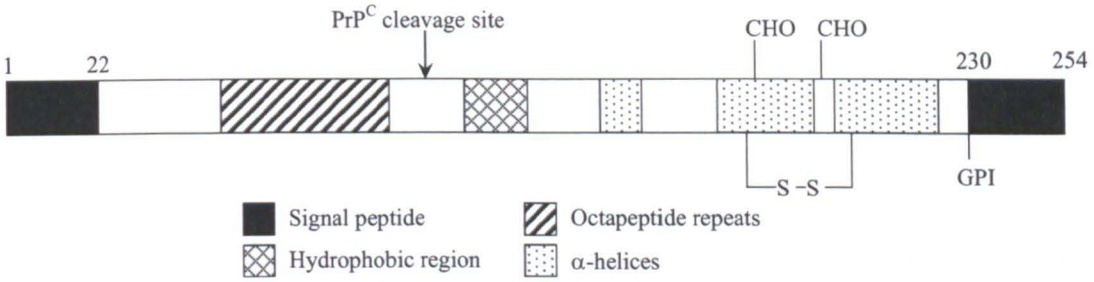

B

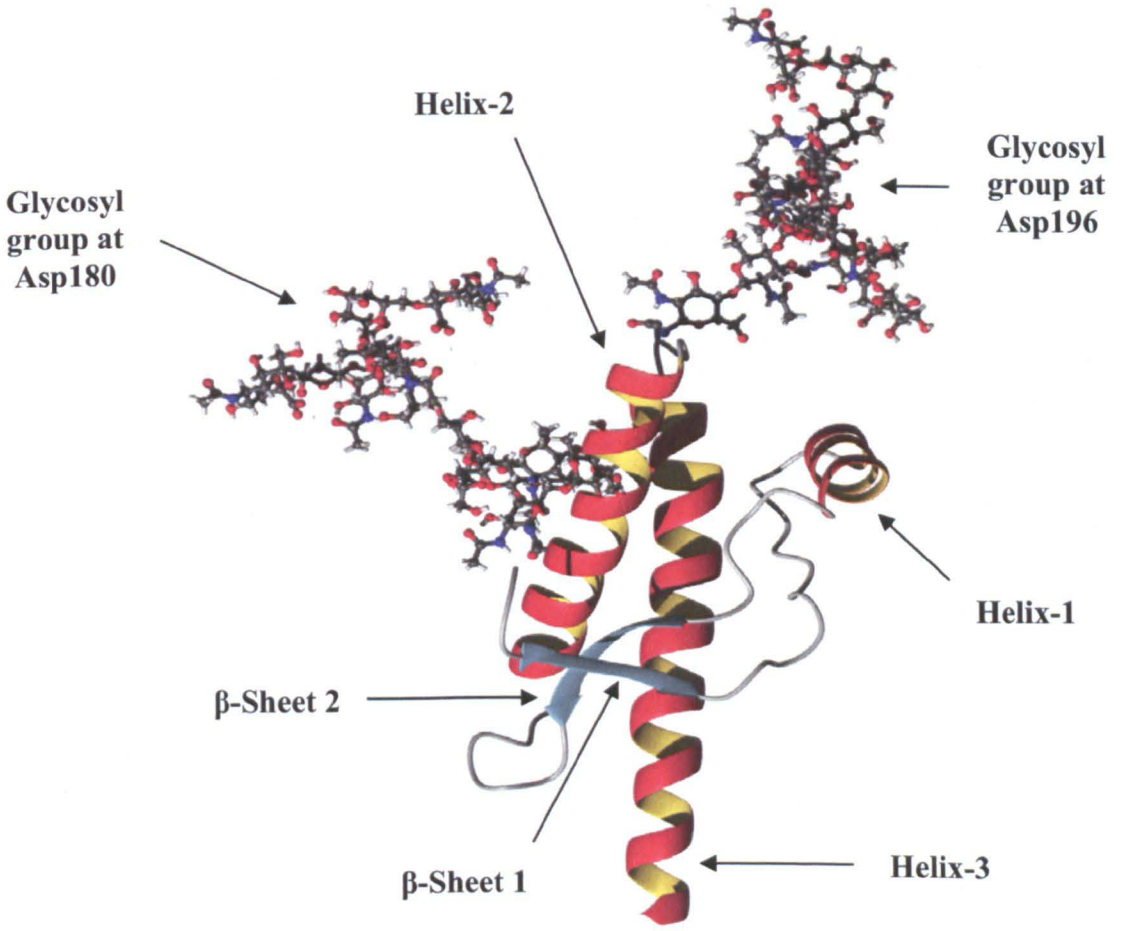

Figure 1.1: Schematic diagrams of PrP^C.

(A) Diagram of the primary structure of PrP^C (B) Ribbon diagram of the structured C-terminus domain of PrP^C where α-helices are represented in red/yellow, β-sheet are represented by blue arrows and the glycosylation of PrP^C as indicated at asparagine residues 180 and 196. (Asp = asparagine, CHO = carbohydrate, GPI = glycosyl-phosphatidylinositol anchor)

and reproduce normally (Manson *et al.*, 1994). This panel of transgenic mice were initially characterised as healthy, however perturbations in circadian rhythm (Tobler *et al.*, 1997), alterations in copper binding and loss of superoxide dismutase activity (Brown *et al.*, 1997) have been attributed to the ablation of PrP. The function of PrP^C, however, is still under debate due to the variation in published data. It is known that PrP is abundant in neurons and has a high selectivity for Copper II (Cu^{2+}) ions through its octapeptide repeat region (Brown *et al.*, 1997). In healthy brain, the prion protein has been hypothesised to localise predominately in the synaptic region of neurons (Taraboulos *et al.*, 1992, Sales *et al.*, 1998). Furthermore, it has been suggested that PrP^C is more precisely localised in the presynatic membrane region, firstly through the co-localisation with the presynapytic protein synaptophysin (Fournier *et al.*, 1995) and secondly, by observations made on the regulation of copper concentration at the presynaptic membrane (Herms *et al.*, 1999).

PrP^C can bind up to six Cu^{2+} ions, depending on species, and these analyses suggest a role for PrP in copper homeostasis or at least a function related to a copper dependent pathway. Functional studies of PrP^C have generated observations that upon copper binding, PrP^C is endocytosed, carrying bound copper ions into the cell (Pauly *et al.*, 1998). Copper binding to PrP^C has also been implicated in the prevention of oxidative stress through the regulation of CuZn superoxide dismutase activity (Brown *et al.*, 2001). This observation was supported by Rachidi and co-workers who demonstrated that copper uptake correlated with detoxification of reactive oxygen species in neurons (Rachidi *et al.*, 2002). However, the same study showed no correlation between copper uptake and copper delivery into the cell interior.

Increasing evidence linking PrP^C function with cellular pathways involved in the elimination of reactive oxygen species suggests a model for PrP^C loss of function being responsible for TSE disease-specific neurodegeneration (Milhavet *et al.*, 2000, Wong *et al.*, 2000, Klamt *et al.*, 2001). The *in vitro* analysis of immortalised hippocampal neurons isolated from $PrP^{0/0}$ transgenic mice were more susceptible to oxidative stress and apoptosis than the same cell type that was expressing PrP^C (Kuwahara *et al.*, 1999). Furthermore, observations made *in vivo* showed that PrP^C

protects the brain against mediated cell death (Behrens *et al.*, 2002, Atarashi *et al.*, 2003).

In this study three lines of $PrP^{0/0}$ transgenic mice (ZrchII, Nsgk and Rcm0) were used to study loss of PrP function. The ablation of PrP and the resultant phenotype was attributed to a gene that was 16 kb downstream of *Prnp* and encoded a PrP-like protein termed Doppel (Dpl). This was because, in the absence of PrP, Dpl then came under control of the PrP promoter in these transgenic mice. Although Dpl shares ~25% amino acid sequence homology with PrP (Moore *et al.*, 1999) it lacks the octapeptide repeat region and structurally resembles a truncated form of PrP (Mo *et al.*, 2001). Experiments using transgenic mice expressing this truncated form of PrP that resembles Dpl, displayed similar ataxic phenotypes (Shmerling *et al.*, 1998). In 1999, Weissmann and Aguzzi proposed that PrP^{C} and Dpl may compete with each other for the same ligand (PrPL). Binding of the ligand by PrP^{C} generates a survival signal whereas binding of Dpl or truncated PrP^{C} fails to produce the necessary survival signal. This raises implications for Dpl in TSE disease where PrP^{C} is sequestered into amyloid and therefore preventing binding to PrPL. However, transgenic studies in mice expressing wild type PrP (PrP^{WT}) and $PrP^{0/0}$ mice comprehensively ruled out any implication of Dpl influencing the clinical phenotype of TSE disease at the terminal stages of disease in these lines of transgenic mice (Tuzi *et al.*, 2002).

Although PrP has been associated with oxidative stress and copper mediated pathways, other functions have been reported. These include a neuroprotective function of PrP^{C} through the interaction with the 37-kDa / 67-kDa laminin receptor. This interaction induces PrP internalisation *via* clathrin-coated pits and it has been proposed that the co-localisation with the laminin receptor initiates a survival signal by either playing a role in important cell to cell communication, or by cellular internalisation (Rieger *et al.*, 1997, Gauczynski *et al.*, 2001). The latter of these hypotheses was supported by data that had been previously published exemplifying the involvement of PrP in the activation of an intracellular tyrosine kinase, Fyn (Mouillet Richard *et al.*, 2000). However, the importance and exact involvement of this tyrosine kinase in cell survival is yet to be determined.

Finally, PrP^C has been implicated in other signal transduction pathways linked to cell survival, specifically mitochondrial mediated apoptosis. PrP^C has been shown to suppress Bax-mediated apoptosis by preventing the conformational change in Bax required to initiate the apoptotic signal (Roucou *et al.*, 2005). This is not through co-localisation of PrP^C with Bax but instead, through the initiation of a signal stemming from PrP^C on the cell membrane.

1.4 PrP^{Sc} and TSE Disease

During TSE disease, the host protein PrP^C is converted to a disease associated isoform that is believed to be the principal component of the infectious agent (Prusiner, 1982). The misfolded isoform of PrP^C is known as PrP^{Sc} where the 'Sc' refers to scrapie-like. Other terms include PrP^d (disease associated isoform), PrP^{res} (protease resistant isoform), $PrP^{27\text{-}30}$ (27-30 kDa proteolytic cleavage product of PrP) and PrP^{TSE}. The conformational changes in PrP^C during disease are associated with an increase in the β-sheet structure of PrP (Caughey *et al.*, 1991*a*). This change in secondary structure is shown in figure 1.2, which is a hypothetical schematic diagram of PrP^{Sc}. This increase in β-sheet causes PrP to form an oligomeric isoform before maturation into fibrils (Hill and Collinge, 2003, Kayed *et al.*, 2003, Wetzel *et al.*, 2007). The formation of amyloid fibrils is a hallmark of neuropathology for most TSE diseases and these plaques are insoluble and partially resistant to proteolytic digestion. When treated with proteases, the unfolded N-terminus is cleaved, leaving behind a 27-30 kDa protease resistant core which can be detected by Western blotting with an antibody that detects a C-terminus epitope. Figure 1.3 shows the Western blot profile when using a C-terminal specific antibody (BC6) or a N-terminal specific antibody (FH11).

Insoluble amyloid plaques composed primarily of PrP^{Sc} are generally associated with neurodegeneration, gliosis (astrocytes and microglial invasion) and spongiform change in the brain, as illustrated in figure 1.4 (Budka, 2003). Typically, PrP^{Sc} deposits are found in the brain, however the distribution and severity of vacuolation

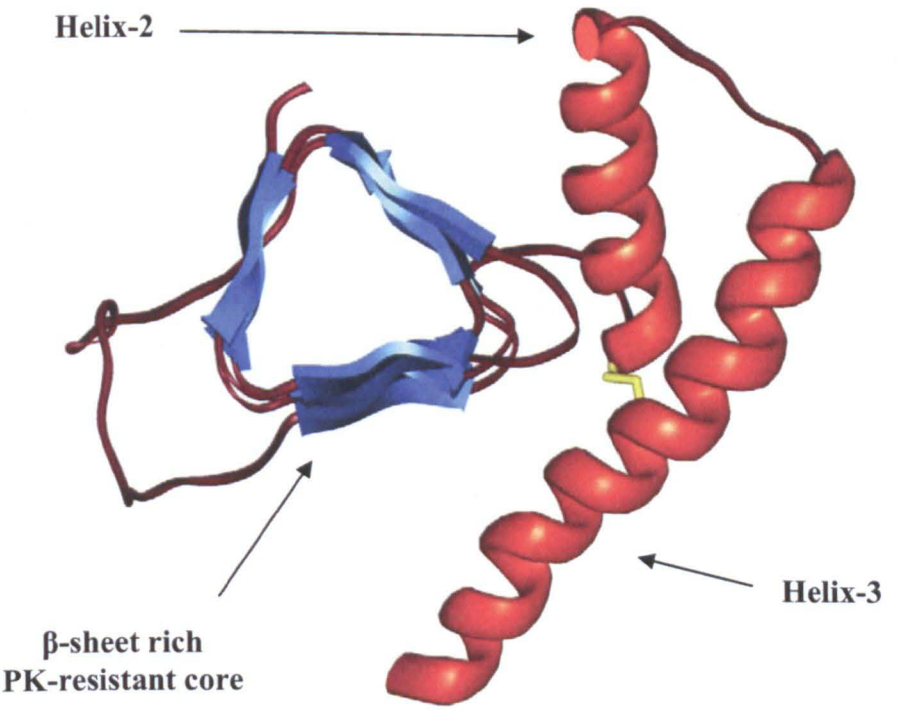

Figure 1.2: Schematic diagram of the secondary structure of PrP^{Sc}.

Hypothetical ribbon diagram of the structured C-terminal domain of PrP^{Sc} where α-helices are represented in red and β-sheet are represented by blue arrows. The disulphide bridge is represented by a yellow line.

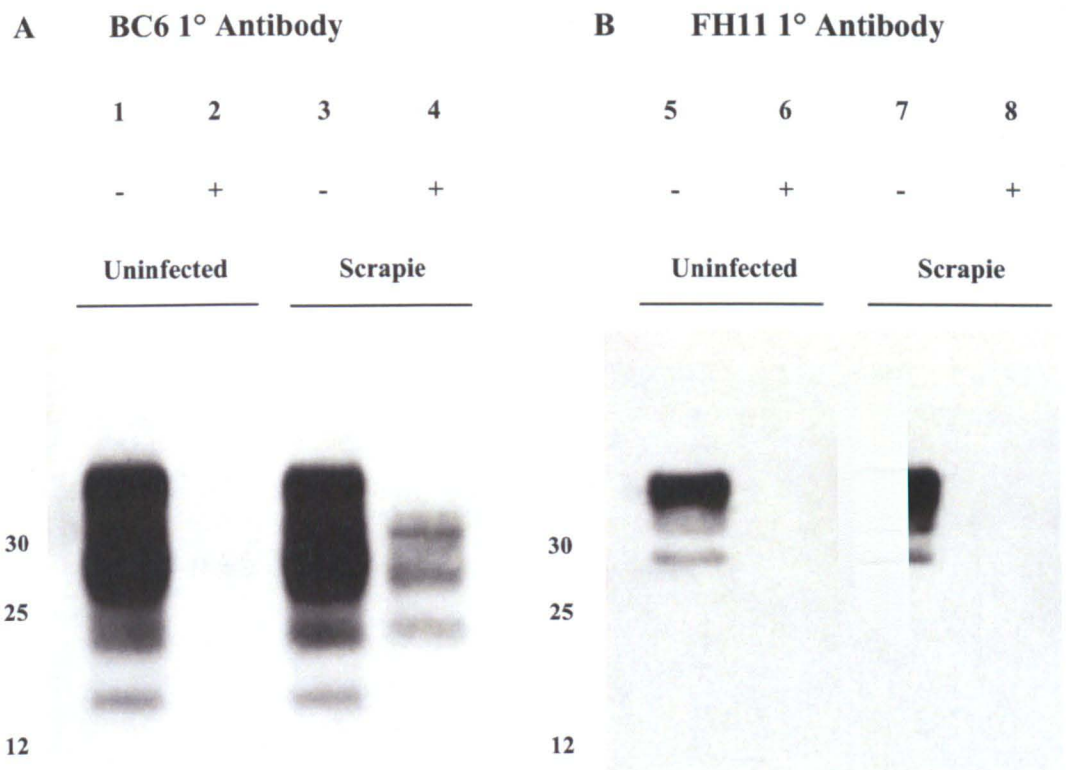

Figure 1.3: Differential identification of the proteolytic resistance of PrP^{Sc} associated with scrapie associated fibrils isolated from brains of TSE infected sheep.

Uninfected and scrapie infected brain homogenates (10 % (w/v)) were treated with and without PK (50 µg/ml) prior to SDS PAGE and Western blotting with the anti-prion primary antibodies (A) BC6 (C-terminal specific epitope at residues 141–152) at 1 µg/ml (lanes 1 to 4) and (B) FH11 (N-terminal specific epitope at residues 54–58) at 1 µg/ml (lanes 5 to 8). Secondary antibody was goat anti-mouse HRP (Dako) at 1:20,000. Lanes 1 and 3 show full length and truncated PrP^{C} whereas lanes 5 and 7 show only full length PrP^{C}. After treatment with PK, PrP^{C} is degraded as shown in lanes 2, 4, 6 and 8. In scrapie infected brain homogenates only BC6 can detect PK-truncated PrP^{Sc} (lane 4) due to the location of the antibody epitope in the PK-resistant C-terminus, whereas the epitope for FH11 has been cleaved off by PK (lane 8). Western blots courtesy of Dr Sandra McCutcheon and Boon Chin Tan (The Roslin Institute).

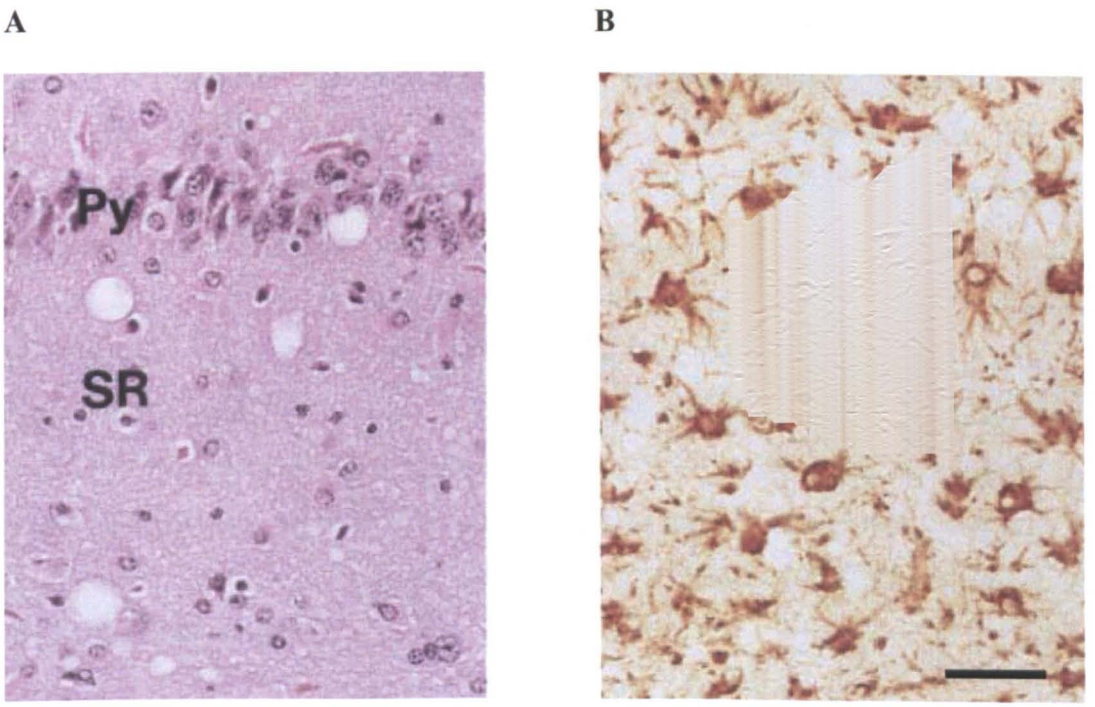

Figure 1.4: Neuropathology of RML infected mouse brains.

Brain sections from Swiss white mice inoculated with Rocky mountain laboratory (RML) strain of scrapie were fixed in 10 % formalin and embedded in paraffin before (A) hematoxylin and eosin staining of the hippocampus and (B) immunohistochemistry of the hippocampus for the astrocyte marker, glial fibrillary acidic protein (GFAP). Py is the pyramidal cell layer and SR is the stratum radiatum (Bar = 50 μm). Reproduced without permission from Prusiner, 1998 (Nobel Prize Lecture).

are used to characterise TSE strains (Fraser and Dickinson, 1968, Bruce *et al.*, 1989, Bruce *et al.*, 1991, Fraser, 1993).

1.5 Human TSEs

Human TSEs were first reported by the German neurologist Hans Gerhard Creutzfeldt in 1920 and then soon afterwards by Alfons Maria Jakob. The term Creutzfeldt-Jacob disease (CJD) was coined in 1922 and used as a general term to describe human TSEs (Spielmeyer, 1922). This term originally encompassed all human TSEs, however it has changed over the years due to the heterogeneity of phenotypes displayed in human TSE patients. The variation in disease phenotypes can be determined by the origin of the prion and the route of infection (Gambetti *et al.*, 2003). Typically the first manifestations of CJD are dementia and memory loss which progress into physical impairments such as speech impairment and ataxia. The disease is invariably fatal and are caused by the progressive loss of neuronal cells in the brain (Budka, 2003).

There are three epidemiological types of human TSEs; sporadic, familial, and acquired (table 1.1). These diseases are rare, with approximately 1:1,000,000 cases per annum being classified as sufferers (Collinge *et al.*, 2001). From this number, 85 % of all TSE patients have sporadic CJD (sCJD) with the majority of the remainder consisting of familial TSEs (familial CJD (fCJD), fatal familial insomnia (FFI) and Gerstmann-Sträussler-Scheinker syndrome (GSS), Kong *et al.*, 2003). Acquired TSEs are the rarest and arise from either the ingestion of TSE contaminated foodstuffs or by iatrogenesis. A recent example of an acquired TSE is variant CJD (vCJD), which was caused by the consumption of meat products contaminated by the prion responsible for bovine spongiform encephalopathy (BSE) (Bruce *et al.*, 1997).

Sporadic human TSEs	Familial human TSEs	Acquired human TSEs
Sporadic CJD	Familial CJD	Iatrogenic CJD
Sporadic FI	FFI	New variant CJD
-	GSS	Kuru

Table 1.1 The spectrum of human TSEs.

Key: Fatal familial insomnia (FFI), fatal insomnia (FI) Gerstmann-Sträussler-Scheinker (GSS), Creutzfeldt-Jacob disease (CJD).

such as blood transfusion (Houston *et al.*, 2000) Transmission studies using sheep infected with scrapie and BSE, identified that TSE infection can be carried efficiently The BSE epidemic in cattle raised concerns for human health and the risk of transmission from not only BSE but other animal prions. More recently it has been the risk of vCJD infected blood and blood-related products used in medical practices by blood transfusion from donor to recipient (Hunter *et al.*, 2002, Houston *et al.*, 2008). Consequently, strict regulations have been put in place to prevent TSE spread by blood transfusion. These include the purchase of plasma from non-UK sources and leucoreduction of whole blood and red-blood cell derived products (Gregori *et al.*, 2004).

1.6 Animal TSEs

Scrapie is an animal TSE and has been endemic in the UK for over 200 years (McGowan, 1922). It is the most abundant TSE and was described as a disease that caused persistent lumbar pruritis and resulted in sheep fatality (Stamp, 1962, Parry, 1983). In 1943, it was observed that the presence of vacuolated nerve cells in the medulla oblongata was indicative of scrapie (Holman & Pattison, 1943), yet it wasn't until 1959 when W. J. Hadlow, explained in a letter to The Lancet, that Kuru, a CNS disorder of the South Fore tribe of Papau New Guinea, and sheep scrapie shared many parallels in terms of clinical and pathological features (Hadlow, 1959). The proposal by Hadlow was that although they were not identical, the lack of evidence of a causative microbiological agent implied pathological similarities. Work by Chandler opened up the possibility of using the mouse to study the disease in a manageable model (1961). In this publication Chandler, demonstrated that scrapie could be transmitted to a mouse model by intracerebral inoculation. After 7 ½ months incubation, neurological disturbances were observed and histological examination showed considerable astrocytosis as well as severe vacuolation of the medulla oblongata.

Since the BSE epidemic in the 1980's, the devastating effect on farming and the rural economy emphasized the importance of TSE research both politically and

economically. The threat of a TSE epidemic in humans from contaminated animal foodstuffs prompted a ban on the recycling of animals unfit for human consumption, into animal feeds. The BSE epidemic may have started from BSE infected meat and bone meal (MBM) that was provided as protein supplements for cattle (Prusiner *et al.*, 1997). However, due to the sudden occurrence of BSE, the origin of the infectious agent is still under review. For example, it is not known whether BSE emerged through a spontaneous mutation of the bovine PrP gene or if the scrapie agent mutated and crossed species from sheep to cattle initially *via* scrapie-infected MBM.

More recently, it was reported that a number of BSE infected cattle in Italy and France exhibited atypical molecular characteristics coupled with differences in amyloid distribution to that of classical BSE. The Italian case showed that the unglycosylated PrP^{Sc} had a lower molecular weight than unglycosylated PrP^{Sc} associated with BSE (Casalone *et al.*, 2004). This new form of BSE is more prevalent in older cattle and was called L-type BSE but has also been described as bovine amyloidotic spongiform encephalopathy (BASE). The French atypical BSE case on the other hand, exhibited a higher molecular weight for unglycosylated PrP and this form of BSE was named H-type BSE (Biacabe *et al.*, 2004).

Atypical BSE may pose a new threat to human health due to the unknown virulence of this strain with regards to the current knowledge regarding susceptibility conferred by different human genotypes. This reasoning was supported by data from the sheep model where the characteristics of atypical scrapie had different pathological characteristics to that of classical scrapie (Benestad *et al.*, 2003). Atypical scrapie predominately affects sheep with genotypes that are associated with resistance to classical scrapie whereas in contrast, sheep that are susceptible to classical scrapie were resistant to atypical scrapie (Benestad *et al.*, 2008). Atypical scrapie was discovered in a Norwegian sheep flock in 1998 and after intensive surveillance, has since been identified in several other countries. This strain differs from classical scrapie most notably in its distribution of neuropathology and its Western blot profile

where a lower molecular weight form of PrP^{Sc} is detected between 7-12 kDa (Benestad *et al.*, 2003).

Another emerging TSE in animals is chronic wasting disease (CWD) of deer and elk. This naturally occurring animal TSE is rapidly spreading through these species in North America by an unknown transmission route, although it has been suggested that environmental contamination is responsible (Williams and Miller, 2002, Miller *et al.*, 2003). Currently, CWD poses an unknown risk to human health; however, studies have crucially shown that CWD prions can be detected in deer skeletal muscle, implying the possibility of a zoonotic transmission to humans *via* infected meat products (Angers *et al.*, 2006).

Other than BSE, scrapie and CWD, other animal TSEs have been reported in the literature. These include feline spongiform encephalopathy (FSE) of domestic and zoological cats and transmissible mink encephalopathy (TME) of farmed mink. TME has been observed in mink since 1947; however outbreaks in mink populations are rare (Marsh and Hadlow, 1992). This TSE is of unknown origin however mink are susceptible to intracerebral inoculation with scrapie and BSE, raising questions over the epidemiology of TME (Hanson *et al.*, 1971, Marsh *et al.*, 1997). However, FSE has been identified as being linked to the BSE epidemic where a total of 15 animal species unknown to of previously developed TSE disease, were transmitted BSE prions. The 15 new species known to have contracted BSE include seven bovid, four felid and four primate species (Sigurdson and Miller, 2003).

1.7 Prion Genetics

In 1968, it was suggested that a gene controls the incubation time of scrapie in mice and has two alleles, s7 and p7 (Dickinson *et al.*, 1968*a*, Dickinson and Meikle, 1971). In these seminal experiments, C57BL mice ($Sinc^{s7}$) gave shorter incubation times for ME7 infection than VM mice ($Sinc^{p7}$). The *Sinc* gene (gene controlling incubation period of ME7) has since been shown to be congruent with *Prnp* and *Prni*

genes (Moore *et al.*, 1998). The following sections (1.7.1 and 1.7.2) describe the influence of prion genetics in humans and animals, respectively.

1.7.1 Human Prion Genetics

As previously discussed, human TSEs can be inherited, in a dominant autosomal manner, acquired or arise sporadically in an individual. Mutations in the human PRNP gene have been associated with determining the clinical and pathological outcome of the disease (Palmer and Collinge, 1993, Horwich and Weissman, 1997). Genetic analysis of PRNP has also identified a number of polymorphic sites throughout the human prion protein that are associated with susceptibility to TSE infection (figure 1.5).

In some family lines, there are mutations in the PRNP gene that mean some individuals develop a familial TSE. In particular, the D178N mutation, in combination with a methionine at residue 129 in PrP^{C}, results in the rare familial human TSE, fatal familial insomnia (FFI). This is an autosomal dominant prion disease that causes plaques of PrP^{Sc} to develop in the thalamus, the region of the brain responsible for sleep. Other mutations in PrP^{C} include the P102L substitution, which is associated with the occurrence of Gerstmann-Sträussler-Scheinker syndrome, another autosomal inherited prion disorder. However, the most common inherited human prion disease is the E200K variant of CJD. The substitution of glutamic acid to lysine at residue 200, results in a very similar disease phenotype to sCJD (Meiner *et al.*, 1997).

Sporadic CJD encompasses a wide variety of polymorphisms and mutations in PrP that cause the misfolding of human PrP to a disease associated isoform. Somatic mutations, which account for 85 % of all sporadic cases, include P105L, A117V, $Y145_{stop}$, F198S and M232R to identify a few (Kitamoto and Tateishi, 1994, Ghetti *et al.*, 1996*a,b*). In addition, the methionine/valine polymorphism at residue 129 has been correlated with variances in clinical phenotype of sCJD, such as survival time

and type of PrP^{Sc} deposited in the brain (Collinge *et al.*, 1991, Palmer *et al.*, 1991, Brown *et al.*, 1994, Parchi *et al.*, 1996). In general, homozygosity for methionine at residue 129 was more abundant in sCJD sufferers and correlates with reduced survival times (Pocchiari *et al.*, 2004). Statistical analysis of this study correlated increased survival time with factors such as the female gender, younger age of clinical disease onset and expression of PrP type. These mutations and other prevalent polymorphisms are detailed in figure 1.5.

1.7.2 Animal Prion Genetics

One of the most extensively studied examples of prion genetics that influence susceptibility and resistance to TSE disease, is the ovine PrP gene. Studies into natural scrapie showed the importance of three codons within the ovine PrP gene; 136, 154 and 171 (Goldmann *et al.*, 1991). These three codons dictated incubation time of disease for natural and experimental scrapie in sheep (Goldmann *et al.*, 1994). Interestingly, of these three codons it is only residues at 136 and 171 that influence the rate of infection for sheep inoculated with BSE (Foster *et al.*, 2001). The most resistant genotype is AA_{136} RR_{154} RR_{171}, which confers resistance to natural and experimental scrapie. On the other hand, sheep with the genotype VV_{136} RR_{154} QQ_{171} are extremely susceptible to scrapie. Table 1.2 summarises the level of susceptibility of the 15 different ovine genotypes to scrapie and their approximate prevalence in the UK sheep population.

Our understanding of how genes influence resistance and susceptibility to TSE infections in other animal species are not as well understood as to the ovine model. In cattle, there are no correlations between polymorphisms in the bovine PrP gene and an increased incidence of BSE in cattle. However, the insertion/deletion (indel) mutations of a 23-bp indel in the promoter region and a 12-bp indel in intron 1 have been significantly associated with an increased susceptibility of cattle to BSE (Juling *et al.*, 2006). The authors of this publication implied that exposure to contaminated feed was likely the main risk factor, out with genetics, for cattle acquiring BSE.

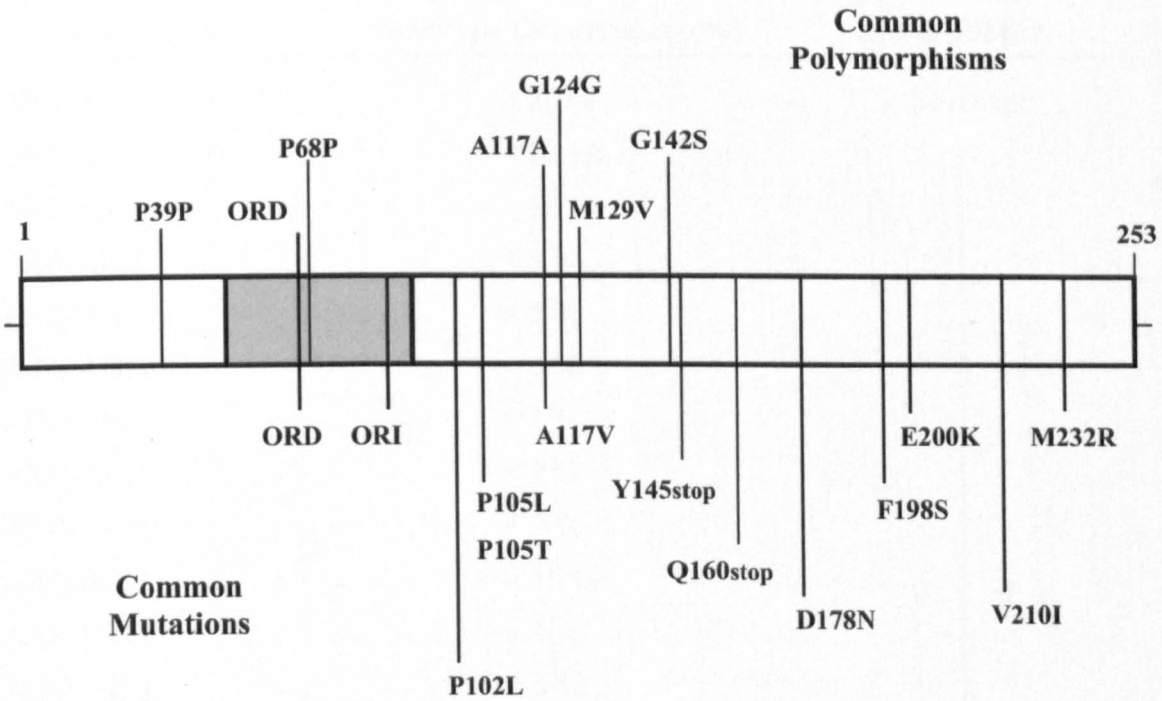

Figure 1.5: Polymorphic variants of human PrP.

Diagram of human PrP with the octapeptide repeat sequence filled in grey. Mutations that are associated with disease are shown below human PrP. Polymorphisms that do not cause disease but are implicated in susceptibility or resistance are shown above human PrP. (ORD = octapeptide repeat deletion, ORI = octapeptide repeat insertion).

Genotype	Genotype Occurrence (%)	Susceptibility
ARR/ARR	> 20 %	Resistant
ARR/AHQ	< 10 %	
ARR/ARQ	> 20 %	
ARR/ARH	< 5 %	
AHQ/AHQ	< 5 %	
ARQ/AHQ	< 5 %	
AHQ/ARH	< 1 %	
ARH/ARH	< 2 %	
ARQ/ARH	< 2 %	
ARQ/ARQ	> 10 %	
ARR/VRQ	< 10 %	
AHQ/VRQ	< 5 %	
ARQ/VRQ	< 10 %	
ARH/VRQ	< 1 %	
VRQ/VRQ	< 1 %	Susceptible

Table 1.2: Ovine PrP genotype and susceptibility to scrapie.

Table listing the ovine prion protein variations at amino acid residues: 136, 154 and 171 and their approximate occurrence in UK sheep populations (Adapted from Baylis *et al.*, 2004).

In cervids a number of polymorphisms in different species have been identified as influencing susceptibility to CWD e.g. mule deer, elk and white-tailed deer. Mule deer that were heterozygous for serine and phenylalanine or homozygous for phenylalanine at codon 225 were suggested to be less susceptible to CWD (Jewell *et al.*, 2005). Elk however, were more susceptible to CWD if homozygous for methionine at codon 132 (O'Rourke *et al.*, 1999) and in white-tailed deer the polymorphisms Q95H and G96S were associated with decreased susceptibility to CWD (Johnson *et al.*, 2006).

1.8 TSE Strains

In 1961, Pattison and Millson published data indicating that genetic susceptibility was not the only significant factor affecting clinical symptoms of the disease. Sheep that had scrapie exhibited two distinct behaviours i.e. scratching or nervous behaviour. Brain homogenate from sheep with the scratching syndrome was intracerebrally (ic) passaged into goats where it was observed that the number of animals that showed scratching symptoms was reproducible. This experiment was repeated with brain homogenate from sheep with the nervous form of scrapie and recipient goats predominantly exhibited the same nervous behaviour characteristics. This was the first study that provided researchers with insights into different strains of the TSE agent (Pattison and Millson. 1961). In the same year, preliminary work published by R. L. Chandler at the Agricultural Research Council Field Station, Compton, showed that Pattison and Millson's nervous scrapie strain could also be transmitted to Swiss white mice by intracerebral inoculation (Chandler, 1961). This work opened up the possibility of using the mouse model to analyse the identity of the infectious agent and the intriguing phenomenon of different strains of the infectious TSE agent (Dickinson *et al.*, 1968*a*,*b*, Fraser *et al.*, 1968, Dickinson *et al.*, 1969).

It is believed that naturally occurring sheep scrapie is a crude mixture of scrapie strains, which, when transmitted into mice, can be characterised into new distinct strains. The incompatibility between PrP^{C} and PrP^{Sc} from different species causes the

selection of the most pathological strain of the agent. Discrimination by semi-quantitative methods such as lesion profiling and incubation period allows for the characterisation of new distinct strains (Pattison and Jones, 1968, Prusiner, 1998). Initial experiments on mouse scrapie described that on the second passage of sheep scrapie in Swiss white mice, the time before the onset of scrapie like symptoms shortened to within 5 to 9 months after intracerebral inoculation (Zlotnik and Rennie, 1963). Today, there are many distinct strains of scrapie that have been identified over multiple passages in mice of different genotypes. Mouse scrapie strains differ in their incubation period, pathology and clinical features. The incubation period of mouse scrapie in mice varies from 4 to 24 months and is incredibly reproducible but is dependent up on the host PrP sequence.

The most notable set of scrapie strain experiments came from the sheep scrapie brain pool (SSBP/1), which was originally generated from three natural scrapie cases in Cheviot sheep (Bruce and Fraser, 1991). The SSBP/1 main passage line involved multiple passes in sheep before cloning into mice homozygous for either the s7 or p7 allele of *Prnp*. From the main line of SSBP/1, mouse passages revealed the presence of 5 strains of scrapie that were called 22A, 22C, 22F, 22H and 22L (Carp and Callahan, 1991, Bruce, 1993). During the initial passages of SSBP/1 in sheep (prior to inoculation into mice), a branch line of experiments was carried out and included the inoculation of the scrapie agent into goats. This approach enabled the separation of scrapie and the isolation of other novel strains. The goats were split into two groups according to whether they displayed scratching or the drowsy clinical phenotypes. Infectious brain homogenate from goats with the drowsy form of goat scrapie were ic inoculated into mice, which resulted in the characterisation of two new strains of scrapie, 79A and 139A (Chandler, 1961, Somerville *et al.*, 2005). During these experiments, a sample of mouse passaged scrapie was sent to the Rocky Mountain Laboratory (USA) where it was propagated firstly in Swiss white mice then Swiss CD-1 mice. The new strain of scrapie was called RML and is biochemically similar to that of 79A (Bruce *et al.*, 1991). Finally, scrapie was also inoculated into Golden hamsters which isolated a novel mutant strain, called 263K, which was pathologically completely different to the original scrapie inoculum (Marsh and Kimberlin, 1975).

Other animal TSEs such as BSE have also been transmitted into mice and these experiments generated additional experimental models of murine TSEs. Infectious material isolated from four BSE infected Holstein-Friesian cows was transmitted into mice that were either homozygous for the s7 or p7 allele of *Prnp*. This resulted in the classification of two mouse-derived strains of BSE, which were called 301C and 301V, respectively (Bruce *et al.*, 1994).

1.9 Species Barrier

The species barrier is one factor believed to control transmission of prions between different species (Bruce and Fraser, 1991). Cross species prion propagation is generally rare and is thought to be limited by the differences in PrP sequence of the donor and the host (Prusiner *et al.*, 1990). Furthermore, the differences in sequence may relate to subtle alterations in conformation resulting in an incompatibility between donor and host PrP molecules. If there is sufficient compatibility enough host PrP molecules will be converted to the disease associated isoform to begin the infection. Generally, effects of a species barrier will cause an elongation in the incubation period. However, studies in mice have demonstrated that on serial passage of the TSE agent can result in a shortening of the incubation period, indicating that the infectious agent has adapted to its new host and overcome the initial species barrier. The species barrier therefore, has been a key factor in the determination and isolation of novel strains of TSEs from a mixture of natural strains.

Since the BSE crisis, the possibility that BSE could cross the species barrier represented a major health threat to human health. This proved to be more than a theoretical risk, as BSE prions crossed the species barrier from cattle to humans causing the TSE termed vCJD (Will *et al.*, 1996). CWD that is sweeping through deer and elk populations in North America poses a new threat, although transmissibility to humans is unknown, its ability to infect cattle, opens a route for a new form of TSE that could potentially effect humans (Miller and Williams, 2004).

Specific traits associated with a species barrier have been replicated *in vitro* using assays such as the cell free conversion assay (CFCA, Kocisko *et al.*, 1995, Raymond *et al.*, 1997, 2000, Kirby *et al.*, 2003). In these publications it was shown that rMoPrP did not convert to a PK-resistant isoform in the CFCA when using the hamster derived strain, 263K. Conversely, HaPrP was also resistant to conversion by the mouse scrapie strains Chandler and 87V in the CFCA.

1.10 Protein X and Co-Factors

Many advances have been made in TSE research in recent years, however the identity and composition of the prion agent is still unclear. Isolation of host PrP from the infectious agent has implicated a pathological change in the conformation of PrP^{C}, which ultimately results in a neurological disorder. Prusiner's protein only hypothesis states, that the interaction between PrP^{C} and PrP^{Sc} is the principal pathological event and occurs in the absence of any nucleic acid (Prusiner, 1982). This hypothesis proposed that the pathological isoform, PrP^{Sc}, propagates itself by interacting and converting PrP^{C} in a still undefined reaction. This hypothesis remains unproven, but in the absence of any alternative theorem, remains the most attractive explanation of prion propagation. Other hypotheses do exist and moreover involve the inclusion of viral nucleic acids as the information coding molecule associated with the infectious agent. However, an alternative theory was proposed in 1991, to answer the question of prion propagation and is known as the unified theory (Weismann, 1991). This data suggests that a small host-specific nucleic acid is a crucial component of PrP^{Sc} and encodes features such as strain specificity but needs not be a virus or viroid. Support for this theory has been reported by the discovery of small RNAs that stimulate prion protein conversion in the protein misfolding cyclic amplification assay (PMCA, Deleault *et al.*, 2003, 2007). This group demonstrated that enhanced propagation of prions *in vitro* was facilitated by accessory polyanion molecules such as RNA. However, in the 2007 study they attempted to make synthetic infectious prions from minimal components which, although causing a neurological disorder in a panel of mice, lacked defining strain characteristics; in other words there was strain convergence. There is a possibility that this is a flaw of

the particular assay used (PMCA is discussed elsewhere) and there is the possibility that small RNA molecules play a valid role in acting as either a scaffold of PrP^{Sc} or a catalyst of conversion.

TSE strains were historically distinguished by differences in disease incubation time and lesion profiles of the brain (Fraser & Dickinson *et al.*, 1968, Bruce *et al.*, 1989). Since then it has been suggested that strain differences are encoded by different conformations of PrP^{Sc} (Bessen *et al.*, 1992, Bessen *et al.*, 1994, Safar *et al.*, 1998, Polymenidou *et al.*, 2005). However, work on yeast prions has revealed that different strains of yeast prions are determined by non-prion components (Toyama *et al.*, 2007). Yeast prions share many biochemical traits with mammalian prions and it is conceivable that PrP^{Sc} conformation, in cooperation with specific co-factors, help to differentiate one strain from another.

Protein X was the first suggested co-factor and was thought to play an important role in prion replication (Telling *et al.*, 1995). The evidence to suggest a prion co-factor was to explain the results acquired when monitoring the susceptibility of transgenic mice expressing either mouse, human or a mouse-human chimeric PrP, to human prions. Mice expressing both mouse and human PrP were resistant to a human prion infection. However, mice expressing both mouse and a mouse-human chimeric PrP were susceptible to infection to the same human prions. It was hypothesised that a murine co-factor (i.e. protein X) that selectively bound to mouse PrP, was responsible and necessary for successful conversion. Protein X had a higher affinity for murine PrP and therefore prevented conversion in mice expressing both murine and human PrP but supported conversion in mice expressing murine and the mouse-human chimeric PrP, by binding to the murine part of the chimeric PrP.

Alternative ideas into the identification of co-factors have included the demonstration that lipids interact with PrP^{C} and PrP^{Sc} and promote conformational changes in PrP during conversion (Sanghera and Pinheiro, 2002, Kazlauskaite *et al.*, 2003). PrP^{C} is localised at the plasma membrane and evidence suggests that this is a

possible site of PrP conversion, thus supporting the potential involvement of lipids in this reaction (Shyng *et al.*, 1994, Fournier *et al.*, 1995).

The search for prion co-factors takes into account the location of PrP^{C} in the cell and the nature of the interaction with PrP^{Sc}. PrP^{C} is a GPI anchored protein that is translated on ribosomes attached to the surface of the rough endoplasmic reticulum (rER) before entering the secretory pathway to the plasma membrane (Campana *et al.*, 2005). Protein degradation will generally occur by entry into the endosomal pathway and degradation in the lumen of lysosomes by acid hydrolases. Therefore, there are many locations within the cell that PrP^{C} will reside, with many interaction partners along the way as described earlier in this chapter and supported by the literature (Lee *et al.*, 2003, Rutishauser *et al.*, 2009). In addition, the site of conversion, or indeed the accumulation of PrP^{Sc}, has been observed in multiple locations, from the plasma membrane to the endosomal pathway (Caughey *et al.*, 1991, Borchelt *et al.*, 1992, Kaneko *et al.*, 1996, Vey *et al.*, 1996, Sanghera and Pinheiro, 2002). If PrP^{Sc} has been detected in these cellular compartments, it was therefore considered to contain the necessary prion co-factors for the successful conversion of PrP^{C}.

1.11 Cell Models of TSE Infection

To research the molecular and biochemical characteristics of PrP *in vivo* is difficult, expensive and time consuming. Transmission experiments into mice rather than sheep or cattle gives increased manageability and reduced costs but incubation times are still relatively long and the use of animals in experiments can be ethically challenging. Cell cultures therefore represent a practical and relevant model to study some major questions in TSE research i.e. PrP^{C} function and PrP^{Sc} infectivity.

There are two approaches to obtain cell culture models that are susceptible to prion replication. Firstly, cell lines can be cultured *ex vivo* and exposed to infectious material, such as brain homogenate from infected animals and cells would

incorporate some of the PrP^{Sc} units and become infected. Over many washes and passages, to dilute the original inoculum, persistent infection would be detectable thus demonstrating that infected cultures are generating newly synthesised PrP^{Sc} molecules. The second approach involves the isolation of an infected cell line directly from infected animals. This was the method used to create the scrapie mouse brain (SMB) cell line, which was derived from cultures of Chandler infected mouse brain (Clarke and Haig, 1970, Birkett *et al.*, 2001). A list of currently available cell lines used in TSE research is shown in table 1.3.

Most cell culture models are of neuronal origin as this is the cell line most affected during disease *in vivo* (DeArmond *et al.*, 1987, Prusiner *et al.*, 1987). The first cell line shown to support infection *in vitro* was the neuroblastoma cell line, N2a (Race *et al.*, 1987). In this study, the cell line was persistently infected with RML and once infected, the cell line remained viable. Other neuronal cell lines investigated include the hypothalamic cell line GT1, which was differentiated from immortalised gonadotropin-releasing hormone neurons (Schatzl *et al.*, 1997). Quite surprisingly, efficient cell culture models have also been found in non-neuronal cell lines such as fibroblasts and myoblast cells.

TSE susceptible cell models offer a convenient and relevant approach to study PrP^{C} and PrP^{Sc} within the cell. The function of PrP^{C} is still unknown, however cell culture models have contributed to our understanding of PrP^{C} and its function as previously described in this chapter. Furthermore, cell models of prion infection allow for the investigation into the subcellular localisation of PrP^{Sc} for the site of PrP conversion (Taraboulos *et al.*, 1990, McKinley *et al.*, 1991, Lehmann *et al.*, 1996, Béranger *et al.*, 2001, Pimpinelli *et al.*, 2005).

Cell cultures susceptible to TSE infection also form good models for therapeutic research into inhibitors of PrP^{Sc} formation. Cell lines can be cultured in 96-wellplate format which allows for the design of a high-throughput assay to determine compounds with anti-prion properties (Brown, 2002). Cell cultures can also be used to search for molecular markers that could be used as a diagnostic test for

Cell Line	Species of Origin	Cell Type	Prion Susceptibility	References
SMB	Mouse	Microglial	22F, 79A, 22C, 87A, 301V	Birkett *et al.*, 2001
N2a	Mouse	Neuroblastoma	RML, Chandler	Race *et al.*, 1987
N2a-58	Mouse	Neuroblastoma	22L, 139A, Chandler	Nishida *et al.*, 2000
N2a-PK1	Mouse	Neuroblastoma	RML, 22L	Mahal *et al.*, 2007
N2a-R33	Mouse	Neuroblastoma	22L	Mahal *et al.*, 2007
GT1	Mouse	Hypothalamic neural cells	22L, 139A, Chandler	Nishida *et al.*, 2000
SN56	Mouse	Septal neural cells	ME7, 22L, Chandler	Magalhães *et al.*, 2005
CAD-5	Mouse	Catecholaminergic cells	RML, 22L, 79A, ME7, 301C	Mahal *et al.*, 2007
HpL3-4	Mouse	Hippocampus cells	22L	Maas *et al.*, 2007
MSC-80	Mouse	Schwann cell	Chandler	Follet *et al.*, 2002
L929	Mouse	Fibroblast	22L, ME7, Chandler	Clarke & Millson, 1976
NIH/3T3	Mouse	Fibroblast	22L	Vorberg *et al.*, 2004
LD9	Mouse	Fibroblast	ME7, 22L, RML	Mahal *et al.*, 2007
C2C12	Mouse	Myoblasts	22L	Dlakic *et al.*, 2007
moRK13	Rabbit	Kidney epithelial	Fukuoka-1, 22L, Chandler	Courageot *et al.*, 2008
ovRK13	Rabbit	Kidney epithelial	Natural sheep scrapie	Vilette *et al.*, 2001
PC12	Rat	Pheochromacytoma	139A	Rubenstein *et al.*, 1984
MDB	Deer	Fibroblast-like	CWD	Raymond *et al.*, 2006

Table 1.3: Prion susceptible cell lines.

distinguishing prion disease. This is a very important aspect of TSE research because the disease has long incubation times with little or no clinical signs. The sooner the disease is detected, the less neurodegeneration has occurred and the better the chance of survival, post therapeutic intervention (Mallucci *et al.*, 2007). Another useful application for cell culture models is to identify the molecular determinants that make up and segregate TSE strains from each other. For instance, the standard scrapie cell assay (SSCA) is a panel of four cell lines that were selectively susceptible to four different strains of mouse scrapie (Mahal *et al.*, 2007). This assay could provide the means to use differences in cell line susceptibilities to identify intrinsic co-factors that are involved in strain specificity.

1.12 *In Vitro* Misfolding of PrP

TSE disease is characterised by long incubation periods, making quick and accurate biochemical analyses of the infectious agent *in vivo*, technically difficult. *In vitro* assays that utilise recombinant PrP have played a major role in determining the misfolding characteristics of PrP and the conformational change it undergoes. Recombinant PrP purified from bacteria folds into an α-monomeric isoform similar to that of PrP^{C}. Recombinant PrP is unglycosylated but it is hypothesised to have very similar misfolding properties to that of PrP^{Sc}, particularly since unglycosylated PrP has been identified in TSE infected individuals (Kascsak *et al.*, 1985, Collinge *et al.*, 1996, Somerville *et al.*, 1997). Recombinant PrP has successfully been incorporated into several seeded *in vitro* assays and has been converted to an infectious PK-resistant isoform, similar to that of PrP^{Sc} (Swietnicki *et al.*, 2000, Castilla *et al.*, 2005). Seeded *in vitro* assays can be used to provide detailed information on strain characteristics, infectivity and the interaction between the infectious agent and PrP^{C}.

1.12.1 Unseeded *In vitro* Misfolding Assays

In addition to *in vitro* seeded assays, unseeded misfolding assays have been developed to understand how refolding of PrP occurs and the intermediate conformations that are possible and in particular, their potential role in neurotoxicity. Multiple pathways of misfolding and the formation of distinct β-sheet rich isoforms have been studied *in vitro*. Early work on the conformational transitions of PrP^{C} to PrP^{Sc} revealed the presence of soluble oligomers of 4 to 6 PrP^{27-30} molecules as viewed by electron microscopy (EM) (Riesner *et al.*, 1996). Although no infectivity was associated with these oligomers, the analysis into PrP misfolding and soluble prions was shown. It was then reported that a β-sheet rich oligomer may represent an intermediate species in the assembly of PrP^{C} to PrP^{Sc} (Swietnicki *et al.*, 2000, Baskakov *et al.*, 2001). However, further analysis by Baskakov and colleagues revealed that the β-oligomer was energetically stable and was unlikely to assemble further into amyloid without prior dissociation back to the monomeric form (2002). Studies in TSEs and other amyloidoses such as Alzheimer's disease, have suggested that insoluble proteinaceous aggregations are instead a neuroprotective process that sequesters smaller, neurotoxic, oligomeric forms of the disease causing agent (Bucciantini *et al.*, 2002, Caughey *et al.*, 2003).

In vitro protein misfolding assays reveal that unglycosylated recombinant PrP can be influenced by partially destabilising conditions, the addition of denaturants or by application of an acidic pH, to misfold PrP into defined structures that have similar biochemical characteristics to PrP^{Sc} (Rezaei *et al.*, 2002, Tahiri-Alaoui *et al.*, 2004, Martins *et al.*, 2006). In chapter 6 the optimisation of an *in vitro* refolding assay is explored to provide an assay that is predictive of PrP misfolding *in vivo* as well as providing an assay to analyse the interaction of co-factors with PrP.

1.12.2 Seeded *In vitro* Misfolding of PrP

The CFCA was first published in 1994 and demonstrated the *in vitro* formation of PrP^{Sc} using purified constituents (Kocisko *et al.*, 1994). Purified ^{35}S-labelled recombinant hamster PrP^{C} from cell culture was incubated with purified PrP^{Sc} from 263K infected hamster brain in the presence of 3 M guanidine hydrochloride for 48 hours at 37 °C. Treatment with proteinase K (PK) produced protease-resistant C-terminal fragment of ^{35}S-labelled PrP^{C} that had been converted by 263K PrP^{Sc}. The PK-resistant product was termed PrP^{res} where 'res' is short for resistance to proteolytic digestion. This assay has since shown to replicate the species barrier as mouse PrP^{C} is not converted by the hamster PrP^{Sc} strain 263K, and *vice versa* (Kocisko *et al.*, 1995). In addition, PrP^{Sc} strain properties have also been replicated using the CFCA (Bessen *et al.*, 1995). Differences in the extent of PK-resistance have been described in the two strains of hamster TME, hyper TME (HY) and drowsy TME (DY). Incubation of the two hamster TME strains with recombinant hamster PrP^{C} resulted in the generation of PrP^{res} that reproduced the extent of PK-resistance in HY and DY hamster TME. Finally, the CFCA has been shown to reflect polymorphic barriers in PrP (Bossers *et al.*, 1997, Bossers *et al.*, 2000). Experiments using recombinant ovine PrP (rOvPrP) and sheep scrapie in the CFCA showed that variations in recombinant ovine PrP sequence altered susceptibility to conversion in the CFCA. Ovine PrP variants linked to increased resistance to scrapie were poorly converted, whereas ovine PrP variants associated with increased susceptibility to scrapie were ably converted in the CFCA.

The CFCA has since been modified to be more physiological relevant and incorporate a biochemically purified recombinant PrP substrate. Originally, the recombinant PrP substrate was purified from cell culture, however this was considered to contain cellular artefacts that may interact or even disrupt conversion. Subsequent publications have shown a baculovirus system where infected insect cells were used to produce rHaPrP that was successfully converted by hamster derived TME in the CFCA (Iniguez *et al.*, 2000). The assay buffer was originally designed with 3 M guanidine hydrochloride, a chaotrope that caused a denaturising effect on

the PrP^{Sc} seed and resulted in increased conversion efficiency. In fact, a recent publication reported that ovine scrapie would only convert rOvPrP to a PK-resistant isoform in the presence of 3 M guanidine hydrochloride (Piening *et al.*, 2006). However, this denaturant has since been omitted from the assay so that it was more representative of cellular conditions (Kirby *et al.*, 2003, Kirby *et al.*, 2006).

1.13 Synthetic Prions

The creation of synthetic prions *in vitro* from defined reaction constituents is the most compelling way to prove the prion hypothesis. Replication of PrP conversion *in vitro* has previously used purified PrP^{C} and PrP^{Sc} to propagate PrP^{res} with strain associated conformations (Kocisko *et al.*, 1994, Kocisko *et al.*, 1995 Bessen *et al.*, 1995). The association of newly synthesised PrP^{res} with PrP^{Sc} makes analysis into the infectivity of newly synthesised PrP^{res} impossible. Alternative unseeded fibrilisation assays impose destabilising conditions on PrP^{C}, molecules causing refolding to a more stable β-sheet rich isoform such as an oligomer or a fibril. The experiment that got closest to proving the prion hypothesis was the fibrilisation of truncated MoPrP (89-230) (Legname *et al.*, 2004). This aggregated peptide caused a neurological disease in transgenic mice, which over-express truncated MoPrP(89-230). However, there were two strong criticisms of this result, firstly *in vitro* generated fibrils were significantly less infectious than PrP^{Sc} and secondly ~30 % of the transgenic mice used in this study have been reported to develop a spontaneous neurological disease.

Recently, a seeded *in vitro* assay has provided an alternative approach to the generation of infectivity from minimal components. The protein misfolding cyclic amplification (PMCA) involves the incubation of small amounts of PrP^{Sc} (~ 1 attogram) with uninfected brain homogenate (Saborio *et al.*, 2001). PrP^{C} in the brain homogenate is converted to PrP^{res} and through cycles of incubation and sonication, amplification of PrP^{res} occurs. After many cycles, 10 % of the reaction is removed and incubated with fresh uninfected brain homogenate and cyclic incubation and sonication is resumed. When the PMCA method is repeated several times, the original PrP^{Sc} seed is diluted out leaving behind only newly generated PrP^{res}.

Infectivity studies in mice of the material generated by PMCA have shown robust infectivity (Castilla *et al.*, 2005, Castilla *et al.*, 2008). In these studies, the newly generated PrP^{res} was comparable to PrP^{Sc}, demonstrating similar disease phenotypes and biochemical characteristics *in vivo* to that of the parental strains used.

In addition to these studies, Supattapone and co-workers used the PMCA method with partially purified components to propagate infectious PrP^{res} (Deleault *et al.*, 2005, Deleault *et al.*, 2007). In these studies, PrP^{C} was purified from uninfected brain material and seeded with PrP^{Sc} together with a synthetic polyanion which helped to stimulate conversion to PrP^{res}. Polyanion molecules that stimulated conversion included poly(A) and poly(dT) nucleic acids and non-nucleic acid molecules such as heparan sulphate proteoglycan. This addition of a polyanion molecule to the PMCA suggests that a non-PrP molecular scaffold is associated with amyloid fibrils helping to support the fibril structure. However, the presence of a polyanion to stimulate PMCA conversion with purified components was not strain specific, thus suggesting a ubiquitous role in prion conversion rather than one that acted as a specific prion co-factor (Deleault *et al.*, 2007). Unfortunately, PMCA generated PrP^{res} seeded from two different strains showed no statistical significance in incubation time or disease phenotype characteristics when inoculated into wild type hamsters. The convergence of strain properties was not explained in this publication; however it would appear that PMCA generated nonspecific aggregates of PrP due to the lack of strain specific co-factors that were previously included by the use of un-purified brain homogenate material.

Deleault and co-workers observed that incubation of purified hamster PrP^{C} with poly(A)RNA molecules caused spontaneous formation of PrP^{res} in an infrequent and stochastic manner (2007). The *de novo* generation of PrP^{res} from the unseeded PMCA reaction was shown to be infectious to wild type hamsters. Incubation times before clinical onset were variable and the guanidine denaturation profile of *de novo* generated PrP^{res} from that of an unseeded PMCA reaction was identical to the control PrP^{Sc} seeded PMCA reaction. These observations question the credibility and validity of PMCA experiments to propagate PrP^{res} that is apparently indicative of

PrP^{Sc} and maintains strain properties such as PrP conformation and its crucial and distinct biochemical profiles.

Recent development of the PMCA has seen the invention of the quaking-induced conversion assay (QUIC), an assay that incorporates periodic shaking, rather than sonication, to convert recombinant PrP to a PK-resistant isoform (Atarashi *et al.*, 2008). Atarashi and co-workers reported no false positive results in negative control experiments which is something that occurs spuriously when using the PMCA and therefore the QUIC assay may represent a more robust assay for future diagnostic tests.

1.14 Scientific Objective and Experimental Approach

In prion diseases, the strain phenomenon is one of the most puzzling and intriguing characteristics associated with the infectious agent. Previous studies have concluded that it is the conformation of PrP^{Sc} that plays a key role in establishing the properties that determine strain variation (Safar *et al.*, 1998, Tanaka *et al.*, 2004, Tanaka *et al.*, 2006). Different strains of TSEs appear to have different conformations of PrP and, as a result, may have different fibril morphologies (Jones and Surewicz, 2005). It has been hypothesised that different interaction partners or prion co-factors are necessary for the propagation of PrP^{Sc}. The identity of these co-factors is likely to be strain specific, either because of the variation in the structural conformations and therefore interaction sites of PrP^{Sc}, or perhaps the involvement of different co-factors with PrP^{Sc}, influences the structural conformation of PrP^{Sc}.

In this project, my aim was to identify the subcellular localisation of strain specific co-factors that are necessary for the efficient conversion of PrP^{C} to PrP^{Sc}. To approach this, TSE susceptible cell lines were acquired to analyse for prion co-factors. As previously indicated in section 1.11, TSE susceptible cell lines can be differentiated based on their susceptibility or resistance to certain mouse scrapie strains. It was hypothesised that differential expression of prion co-factors dictate

whether a cell line is susceptible to infection from a TSE strain. The location of co-factors within the cell was unknown and therefore subcellular fractionation of the cell into distinct compartments provided a series of fractions enriched for different organelles, which enabled the testing for the presence of prion co-factors. This was carried out on two different cell lines, LD9 fibroblasts and SMB-PS microglial cells which are susceptible to the mouse-adapted scrapie strains, ME7 and 79A respectively.

Subcellular fractions from LD9 and SMB-PS cell lines were tested in the cell free conversion assay (CFCA) and the effect on conversion assessed. This involved the incubation of recombinant MoPrP with either ME7 or 79A and supplemented with LD9 or SMB-PS subcellular fractions. During these experiments it was identified that LD9 plasma membrane-enriched fractions significantly enhanced the conversion efficiency of ME7. However, this effect was not cell line specific as SMB-PS low density subcellular fractions also significantly enhanced ME7 conversion. It was hypothesised that the lipid bilayer of the plasma membrane provided a scaffold support that increased the interaction between PrP^{C} and PrP^{Sc}. Interestingly, SMB-PS Golgi body enriched fractions enhanced the conversion efficiency of 79A in the CFCA, thus suggesting a different site of conversion and therefore a different set of co-factors involved in the conversion of PrP^{C} by the 79A strain of mouse scrapie.

In addition to the CFCA, I optimised an alternative *in vitro* PrP misfolding assay for the analysis of interactions between PrP and fractions that enhance conversion in the CFCA. This oligomerisation assay involved the refolding of recombinant PrP to β-sheet rich oligomers when incubated at 45 °C in an acidic buffer. Comparisons of the rate of oligomerisation of wild type rMoPrP were made in the absence or presence of fractions that enhanced the conversion of SAF in the CFCA. Surprisingly, low density subcellular fractions from the LD9 cell line inhibited the oligomerisation of rMoPrP to β-sheet rich oligomer isoforms.

I also used mass spectrometry to identify prion co-factors of SAF preparations. Amyloid fibrils were crudely purified from mouse scrapie infected mouse brains and

are hypothesised to contain prion co-factors that have co-aggregated with PrP^{Sc} during polymerisation of the amyloid fibril. Tryptic digestion of SAF preparations in the presence of a low molar urea buffer provided tryptic peptides for the analysis and identification by mass spectrometry. Different strains of mouse scrapie associated fibrils (ME7, 79A and 22F) were compared to attempt to identify strain specific co-factors. Different proteins were identified from each of the three strains, indicating the possibility of strain specific markers. Pre-treatment of the isolated SAF narrowed down the list to single protein identifications for each mouse scrapie strains. Analysis of the literature provided insights into the function of these proteins.

2. Materials and Methods

2.1 Methods

All chemicals were sourced from Sigma Aldrich except where otherwise stated.

2.1.1 DNA methods

2.1.1.1 Transformation of *E. coli* with plasmid DNA

The following ligation was carried out by a previous co-worker, Dr Louise Kirby. The plasmids pTrcHis (Invitrogen) and pTrcHisB (Invitrogen) were digested with the restriction enzymes *NcoI* and *EcoRI* to remove the six histidine tag. Recombinant vectors were ligated with polymerase chain reaction (PCR) fragments that code for full length recombinant mouse PrP and full length recombinant ovine PrP respectively.

Both modified vectors were separately transformed into the *Escherichia coli* (*E.coli*) strain 1B392 (Wright *et al.*, 1986). On ice, 40 µl of competent *E.coli* cells were combined with 1 µl of plasmid DNA and incubated for 30 minutes. Competent cells were heat shocked at 42 °C for 45 seconds, followed by 2 minutes incubation on ice. Using a sterile spreader, competent cells were spread on a Luria Bertani (LB) agar plate (10 g tryptone, 5 g yeast extract, 0.5 g sodium chloride, 1.5 % (w/v) agar and made up to 1 litre with dH_2O) with ampicillin (from IAH media services, 100 µg/ml) and incubated overnight at 37 °C.

2.1.1.2 Glycerol stocks of transformed *E.coli*

One colony of 1B392 *E.coli* bacteria was isolated from an LB agar plate of transformed *E. coli* and used to inoculate 10 ml of LB media (10 g tryptone, 5 g yeast extract, 0.5 g sodium chloride and made up to 1 litre with dH_2O). This was incubated overnight at 37 °C, shaking at 220 rpm (Innova, New Brunswick Scientific). From this culture, 100 µl was pipetted into 10 ml of LB, with ampicillin (100 µg/ml) and incubated for 4 hours at 37 °C, shaking at 220 rpm. 500 µl of this culture was mixed with 500 µl of a glycerol solution (30 % (v/v) glycerol in LB media) in a 1.5 ml

screw top eppendorf (Sarstedt). Glycerol stocks were snap frozen in liquid nitrogen prior to storage at -80 °C.

2.1.2 Protein methods

2.1.2.1 SDS PAGE

Samples to be analysed by SDS PAGE were mixed 3:1 with LDS sample buffer (4x) (Invitrogen) and heated at 100 °C for 10 minutes. For silver staining of SDS PAGE gels, samples were suspended in modified Laemmli sample buffer (MLSB, 4 M urea, 5 % (v/v) glycerol, 5 % (w/v) SDS, 5 % (v/v) β-mercaptoethanol, 65 mM Tris (pH 6.8)) rather than LDS sample buffer. Samples were centrifuged at 10,000 *g* for 15 seconds prior to loading samples into separate wells of a 12 % bis-tris pre-cast NuPAGE gel (Invitrogen). For every gel used, 10 µl of SeeBlue Plus2 pre-stained marker (Invitrogen) was used as the molecular weight standard. Pre-cast gels were subjected to 180 volts for approximately one hour and either stained with Instant Blue coomassie (Expedeon Solutions), silver nitrate or transferred onto PVDF membrane (Millipore) by semi-dry blotting followed by Western blotting.

2.1.2.2 Coomassie staining

Instant Blue Coomassie stain was added to SDS PAGE gels and protein bands resolved within 5 minutes.

2.1.2.3 Silver staining

All buffers were prepared with freshly de-ionized H_2O (dH_2O). Silver nitrate staining of SDS PAGE gels was carried out by following the Plus One silver staining protocol as suggested by GE Healthcare (www.gelifesciences.com). Briefly, this protocol involved the submersion of the SDS PAGE gel in 20 ml fixing buffer (30 % (v/v) ethanol, 15 % (v/v) glacial acetic acid) in a clean petri dish for 1 hour with gentle shaking on a platform shaker (Innova 2100, New Brunswick Scientific) at 50 rpm. The gel was then transferred to sensitizing buffer (30 % (v/v) ethanol, 0.2 % (w/v) sodium thiosulphate, 6.8 % (w/v) sodium acetate, 0.5 % (v/v) glutardialdehyde) for 1

hour with shaking. The gel was then washed with 20 ml dH_2O for 15 minutes, four times. Next, the gel was submerged in silver solution (0.25 % (w/v) silver nitrate and 0.1 % formaldehyde) for 1 hour with gentle shaking. Silver solution was removed and the gel was washed twice with 20 ml dH_2O for precisely 1 minute for each wash. Finally, the gel was placed in development buffer (2.5 % (w/v) sodium carbonate, 0.025 % formaldehyde) and development was halted by transferring the gel to a clean petri-dish with 20 ml of stop solution (40 mM EDTA)

2.1.2.4 Western blotting

Immobilon-P PVDF transfer membrane with a pore size of 0.45 μm and grade 1 filter paper (Whatman) were cut to 8 cm x 9 cm. Eight pieces of filter paper were stacked together and submerged in transfer buffer (0.19 M glycine, 0.1 M tris-HCl, 5 % (v/v) methanol). Wet filter paper was mounted on the semi-dry blotter (Invitrogen), and air bubbles rolled out. The PVDF membrane was soaked in methanol for 2 minutes followed by submersion in transfer buffer and layering on top of the stack of eight pre-soaked filter papers. The SDS PAGE gel was briefly washed in transfer buffer and placed on top of the pre-soaked PVDF membrane and filter paper stack. Finally, the stack was completed by eight pieces of filter paper also pre-soaked in transfer buffer. Air bubbles were rolled out and semi-dry blotter unit was closed and connected to a Pharmacia Biotech EPS-1000 electrophoresis power supply at 100 mA per blot for 1 hour 30 minutes. The membrane was removed and placed in block solution (5 % marvel (w/v) dissolved in TBS-T (0.13 M sodium chloride, 10 mM tris-HCl, 0.05 % (v/v) Tween-20)) for one hour at room temperature (RT). The blocking buffer was replaced with primary antibody solution (primary antibody in 1 % marvel (w/v) in TBS-T) and the membrane was incubated at RT for one hour. The membrane was washed initially in TBS-T for 30 seconds followed by a further 3 x 15 minute washes in TBS-T. The final wash solution was removed and the membrane incubated in the secondary antibody solution (secondary antibody in 1 % marvel (w/v) in TBS-T)) at RT for 1 hour. The membrane was washed, initially in TBS-T for 30 seconds, followed by a further 3 x 15 minutes in TBS-T. The final wash solution was removed and the membrane incubated for 1 minute in ECL Western blotting detection reagent (GE Healthcare). The membrane

was dried and exposed to hyperfilm-MP (GE Healthcare) for varying time intervals. Film was developed by a Compact Xograph X4 (Xograph Imaging Systems).

2.1.2.5 Densitometry analysis

To capture images for densitometric analysis, films were scanned using an Image Scanner III (GE Healthcare) with the operating program Labscan 6.0 (GE Healthcare) was used. The image scanner was calibrated every 30 days using a photographic step tablet (Kodak) between a density range 0.07 – 4.27 optical density (OD).

Scanned images were transported into ImageQuant TL (GE Healthcare) where a 1D gel analysis was carried out to determine densitometric values of protein bands relative to bands of known protein concentrations as indicated where appropriate.

2.1.2.6 Reduction and alkylation of PrP

All solutions in sections 2.1.2.6 and 2.1.2.7 were prepared with LC-MS grade water (Fischer Scientific).

To enhance tryptic digestion of protein samples, disulphide bonds were reduced and alkylated to prevent reforming of the disulphide bridge. To do this, 19 µl of 6 M guanidine hydrochloride, 100 mM ammonium bicarbonate (pH 8.5) were added for every 1 µl of protein sample. Dithiothrietol (DTT) solution (5 mg/ml) was added to give a 5 fold molar excess over the number of cysteines in the protein. There are 2 cysteines in PrP and with a PrP concentration of 1 mg/ml, 40 µM of DTT was added. Samples were incubated at RT overnight, whereupon 5 mg/ml iodoacetamide (IAA) was added to give a 4 fold molar excess over the concentration of DTT used. To this, 1 µl of 100 mM ammonia bicarbonate solution was added to keep the pH alkaline. Samples were incubated in the dark at room temperature for 1 hour.

2.1.2.7 Tryptic digestion of PrP

Tryptic digestion of proteins provided tryptic peptides for mass spectrometric analysis. To concentrate and purify protein from the previously added DTT and IAA, reduced and carboxylmethylated proteins were precipitated at -20 °C for 12 hours in 20 volumes of ethanol. Samples were centrifuged at 13,000 *g* for 15 minutes at 10°C to pellet precipitated species. The supernatant was removed and discarded and pellets were incubated for 2 hours at RT to ensure the pellet was completely dry. The pellet was re-suspended in 100 µl of re-suspension buffer (4 M urea, 100 mM ammonium bicarbonate). Calculating $1/20^{th}$ of the approximate amount of protein in the sample is the mass of trypsin (Promega) to be added. Samples were incubated at 37 °C for 8 hours. Tryptic digestion was stopped by snap freezing at -20 °C.

2.1.2.8 Mass spectrometry

All mass spectrometry was carried out in the proteomics facility of the Institute for Animal Health by proteomics staff. Samples were thawed and tryptic peptides were concentrated using a 180 µm x 20 mm, 5 µm Symmetry C18 trap (Waters) for 3 min at 10 µl/min, and resolved on a 1.7 µm, 100 µm x 100 mm, BEH 130 C18 column (Waters) at 400 nl/min that was attached to a nano Acquity UPLC (Waters). Peptides were eluted over a linear gradient of 0-50 % (v/v) acetonitrile, 0.1 % (v/v) formic acid for 30 minutes with a flow rate of 400 nl/min. To complete elution, the column was washed with 85 % (v/v) acetonitrile, 0.1 % (v/v) formic acid for 7 minutes. Ionised peptides were analysed by a quadrupole time of flight (Q-ToF) Premier mass spectrometer (Waters) and the acquired data analysed by ProteinLynx Global Server version 2.2.5 (Waters) to generate the list of peptides detected. This peptide list was submitted to MASCOT version 2.2 (Matrix Science, UK) and searched against the IPI murine protein database.

2.1.2.9 Circular dichroism

Far-UV circular dichroism (CD) spectra were recorded on a Jasco J-710 spectropolarimter using a scanning speed of 100 nm/min and a step resolution of 1 nm. For each sample, 20 spectra were accumulated at RT between wavelengths as

indicated on each CD spectra. Cell path lengths were dependent on protein concentrations and are indicated where appropriate.

2.1.2.10 UV spectroscopy

A Beckman DU-650 spectrophotometer was used to determine the concentration of recombinant protein by measuring the absorbance of the sample between 200 nm and 400 nm in a 10 mm path length quartz cuvette (Hellma). The amino acids tyrosine and tryptophan absorb UV light typically with a wavelength of 280 nm. The absorbance value obtained allows for the quantification of protein concentration. To accurately predict protein concentration, a background absorbance at 320 nm was subtracted from the absorbance measured at 280 nm. Serial dilutions were made of the sample to further ensure an accurate measurement of protein concentration was determined. Molecular weight and extinction coefficients used to calculate protein concentration are summarised in Table 2.1 (Gill and Von Hippel, 1989).

2.1.2.11 Induction of recombinant PrP expression

Glycerol stocks of *E.coli* bacteria used for the expression of recombinant PrP were streaked out onto LB (10 g tryptone, 5 g yeast extract, 0.5 g sodium chloride and made up to 1 litre with dH_2O) agar plates with ampicillin (100 µg/ml) and incubated at 37 °C overnight. Single colonies were picked and used to inoculate 10 ml LB aliquots with ampicillin (100 µg/ml) and these were incubated overnight at 37 °C in a shaking incubator at 220 rpm (Innova, New Brunswick Scientific). 4 ml of confluent overnight growth cultures were used to inoculate 400 ml of terrific broth (TB) growth media (12 g tryptone, 24 g yeast extract, 4 ml glycerol in 900 ml dH_2O. Media was autoclaved at 121 °C after which 0.017 M potassium phosphate and 72 mM di-potassium phosphate was added and media made up to 1000 ml) plus ampicillin (100 µg/ml) in a 2 litre flask. Cultures were grown at 37 °C in a shaking incubator at 220 rpm until an OD_{600} between 0.6 - 1 was reached. Recombinant PrP expression was induced by the addition of 1 µl /ml of 1M IPTG and cultures were incubated for a further 7 hours at 37 °C. Bacterial cells were harvested by centrifugation at 10,000 rpm for 10 minutes in a Sorvall RC5B centrifuge with a

Recombinant Protein	Molecular Weight	Extinction Coefficient
Full length Murine PrP	23113.6	62280
Full length Ovine PrP	22902.2	57780

Table 2.1: Molecular weight and extinction coefficients of various PrP types (Gill and von Hippel, 1989).

Sorvall SLA1500 rotor. The resultant supernatant was discarded and cell pellets were stored at -20 °C overnight.

2.1.2.12 Bacterial cell lysis

Bacterial cell pellets were thawed from -20 °C storage and re-suspended in 10 ml/g of bacterial lysis buffer (100 mM sodium chloride, 1 mM EDTA, 50 mM tris-HCl (pH 8)) and 2 µl/ml of phenylmethylsulfonyl fluoride (PMSF) for 2 hours. The cell suspension was treated with 20 µl/ml of lysozyme and incubated at 4 °C for 20 minutes. To solubilise membrane components, 1 mg/ml of sodium deoxycholate was added. Suspensions were vortexed followed by incubation at RT until viscous. Once viscous, 5 µl/ml of 1 mg/ml bovine deoxyribonuclease (DNase) and 500 µl of 2 M magnesium chloride were added and suspensions incubated at RT for 15 minutes. Suspensions were centrifuged in the RC5B centrifuge with the SLA1500 rotor at 10 °C for 15 minutes at 15,000 rpm. Supernatants were discarded and the inclusion body pellets stored at -20 °C.

2.1.2.13 Purification of recombinant PrP with Ni-IMAC

This protocol was used for the generation of rMo3F4PrP for its use in the CFCA. Inclusion body pellets were suspended in 10 ml/g immobilised metal anion chromatography (IMAC) buffer A (8 M urea, 0.1 M sodium phosphate, 10 mM tris-HCl (pH 8), 0.07 % (v/v) β-mercaptoethanol), vortexing thoroughly to ensure maximum solubilisation of recombinant protein. Suspensions were centrifuged at 15,000 rpm for 15 minutes in the RC5B centrifuge with the SLA1500 rotor. The supernatant was retained for rPrP purification using an ÄKTA FPLC (Pharmacia Biotech).

A nickel-sepharose superflow column (Amersham Biosciences) was packed with 5 ml superflow resin and attached to the FPLC and the column equilibrated with IMAC A. Solubilised material from the inclusion body pellet was loaded into a superloop collection tube for injection onto the IMAC column. Full length rMoPrP is purified without a six histidine tag and instead relies upon the natural nickel chelating affinity of the octapeptide repeat sequence. Once protein was loaded, the column was washed

with 50 ml of IMAC A buffer and eluted with IMAC buffer B (8 M urea, 0.1 M sodium phosphate, 10 mM tris-HCl (pH 4.5)). Samples were collected in 5 ml fractions. Samples from all stages of growth and purification were analysed by SDS PAGE and stained with Instant Blue coomassie to determine which fraction contained recombinant PrP.

IMAC eluted fractions that contained the highest concentrations of recombinant PrP, as revealed by SDS PAGE, were pooled together and the total volume doubled with ion exchange buffer A (8 M urea, 50 mM HEPES-NaOH (pH 8)). Second stage purification was cation exchange chromatography and was also performed on an ÄKTA FPLC system. A 5 ml SP Sepharose fast flow (Amersham Biosciences) column was prepared and attached to the FPLC and the column equilibrated with ion exchange buffer A. Pooled fractions of Ni-IMAC elute were loaded into a superloop collection tube for injection onto the ion exchange column at a flow rate of 2 ml/min. Once loaded, the column was washed with 50 ml of ion exchange buffer A. Protein bound to the column by ion exchange affinity were eluted over a 0-100 % gradient with ion exchange buffer B (8 M urea, 1.5 M sodium chloride, 50 mM HEPES-NaOH (pH 8)) over 30 minutes. Samples were collected in 5 ml fractions. From each stage of the purification, 100 µl samples were retained for separation by SDS PAGE and resolution of protein species by staining with Instant Blue coomassie stain. Elution fractions that contain purified recombinant PrP were pooled and their protein concentration determined by use of a UV spectrophotometer at a wavelength of 280 nm.

2.1.2.14 Refolding and concentration of purified recombinant PrP

Pooled fractions from ion exchange were diluted to 0.1 mg/ml and oxidised in the presence of a 5-fold molar excess of Cu^{2+} ions for 12 hours at 4 °C. Recombinant PrP was refolded into its native conformation by dialysis against 5 litres of 50 mM sodium acetate, 10 mM EDTA (pH 5.5). Dialysis buffer was replaced every 4 hours over a 20 hour period. The first 5 litres of dialysis buffer included 10 mM EDTA to remove any free Cu^{2+} ions from solution.

After 20 hours of dialysis, samples were recovered and centrifuged at 4,000 *g* for 15 minutes at 10 °C to pellet any precipitated protein. The supernatant was removed and concentrated to approximately 2 mg/ml by ultra filtration with a 10 kDa filter (Amicon). Samples were snap frozen in liquid nitrogen and stored at -80 °C until used.

2.1.2.15 Purification of scrapie associated fibrils

Based on a method described by Hope *et al.* 1986, PrP^{Sc} was purified from the brains of terminally TSE infected animals. A 5 % (w/v) brain homogenate was prepared from 4 mouse brains infected with mouse scrapie by homogenisation with a dounce homogeniser, in a buffer containing 10 % (w/v) *N*-lauroylsarcosine, 0.1 M sodium phosphate (pH 7.4). The homogenate was centrifuged at 22,000 *g* for 30 min at 10 °C. The pellet was discarded and the supernatant centrifuged at 215,000 *g* for 150 minutes at 10 °C. The pellet was re-suspended in 3 ml H_2O by repetitive vortexing followed by incubation at RT for 1 hour. To this, 9 ml of a solution containing, 0.9 M potassium iodide, 15 mM sodium phosphate, 9 mM sodium thiosulphate, 1.5 % (w/v) *N*-lauroylsarcosine (pH 8.5) was added. Finally, the suspension was centrifuged at 285,000 *g* for 90 minutes at 10 °C through a cushion of 20 % (w/v) sucrose in 0.6 M potassium iodide, 10 mM sodium phosphate, 6 mM sodium thiosulphate, 1 % (w/v) *N*-lauroylsarcosine sodium salt (pH 8.5). The resultant pellet was washed in dH_2O and centrifuged at 13,000 *g* for 30 minutes at RT. The final SAF pellet was re-suspended in dH_2O by sonication to approximately 1 µg/µl, as estimated by 10 µg/mouse brain. Western blotting using the AG4 antibody against a serial dilution of rMoPrPWT of known concentrations gave a more accurate concentration and appropriate modifications were made to give 1 µg/µl.

2.1.2.16 Proteinase K Digest of SAF

Samples of SAF were sonicated in 3 x 15 second bursts to disrupt PrP^{Sc} aggregates and yield a homogeneous suspension. The equivalent of 1 µg of PrP^{Sc} was made up to 18 µl with water and 2 µl of 600 µg/ml proteinase K (PK) to give a final PK concentration of 60 µg/ml. The SAF sample was incubated for 1 hour at 37 °C before

adding 25 mM pefabloc *sc* to stop PK digestion. Samples were precipitated for 1 hour at -20 °C by adding 20 µg of BSA and 4 volumes of ice cold methanol. Samples were centrifuged at 13,000 *g* for 30 minutes to pellet digest products. The resultant pellets were analysed by SDS PAGE and Western blotting.

2.1.2.17 CFCA

Scrapie isolated fibrils were disrupted by sonication to yield a homogenous solution. In an eppendorf, 1 µl of fibrils was mixed with 16.5 µl of conversion buffer (100 mM sodium chloride, 50 mM sodium citrate, 50 mM potassium chloride, 10 mM magnesium chloride, 0.1 % (v/v) Nonident P-40 (pH6.5)) and 200 ng of recombinant mouse 3F4 PrP and then made up to a final volume of 20 µl with water. In some experiments, water was replaced with re-suspended pellets from subcellular fractionation. Reaction mixtures were incubated at 37 °C for 24 hours. Samples were briefly centrifuged in the benchtop centrifuge to pull down condensate from the sides of tubes. 20 µl of water was added, vortexing to mix. From this, 2 µl ($1/20^{th}$, which is abbreviated to -PK) of sample was removed for future analysis and the remaining 38 µl ($19/20^{th}$, which is abbreviated to +PK) was treated with 4 µl of diluted PK and incubated at 37 °C for 1 hour. To stop the PK treatment, 4 µl of pefabloc was added and sample was incubated at room temperature for 5 minutes. To these PK treated samples, 20 µl of 600 µg/µl BSA and four volumes of ice-cold methanol were added prior to incubation at -20 °C for 1 hour. The 2 µl sample removed prior to treatment with PK, represented the non-PK treated sample. To this, 20 µl of 600 µg/µl BSA and four volumes of ice-cold methanol was added, followed by incubation at -20 °C for 1 hour. All samples were centrifuged at 13,000 rpm for 30 minutes to pellet precipitate. The supernatant was removed and discarded and the pellets resuspended in SDS PAGE loading buffer. This was then followed up by the protocols described in sections 2.1.2.1 (SDS PAGE), 2.1.2.4 (Western blotting) and 2.1.2.5 (densitometric analysis).

2.1.2.18 Purification of recombinant PrP for the oligomerisation assay

Inclusion body pellets from 1B392 *E.coli* expressing rMoPrP and rOvPrP (see sections 2.1.2.11 and 2.1.2.12) were used as the starting material to generate purified

recombinant PrP in the required oligomerisation buffer. Protocols for the purification of recombinant PrP from inclusion bodies for each of the different oligomerisation assays are described in chapter 6.

2.1.3 Cell Culture Methods

All cell manipulations took place in a class II microbiological safety cabinet (Envair UK Limited) and all cell culture flasks (TPP) were incubated in a Hera Cell 240 incubator (Heraeus) at 37 °C and 5 % CO_2.

Aliquots of the LD9 fibroblast cell line were acquired frozen on dry ice from Dr Sukhvir Mahal (Scripps, Florida) and are cultured in Eagles's minimal essential media (EMEM) media (Gibco) supplemented with 10 % (v/v) foetal calf serum (FCS). The SMB-PS cell line was acquired from Ruth Hennion (TSE Resource Centre, IAH) who supplied aliquots from a liquid nitrogen frozen cell bank and are cultured in media 199 (IAH in-house media services) supplemented with 10 % (v/v) newborn bovine serum (NBBS) and 5 % FCS.

2.1.3.1 Cell culture

Frozen cell lines were thawed in a 37 °C waterbath (Grant) for 2 minutes. LD9 cell line samples were gently mixed with 4 ml of EMEM media and SMB-PS cell line samples were mixed with 4 ml of media 199. Samples were transferred to a T25 flask and incubated overnight at 37 °C and 5 % CO_2. Media was replaced to remove DMSO that was present in the freezing media. Cell monolayers were returned to the incubator to grow until 90 % confluency, replacing media every 3 days.

2.1.3.2 Cell passaging

When cell monolayers reached 90 % confluency, media was removed and cell monolayers were washed twice with 10 ml of Hank's buffered salt solution (HBSS). HBSS was removed and the cells were treated with trypsin according to the method under liquid N_2 storage section. Cell suspensions were split 1:4 (SMB-PS) or 1:20

(LD9). Flasks were labelled and the passage number of the cell line incremented by one.

2.1.3.3 Liquid N_2 storage

Cell lines were stored in liquid nitrogen to preserve cell line viability. Cell monolayer was washed twice with HBSS prior to incubation with 5 ml trypsin (Gibco) at RT for 2 minutes with gentle agitation. Trypsin solution was removed and flask incubated for 5 minutes at 37 °C. Detached cells were re-suspended in 1 ml of freezing media (90 % (v/v) foetal calf serum (FCS), 10 % (v/v) dimethyl sulfoxide (DMSO)). The cell suspensions were transferred to 2 ml cryovials (Greiner), labelled and placed in a Mr Frosty container (Nalgene) filled with isopropanol and cooled to -80°C. After 24 hours, cryovials were transferred to liquid N_2 storage.

2.1.3.4 Subcellular fractionation

Samples were kept on ice for all steps of the subcellular fractionation. Subcellular fractions were prepared from 3 x T75 culture flasks of confluent cells. Each flask was washed twice with 10 ml PBS and twice with 10 ml homogenisation buffer (0.25 M sucrose, 1 mM EDTA, 20 mM HEPES/NaOH (pH 7.4)) containing complete EDTA-free protease inhibitors (Roche). Cell monolayers were collected by using a cell-scraper (Greiner) and scraping off into 9 ml of homogenisation buffer and placed in a tight-fitting glass dounce and homogenised with 10 strokes of the Teflon homogneiser. Homogenate was transferred to 1.5 ml centrifuge tubes and centrifuged at 1000 *g* for 10 minutes in a Sorvall biofuge fresco to pellet nuclei and cell debris. The postnuclear supernatant (PNS) was removed and a protein assay (2D Quant Kit, Amersham Biosciences) performed, with 1.5 mg of PNS layered on top of a continuous 10 - 20 % OptiPrep gradient diluted in 0.25M sucrose, 6 mM EDTA, 120 mM HEPES/NaOH. The gradient was generated by placing 2 ml of 20 % OptiPrep™ in a Beckman Ultraclear tube (14 x 89 mm) and layering this with subsequent 2 ml volumes of 17.5 %, 15 %, 12.5 % and 10 % OptiPrep™ followed by a 12 hour incubation at 4 °C to generate a continuous gradient. The gradient was centrifuged in a Sorvall TH-641 rotor at 228,000 *g* for 8 hours at 10 °C. After centrifugation, 500 µl fractions were removed starting from the top of the gradient and each fraction was

precipitated by incubation with 1000 µl ice cold methanol for 12 hours. To recover precipitate, fractions were centrifuged at 13,000 *g* for 30 minutes and supernatant removed. Pellets were either re-suspended in Laemmli's sample buffer for SDS PAGE and Western blotting or were re-suspended in dH_2O for addition to the CFCA.

2.1.4 Statistical analysis of CFCA Western blots

To analyse the effect of subcellular fractions on the effect of different strains of mouse scrapie in the CFCA the protocols outlined in sections 2.1.3.4 and 2.1.2.17 were followed. Densitometric analysis of the resultant photographic exposures provided data on the conversion efficiency of each strain of mouse scrapie. These experiments were repeated and data points were plotted ± SEM. Statistical analysis was applied to the data to determine the significance of each result against the conversion efficiency of a particular strain of mouse scrapie in the CFCA in the absence of any subcellular fraction supplement. A one-sample t-test was applied using the following equations.

$$t = \frac{X - \mu}{S_x}$$

X is the sample mean

μ is the population mean

S_x is the sample estimate of the standard error of the mean

The sample estimate of the standard error of the mean (S_x) is based on the sample standard deviation (S) and the square root of the sample size (n).

$$S_x = \frac{S}{\sqrt{n}}$$

To test the statistical hypothesis I used the t distribution or student's distribution which required the t statistic (t) and the degrees of freedom (sample size minus one) and was calculated using the Microsoft Excel package.

3. Preparation and validation of subcellular fractions from LD9 and SMB-PS cells

3.1 Introduction

In vitro studies on TSE susceptible cell lines provide a model system with which to study the function of PrP^C as well as the molecular and cellular basis of PrP conversion. Principally, they can be used to identify the localisation of PrP^C conversion, the identity of the infectious agent and how the subsequent cell to cell spread of prions occurs (Vey *et al.*, 1996, Naslavsky *et al.*, 1997 Kanu *et al.*, 2002, Ben-Zaken *et al.*, 2003). To propagate prions *ex vivo*, infected brain homogenates or purified scrapie associated fibrils (SAF) are added to the cell culture. After multiple washes and sufficient passages to dilute out exogenous infectivity, the presence of newly replicated PrP^{Sc} can be detected using PrP antibodies by Western blot analysis of cell lysates for proteinase-K resistant PrP.

The susceptibility of TSE susceptible cell lines is often strain specific, such that only a selection of TSE strains will infect any given cell line. Susceptibility is believed to come primarily from the presence or absence of strain specific co-factors within each cell line. If a certain cell line does not express a protein that is necessary for the efficient conversion of PrP^C to PrP^{Sc}, then the cell will survive infection. This hypothesis predicts that strain specific co-factors exist within certain cells and that this explains how some cells are susceptible and others are resistant to a given strain of TSE.

This chapter describes the use of TSE susceptible cell lines and their subsequent fractionation by differential centrifugation to give fractions associated with different subcellular organelles. Purified organelles were identified and validated by the detection of specific protein markers using Western blotting. Fractions were then used to supplement the CFCA and conversion efficiency assessed in a range of experiments, as described in chapter 4. This strategy assumes that the susceptible cell lines have strain specific co-factors required for the replication of set prion strains.

I considered many factors before selecting the TSE susceptible cell line for my experiments. Firstly, the cell line needed to be murine in origin as the SAF preparations I had used to seed the CFCA were taken from infected mouse brains and to alleviate any potential problems posed by a species barrier effect, the cell line and

CFCA seed were selected from a homologous species. Secondly, the selected cell line would need to be susceptible to the mouse scrapie strain used in the CFCA. Table 1.3 summarises the cell lines that have been described in the literature to be susceptible to one or more strains of mouse scrapie. The CFCA however was the limiting factor as there were only a few strains of mouse scrapie known to catalyse the conversion reaction. Typically, the mouse scrapie strain 87V was used to convert rMoPrP to a PK-resistant isoform, however there were no cell lines known to be susceptible to this particular strain of mouse scrapie. Previous work in the lab had shown that ME7, 22F, 79A and the mouse derived BSE strain 301V, can all convert rMoPrP in the CFCA with varying efficiencies. The mouse derived BSE strain 301V was excluded however, on the grounds that it required higher containment facilities. That left three strains; ME7, 22F and 79A, with which to test subcellular fractions in the CFCA.

The mouse scrapie strain ME7 was derived from mice intracerebrally inoculated with mouse brain homogenates that previously had been infected with spleen tissue from sheep with natural scrapie (Zlotnik & Rennie, 1963). ME7 has been used to infect different cell culture models. Neuronal cell models such as N2a neuroblastoma cells, however, required unglycosylated PrP to be expressed for a persistent infection (Korth *et al.*, 2000). Other neuronal cell lines include the septal neural cell line SN56, which had a low efficiency of infection by ME7 and only an acute infection was possible whereas the PC12 cell line required growth factor to sustain prion infection (Chiesa and Harris, 2000). The requirement for growth factor suggests that prion co-factors have low expression in PC12 cells and to rectify this prion co-factor deficiency, growth factor was required. To increase the chance of detection of strain specific co-factors I concluded that this cell line was likely unsuitable. The non-neuronal cell line L929 is of fibroblast origin and can sustain ME7 infection for a maximum of 10 passages (Personal communication with Dr I. Vorberg). It is unknown how the cells were able to overcome infection, however, it was hypothesised that an unknown biological clearance mechanism maybe in place and potentially in addition to deficiencies in co-factor expression. However, the L929 cell line was subsequently cloned and selected for susceptibility to the scrapie strain RML (Mahal *et al.*, 2007). This led to the demonstration of the L929 clone, LD9, being susceptible to a persistent infection with ME7 scrapie. This cell line was

therefore identified as a candidate cell line to fractionate and test for the presence of co-factors in the CFCA.

The mouse scrapie strains 79A and 22F have not been extensively used *in vitro* and the only known cell line that is susceptible to infection by these strains, is the SMB-PS cell line. The mouse scrapie strain 79A originates from an s7/s7 mouse line that was infected with drowsy goat strain of scrapie (Chandler, 1961). The 22F strain of mouse scrapie originates from SSBP/1, which when inoculated first into a p7/p7 mouse line results in a strain of scrapie called 22A. When the 22A strain of scrapie was inoculated into mice with an s7/s7 PrP background, a new strain with a novel disease phenotype was selected for and this was termed 22F.

I reasoned that the fibroblastic cell line LD9 and the microglial cell line SMB-PS were therefore suitable candidates to fractionate into subcellular compartments based on biological relevance, practicability and susceptibility to infection by more than one strain.

3.2 Tissue culture

The LD9 fibroblastic cell line was a gift from Dr Sukhvir Mahal, (Scripps, Florida) and the SMB-PS cell line was provided by Ruth Hennion (TSE Resource Centre, IAH). Following tissue culture protocols for cell growth, both cell lines were cultured to confluence as described in chapter 2 section 2.1.3.2. Cell lines were visualised using an inverted light microscope (Leica Microsystems) where morphological observations were made, as shown in figure 3.1. The LD9 cell line is of fibroblastic origin and therefore heterogeneous in size and shape (see figure 3.1 part A). Conversely, the SMB-PS cell line is a microglial cell line and figure 3.1 part B, shows classic glial morphology where long branching processes emanate from the cellular body.

3.3 Subcellular organelle detection

Subcellular fractionation of TSE susceptible cell lines provided the basis for the investigation into the presence of strain specific prion co-factors. It has been

A B

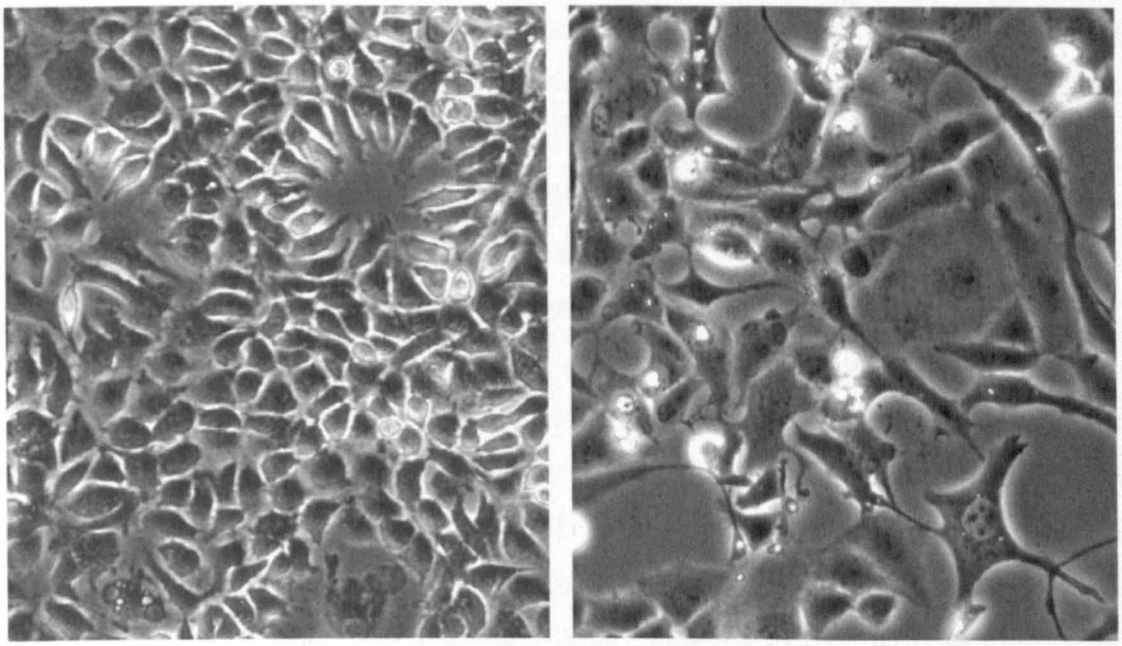

Figure 3.1: Visualisation of LD9 and SMB-PS cell lines.

(A.) LD9 fibroblast cell line cultured at 37 °C and 5 % CO_2 in EMEM media supplemented with 10 % (v/v) FCS. These fibroblasts are typically heterogeneous in size and shape. (B.) SMB-PS cell line cultured at 37 °C and 5 % CO_2 in media 199 supplemented with 10 % NBBS and 5 % FCS. Microglial morphology shows that these cells have long branching processes that emanate from the cellular body. Images captured with an inverted Leica DM IRB microscope (Leica Microsystems) using Leica FW4000 software (Diagnostic Instruments). Magnifications were at 100 x for both A and B.

hypothesised that different TSE strains replicate in different cellular compartments thus suggesting that co-factors can be found in different subcellular locations. The subcellular fractionation of a cell line by ultracentrifugation through a density gradient separates organelles based on their densities. Analysis by immunoblotting for antibodies specific for organelle markers validated the presence of organelles in each of the fractions prepared. I selected a range of subcellular markers based on extensive literature searches on proteins associated with organelles from either fibroblasts or glial cell origin. Organelles to be isolated were based on the likelihood of their association with PrP i.e. trafficking of PrP through the cell means that PrP will be associated with many different organelles which may play a role in the conversion of PrP and may potentially be the site of conversion. In addition to the organelles PrP experiences during normal trafficking (as discussed below), the mitochondria have been implicated in TSE disease through the observations of abnormalities in energy metabolism and the detection of PrP^{Sc} in the mitochondria (Hachiya *et al.*, 2004, Rossi *et al.*, 2004). Therefore, as part of my aims, mitochondria were also purified from LD9 and SMB-PS cells.

Ribosomes on the surface of the rough endoplasmic reticulum (rER) are the location where mRNA is translated into an amino acid sequence. The amino acid residues are connected by a peptide bond and the nascent protein interacts with various chaperones to fold the protein into its appropriate structure (Harris, 2003). A common rER marker is the chaperone BiP and has been demonstrated to be present in the rER of fibroblasts (Chessler and Byers 1993) and microglia (Kakimura *et al.*, 2001). When PrP^{C} is folded correctly in the ER, it is trafficked to the Golgi body for structural modifications and processing prior to being shuttled to the plasma membrane. Three markers for Golgi body were tried, including antibodies for GM130, 58K and ERGIC53, all of which were unsuccessful on LD9 and SMB-PS homogenates. However, a known marker for the Golgi body in microglial cells, is the protein TCP1(23C), which had been previously detected in the SMB cell line (Personal communication from Dr Enrico Cancellotti, The Roslin Institute). Once PrP^{C} has been processed in the Golgi body it buds off in a membrane vesicle, which relocates to the plasma membrane. The plasma membrane is a proposed site for PrP^{C} function and has been extensively reported to be the site of PrP conversion (Kazlauskaite *et al.*, 2002, Sanghera *et al.*, 2002). A suitable marker for plasma

membrane is the protein annexin-II which has been previously demonstrated to be present in both fibroblasts (Barwise and Walker, 1996) and microglia (Eberhard *et al.*, 1994). Plasma membrane proteins, such as PrP^C, only remain on the cell surface for a specific period of time, after which they will be endocytosed via clathrin-coated pits. At this point, PrP^C will either be recycled back to the plasma membrane, if it is found to be undamaged, or will instead enter into the lysosomal pathway for digestion by acidic enzymes present in the cavity of the lysosomal compartment. Lysosomes have been hypothesised to be instrumental in the pathogenesis of cell death and were considered to be a highly relevant organelle to investigate (Laszlo *et al.*, 2005). Locating a suitable marker for the detection of lysosomes in fibroblast and microglial cells was difficult, with both cathepsin D and LAMP1 tested without success. The marker LAMP2, however, proved to be a marker that was present in both cell types (Maurin and Raoult, 1999, Djukic *et al.*, 2006). Unfortunately, antibody cross reactivity was a problem when probing multiple fractions from SMB-PS and LD9 cells. Table 3.1 outlines the organelle markers and antibodies used to detect these markers. Figure 3.2 shows the detection of organelle markers in LD9 and SMB-PS cellular homogenates after separation by SDS PAGE and Western blotting.

The endocytic pathway, from the plasma membrane to the lysosomes, transports plasma membrane bound proteins initially through endocytic vesicles which fuse with early endosomes. Early endosomes mature into late endosomes which in turn are suggested to convert into lysosomes (Gruenberg, 2001). Endosomes have previously been suggested to be important in the conversion of PrP^C to PrP^{Sc} and that conversion occurs after PrP^C has been to the plasma membrane (Borchelt *et al.*, 1992, Campana *et al.*, 2005, Marijanovic *et al.*, 2009). A marker of early endosomes is the protein EEA-1, which is instrumental in tethering and docking of the early endosome with endocytic vesicles from the plasma membrane (Wilson *et al.*, 2000). Unfortunately this marker was not detected in either the SMB-PS or LD9 cell line. An alternative early endosomal protein marker is Rab5 which is a small GTPase that modulates effector proteins such as EEA-1 and rabaptin-5 (Horiuchi *et al.*, 1997, Patki *et al.*, 1997, Deneka and van der Sluijs, 2002). Howevèr, Rab5 was also not detected in homogenates from either the SMB-PS or LD9 cell line.

Organelle	Marker	MW	Antibody	Sourced From
Endoplasmic Reticulum	BiP/GRP78	78 kDa	Mouse IgG2a	BD Biosciences
Golgi Body	TCP1(23C)	60 kDa	Rat Monoclonal	Abcam
Plasma Membrane	Annexin II	36 kDa	Mouse IgG1	BD Biosciences
Lysosomes	LAMP2	100 kDa	Rat Monoclonal	Abcam
Mitochondria	Bcl-2	26 kDa	Mouse IgG1	BD Biosciences

Table 3.1: Antibodies for immunoblot detection of mammalian cell culture derived organelles.

Detection of markers was demonstrated by the analysis of crude cell lysates that were separated by SDS PAGE and probed with appropriate antibodies to detect a given organelle. The reactivity of the antibodies against the purified organelles was validated in figure 3.2 where Western blot analysis of LD9 and SMB-PS cell lysates confirms detection of organelles as assessed by the specificity of antibodies for target proteins and correct molecular weight.

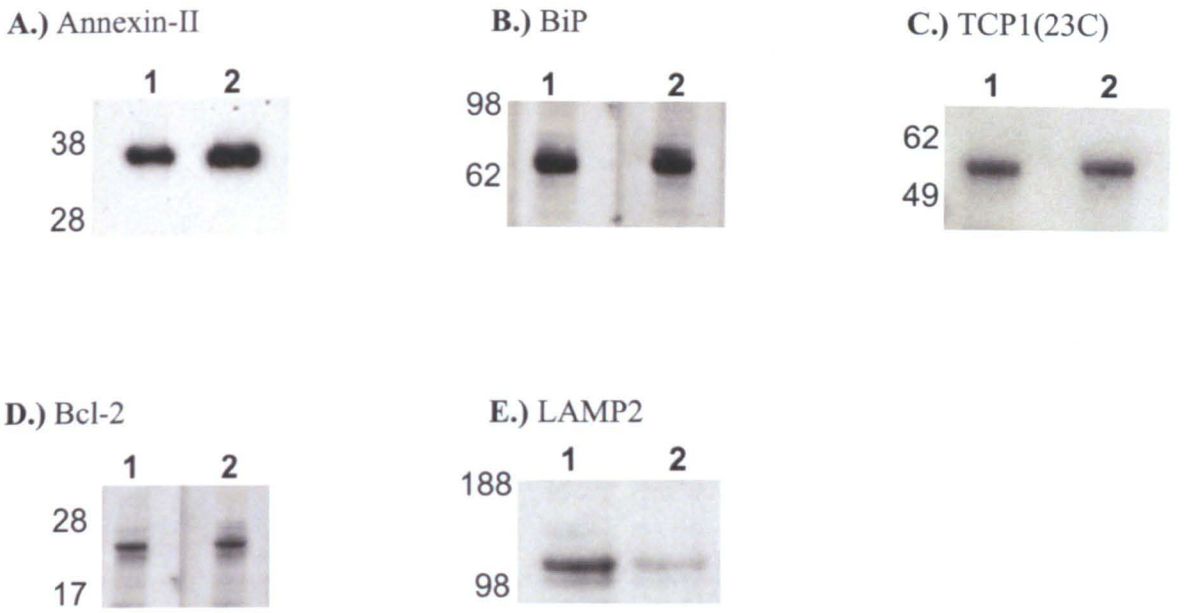

Figure 3.2: Western blot analysis of LD9 and SMB-PS cell homogenates.

Homogenates from LD9 and SMB-PS cells (lane 1 and 2, respectively) were analysed by SDS PAGE and detected by Western blotting with (A.) plasma membrane marker annexin II (1:1000) and using a secondary anti-mouse HRP (1/2000) antibody, (B.) endoplasmic reticulum marker BiP (1:500) and using a secondary anti-mouse HRP (1/2000) antibody, (C.) Golgi body marker TCP1(23C) (1:2000) and using a secondary anti-rat HRP (1/2000) antibody, (D.) mitochondria marker Bcl-2 (1:1000) and using a secondary anti-mouse HRP (1/2000) antibody, (E.) lysosomal marker LAMP2 (1:600) and using a secondary anti-rat HRP (1/2000) antibody for chemiluminescence detection. Molecular weight, in kDa, is shown on the left hand side of each Western blot.

3.4 Subcellular fractionation method development

My experimental aim was that strain specific co-factors are necessary for prion conversion. To do this, subcellular fractionation of TSE susceptible cell lines was performed to analyse for the presence of cellular co-factors associated with distinct organelles. The assay that I chose to assess this was the CFCA, to which I added organelles to rMoPrP seeded by different strains of mouse scrapie.

There is no definitive protocol for the subcellular fractionation of tissue culture cells that can be applied to every cell line. Membrane particle separation by density gradient media is determined predominately by the content ratio of protein and lipids within the membrane (Pasquali *et al.*, 1999). For instance, mitochondrial membranes are protein rich and thus have a high density, whereas lysosomes are lipid rich and therefore are low in density. Organelle content also plays a part in density and this is best demonstrated by the low density lipoproteins within the Golgi body resulting in more buoyancy when compared to the high concentrations of secretory proteins that reside within secretory vesicles. Sucrose is the most common choice of gradient media, however medias such as Percoll, Ficoll, Nycodenz and OptiPrep™ are readily available and are often more practical. Crucially, sucrose solutions are required to be freshly made up every time to prevent bacterial infection and therefore there can be reproducibility issues when making up fresh sucrose gradients. I tested OptiPrep™ first because it was readily available as a 60 % sterile solution and reportedly offered superior osmotic control and balance, which I hoped would enhance organelle viability and reproducibility in downstream assays.

3.4.1 Homogenisation of cultured cells

The first critical step of subcellular fractionation was to apply the most relevant and appropriate homogenisation conditions for the generation of a cell homogenate that could be reproducibly separated by ultracentrifugation. The homogenisation procedure was aimed at efficiently disrupting the cell membrane without shearing internal organelles. The homogenisation medium (0.25 M sucrose, 1 mM EDTA, 20 mM HEPES-NaOH (pH 7.4)) was adapted from Yang *et al.*, 1997 and Zhang *et al.*,

1998 and was iso-osmotic to aid effective cell disruption and maintain organelle viability during homogenisation.

Several methods are commonly used to homogenise cells including manual grinding, mechanical disruption and liquid homogenization and selected methods are listed in table 3.2. I trialled four methods of homogenisation to ascertain a practical and reproducible technique for the complete breakage of outer cellular membrane without compromise to internal organelles. These included Potter-Elvehjem homogenisation, narrow bore syringe needle, sonication and freeze/thaw techniques. The homogenisation method also incorporated a post-nuclear spin (PNS) immediately after homogenisation. This step pelleted cellular debris and nuclei which prevented DNA leakage and aggregation during ultracentrifugation (Graham and Rickwood, 1996).

The freeze/thaw technique was tested first using both the LD9 and SMB-PS cell lines; however this did not cause sufficient lysis of the cells. This was determined at the first centrifugation step where the PNS is separated from cellular debris and free nuclei. The PNS did not contain any organelles as validated by Western blotting and therefore the conclusion was that whole cells rather than just cellular debris and free nuclei were pelleted at this stage (data not shown).

The second homogenisation technique investigated was passage of the cell suspension through a narrow bore syringe. Aspiration and ejection through a narrow orifice causes shearing of cellular membranes and the release of internal organelles. A range of gauges from 16 to 24 gauge were tested, however, this technique also proved to be inefficient at cell disruption for both LD9 and SMB-PS cells. Observations made by Western blotting of organelles indicated that it was more efficient than freeze/thawing but the majority of cells remained intact and were pelleted out of the PNS (data not shown).

Liquid based homogenisations are commonly used to disrupt tissue culture cells in small volumes of buffer. Cells are lysed by forcing the cell suspension through a narrow opening which causes shearing of cellular membranes. Dounce homogenisers and Potter-Elvehjem homogenisers consist of glass or PTFE pestles respectively,

Shearing Method	Details
Dounce homogeniser	Liquid shear with a round glass pestle
Potter-Elvehjem homogeniser	Liquid shear with a PTFE pestle
Syringe needle	Aspiration and ejection
Cell Cracker	Ball bearing homogeniser
Stansted Cell Disruptor	High pressure
Nitrogen cavitation	Rapid loss of pressure causes dissolved gas to form bubbles
Sonication	Pulsed high frequency sound waves
Freeze/Thaw	Lysis by cyclic formation of ice crystals

Table 3.2: The principal techniques used for effective and efficient cell disruption.

Table lists the techniques used to physically lyse cells and the details on how this is performed.

which are manually or mechanically forced into a glass tube. I selected a tight fitting manual Potter-Elvehjem homogeniser with a volume of 2 ml because it was easily acquired. Figure 3.3 shows that there was an improvement on the previous attempted homogenisation techniques, freeze/thaw and passage through a narrow bore syringe. The main variable with a tight fitting Potter-Elvehjem homogeniser was the number of strokes required to shear (>90 %) of cells but without shearing the nuclear membrane and causing subsequent DNA aggregation within the sample.

The homogenisation protocol in chapter 2 section 2.1.3.4 was used with the following alterations. One flask of LD9 cells was resuspended in 1.5 ml of homogenisation buffer with 1000 µl homogenised by 5 strokes of the pestle. From this, 250 µl was removed and stored on ice. The remaining 750 µl was homogenised by a further 5 strokes of the pestle (total of 10 strokes) from which another 250 µl was removed and stored on ice. This was repeated to achieve a total number of 15 and 20 strokes which resulted in homogenised samples ranging from 5, 10, 15 and 20 strokes. Each sample was crudely fractionated by the following protocol: a post-nuclear spin to pellet cellular debris was performed at 1000 *g* for 10 minutes; supernatant was collected and centrifuged at 3000 *g* for 10 minutes, generating a heavy mitochondrial fraction (HMF) pellet. Next, the supernatant was collected and further centrifuged at 15,000 *g* for 10 minutes to generate a light mitochondrial fraction (LMF) pellet. The supernatant from this was collected and centrifuged at 100,000 *g* for 45 minutes in an ultracentrifuge which generated a microsomal pellet. Each pellet was retained on ice, dried and resuspended in 40 µl of SDS PAGE loading buffer for subsequent Western blot analysis. Cell debris and nuclear pellet was also treated with DNase (5 µg) / $MgCl_2$ (0.25 M). Western blotting for organelle markers representing mitochondria (Bcl-2) and Golgi body (TCP1(23C)) are shown in figure 3.3. In addition, sonication of the cell suspension was investigated incorporating a 5 second, 10 second or 15 second pulse to disrupt cellular membranes. Samples were also analysed by SDS PAGE and Western blotting to determine the homogenisation efficiency of sonication and compare against a Potter-Elvehjem homogeniser.

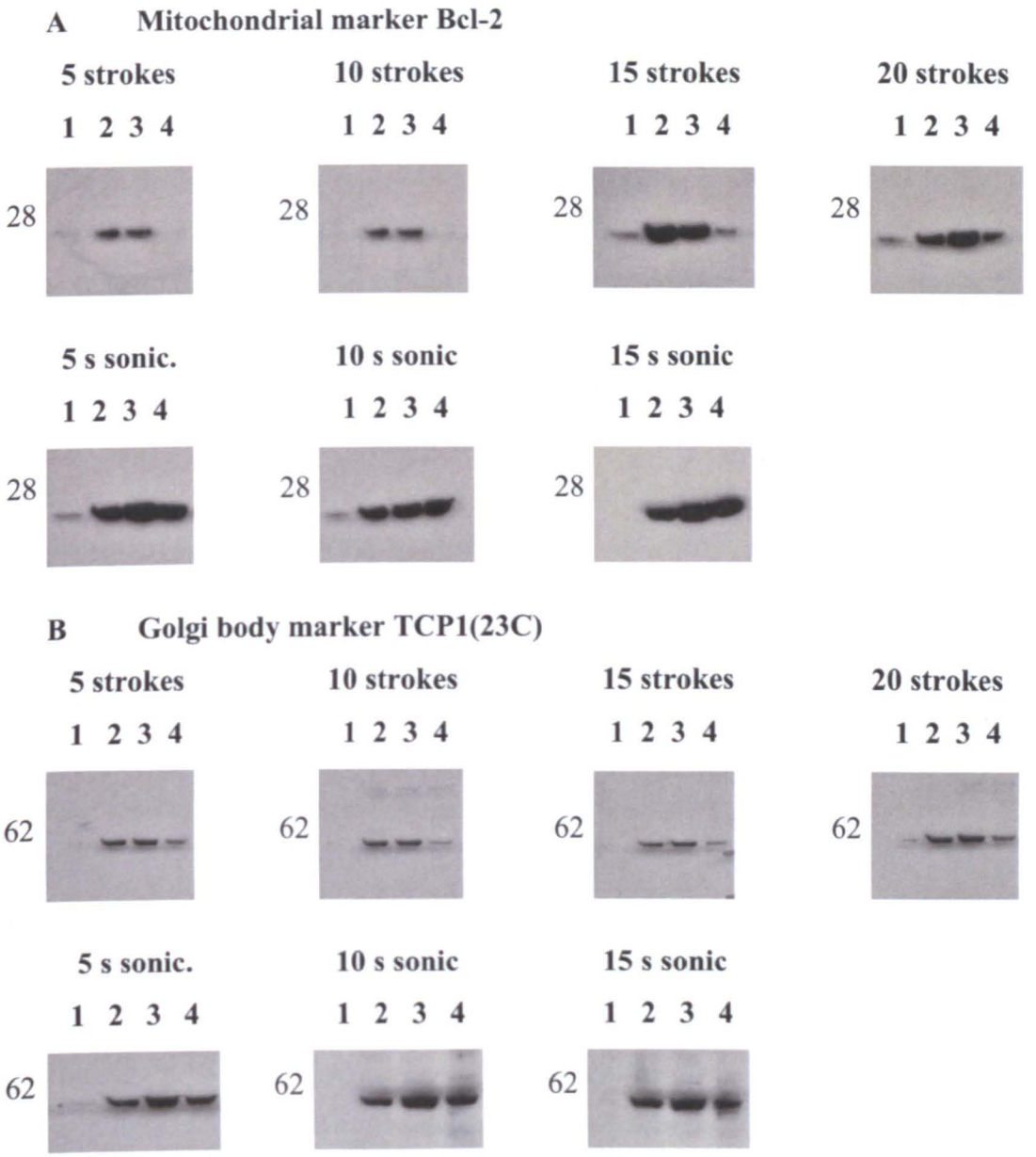

Figure 3.3: Analysis of homogenisation techniques by crude subcellular fractionation of LD9 cells.

The above Western blots are divided into, (A) detection of mitochondrial marker Bcl-2 and, (B) detection of Golgi body marker TCP1(23C). For both A and B, they are subdivided into 7 different approaches to homogenise LD9 cells: 5, 10, 15 or 20 strokes of the pestle and 5, 10 or 15 second (s) sonication pulses. There are four samples from each stage of the crude subcellular fractionation and are labelled as (1.) PNS pellet, (2.) HMF pellet, (3.) LMF pellet and, (4.) microsomal pellet and are generated as described in the main text on page 13. Molecular weight, in kDa, is shown on the left hand side of each Western blot.

Figure 3.3 illustrates the results of increasing the number of strokes of the pestle to release subcellular organelles, on two organelles, mitochondria and the Golgi body. Mitochondria is the most dense of the organelles studied and therefore I rationalised that if homogenisation was effective, mitochondria would be present in fractions 2 (HMF) and fraction 3 (LMF) and absent in fraction 4 (microsomes). The Golgi body was also chosen because of the nature of the Golgi body to form stacks that are susceptible to shearing into indistinct microsomes. I believed that the Golgi body would be a good indicator of homogenisation force in relation to organelle viability.

A number of conclusions can be drawn from the experiment outlined above and shown in figure 3.2. Firstly, as the number of pestle strokes increase, there is an increase in organelle shearing. This was interpreted from the observation of mitochondria in fraction 4 (microsomes) after 15 strokes. This is not true for 5 or 10 strokes of the pestle where mitochondria is present only in fraction 2 (HMF) and fraction 3 (LMF) as expected. This suggests that the mitochondria have been sheared into smaller indistinct microsomes after 15 strokes. In section B of figure 3.3, the Golgi body blots were difficult to interpret as the organelle marker was detected throughout fractions 2 to 4, regardless of the number of strokes of the homogeniser. These observations were suggested to be because of the large number of Golgi body apparatus present in the LD9 cell line and therefore were particularly prone to shearing even under the minimal of forces. As discussed later this result is congruent with later observations on the subcellular fractionation of LD9 cells (figure 3.6).

Secondly, sonication appeared to be an aggressive form of homogenisation. This was demonstrated by the increased presence of mitochondria in fraction 4 (microsomes), which was evident even after only a 5 second sonication pulse. In addition, there was increased detection in organelle markers detected by the mitochondrial marker Bcl-2, after sonication, than when generally compared against the Potter-Elvehjem homogenisation method. This was presumed to be caused by the complete homogenisation of all membrane surfaces by sonication and therefore more organelle marker i.e. more Bcl-2 and TCP1(23C) was released and detected. In section B of figure 3.3, the effect of sonication on the Golgi body was similar to that on mitochondria.

From figure 3.3 I concluded that all future experiments would incorporate 10 strokes of a Potter-Elvehjem pestle, which was sufficient to disrupt cellular membranes but not too forceful as to shear open the nucleus or other organelle membranes.

3.5 Optimisation of OptiPrep™ density gradient media for subcellular fractionation

OptiPrep™ density gradient media is a 60 % sterile solution of iodixanol, 5,5'-[(2-hydroxy-1-3 propanediyl)-bis(acetylamino)] bis [N,N'-bis(2,3dihydroxypropyl-2,4,6-triiodo-1,3-benzenecarboxamide)] designed for the *in vitro* isolation of biological compartments by centrifugation. I required preparing an OptiPrep™ gradient that would separate the complete list of organelles associated with PrP conversion. Therefore I investigated a range of gradients, including 10-20 %, 15-25 %, 20-30 % and 10-30 % iodixanol. These gradients covered a wide range of OptiPrep™ concentrations that could potentially be utilised to isolate any given subcellular organelle.

One T75 flask of confluent LD9 cells was resuspended in 1 ml homogenisation buffer and homogenised by 10 strokes of a Potter-Elvehjem pestle followed by a PNS spin of 1000 *g* for 10 minutes to pellet cellular debris. From a 50 % iodixanol working solution (OptiPrep™ diluted with homogenisation buffer), Optiprep™ solutions were made up to the previously indicated concentrations of iodixanol, including every 2.5 % between the highest and lowest concentrations of iodixanol. For example, 10 %, 12.5 %, 15 %, 17.5 % and 20 % iodixanol solutions were made up to form a 10-20 % gradient. For each concentration of iodixanol, 1000 µl was placed in the ultracentrifuge tube, resulting in a total column volume of 5 ml. Discontinuous gradients were left at room temperature for 30 minutes to equilibrate into continuous gradients, after which 500 µl (10 % of column volume) of LD9 PNS sample was loaded on top of each of the four gradients and ultracentrifuged at 145,000 *g* for 4 hours. For each of the 4 gradients investigated, opaque layers of 'banded' cellular material were observed and the distance from the top of the gradient was measured. Figure 3.4 is a schematic diagram indicating the recorded heights within the tubes of each of the bands. These opaque bands presumably represented different organelles separated by OptiPrep™ gradient following

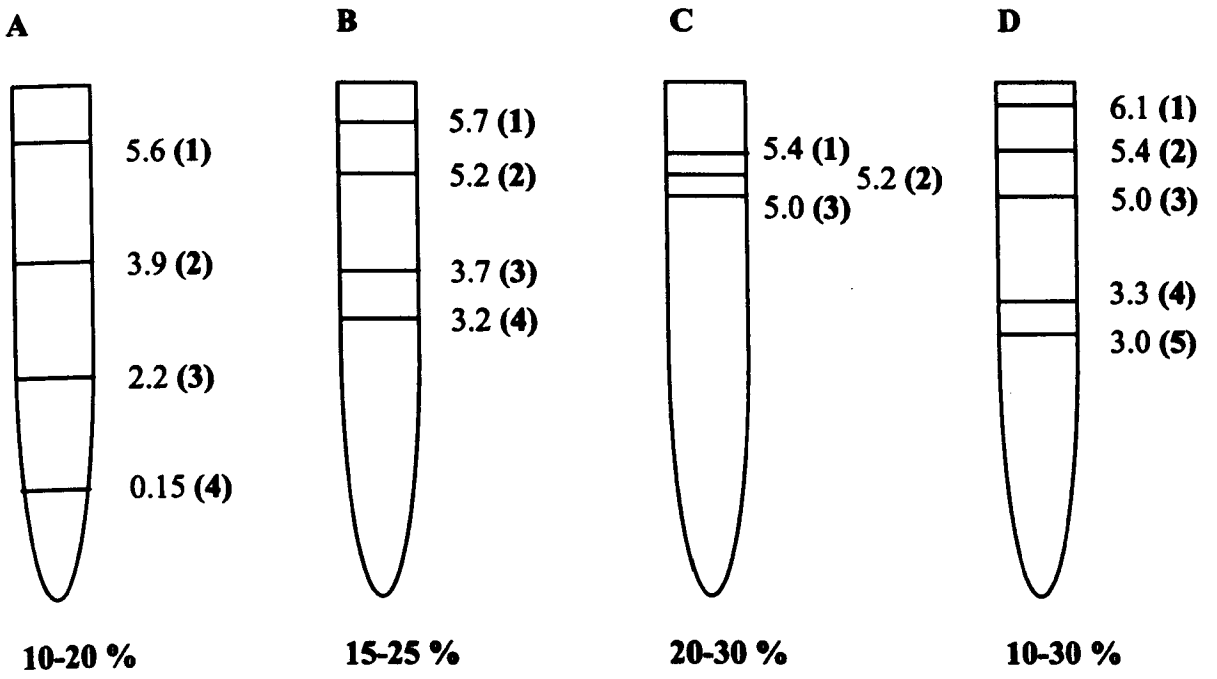

Figure 3.4: Diagrammatic representation of cellular material forming bands, within a density gradient post ultracentrifugation.

Schematic representation of ultracentrifuge tubes whereby the black lines represent the location of opaque bands of cellular material within the density gradient. The values shown for each gradient are a measurement of distance (centimetres) from base of ultracentrifuge tube. Density gradient was recorded as a concentration of iodixanol from top of the tube to the base where in (A.) there was a 10-20 % gradient, (B.) 15-25 % gradient, (C.) 20-30 % gradient and, (D.) 10-30 % gradient. Sample was 500 µl of PNS supernatant from LD9 homogenate and was ultracentrifuged at 145,000 *g* for 4 hours prior to measurement of opaque bands within density gradient.

ultracentrifugation. From each organelle band, a 300 µl sample was removed using a Hamilton 1000 µl syringe, then precipitated and resuspended as per the protocol in chapter 2 (section 2.1.3.4) for preparation of gradient fractions prior to SDS PAGE and Western blot analysis. Samples from the 20-30 % gradient were not processed in this way due to the close proximity of the 3 opaque bands to each other, which made isolation without contamination, technically difficult (see figure 3.4 panel C). Figure 3.5 shows the Western blot analyses of the subcellular fractions that were removed from each of the three gradients. Fraction 1 is at the top of the gradient and fraction 4 is towards the bottom of the gradient.

Figure 3.5 panel A illustrates the separation of lysosomes, mitochondria and Golgi body using the 10-20 % OptiPrep™ gradient as assessed by Western blotting using the antibodies LAMP2, Bcl-2 and TCP1(23C) respectively. Lysosomes were enriched in fraction 2 whereas mitochondria are mainly present in fraction 4. The Golgi body is distributed throughout fractions 1 to 4, however there appeared to be an increase in fraction 3 which maybe due to variable sample loading doing SDS-PAGE. The schematic diagram in figure 3.4 section A clearly demonstrates good separation between each of the four fractions.

Figure 3.5 panel B shows the Western blot of the separation of lysosomes, mitochondria and Golgi body when using a 15-25 % OptiPrep™ gradient resulted in lysosomes being represented in fraction 1. The manipulation of the OptiPrep™ gradient concentration resulted in an enrichment of lysosomes in fraction 1 only, as of when using a 10-20 % OptiPrep™ gradient. Mitochondria were enriched in fraction 4 and the Golgi body have been co-purified in fractions 1, 2 and 3. The shift in concentrations has resulted in mitochondria travelling further down through the gradient into concentrations of iodixanol that are too dense for Golgi body.

Finally, upon testing a 10-30 % gradient resulted in an extra cellular fraction observed in the gradient (figure 3.5 panel D). Of these five fractions, lysosomes were enriched in fraction 2, whereas mitochondria whilst being detected in all fractions, were enriched in fraction 5. Golgi body on the other hand was present throughout fractions 1 to 4. In combination with figure 3.4 panel D, it appeared that the organelles were less efficiently purified using this gradient when compared to the 10

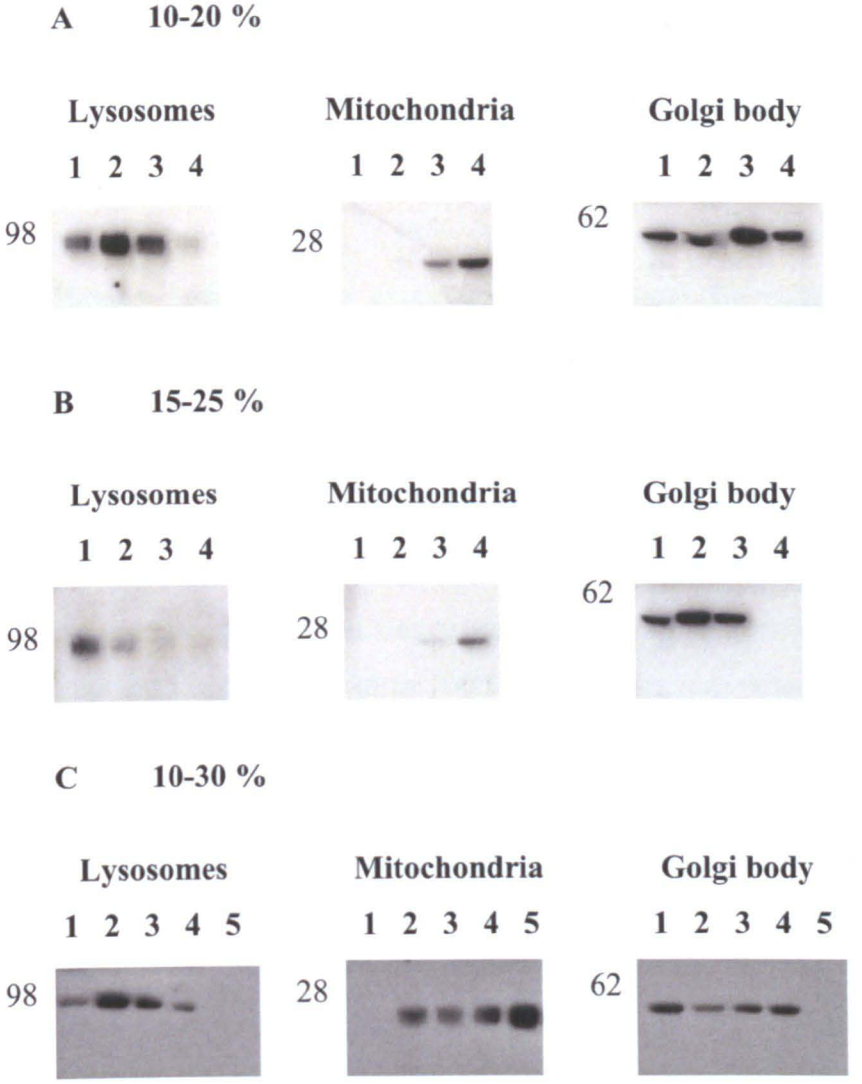

Figure 3.5: Analysis of subcellular fractionation of LD9 post nuclear supernatant by ultracentrifugation of different density gradients of iodixanol.

The above Western blots are divided into, (A) 10-20 % gradient, (B) 15-25 % gradient and, (C.) 10-30 % gradient. For both A, B and C, they are subdivided into 3 different Western blots probed by 3 different primary antibodies: lysosomal marker LAMP2 (1/600), mitochondrial marker Bcl-2 (1/1000) and Golgi body marker TCP1(23C) (1/2000). There are four subcellular fractions from both the 10-20 % and the 15-25 % gradients and five subcellular fractions from the 10-30 % gradient. Each subcellular fractions represents the fraction removed from the gradient where 1 is nearest to the top of the gradient and 4 or 5 is nearest to the base of the gradient. Molecular weight, in kDa, is shown on the left hand side of each Western blot.

-20 % gradient. Using this data I concluded that a 10-20 % gradient of iodixanol would provide the best conditions for the separation of lysosomes, mitochondria and Golgi body from the LD9 cell line as validated by Western blotting of these organelles.

Having optimised the experimental conditions for subcellular fractionation, the protocol was repeated and resultant subcellular fractions were subjected to methanol precipitation. The precipitate was resuspended in a standard volume of dH_2O prior to incorporation to the CFCA. To maximise the amount of organelles that could be added to the CFCA, multiple subcellular fractionations were centrifuged together and pooled prior to addition to the CFCA. A second approach to increase sample organelle concentration was to increase sample volume applied to each OptiPrep™ gradient i.e. from 500 µl to 1000 µl. However, the volume of the sample applied to each gradient should represent no more than 10 % of the total column volume. This is because large sample volumes can cause damage to the gradient and subsequently alter organelle movement through the gradient. Therefore, the column volume was increased from 6 ml to 12 ml which consequently meant that the centrifugal force would have to be increased to accommodate the increase in gradient length. This increase in column volume was calculated to represent an increase in centrifugal force to 225,000 *g* for a period of 8 hours (Graham and Rickwood, 1996).

3.6 Subcellular fractionation of SMB-PS and LD9 cell lines

Following extensive optimisation, the final method for subcellular fractionation entailed the cellular homogenisation of either LD9 or SMB-PS cells in a Potter-Elvehjem homogeniser. Cellular debris was pelleted at 1000 *g* for 10 minutes and 1000 µl of the supernatant added to the top of a continuous 10-20 % gradient. Ultracentrifugation in a Sorvall TH-641 rotor at 225,000 *g* for 8 hours separated the PNS by the unique density properties of each of the organelle types. The method is described in more detail in chapter 2 (section 2.1.3.4). The gradient had a total volume of 11 ml and after centrifugation, was separated into 500 µl fractions. This volume was thought to be firstly, small enough to give adequate resolution to provide precise analysis on organelle distribution and secondly, large enough for reproducibility and ease of handling. Starting from the top of the gradient, 500 µl

fractions were taken and numbered 1 to 22. Subcellular fractionation of LD9 and SMB-PS cell lines were assessed and validated by Western blot as shown by representative Western blots in figures 3.6 and 3.7, respectively.

In figure 3.6, LD9 subcellular fractionation showed that the plasma membrane marker annexin-II was detected predominately in fractions 1 to 5 at a density of 1.040 g/ml. The observation of plasma membrane marker also present in fractions 19 to 21 presumably reflects the presence of plasma membrane derived cellular debris. This is due to contamination of the PNS with cellular debris that became detached from the pellet at this stage. The lysosomal marker LAMP2 was detected in fractions 3 to 7 between a density of 1.043 g/ml and 1.047 g/ml. The Golgi body marker TCP1(23C) was detected over a wide range of fractions covering densities of 1.046 g/ml to 1.078 g/ml. The endoplasmic reticulum marker BiP on the other hand was detected from fraction 11 to 16 at densities of 1.073 g/ml to 1.085 g/ml. Finally, in fractions 15 to 22 the mitochondrial marker Bcl-2 was enriched, which covered densities of 1.081 g/ml to 1.139 g/ml. There was the detection of Bcl-2 in fractions 2 to 5 which could represent shearing of the mitochondria into smaller less dense microsomes. Example Western blots of the subcellular fractionation of the LD9 cell line are shown in figure 3.6.

Like the results with the LD9 cell organelle purification, SMB-PS subcellular fractionation also showed that the plasma membrane from marker annexin-II was also enriched at the top of the gradient in fractions 1 to 6 at a density of 1.040 g/ml. However, unlike LD9 cells, SMB-PS lysosomes ranged from fraction 3 to 12, covering density of 1.04 g/ml to 1.079 g/ml. The Golgi body marker TCP1(23C) was detected in fractions 15 to 19, which had a density of 1.081 g/ml to 1.01 g/ml. Finally, the mitochondrial marker Bcl-2 was detected in fractions 16 to 22, which had densities of 1.085 g/ml to 1.139 g/ml. The presence of Bcl-2 at lower densities could be due to the shearing of large mitochondria during homogenisation, into a range of mitochondria-derived microsomes of different sizes and densities. Together, these results indicate that both LD9 and SMB-PS cell lines can be homogenised and fractionated into distinct fractions of subcellular organelles. Example Western blots of the subcellular fractionation of the SMB-PS cell line are shown in figure 3.8.

Figure 3.6: Enrichment of different LD9 organelles as determined by Western blotting detection of organelle specific proteins after subcellular fractionation using an ultracentrifugation gradient.

LD9 subcellular fractions were prepared as outlined in section 3.6. Fractions of equal volumes were methanol precipitated, separated on a 12 % bis tris SDS PAGE and blotted onto PVDF membrane for immunodetection to show organelle distribution through the gradient. Primary antibodies used were (A.) endoplasmic reticulum marker BiP, (B.) Golgi body marker TCP1(23C), (C.) plasma membrane marker annexin II, (D.) lysosomal marker LAMP2, (E.) mitochondrial marker Bcl-2. Molecular weight, in kDa, is shown on the left hand side of each Western blot.

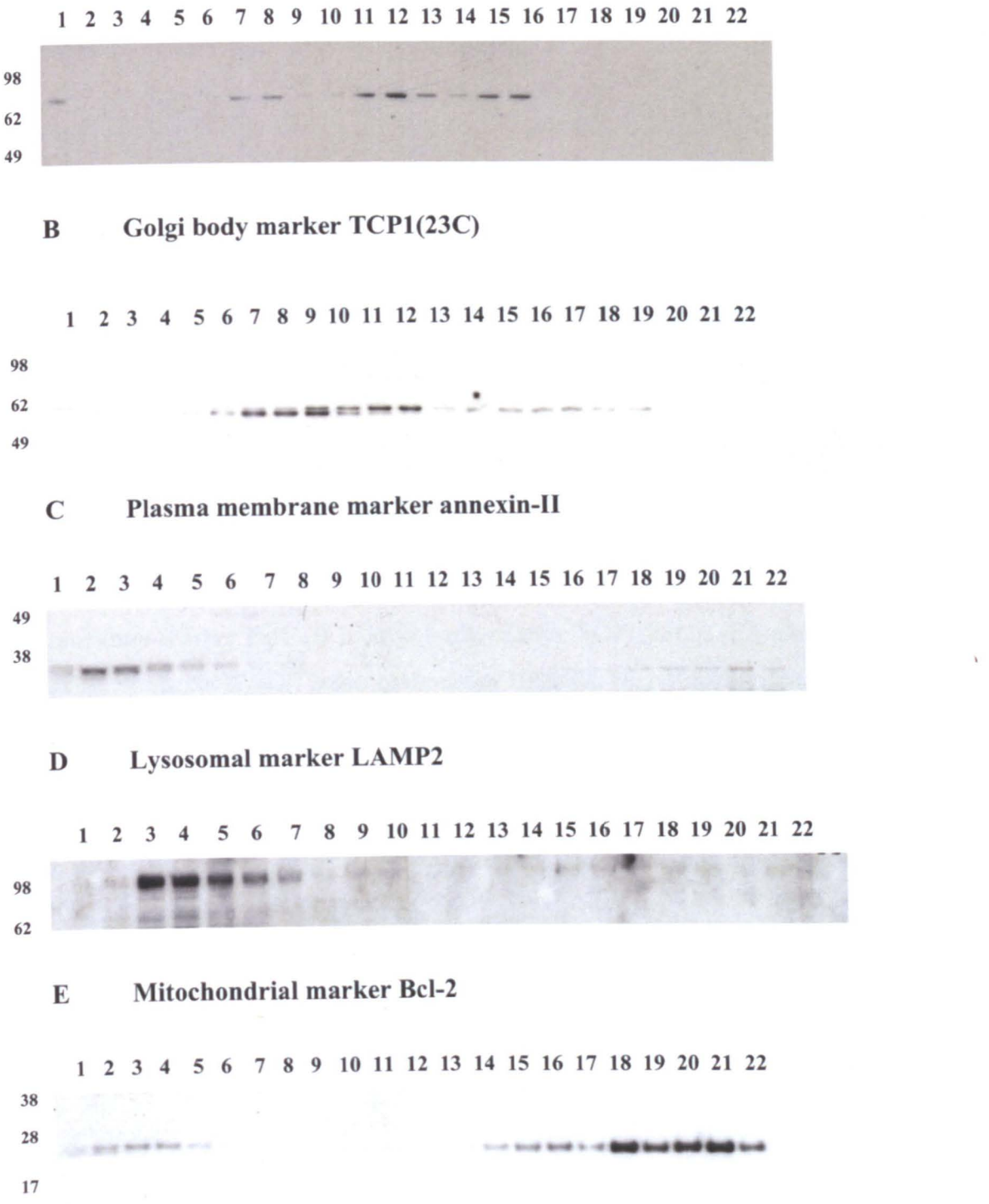

Figure 3.6: Enrichment of different LD9 organelles as determined by Western blotting detection of organelle specific proteins after subcellular fractionation using an ultracentrifugation gradient.

Figure 3.7: Enrichment of different SMB-PS organelles as determined by Western blotting detection of organelle specific proteins after subcellular fractionation using an ultracentrifugation gradient.

SMB-PS subcellular fractions were prepared as outlined in section 3.6. Fractions of equal volumes were methanol precipitated, separated on a 12 % bis tris SDS PAGE and blotted onto PVDF membrane for immunodetection to show organelle distribution through the gradient. Primary antibodies used were (A.) endoplasmic reticulum marker BiP, (B.) Golgi body marker TCP1(23C), (C.) plasma membrane marker annexin II, (D.) lysosomal marker LAMP2, (E.) mitochondrial marker Bcl-2. Molecular weight, in kDa, is shown on the left hand side of each Western blot.

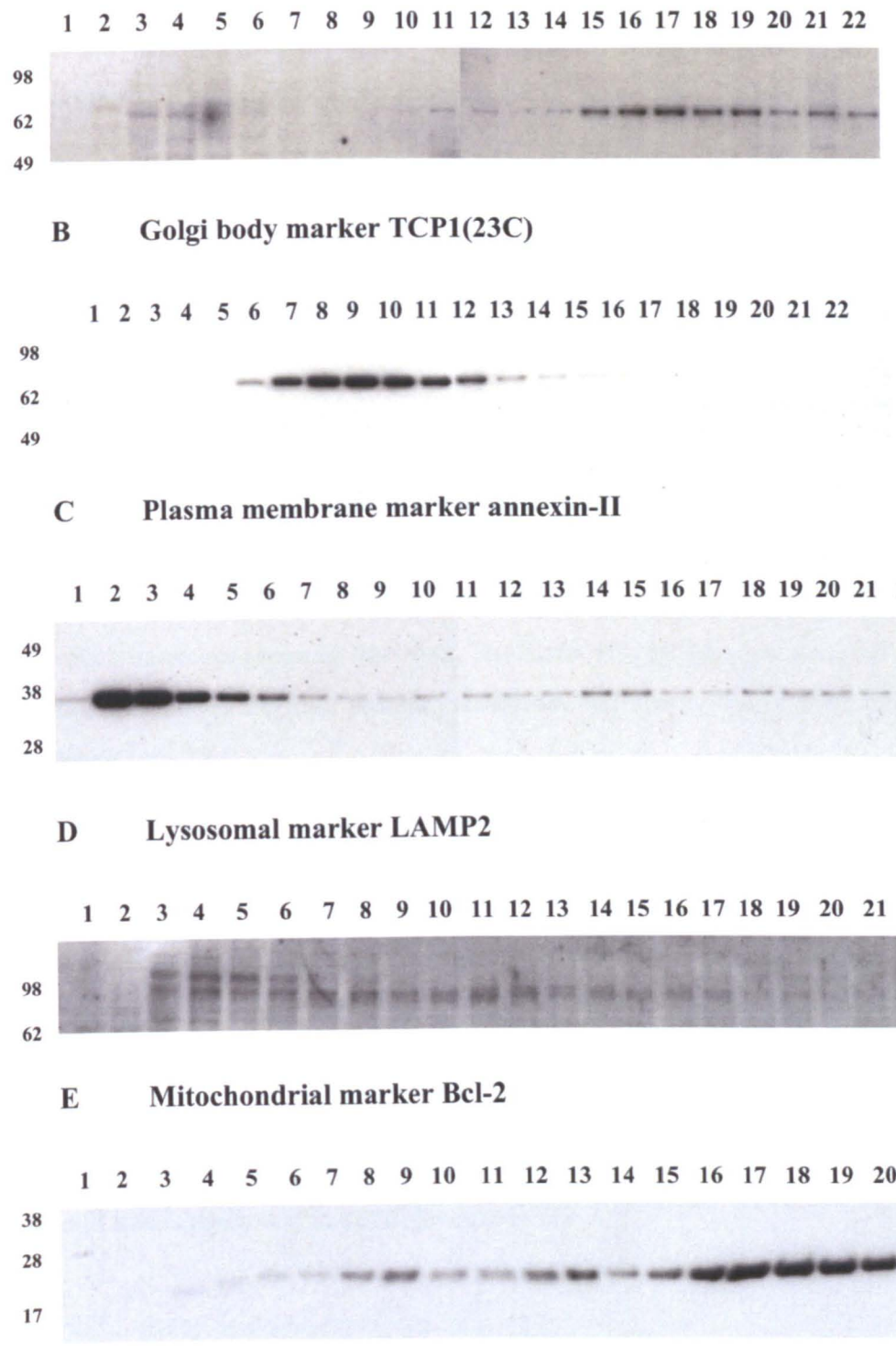

Figure 3.7: Enrichment of different SMB-PS organelles as determined by Western blotting detection of organelle specific proteins after subcellular fractionation using an ultracentrifugation gradient.

Densitometric analysis of these Western blots allowed for the data to be plotted on a bar chart to represent organelle distribution through the gradient. These are exhibited as figures 3.8 and 3.9 for LD9 and SMB-PS organelle distribution, respectively, and represent a minimum of four repeats and in some cases a maximum of seven repeats.

Figure 3.8 and 3.9 shows that most organelles are distributed over a range of fractions; however there is a definite enrichment of each of the organelles detected. The LD9 Golgi body marker TCP1(23C) was detected throughout the gradient indicating a wide distribution of Golgi body densities. This was most likely due to the nature of fibroblasts to secrete protein fibres and as such have prominent Golgi body apparatus. The stacks of these Golgi body would be more prone to shearing during homogenisation and therefore the Golgi body would subsequently be rendered into various different sizes and densities. The converse can be seen with the detection of TCP1(23C) in SMB-PS cells where this Golgi body marker was detected over a much narrower range of fractions. The SMB-PS cell line is microglial in origin and is not specialised for high protein production and secretion like the LD9 fibroblast cell line.

3.7 Discussion

In this chapter, I have demonstrated the enrichment of subcellular organelles from two different lines of cultured cells, LD9 fibroblasts and SMB-PS microglia. Moreover, I have provided a means to assay organelle distribution and provide samples for analysis in the CFCA. The impact of organelle supplementation on the conversion efficiency of different strains of mouse scrapie in the CFCA was assessed and this is discussed in detail in chapter 4.

TSE susceptible cell lines are rare with only a few cell lines known to support a persistent TSE infection (see table 1.3). Cell lines used for subcellular fractionation were chosen based on a number of criteria, including species of origin, mouse scrapie strain susceptibility and availability. In previous studies the L-fibroblast cell line L929, was reported to be capable of replicating 22L, ME7 an RML prions (Vorberg *et al.*, 2004). The L929 cell line has subsequently been cloned to alter its strain susceptibility to be permissive to RML prions (Mahal *et al.*, 2007).

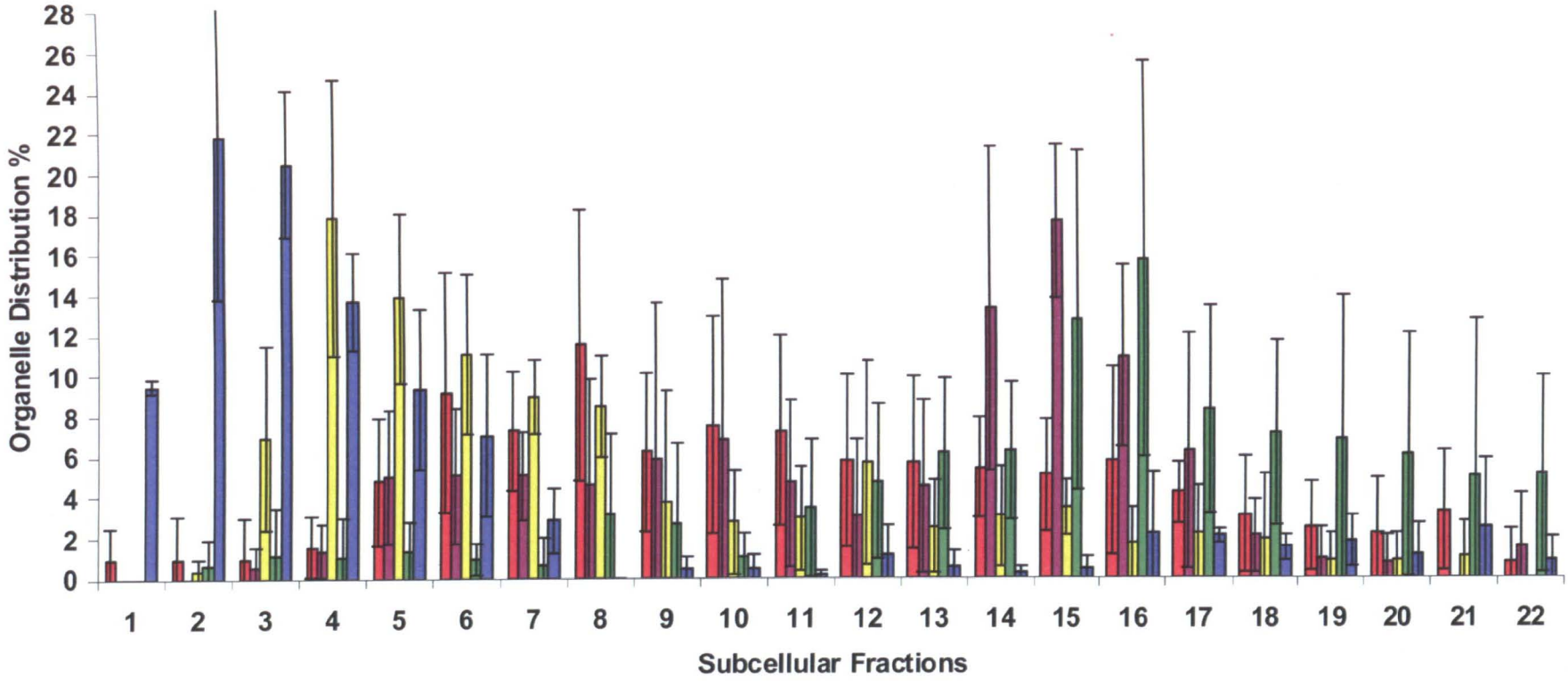

Figure 3.8: LD9 organelle distribution profile after subcellular fractionation by density gradient centrifugation.

This figure illustrates the subcellular distribution of LD9 organelles through a 10 to 20 % density gradient after ultracentrifugation. The data are presented as percentage of organelle in each fraction from 1 (low density) to 22 (high density) including plasma membrane (blue), lysosomes (yellow), Golgi body (red), endoplasmic reticulum (purple) and mitochondria (green).

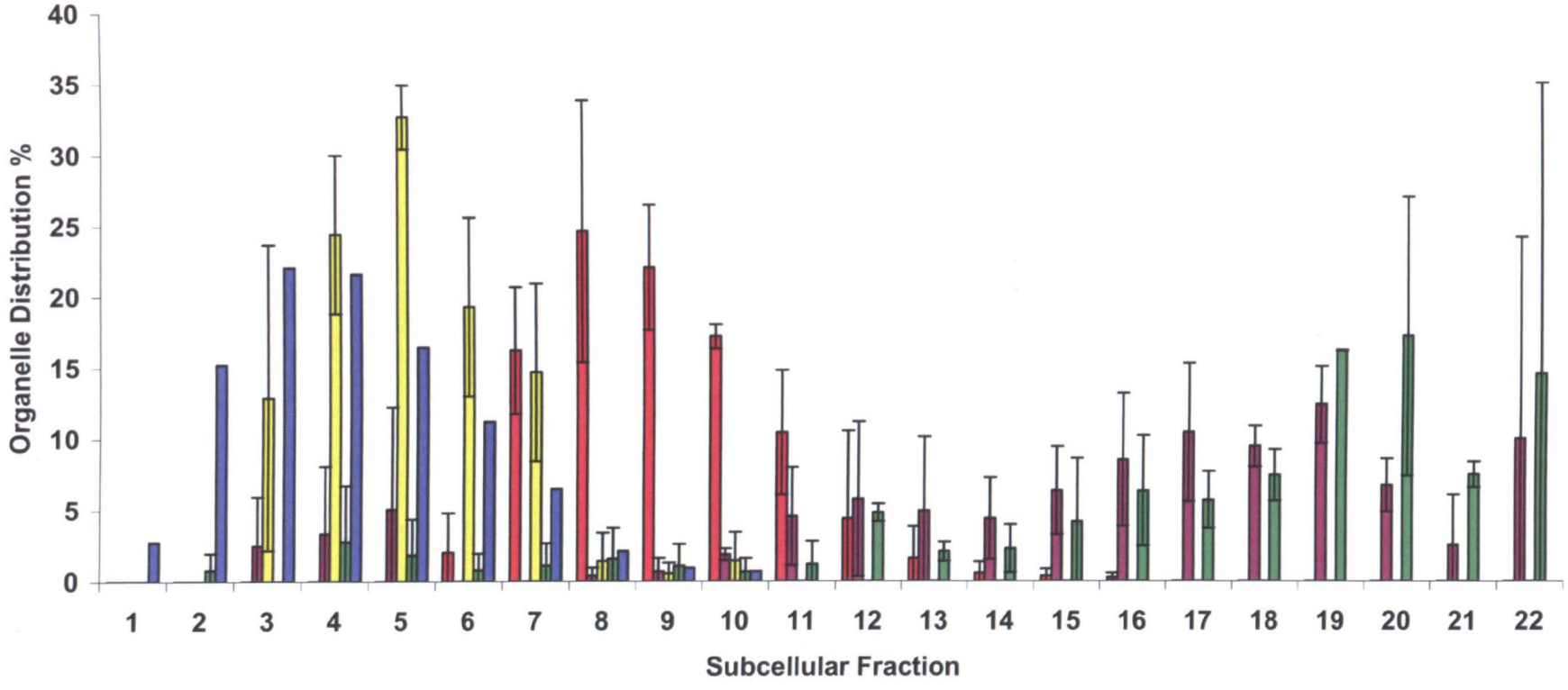

Figure 3.9: SMB-PS organelle distribution profile after subcellular fractionation by density gradient centrifugation.

This figure illustrates the subcellular distribution of SMB-PS organelles through a 10 to 20 % density gradient after ultracentrifugation. The data are presented as percentage of organelle in each fraction from 1 (low density) to 22 (high density) including plasma membrane (blue), lysosomes (yellow), Golgi body (red), endoplasmic reticulum (purple) and mitochondria (green).

The new clone of L929 cell line was called LD9 and was susceptible to not only the RML strain but to ME7 and 22L prions.

The LD9 cell line was procured from Dr Sukhvir Mahal to supplement CFCA reactions seeded with the mouse scrapie strain ME7. The LD9 cell line was highly susceptible to ME7 mouse scrapie and was successfully included in the standard scrapie cell assay (SSCA) thus demonstrating that fibroblasts are a valid and valuable cell culture line to study TSE infectivity (Mahal *et al.*, 2007). The SSCA consists of a panel of cell lines grown *ex vivo* that have different susceptibilities to different strains of mouse scrapie. The aim of this assay is to discriminate one strain of mouse scrapie from another within 2 weeks. In addition the SSCA can be used to understand strain variation and strain specific co-factors.

A second cell line that met the selection criteria for the subcellular fractionation of a TSE susceptible cell line with the downstream application of incorporating fractions into *in vitro* refolding assays was the SMB-PS cell line. This cell line was originally isolated from scrapie infected mouse brains and subsequently cured of TSE infection with pentosan polysulphate (Birkett *et al.*, 2001). Historically, this cell line was one of the first cell lines to be grown *ex vivo* and established as a TSE susceptible cell line. The SMB-PS cell line was only until recently revealed to be of microglial origin and is susceptible to a number of mouse scrapie strains including 22F, 79A and 22C. This cell line was fractionated into endoplasmic reticulum, Golgi body, plasma membrane, lysosomes and mitochondria to supplement the CFCA seeded by 22F and 79A.

Subcellular fractionation involves the separation of organelles into distinct fractions. The components of each of the fractions were determined using an array of antibodies that detect unique protein markers associated with each organelle. The murine L929 fibroblast cell line is commonly used in many different experiments out with TSE research. This provided a catalogue of publications to search for organelle markers that already have commercially available antibodies directed against them.

An organelle detector sampler kit (BD Transduction Laboratories) contained an extensive list of antibodies that can be used for examining each organelle. Crucially,

the kit contained the endoplasmic reticulum antibody for BiP/GRP78, the plasma membrane antibody for annexin-II, and the mitochondrial antibody for Bcl-2, which all showed reactivity to the corresponding organelle markers after Western blotting of LD9 and SMB-PS cell lysates. The antibody for the Golgi body marker GM130 and the antibody for the lysosomal marker LAMP1 were investigated by reactivity on a Western blot; however no signal on exposure to photographic film was detected. Further investigation into antibodies directed against Golgi body markers led to the investigation using the antibodies GS28 (Stressgen Bioreagents), 58K (Abcam) and ERGIC53 (Alexis Biochemicals), with all three proving to be ineffective at detecting the Golgi body. Personal communication with Dr Enrico Cancellotti however, confirmed that the Golgi body marker TCP1(23C) was a reliable marker for SMB-PS Golgi. This antibody was successful and I applied this antibody to detect Golgi body in the LD9 fibroblast cell line with success. After the failure of LAMP1 to detect lysosomes, the antibodies for LAMP2 and cathepsin-D were studied for both LD9 and SMB-PS cell lines. Cathepsin-D was completely ineffective and did not give a positive identification by Western blotting. The LAMP2 antibody on the other hand gave a positive identification of the LAMP2 protein in cell lysates of both LD9 and SMB-PS cell lines. Unfortunately, this antibody has a degree of cross reactivity with a number of other proteins resulting in the detection of multiple bands on the blot. Finally, two antibodies were purchased to identify markers associated with endosomes. This organelle forms part of the endosomal pathway and has been implicated in TSE disease (Taraboulos *et al.*, 1992). The cell lysates were probed with the antibodies EEA-1 (BD Transduction Laboratories) and Rab5 (Abcam) with both antibodies proving to be unsuccessful at detecting endosomes within cell lysates. This line of investigation into early endosomal markers was halted due to time and financial constraints. The selection of antibodies for the range of organelles selected at this stage was deemed to be sufficient for the analysis of crude subcellular fractionation. However, future work would include the isolation of early and late endosomes, amongst others, because of the possible involvement of the endocytic pathway in prion conversion (Borchelt *et al.*, 1992, Beranger *et al.*, 2002, Marijanovic *et al.*, 2009).

Homogenisation of cultured cells followed by subcellular fractionation by ultracentrifugation using a density gradient media is an experimental approach for

the isolation of organelles based on their densities. Homogenisation combined with a low speed centrifugation step generated a post nuclear supernatant that contained the cellular constituents. This cellular suspension was then applied to an OptiPrep™ gradient and centrifuged under high *g* forces to separate individual organelle components based on size and density. Fractions were collected from top to bottom and cellular constituents in each fraction were concentrated by methanol precipitation for separation by SDS PAGE. Western blotting onto PVDF membrane followed by immunodetection of organelle markers by relevant antibodies provided the means for analysis of organelle distribution. Western blots were evaluated by densitometric analysis to accurately predict the enrichment of a given organelle within the gradient.

The first critical step in subcellular fractionation is the homogenisation of cellular material to release internal organelles from their compartments. Organelles include nuclei, mitochondria, Golgi body, lysosomes, early and late endosomes, peroxisomes, microsomes and the cytosol. The homogenisation step is critical to produce a homogenate that is a suspension of free and intact organelles. The forces applied to disrupt the cell membrane are required to be adequate to rupture the plasma membrane but not sufficient to break open organelle membranes. Several homogenisation procedures were trialled, with the Potter-Elvehjem homogeniser providing a manual and controllable procedure that generated reproducible levels of membrane disruption. The Potter-Elvehjem homogeniser offered greater stability and reproducibility during the downward strikes of the PTFE pestle than other attempted homogenisation methods.

There are many subcellular fractionation techniques that can be applied to separate organelles from a cellular homogenate. Typically, subcellular fractionation utilises density gradients that are coupled with centrifugation to efficiently separate organelles. However, this conventional method is not without its limits. Often different organelle groups share similar densities, which make separation into homogenous organelle populations problematic.

Other subcellular fractionation methods have been previously described in the literature. Firstly, these include immunoisolation using antibodies to bind to

organelle specific antigens (Howell *et al.*, 1988, Howell *et al.*, 1989). The antibodies are tagged and purification is effected by binding the antibody to magnetic beads prior to retrieval. Secondly, organelles can be separated by the characteristic charge density associated with membrane bound particles (Heidrich and Dew, 1976). Different organelles display differences in the composition of charged surface molecules and when subjected to an electric current, will influence electrophoretic mobility. This method is known as free flow electrophoresis (FFE) and has been effectively used as a preparative technique in combination with other fractionation techniques (Marsh *et al.*, 1987). FFE has since been modified to incorporate a density gradient that is separated by two electrodes and offers high resolution of charged organelles (Tulp *et al.*, 1993). Both FFE and density gradient electrophoresis (DGE) have only been used successfully for organelles in the endosomal pathway. The current method of crude subcellular fractionation provided a method for producing fractions that have been enriched for different organelles. This method satisfied the aim: to analyse the effect of a range of fractions containing different constituents and correlate conversion efficiency with organelle distribution. The knowledge that further organelle purification is possible is something to consider for future experiments that would require more refined samples.

The isolation of subcellular compartments provided enriched samples for input into the CFCA. It was hypothesised that some fractions would contain the necessary factors, proteinaceous or non-proteinaceous, to increase efficiency of PrP^{Sc} to convert rMoPrP to a PK-res isoform *in vitro*. The results on the addition of LD9 and SMB-PS fractions to the CFCA in the presence of different seeds is analysed and discussed in chapter 4.

4. The addition of subcellular fractions from TSE susceptible cell lines to the cell free conversion assay

4.1 Introduction

The hypothesis of the project was to identify co-factors that interact with PrP^{C} and/or PrP^{Sc} during prion conversion, which may provide a mechanism of strain differentiation. Subcellular fractionation of TSE susceptible cell lines, as described in chapter 3, provided enriched subcellular organelle samples for the analysis of co-factors in the CFCA. It was hypothesised that subcellular fractions would provide the necessary co-factors required by different strains of mouse scrapie to convert rMoPrP to a PK-resistant isoform in an *in vitro* system.

The CFCA is the primary assay used in this project to analyse samples for potential PrP conversion-enhancing properties. The assay was originally designed to use ^{35}S-labelled rPrP purified from cell culture as a substrate and entailed a 48 hour incubation with a PrP^{Sc} seed at 37 °C (Kocisko *et al.*, 1994). Over 48 hours, the PrP^{Sc} seed converts the rPrP substrate into a PK-resistant isoform. Treatment with proteinase-K generates a PK-resistant fragment that can be resolved using SDS PAGE and assessed by Western blotting. Previous publications on the CFCA have documented replication of the species barrier, strain properties and conversion efficiency of polymorphic variants of PrP (Kocisko *et al.*, 1995, Bessen *et al.*, 1995, Bossers *et al.*, 1997, Raymond *et al.*, 1997, Bossers *et al.*, 2000, Horiuchi *et al.*, 2000).

Successful modifications to this assay involve incorporation of rMoPrP purified from bacteria and use of an incubation buffer that omits any denaturant (Kirby *et al.*, 2003). The rMoPrP contains the hamster epitope 3F4 (tetra-peptide: Met-Lys-His-Met, between residues 109-112), which allows for the specific identification of protease-resistant isoforms of rMoPrP that have been converted by the murine SAF seed. These modifications make the assay more physiological and therefore a better *in vitro* model for prion conversion. This version of the CFCA was capable of mimicking the species barrier and in addition was also inhibited by Congo red analogues, a known inhibitor of PrP conversion (Kirby *et al.*, 2003). Recently, the CFCA was used to study the effect of a novel ovine polymorphism that was associated with resistance to scrapie and BSE transmission (Kirby *et al.*, 2006). The ovine PrP variant $ARL^{168}Q$ was resistant to conversion in the CFCA, displaying

similar resistance characteristics to the resistance-associated ovine variant, ARR. The CFCA therefore represents an ideal model to analyse the effect of subcellular fractions from TSE susceptible cell lines on conversion.

TSE susceptible cell lines offer a valuable resource for the *in vitro* analysis of potential prion co-factors. The cell lines LD9 and SMB-PS form the basis for this project due to the unique characteristics of both cell lines. The cell line LD9 is of fibroblastic origin and has only recently been cloned from the L929 fibroblast cell line (Mahal *et al.*, 2007). Mahal and co-workers described the successful incorporation of LD9 cells into the standard scrapie cell assay (SSCA) and demonstrated variability in susceptibility to different prion strains. The LD9 fibroblast was derived from the L929 fibroblast cell line by serial cloning against RML infection. The LD9 cell line and other non-neuronal cell lines have proved to be surprisingly susceptible to prion infection and have added to the arsenal of cellular models of TSE infection.

The SMB cell line was derived by culturing, *ex vivo*, mouse brains infected with the mouse scrapie strain Chandler (Clarke and Haig, 1970). Subsequent cloning of the cell line produced cells that were stably TSE infected. The SMB cell line has since been cured by incubation with pentosan sulphate (PS) and the cured cell line, SMB-PS, is susceptible to multiple strains of mouse scrapie (Birkett *et al.*, 2001, personal communication with Ruth Hennion). Table 1.3 illustrates the variety of mouse scrapie strains that can infect the SMB-PS cell line in an acute or persistent manner. This brain derived cell line is selectively susceptible, depending on the strain of mouse scrapie and therefore was a suitable and relevant model to investigate for the presence of co-factors.

4.2 Proteinase K Digest of Scrapie Associated Fibrils

The CFCA requires a PrP^{Sc} seed to convert the rMo3F4PrP substrate into a PK-resistant isoform. In this study I isolated scrapie associated fibrils from infected mice and this process required verification to determine the success of purification and validation of the identity of the scrapie strain. Scrapie associated fibrils for four different mouse scrapie strains (87V, ME7, 79A and 22F) were isolated from

infected mouse brains by detergent separation and differential centrifugation as described in chapter 2 using methods described by Hope *et al.*, (1986). The presence of PrP^{Sc} was confirmed by treatment of the sample with PK, which after Western blotting reveals the characteristic three bands associated with di-, mono- and unglycosylated PrP^{res}. Treatment with PK cleaves the N-terminus of PrP^{Sc} resulting in isoforms that are detectable by Western blotting with the PrP C-terminus antibody, 8H4. Densitometric analysis yields the relative amount of PrP^{Sc} as well as the ratio of diglycosylated to monglycosylated to unglycosylated for each mouse scrapie strain. Figure 4.1 shows the differential occupation of glycosylation sites of 79A, ME7, 87V and 22F when compared against each other. Densitometric analysis of these allowed comparison of the relative proportions of the three glycosylation states for each of the four strains. Values are a percentage of the total PK-resistant core of PrP^{Sc} and are shown in table 4.1. The values for glycosylation states are consistent with previous publications (Somerville *et al.*, 1997, Kuczius *et al.*, 1998).

4.3 Cell free conversion assay with different mouse scrapie seeds

The cell free conversion assay traditionally used the mouse scrapie strain 87V as a seed for which there are multiple publications illustrating the successful conversion of recombinant mouse PrP when using this strain (Kocisko *et al.*, 1994, Wong *et al.*, 2001, Kirby *et al.*, 2003, Eiden *et al.*, 2006). In order to demonstrate that other strains could be used, SAF preparations for ME7, 79A and 22F were added to the CFCA at a PrP^{Sc} concentration of 1 µg/µl. Figure 4.2 shows the different conversion efficiencies of four different mouse scrapie strains to convert recombinant mouse 3F4 PrP (rMo3F4PrP) to a PK-resistant isoform. Briefly, after rMo3F4PrP was incubated with a mouse-adapted scrapie seed at 37 °C for 24 hours, $19/20^{th}$ of the reaction volume was treated with PK (abbreviated to +PK) and the remaining $1/20^{th}$ was not treated (abbreviated to -PK). Proteins in both samples were resolved using SDS PAGE and assay products detected by Western blotting with the Syrian hamster antibody 3F4. Proteolytic treatment of the conversion reaction shows a ~ 17 kDa which represents the protease-resistant core of PrP^{Sc}. Densitometric analysis of the intensity of the bands representing +/- PK treated samples provided data on the amount of rMo3F4PrP converted to a PK-resistant isoform by the particular strain of mouse scrapie tested (figure 4.2). Typically, 87V, ME7, 79A and 22F strains of

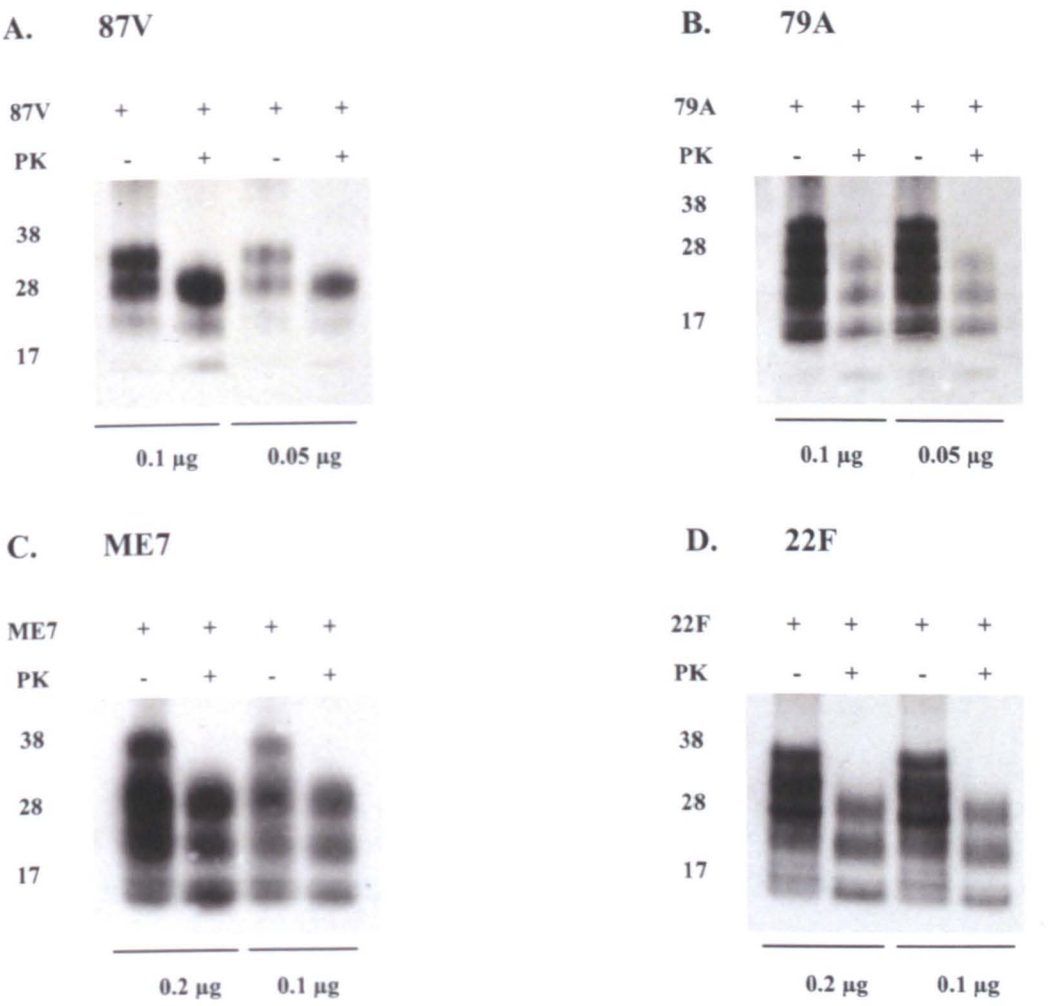

Figure 4.1: Proteinase K digestion of scrapie associated fibrils for multiple strains.

Scrapie associated fibrils were isolated from scrapie infected mouse brains and SAF preparations were treated with and without PK. Samples were serially diluted and separated by SDS PAGE. Western blotting was carried out by use of the murine prion antibody 8H4: (A) 87V fibrils treated with (+) and without (-) PK. Lane 1 and lane 2 have a $1/10^{th}$ dilution of the sample and lane 3 and lane 4 have $1/20^{th}$ dilution of the sample. (B) 79A fibrils treated with (+) and without (-) PK. Lane 1 and lane 2 have a $1/5^{th}$ dilution of the sample and lane 3 and lane 4 have $1/10^{th}$ dilution of the sample. (C) ME7 fibrils treated with (+) and without (-) PK. Lane 1 and lane 2 have a $1/10^{th}$ dilution of the sample and lane 3 and lane 4 have $1/20^{th}$ dilution of the sample. (D) 22F fibrils treated with (+) and without (-) PK. Lane 1 and lane 2 have a $1/4^{th}$ dilution of the sample and lane 3 and lane 4 have $1/8^{th}$ dilution of the sample.

	Diglycosylated	Monoglycosylated	Unglycosylated
87V	76 %	20 %	4 %
79A	19 %	37 %	34 %
ME7	35 %	37 %	21 %
22F	51 %	32 %	17 %

Table 4.1: Glycoform ratio of different mouse scrapie isolates.

The ratio of the three protease-resistant PrP glycoforms in four different strains of mouse scrapie. Data represents the mean relative proportions of di-, mono- and un-glycosylated PrP as a percentage for 87V, 79A, ME7 and 22F. Total percentage of the glycoforms of 87V and 22F equal 100 %, however 79A and ME7 equal 90 % and 93 %, respectively. This is because 79A and ME7 have a protease-resistant isoform of lower molecular weight that corresponds to a truncated isoform of PrP^{Sc}.

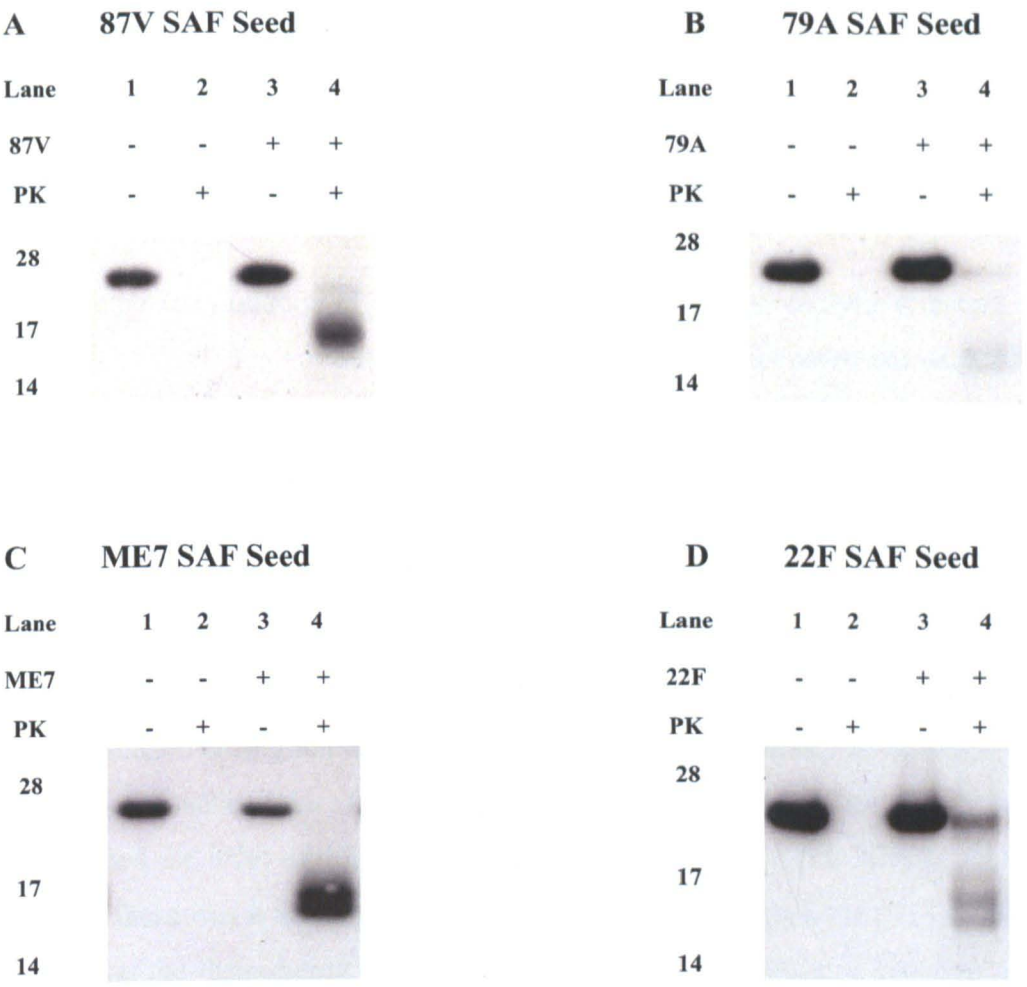

Figure 4.2: Cell free conversion assay with four different mouse scrapie seeds.

200 ng rMo3F4PrP with 1 µg of mouse adapted scrapie associated fibrils in conversion buffer for 24 hours at 37 °C. From this, the reaction volume was divided into +PK sample (lane 4) and –PK sample (lane 3). Both samples were separated by SDS PAGE and assessed by Western blotting with the Syrian hamster antibody, 3F4. A control experiment involved the incubation of 200 ng rMo3F4PrP with no mouse scrapie associated fibrils in conversion buffer for 24 hours at 37 °C. This was done for four mouse adapted scrapie strains; (A) detection of 87V converted products (B) detection of 79A converted products (C) detection of ME7 converted products (D) detection of 22F converted products.

mouse scrapie convert 20 %, 18 %, 3.5 % and 2.5 % of the rMo3F4PrP substrate, respectively.

4.4 Optimisation of the addition of exogenous material to the CFCA

Subcellular fractionation of cells will inevitably release proteolytic enzymes that are used by the cell for various functions. In particular, lysosomes are organelles that contain the majority of cellular acid hydrolases that destroy engulfed foreign particles, excess proteins and damaged organelles (De Duve and Wattiaux, 1966, Holtzmann, 1989). In preliminary experiments the addition of total LD9 cell homogenates to the CFCA degraded the recombinant PrP substrate as indicated by no signal on the membrane after Western blotting (data not shown). This was presumably due to the presence of proteases that had been released by lysosomes that were damaged during homogenisation. To counteract the effect of proteases in future analyses of subcellular fractions, serial dilution of the LD9 cell homogenate established the level of dilution required prior to addition to the CFCA. At a 1/4000 dilution there was a minimal degree of proteolytic activity within the sample. Figure 4.3 shows the degradation effect of proteases when recombinant PrP was incubated with serial dilutions of LD9 cell homogenate. To protect the CFCA substrate from proteases would require the inclusion of protease inhibitors in the subcellular fractions. However this was not possible due to the PK treatment included later on in the CFCA protocol. Analogous experiments involving the incubation of rMo3F4PrP with SMB-PS homogenates suggested significantly lower levels of proteolytic activity (data not shown).

To discount the effect of any endogenous PrP in these cell lines, I assessed PrP^C content and distribution by Western blotting with an ant-PrP antibody (8H4, appendix 1). Assessment of PrP distribution against a $rMoPrP^{WT}$ control of known concentration showed that endogenous PrP^C was negligible.

4.5 Addition of exogenous material to the CFCA

The subcellular fractionation of TSE susceptible cell lines provided samples that were added to the CFCA, for which conversion efficiency was monitored by

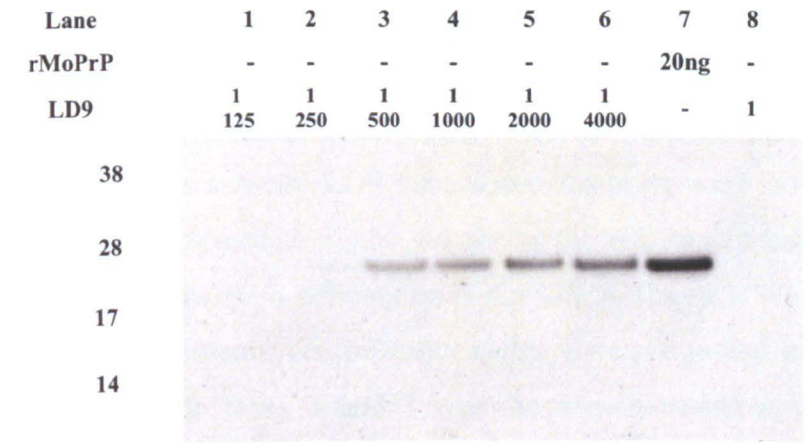

Figure 4.3: Incubation of recombinant mouse 3F4 PrP with LD9 cell lysates.

Incubation of 20 ng recombinant Mo3F4PrP with serial dilutions of LD9 cell lysate for 24 hours at 37 °C followed by SDS PAGE and Western blotting. Serial dilutions of cell lysates comprise of 1/125 (lane 1), 1/250 (lane 2), 1/500 (lane 3), 1/1000 (lane 4), 1/2000 (lane 5) and 1/4000 (lane 6) of one confluent T75 tissue culture flask of LD9 cells. Lane 7 shows 20 ng of rMo3F4PrP and lane 8 shows the absence of any rMo3F4PrP in a LD9 cell lysate.

densitometric analysis of Western blots. Due to the susceptibility of TSE susceptible cell lines to specific prion strains, they were hypothesised to contain the necessary strain specific co-factors required for the conversion of PrP^{C} to PrP^{Sc}. The LD9 cell line is susceptible to ME7 infection and the SMB-PS cell line is susceptible to 79A infection. The subcellular fractionation of LD9 and SMB-PS cell lines was covered in chapter 3, which describes the generation of fractions that were enriched for different organelle subsets. LD9 subcellular fractions were initially added to the assay using ME7 as a seed. Figure 4.4 shows the effects of those different fractions of LD9 had on conversion efficiencies in the CFCA. On each Western blot generated from CFCA experiments, control experiments were positioned in lanes 1 to 4 of the SDS PAGE gel. In lanes 1 and 2 was the negative control CFCA whereby the substrate, rMo3F4PrP, was incubated at 37 °C for 24 hours in the absence of a mouse scrapie seed. In lanes 3 and 4 was the positive control whereby the reaction was complete with substrate and seed but in the absence of any subcellular fraction. Lane 4 contained the +PK sample of one assay and demonstrated the amount of conversion i.e. the ~ 17 kDa band, that was anticipated when in the absence of any subcellular fractions. Upon the addition of LD9 subcellular fractions to the CFCA, the conversion efficiency of ME7 in these new conditions was monitored by comparing against the positive control PK-resistant product in lane 4. To aid in this comparison, the samples were arranged in adjacent lanes of the gel prior to SDS PAGE.

4.5.1 Addition of LD9 subcellular material to the CFCA seeded with ME7

In figure 4.4 (panels A to E) the effect of the addition of LD9 fractions 1 to 22 on the conversion of rMo3F4PrP by ME7 in the CFCA is shown. Panel A illustrates that upon the addition of LD9 fractions 1 to 5, which are enriched for plasma membrane (figure 3.6), there is an increase in the amount of rMo3F4PrP converted to a PK-resistant isoform (lanes 5 to 9) when compared against the positive control in lane 4. Panels B and C however, show the degradation of the rMo3F4PrP substrate by cellular proteases. This was deduced from the reduction in conversion followed by almost the complete absence of conversion, when in the presence of LD9 fractions 8 to 13. However, more crucially, it was observed that the -PK samples exhibit bands that are either noticeably less dense or are absent. This clearly suggested that the substrate had been depleted and this was likely to be from the presence of cellular

Figure 4.4: The addition of LD9 subcellular fractions to the CFCA that was seeded with ME7.

200 ng rMo3F4PrP was incubated with 1 μg ME7 scrapie associated fibrils in conversion buffer for 24 hours at 37 °C. From this, the reaction volume was divided into +PK sample (lane 3) and –PK sample (lane 4). Both samples were assayed by separation on SDS PAGE and assay products detected by Western blotting and probing with Syrian hamster antibody 3F4.

(**A**) The CFCA was supplemented with LD9 fractions 1 to 5 for which +PK and -PK samples were taken from each of the five assays. Samples treated with PK are in lanes 5-9 (fractions 1-5) and the corresponding samples that were not treated with PK are in lanes 10 - 14 (fractions 1-5).

(**B**) The CFCA was supplemented with LD9 fractions 6 to 10 for which +PK and -PK samples were taken from each of the five assays. Samples treated with PK are in lanes 5-9 (fractions 6-10) and the corresponding samples that were not treated with PK are in lanes 10-14 (fractions 6-10).

(**C**) The CFCA was supplemented with LD9 fractions 11 to 15 for which +PK and -PK samples were taken from each of the five assays. Samples treated with PK are in lanes 5-9 (fractions 11-15) and the corresponding samples that were not treated with PK are in lanes 10-14 (fractions 11-15).

(**D**) The CFCA was supplemented with LD9 fractions 16 to 20 for which +PK and -PK samples were taken from each of the five assays. Samples treated with PK are in lanes 5-9 (fractions 16-20) and the corresponding samples that were not treated with PK are in lanes 10-14 (fractions 16-20).

(**E**) The CFCA was supplemented with LD9 fractions 21 and 22 for which +PK and -PK samples were taken from each of the five assays. Samples treated with PK are in lanes 5 and 6 (fractions 21 and 22) and the corresponding samples that were not treated with PK are in lanes 7 and 8 (fractions 21 and 22).

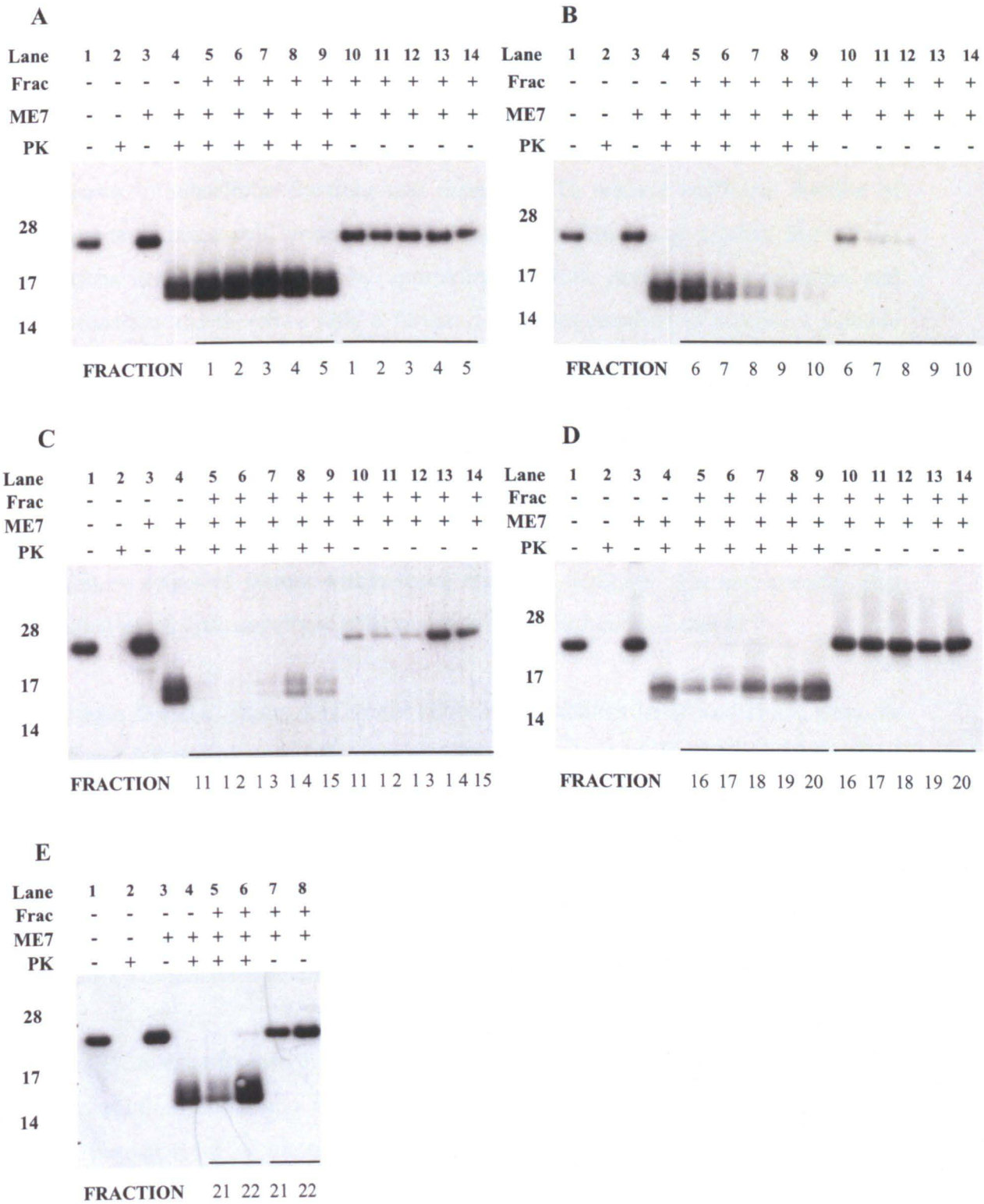

Figure 4.4: The addition of LD9 subcellular fractions to the CFCA that was seeded with ME7.

proteases in subcellular fractions 8 to 13. To observe the effect of LD9 fractions 7 to 13 on the conversion efficiency of ME7 required the dilution of these fractions to a point where protease activity was negligible. Earlier in this chapter, under optimisation of the addition of exogenous material (section 4.4), the presence of proteases in subcellular fractions was discussed. To achieve sufficient dilution of proteases within a cell lysate required a minimum dilution of 1/2000. Subcellular fractions are already diluted by approximately 1/10 during homogenisation and fractionation and therefore only a further 1/200 was required to achieve a suitable protease activity dilution. These fractions were diluted appropriately in dH_2O prior to addition to the CFCA and the results are illustrated in figure 4.5. These data at the dilutions used indicate that the rMo3F4PrP substrate was not degraded by cellular proteases. Conversion efficiency of ME7 in the presence of LD9 fractions 8 to 13 were slightly reduced when compared to the positive control. This could be due to an inhibitory effect of factors within these fractions, however it is also possible that residual proteolytic activity is still present in the LD9 fractions added.

In panels D and E (figure 4.4) are the subcellular fractions 16-20 and 21-22, from the LD9 cell line added to an ME7-seeded CFCA. Fractions 16 and 17 appeared to give a reduction in conversion efficiency however this could be attributed to the presence of proteases. However, fractions 18 to 20 appear to have no discernible effect on the conversion efficiency of ME7. Finally, in panel E, the subcellular fractions 21 and 22 were also added to the ME7-seeded CFCA, which also showed no discernible effect on ME7 conversion efficiency.

The CFCA experiments that were supplemented with LD9 fractions 1 to 22 were repeated four times and this allowed for the standard deviation and statistical significance to be calculated. Densitometric analysis of the Western blots associated with the addition of LD9 subcellular fractions was presented in a bar chart format (figure 4.6) which allowed for easier analysis of the results.

4.5.2 Addition of SMB-PS subcellular material to the CFCA seeded with 79A

In section 4.4 I have shown that the conversion efficiency of the ME7 strain of mouse scrapie was enhanced by low density subcellular fractions from the LD9

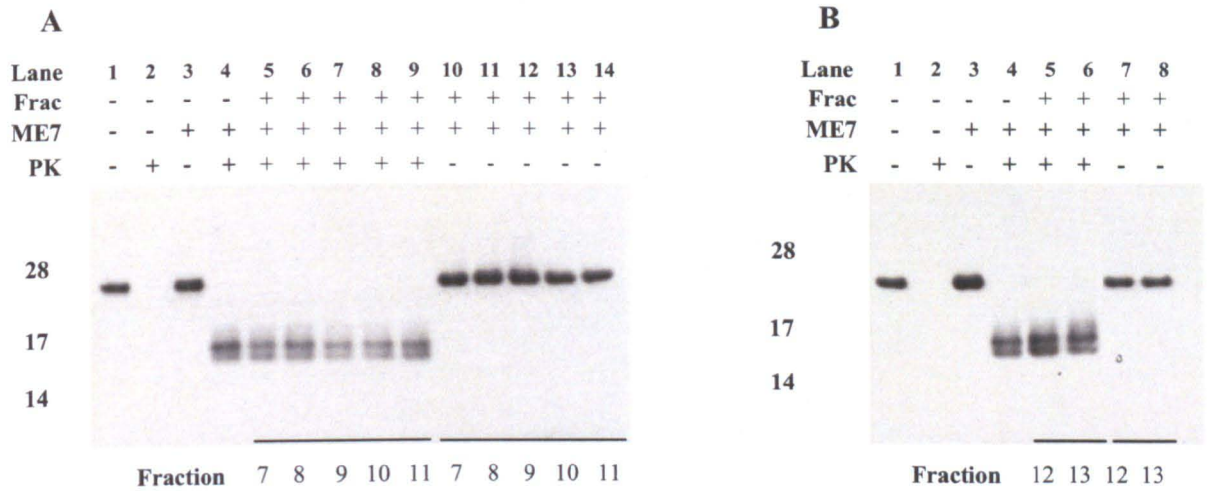

Figure 4.5: The addition of diluted LD9 subcellular fractions 8 to 13 to the CFCA that was seeded with ME7.

200 ng rMo3F4PrP was incubated with 1 µg ME7 scrapie associated fibrils in conversion buffer for 24 hours at 37 °C. From this, the reaction volume was divided into +PK sample (lane 3) and –PK sample (lane 4). Both samples were assayed by separation on SDS PAGE and assay products detected by Western blotting and probing with Syrian hamster antibody 3F4. (A) The CFCA was supplemented with LD9 fractions 7-11 for which +/-PK samples were taken from each of the five assays for treatment with and without PK, respectively. Samples treated with PK are in lanes 5-9 (fractions 7-11) and the corresponding samples that were not treated with PK are in lanes 10-13 (fractions 7-11). (B) The CFCA was supplemented with LD9 fractions 12 and 13 for which +/-PK samples were taken from each of the five assays for treatment with and without PK, respectively. Samples treated with PK are in lanes 5 and 6 (fractions 12 and 13) and the corresponding samples that were not treated with PK are in lanes 7 and 8 (fractions 12 and 13).

Figure 4.6 Relative conversion percentage of ME7 in the CFCA when in the presence of LD9 subcellular fractions 1 to 22.

The ME7-seeded CFCA was supplemented with LD9 fractions 1 to 22 for which +/- PK samples were taken. SDS PAGE and Western blotting of these samples with the Syrian hamster monoclonal antibody, 3F4, allows for densitometric measurements on conversion efficiency of ME7 in the presence of different subcellular fractions of the LD9 cell line. Relative conversion percentage in the presence of subcellular fractions was calculated using the control ME7 seeded CFCA without any subcellular fractions added as 100 % conversion. This is represented by a black line at 100 % relative conversion. Data points are displayed as a bar chart ± SEM with the percentage of total plasma membrane marker, annexin-II, in fractions 1 to 5 indicated. A one-sample t-test was applied to compare the significance of the change in conversion percentage against 100 % conversion efficiency of ME7 in the absence of any added subcellular fractions (* represents a significant difference from the positive control).

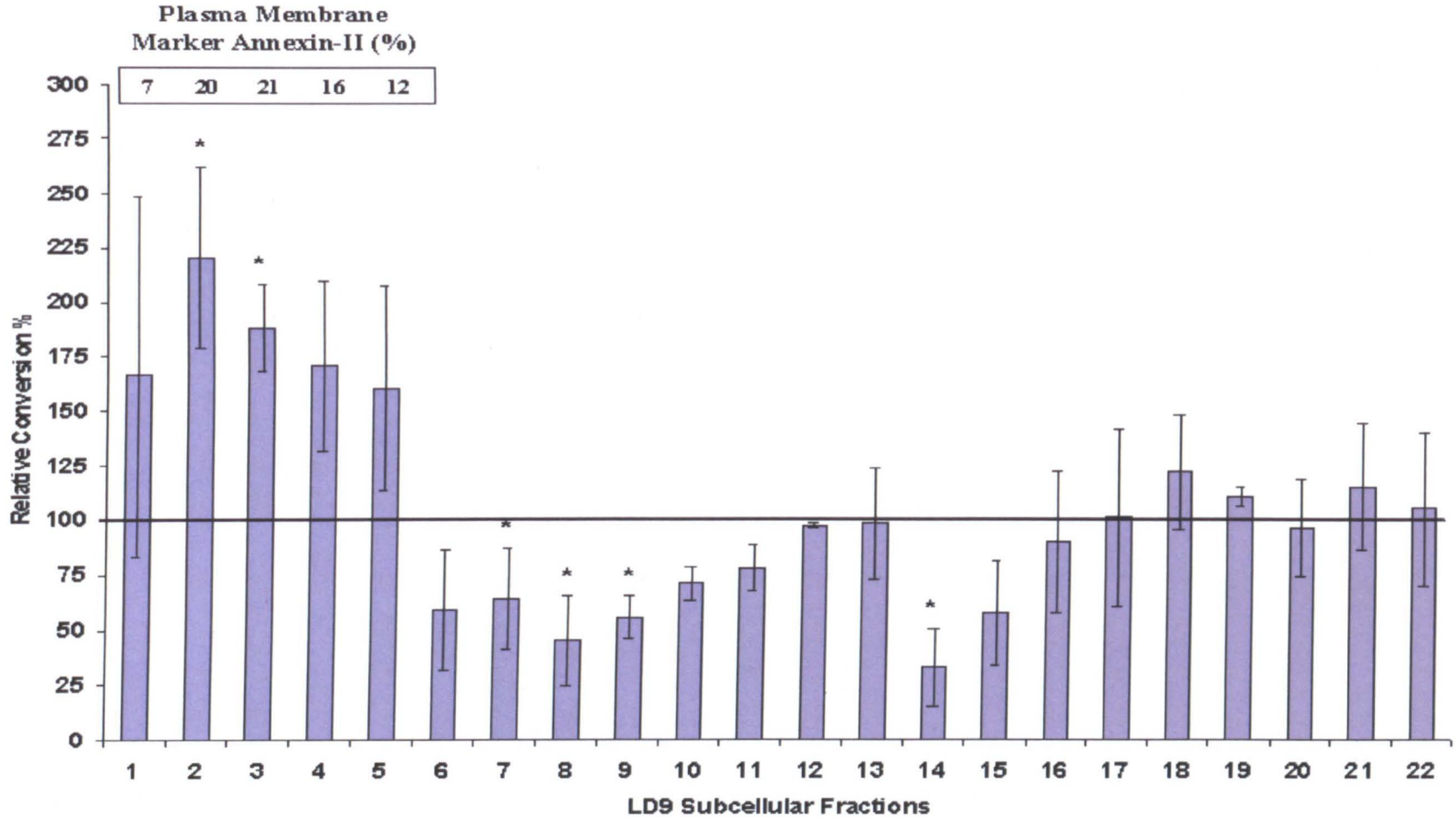

Figure 4.6 Relative conversion percentage of ME7 in the CFCA when in the presence of LD9 subcellular fractions 1 to 22.

Figure 4.7: The addition of SMB-PS subcellular fractions to the CFCA that was seeded with 79A.

200 ng rMo3F4PrP with 1 μg 79A scrapie associated fibrils in conversion buffer for 24 hours at 37 °C. From this, the reaction volume was divided into +PK sample (lane 3) and –PK sample (lane 4). Both samples were assayed by separation on SDS PAGE and assay products detected by Western blotting and probing with Syrian hamster antibody 3F4.

(A) The CFCA was supplemented with SMB-PS fractions 1 to 5 for which +PK and -PK samples were taken from each of the five assays. Samples treated with PK are in lanes 5-9 (fractions 1-5) and the corresponding samples that were not treated with PK are in lanes 10-14 (fractions 1-5).

(B) The CFCA was supplemented with SMB-PS fractions 6 to 10 for which +PK and -PK samples were taken from each of the five assays. Samples treated with PK are in lanes 5-9 (fractions 6-10) and the corresponding samples that were not treated with PK are in lanes 10-14 (fractions 6-10).

(C) The CFCA was supplemented with SMB-PS fractions 11 to 15 for which +PK and -PK samples were taken from each of the five assays. Samples treated with PK are in lanes 5-9 (fractions 11-15) and the corresponding samples that were not treated with PK are in lanes 10-14 (fractions 11-15).

(D) The CFCA was supplemented with SMB-PS fractions 16 to 20 for which +PK and -PK samples were taken from each of the five assays. Samples treated with PK are in lanes 5-9 (fractions 16-20) and the corresponding samples that were not treated with PK are in lanes 10-14 (fractions 16-20).

(E) The CFCA was supplemented with SMB-PS fractions 21 and 22 for which +PK and -PK samples were taken from each of the five assays. Samples treated with PK are in lanes 5 and 6 (fractions 21 and 22) and the corresponding samples that were not treated with PK are in lanes 7 and 8 (fractions 21 and 22).

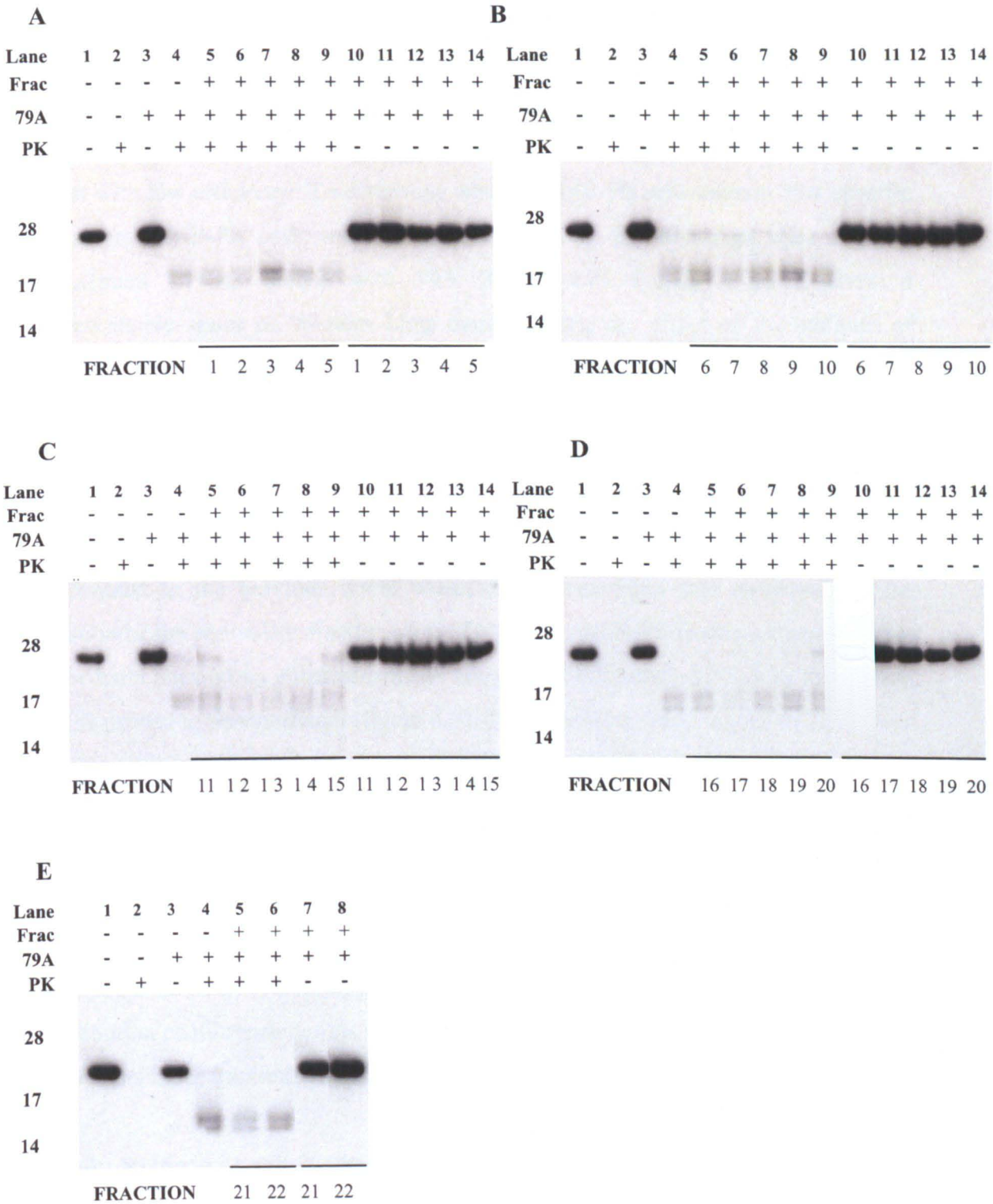

Figure 4.7: The addition of SMB-PS subcellular fractions to the CFCA that was seeded with 79A.

cell line. However, were these results repeatable using a different strain of mouse scrapie in the CFCA and a corresponding susceptible cell line, or would a different set of subcellular fractions enhance conversion? As shown in figure 4.2, the 79A strain of mouse scrapie converts rMo3F4PrP *in vitro* into a PK-resistant isoform, albeit with low efficiency. To determine whether SMB-PS cells contain 79A specific co-factors, SMB-PS cells were fractionated into 22 fractions that were used to supplement CFCAs seeded with 79A (figure 4.7). Panels A to E show a representative series of Western blots demonstrating the effect of the addition of SMB-PS fractions 1 to 22 on conversion of rMo3F4PrP by 79A in the CFCA. Densitometric analysis of these results highlighted that the inclusion of fractions 1 to 5 to the CFCA caused a decrease in the conversion efficiency of 79A. This was repeated seven times and averaged densitometry values for this highlighted that for fraction 2 and 3 there was a significant reduction in conversion efficiency. This was in contrast to the previous result where ME7 conversion was increased by the addition of the equivalent fractions from LD9 cells. SMB-PS fraction 8 and 9 on the other hand showed an enhancement on conversion efficiency of 79A in the CFCA, which proved to be significant (figure 4.8). The remaining fractions, 10 to 22 showed variable effects on conversion with fractions 11, 12, 15, 17 and 19 in particular showing a significant decrease in conversion efficiency. Densitometry values for fractions 6 to 22 were averaged from three replicate experiments. Densitometric values for fractions 6 to 11 was suggestive of a normal distribution profile for increasing conversion efficiency, with the apex of the distribution showing a significant increase in conversion by the addition of fractions 8 and 9. This normal distribution profile matches the distribution of Golgi body within the density gradient after subcellular fractionation of a SMB-PS homogenate (figure 3.9).

Finally fractions 21 and 22 show an increase on conversion efficiency however this effect was not statistically significant after applying a one-sample t-test. Fractions 21 and 22 contained a wide spectrum of constituents that ranged from cell debris to heavy mitochondria. This precipitate at the bottom of the ultracentrifuge tube is therefore likely to contain a variable range of conversion enhancing factors. The data from these two fractions are variable due to the differing amounts of precipitate present in each preparation which could not be controlled.

Figure 4.8 Relative conversion percentage of 79A in the CFCA when in the presence of SMB-PS subcellular fractions 1 to 22.

The 79A seeded CFCA was supplemented with SMB-PS fractions 1 to 22 for which +/-PK samples were taken from each of the five assays for treatment with and without PK, respectively. SDS PAGE and Western blotting of these samples with the Syrian hamster monoclonal antibody, 3F4, allows for densitometric measurements on conversion efficiency of 79A in the presence of different subcellular fractions of the SMB-PS cell line. Relative conversion percentage in the presence of subcellular fractions was calculated using the control 79A seeded CFCA without any subcellular fractions added as 100 % conversion. This is represented by a black line at 100 % relative conversion. Data points are displayed as a bar chart ± SEM with the percentage of total Golgi body marker, TCP1(23C), in fractions 6 to 11 indicated.. A one-sample t-test was applied to compare the significance of the change in conversion percentage against 100 % conversion efficiency of 79A in the absence of any added subcellular fractions (* represents a significant difference against the positive control).

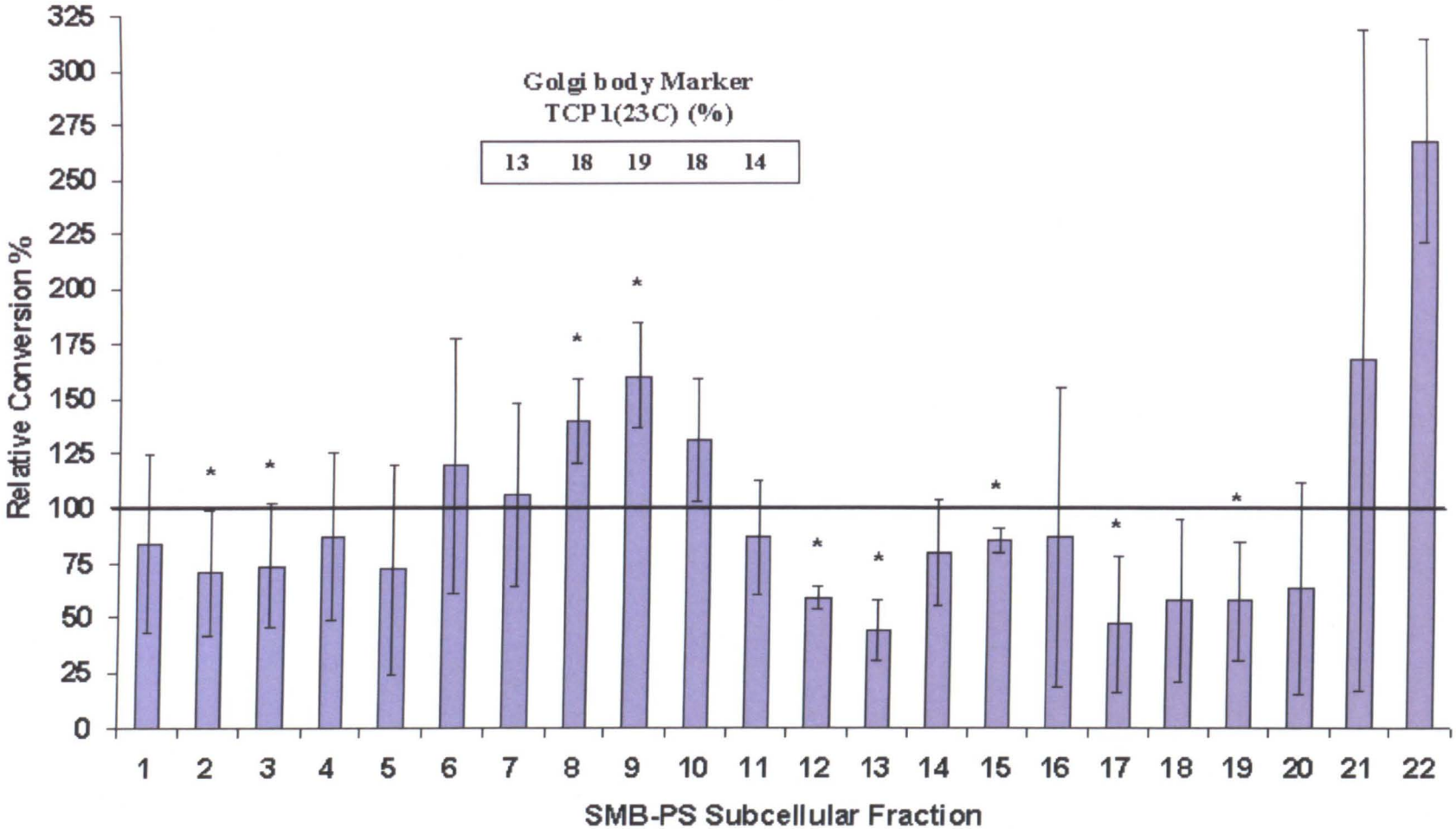

Figure 4.8: Relative conversion percentage of 79A in the CFCA when in the presence of SMB-PS subcellular fractions 1 to 2.

4.6 Mass spectrometric analysis of LD9 low density subcellular fractions

The ME7-seeded CFCA was supplemented with subcellular fractions from the ME7 susceptible cell line LD9, for which fractions 1 to 5 (plasma membrane enriched) enhanced ME7 conversion. Subcellular fractionation of the LD9 cell line in a 10-20 % OptiPrep™ gradient produced discrete fractions that were enriched for different compartments of the cell. The low density fractions which enhanced conversion were positive for the plasma membrane marker annexin-II as assessed by Western blotting (figure 3.6). To validate the presence of the LD9 plasma membrane-specific proteins in these fractions, samples were reduced and alkylated prior to trypsinisation and tryptic peptides were then processed for proteomic analysis by Q-ToF mass spectrometry.

Mass spectrometric analysis of fraction 3 (highest enrichment of plasma membrane) from the subcellular fractionation of a LD9 homogenate provided a list of 42 positive protein identifications as shown in table 4.2. Of these 42 protein identifications, there were 27 cytoplasmic proteins, 4 plasma membrane proteins, 4 secretory proteins, 3 cytoskeletal proteins and one protein ID each from the mitochondrial, lysosomal and ribosomal proteins. There is an abundance of cytoplasmic proteins in LD9 fraction 3, however this fraction was originally believed to be enriched for plasma membrane as assessed by Western blotting (figure 3.6). It is known that plasma membrane proteins are problematic to analyse by mass spectrometry (Mirza *et al.*, 2007). Plasma membrane derived proteins interact with the lipid bilayer and as such have very strong hydrophobic and hydrophilic regions making them difficult to solubilise and analyse using this technique (Santoni *et al.*, 2000). The protocol for mass spectrometry sample preparation that was used incorporates established techniques that increase plasma membrane protein extraction and solubilisation i.e. inclusion of a methanol precipitation step increases protein extraction from the lipid bilayer and solubilisation of the precipitate in a urea-ammonium bicarbonate buffer helps to solubilise more membrane associated proteins. Whilst these steps help to improve the detection of plasma membrane proteins using mass spectrometry, coverage is not always comprehensive. Nevertheless, the presence of at least four plasma membrane proteins suggests that there is LD9 plasma membrane present in fraction 3.

Protein ID	Gene ID	Subcellular Location	Peptides
Actin, cytoplasmic 1	Actb	Cytoplasm	20
Tubulin alpha 1b chain	Tuba1b	Cytoplasm	12
Tubulin beta 2c chain	Tubb2c	Microtubules	12
Tubulin beta 5 chain	Tubb5	Microtubules	3
Heat shock cognate 71 kDa protein	Hspa8	Cytoplasm	13
Heat shock 70 kDa protein 4	Hspa4	Cytopalsm	2
Heat shock protein HSP 90-alpha beta	Hsp90ab1	Mitochondria	14
Heat shock protein HSP 90-alpha	Hsp90aa1	Cytoplasm	3
Peptidyl-prolyl cis-trans isomerise	Ppia	Cytoplasm	4
Peroxiredoxin-6	Prdx6	Lysosome	4
Alpha-enolase	Eg433182	Cytoplasm	11
Aspartate aminotrasferase	Got1	Cytoplasm	4
Triosephosphate isomerise	Tpi1	Cytoplasm	7
14-3-3 protein theta	Ywhaq	Cytoplasm	2
14-3-3 protein zeta/delta	Ywhaz	Cytoplasm	7
Isoform long of 14-3-3 protein beta/alpha	Ywhab	Cytoplasm	3
Isoform 1 of gelsolin	Gsn	External matrix	6
Isoform 1 of Rab GDP	Gdi2	Plasma membrane	3
Eukaryotic translation initiation factor 4b	Eif4b	Ribosomes	2
D-3-phosphoglycerate dehydrogenase	Phgdh	?	3
Phosphoglycerate mutase	Pgam1	Cytoplasm	4
Phosphoglycerate kinase 1	Pgk1	Cytoplasm	7
Glutathione Transferase omega-1	Gsto1	Cytoplasm	3
Farnesyl pyrophosphate synthetase	Fdps	Cytoplasm	4
Rho GDP-dissociation inhibitor 1	Arhgdia	Cytoplasm	6
Rho GDP-dissociation inhibitor 2	Arhgdib	Cytoplasm	3
Annexin A1	Anxa1	Plasma membrane	2
Annexin A3	Anxa3	Plasma membrane	2
Annexin A5	Anxa5	Extracellular matrix	5
Fascin	Fscn1	Cytoplasm	3
Galectin-1	Lgals1	Extracellular matrix	3
Nucleoside diphosphate kinase B	Nme2	Plasma membrane	2
Glyceraldehyde-3-phosphate dehydrogenase 1	Gapdh	Cytoplasm	4

Table 4.2: Identification of peptides detected by mass spectrometric analysis of LD9 fraction 3.

Protein ID	Gene ID	Subcellular Location	Peptides
Aldose reductase	Akr1b3	Cytoplasm	4
Ubiquitin-like modifier-activiating enzyme 1	Uba1	Cytoplasm	4
Alpha-actinin-4	Actn4	Cytoskeleton	2
Serpin B6	Serpinb6a	Cytoplasm	2
GTP-binding nuclear protein Ran	Ran	Cytoplasm	2
Lactoglutathione lyase	Glo1	Cytoplasm	2
Malate dehydrogenase, cytoplasmic	Mdh1	Cytoplasm	3
Isoform 1 of Sorcin	Sri	Cytoplasm	2
Slit homolog 2 protein	Slit2	Extracellular matrix	2

Table 4.2 continued: Identification of peptides detected by mass spectrometric analysis of LD9 fraction 3.

List of protein identifications that were detected in a LD9 plasma membrane enriched fraction (fraction 3). A minimum of two peptide identifications by Mascot were required to confirm significant protein identification.

4.7 Specificity of low density fractions to increase conversion efficiency on the CFCA

The results from the ME7-seeded CFCA experiments supplemented with low density subcellular fractions following the subcellular fractionation of the LD9 cell line, indicated that potential strain specific co-factors may be present (figure 4.4 and figure 4.6). To analyse the specificity of the low density subcellular fractions they were tested in the CFCA with the 79A strain of mouse scrapie. The 79A strain of mouse scrapie is unknown to cause infection in LD9 cell line or indeed the original L929 fibroblast cell line.

Therefore, low density subcellular fractions (fractions 2 to 4) from the LD9 cell line were used to supplement the CFCA seeded with the 79A strain of mouse scrapie (figure 4.9). The inclusion of LD9 fraction 2 had no effect on the conversion efficiency of 79A. LD9 fractions 3 and 4 caused an increase in the conversion as observed using Western blotting, however statistical analysis (following densitometric analysis) showed that this increase was not significant (figure 4.10). This data was acquired from only two replicates and therefore it is unknown if LD9 low density subcellular fractions 3 and 4 were restricted to increasing ME7 conversion in the CFCA. However, an alternative explanation of these results is that fraction 3 and 4 contain small quantities of LD9 Golgi body which may have an effect on the conversion efficiency of 79A. If LD9 fractions 5, 6 and 7 had of been tested then this may have strengthened this argument. Unfortunately, this experiment was not done due to time and SAF material constraints.

To further understand the specificity of the effect LD9 plasma membrane-enriched fractions have on ME7 conversion efficiency the ME7 seeded CFCA was supplemented with low density subcellular fractions from the SMB-PS cell line. The SMB-PS cell line is not susceptible to ME7 infection, however the conversion efficiency of 79A in the CFCA was increased by the presence of SMB-PS plasma membrane (figure 4.11). Densitometric analysis of the effect of SMB-PS low density subcellular fractions 1 to 5 showed that SMB-PS fractions 2 and 3 gave a significant increase in the conversion efficiency of ME7 (figure 4.12).

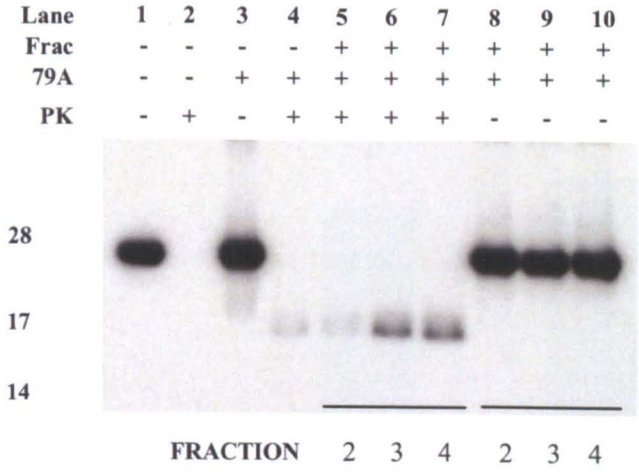

Figure 4.9: The addition of fractions 2 to 4 from a LD9 subcellular fractionation to the CFCA that was seeded with the mouse scrapie strain 79A.

Cell free conversion assay involved the incubation of 200 ng rMo3F4PrP with 1 μg 79A scrapie associated fibrils in conversion buffer for 24 hours at 37 °C. From this, the reaction volume was divided into the +PK sample (lane 3) and the -PK sample (lane 4). Both samples were assayed by separation on SDS PAGE and assay products detected by Western blotting and probing with Syrian hamster antibody 3F4. The CFCA was supplemented with LD9 fractions 2 to 4 for which +/-PK samples were taken. Samples treated with PK are in lane 5 (fraction 2), lane 6 (fraction 3) and lane 7 (fraction 4). The corresponding samples that were not treated with PK are in lane 8 (fraction 2), lane 9 (fraction 3) and lane 10 (fraction 4).

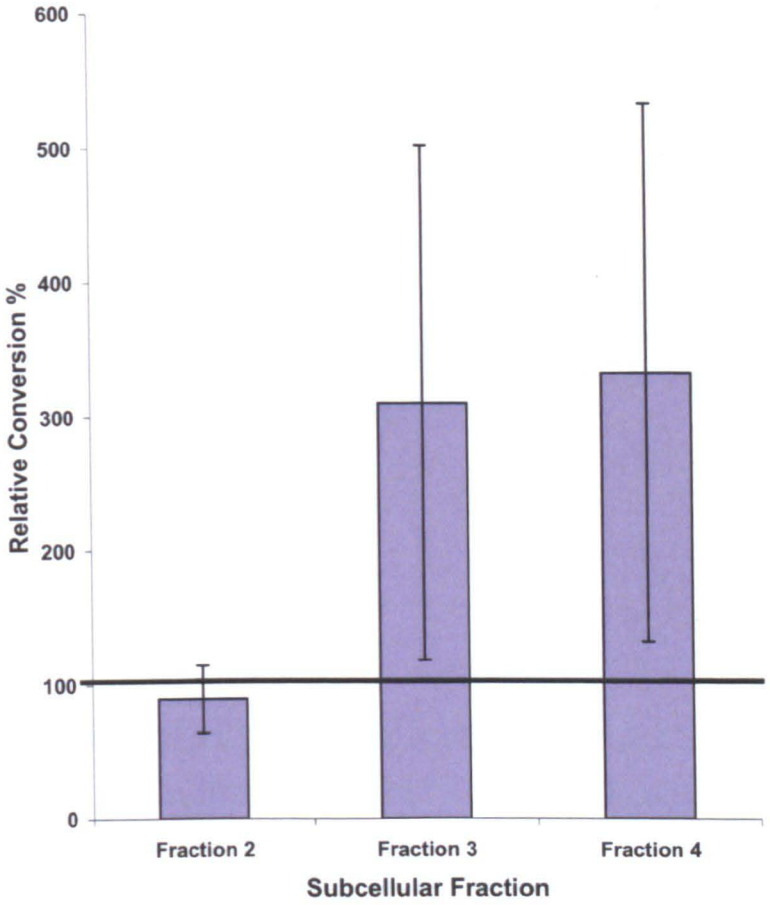

Figure 4.10: Relative conversion percentage of 79A in the CFCA when in the presence of LD9 subcellular fractions 2 to 4.

The 79A seeded CFCA was supplemented with LD9 fractions 2 to 4 for which +/- PK samples were taken. SDS PAGE and Western blotting of these samples with the Syrian hamster monoclonal antibody, 3F4, allows for densitometric measurements on conversion efficiency of 79A in the presence of different subcellular fractions of the LD9 cell line. Relative conversion percentage in the presence of subcellular fractions was calculated using the control 79A seeded CFCA without any subcellular fractions added as 100 % conversion. This is represented by a black line at 100 % relative conversion. Data points are displayed as a bar chart ± SEM. A one-sample t-test was applied to compare the significance of the change in conversion percentage against 100 % conversion efficiency of 79A in the absence of any added subcellular fractions.

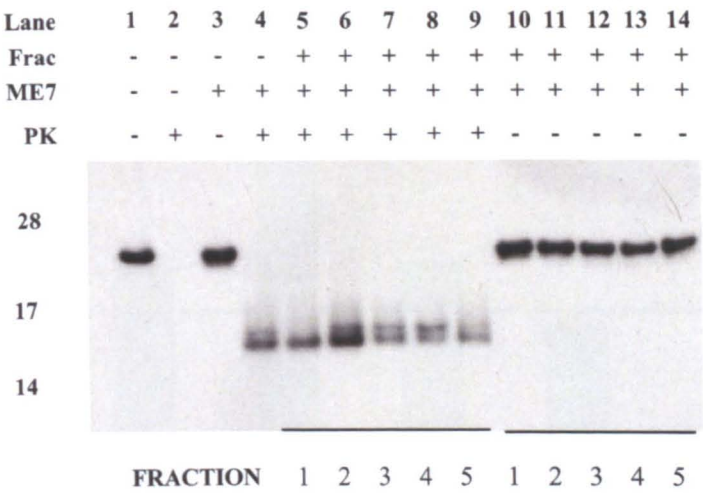

Figure 4.11: The addition of low density fractions from a SMB-PS subcellular fractionation to the CFCA that was seeded with the mouse scrapie strain ME7.

200 ng rMo3F4PrP was incubated with 1 µg ME7 scrapie associated fibrils in conversion buffer for 24 hours at 37 °C. From this, the reaction volume was divided into +PK sample (lane 3) and -PK sample (lane 4). Both samples were assayed by separation on SDS PAGE and assessed by Western blotting with the Syrian hamster antibody, 3F4. The CFCA was supplemented with SMB-PS fractions 1 to 5 for which +/- PK samples were taken from each of the five assays for treatment with and without PK, respectively. Samples treated with PK are in lane 5 (fraction 1), lane 6 (fraction 2), lane 7 (fraction 3), lane 8 (fraction 4) and lane 9 (fraction 5). The corresponding samples that were not treated with PK are in lane 8 (fraction 1), lane 9 (fraction 2), lane 10 (fraction 3), lane 11 (fraction 4) and lane 12 (fraction 5).

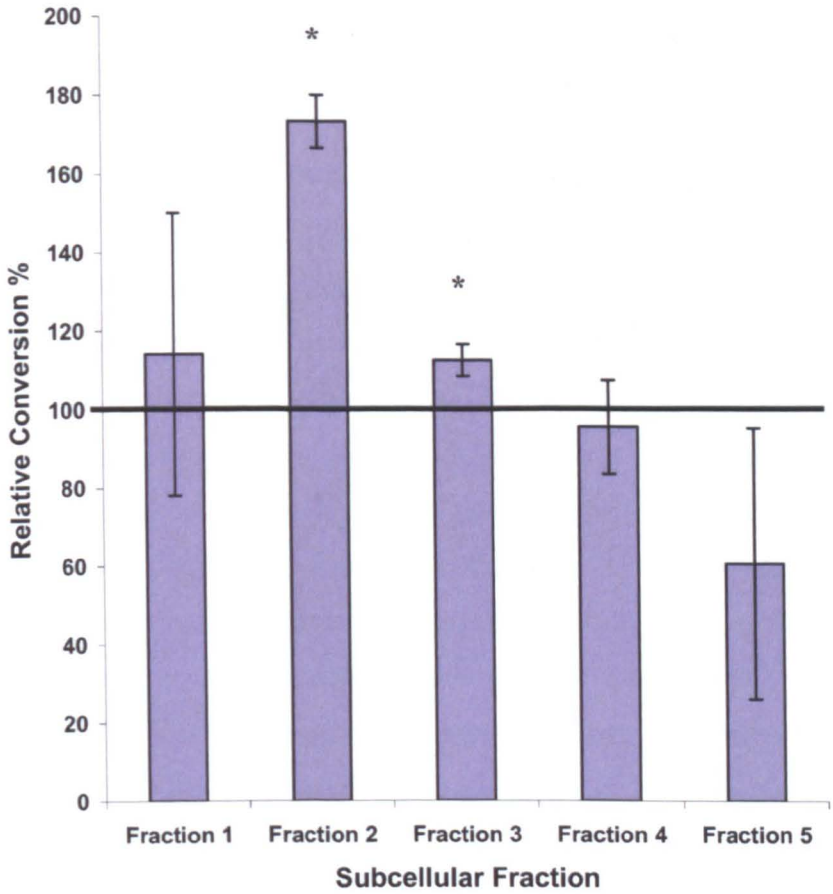

Figure 4.12: Relative conversion percentage of ME7 in the CFCA when in the presence of SMB-PS subcellular fractions 1 to 5.

The ME7 seeded CFCA was supplemented with SMB-PS fractions 1 to 5 for which +/- PK samples were taken. SDS PAGE and Western blotting of these samples with the Syrian hamster monoclonal antibody, 3F4, allows for densitometric measurements on conversion efficiency of ME7 in the presence of different subcellular fractions of the SMB-PS cell line. Relative conversion efficiency in the presence of subcellular fractions was calculated using the control ME7 seeded CFCA without any subcellular fractions added as 100 % conversion. This is represented by a black line at 100 % relative conversion. Data points are displayed as a bar chart ± SEM. A one-sample t-test was applied to compare the significance of the change in conversion percentage against 100 % conversion efficiency of ME7 in the absence of any added subcellular fractions (* represents a significant difference against the positive control).

This experiment was repeated three times and fraction 2 and 3 gave relative conversion efficiencies of 173 % and 110 %, respectively.

4.8 Dilution of plasma membrane enriched LD9 subcellular fractions

The low density LD9 subcellular fractions, which are enriched for plasma membrane and cause an increase in ME7 conversion efficiency, were serially diluted and conversion efficiency monitored. This was to confirm that the effects of the LD9 plasma membrane fractions can be diluted out. The effect was monitored using the CFCA and densitometric analysis of the resultant Western blots allowed for comparison of serial dilutions. Undiluted fractions 2 and 3 resulted in the characteristic increase in ME7 conversion efficiency, however fraction 4 did not. This can be explained by experimental variability with this particular fractionation experiment containing less conversion inducing factors than previous separations. By diluting fraction 2 to 1/200 and fraction 3 to 1/100, the conversion increasing effect was greatly reduced, with conversion efficiencies returning to the same level as an unsupplemented ME7 CFCA (Figure 4.13).

4.9 CFCA supplemented with glycogen

I also hypothesised that the lipid bilayer of the plasma membrane could be acting as a scaffold molecule that sequesters rMo3F4PrP and PrP^{Sc} and thereby encouraging conversion in a nonspecific manner. To replicate this *in vitro*, an alternative molecule, such as glycogen was supplemented into the CFCA. Globular units of glycogen are composed of a protein core, glycogenin, surrounded by glucose subunits (Rybicka, 1996). Glycogen is stored as granules in the cytoplasm of most cell types, including the liver, muscle and brain (Gruetter, 2003).

Glycogen is a polysaccharide that was identified as a component of the TSE agent and was described as a non-proteinaceous scaffold (Appel *et al.*, 1999, Dumpitak *et al.*, 2005). Panza and co-workers demonstrated that by use of an *in vitro* fibrilisation assay, glycogen accelerated the conformational change of α-monomeric rSHaPrP to a β-sheet rich fibril and co-aggregated with glycogen polymers (Stöhr *et al.*, 2008).

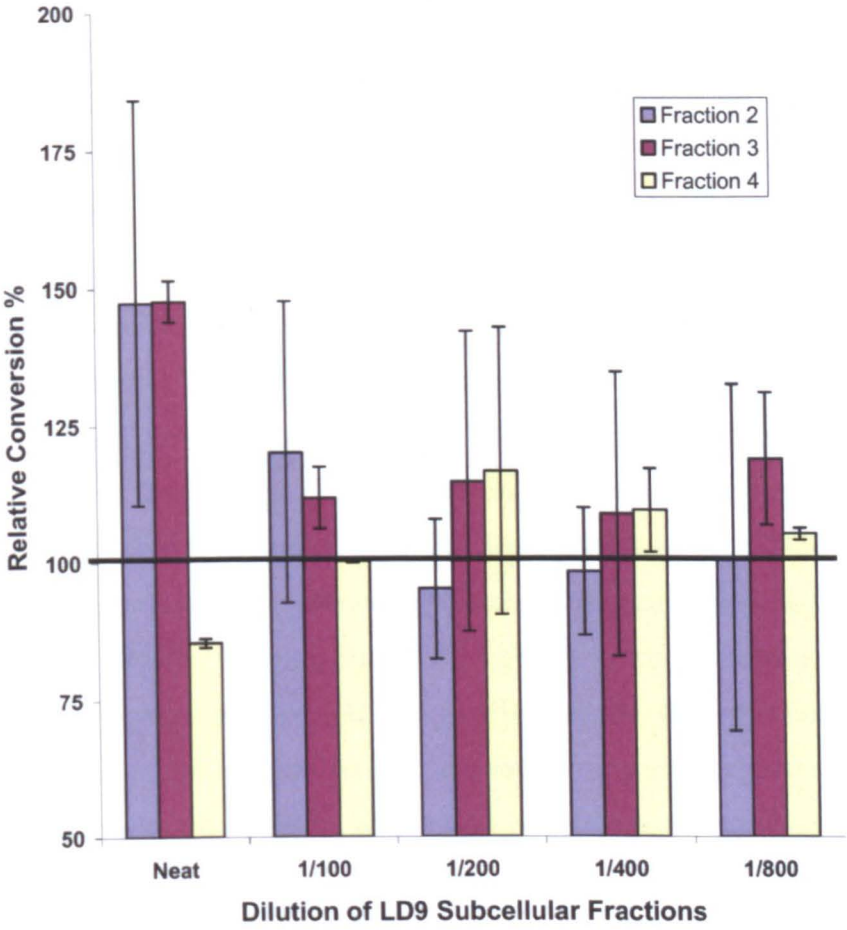

Figure 4.13: The effect of serial dilution of LD9 fractions 2 to 4 on the conversion efficiency of ME7 *in vitro*.

The ME7 seeded CFCA was supplemented with serial dilutions of LD9 fractions 2 to 4 for which +/-PK samples were taken from each of the five assays for treatment with and without PK, respectively. SDS PAGE and Western blotting of these samples with the Syrian hamster monoclonal antibody, 3F4, allows for densitometric measurements on conversion efficiency of ME7 in the presence of serial dilutions of subcellular fractions 2 to 4 of the LD9 cell line. Relative conversion percentage in the presence of subcellular fractions was calculated using the control ME7 seeded CFCA without any subcellular fractions added as 100 % conversion. This is represented by a black line at 100 % relative conversion. Data points are displayed as a bar chart ± SEM.

Glycogen was therefore believed to play an important role in the conversion of PrP^C to the disease related isoform, PrP^{Sc}.

Glycogen (Fluka) was added to the CFCA and the effect on ME7-seeded conversion determined. Glycogen was re-suspended in dH_2O to a concentration of 100 mg/ml and serial dilutions made to give the required final concentration of glycogen in a CFCA reaction mixture. To the CFCA, 7 µl of glycogen at various concentrations were added to make up the final volume to 20 µl. The CFCA constituents are described in detail in the methods chapter. Initially, serial dilutions from 1 mg/ml to 0.0625 mg/ml final concentration of glycogen were added to the CFCA. Samples were taken for -/+ proteinase K treatment and analysis was carried out by separation by SDS PAGE and Western blotting. Figure 4.14 shows that at low concentrations of glycogen, ME7 conversion of rMo3F4PrP was inhibited. As glycogen concentration increases up to 1 mg/ml there is an increase in relative conversion efficiency of ME7 in the CFCA to a maximum of 124 %, as determined using densitometry.

To further understand and validate this result the experiment was repeated, covering a greater range of concentrations. Serial dilutions from 4 mg/ml to 0.03125 mg/ml were made and added to the CFCA in duplicate and the effect on ME7 conversion efficiency was determined (figure 4.15). Similar results were obtained and suggested that at very low concentrations of glycogen there was no discernible effect. However, as glycogen concentration gradually increased, the initial observation was inhibition of conversion at a 0.125 mg/ml glycogen concentration. As glycogen concentration increased up to 4 mg/ml, inhibition of conversion was replaced with an enhancement whereby an increase to 130 % in the relative conversion efficiency was observed (lanes 12 to 14).

From the data shown in figures 4.14 and 4.15, a trend appeared to be emerging; such that there was an inhibitory mechanism of conversion at lower concentrations of glycogen and an enhancing mechanism of conversion at higher concentrations. However, the exclusion of the –PK samples in the previous experiment (figure 4.15), made it difficult to analyse and quantify the significance of the result.

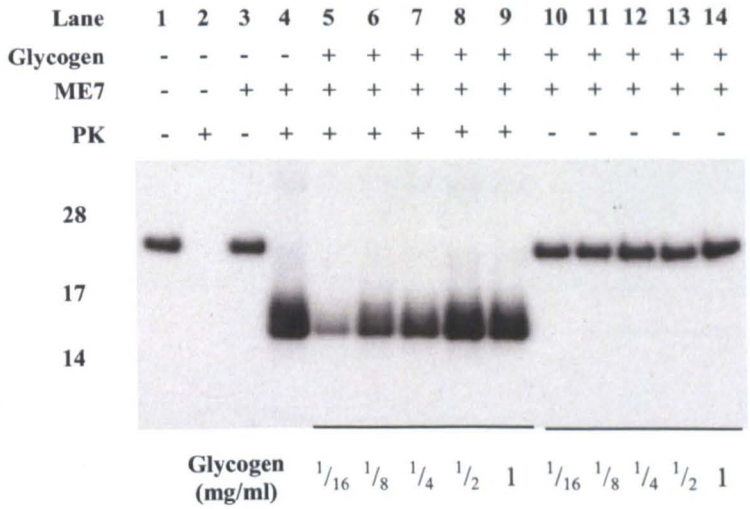

Figure 4.14: The effect of glycogen (0.0625 mg/ml to 1 mg/ml) on the conversion of rMo3F4PrP by ME7 in the CFCA.

Cell free conversion assay involved the incubation of 200 ng rMo3F4PrP with 1 µg ME7 scrapie associated fibrils in conversion buffer for 24 hours at 37 °C. From this, the reaction volume was divided into +/-PK samples. Samples were assayed by separation on SDS PAGE and assay products detected by Western blotting and probing with Syrian hamster antibody 3F4. The CFCA was supplemented with glycogen for which +/-PK samples were taken. Samples treated with PK are in lane 5 (0.0625 mg/ml glycogen), lane 6 (0.125 mg/ml glycogen), lane 7 (0.25 mg/ml glycogen), lane 8 (0.5 mg/ml glycogen) and lane 9 (1 mg/ml glycogen). The corresponding samples that were not treated with PK are in lane 10 (0.0625 mg/ml glycogen), lane 11 (0.125 mg/ml glycogen), lane 12 (0.25 mg/ml glycogen), lane 13 (0.5 mg/ml glycogen) and lane 14 (1 mg/ml glycogen).

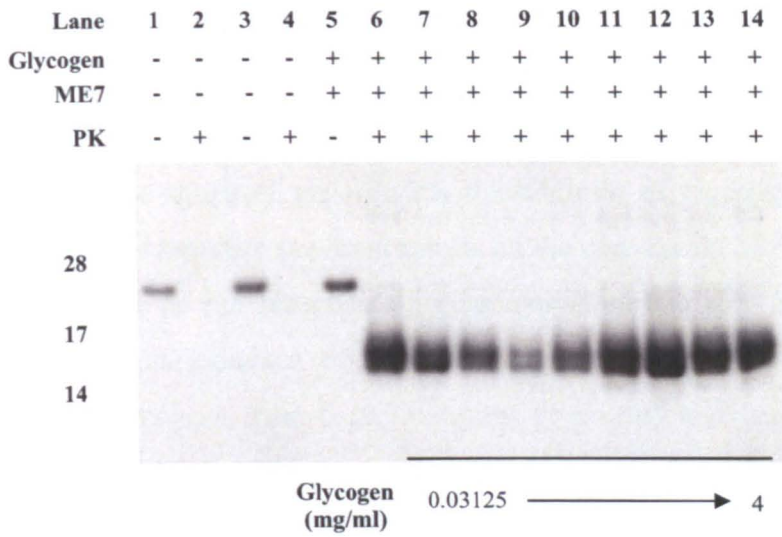

Figure 4.15: The effect of glycogen (0.03125 mg/ml to 4 mg/ml) on the conversion of rMo3F4PrP by ME7 in the CFCA

Cell free conversion assay involved the incubation of 200 ng rMo3F4PrP with 1 μg ME7 scrapie associated fibrils in conversion buffer for 24 hours at 37 °C. From this, the reaction volume was divided into +/-PK samples. Samples were assayed by separation on SDS PAGE and assay products detected by Western blotting and probing with Syrian hamster antibody 3F4. The CFCA was supplemented with glycogen for which +/-PK samples were taken. Samples treated with PK are in lane 7 (0.03125 mg/ml glycogen), lane 8 (0.0625 mg/ml glycogen), lane 9 (0.125 mg/ml glycogen), lane 10 (0.25 mg/ml glycogen), lane 11 (0.5 mg/ml glycogen), lane 12 (1 mg/ml glycogen), lane 13 (2 mg/ml glycogen) and lane 14 (4 mg/ml glycogen). Control experiment to monitor the effect of 4 mg/ml glycogen on the misfolding of 200 ng rMo3F4PrP are shown in lane 1 (-PK sample) and lane 2 (+PK sample).

Therefore, a repeat experiment was done, in duplicate and covering a larger range of glycogen concentrations, from 0.03125 mg/ml to 32 mg/ml. By increasing the effective concentration of glycogen, a trend of the effect of glycogen on conversion may be revealed.

Surprisingly, in these series of experiments the addition of glycogen to the ME7-seeded CFCA did not replicate previous results on the conversion of rMo3F4PrP to a PK-resistant isoform in the presence of glycogen (figure 4.16). In some of the experiments there was evidence of significant increases in conversion in lane 3 (0.03125 mg/ml glycogen), lane 6 (0.25 mg/ml glycogen) and lane 10 (4 mg/ml glycogen) of figure 4.16 that demonstrated no discernable pattern. The corresponding -PK samples in lanes 14, 17 and 21 all demonstrated a significant loss of rMo3F4PrP from the sample. To explain the apparent stochastic nature of this result, it is possible that fibrilisation is also taking place and is working in conjunction with the seeded conversion of rMo3F4PrP to produce another PK-resistant PrP isoform. In addition, if these anomalous results were excluded from figure 4.16 then a similar result would have been achieved as shown in figures 4.14 and 4.15.

4.10 Discussion

The CFCA is an *in vitro* assay that involves incubation of recombinant PrP, over-expressed in bacteria, with SAF purified from the brains of TSE-infected animals. This reaction causes a proportion of recombinant PrP molecules to be converted to a protease-resistant isoform. The principal method of analysis of this reaction is to take a sample for treatment with proteinase K, separate by SDS PAGE, and assess by Western blotting. In these set of experiments, the substrate is recombinant mouse PrP and the SAF-seed is mouse derived scrapie. To detect only the newly converted rMoPrP molecules, the rMoPrP substrate has the 3F4 hamster epitope (109-112) engineered into it allowing specific detection by the monoclonal antibody 3F4 (Kascsak *et al.*, 1987, Rogers *et al.*, 1991). Unlike the SAF-seed, the recombinant PrP substrate is unglycosylated and therefore only a single band is observed on the blot after immunodetection. Scrapie associated fibrils were isolated from scrapie infected mouse brains by detergent extraction and differential centrifugation.

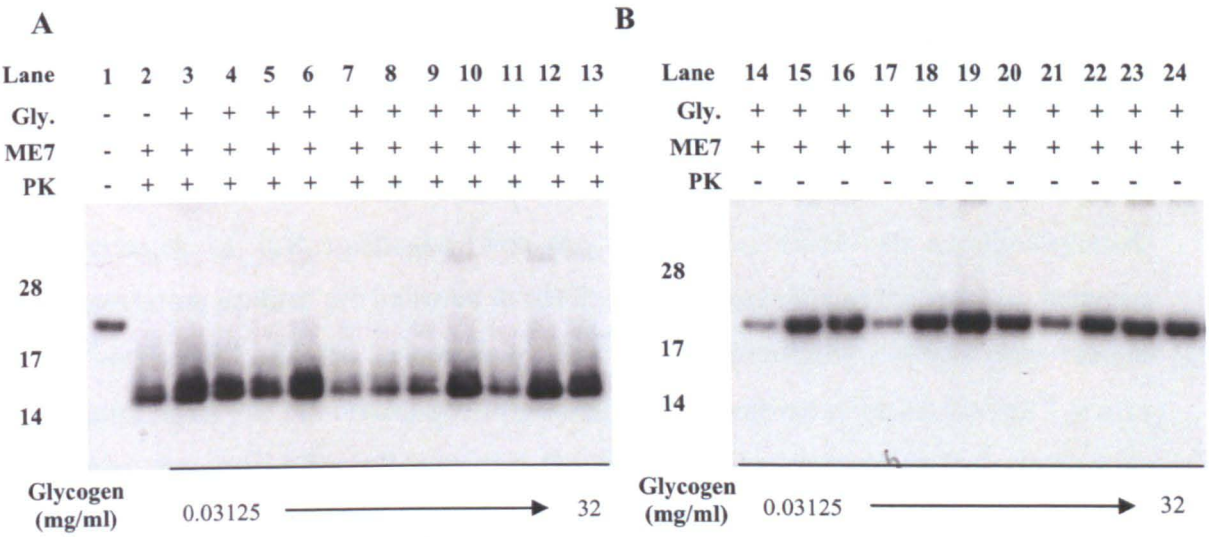

Figure 4.16: The effect of glycogen (0.03125 mg/ml to 32 mg/ml) on the conversion of rMo3F4PrP by ME7 in the CFCA.

Cell free conversion assay involved the incubation of 200 ng rMo3F4PrP with 1 µg ME7 scrapie associated fibrils in conversion buffer for 24 hours at 37 °C. From this, the reaction volume was divided into +/-PK samples. Samples were assayed by separation on SDS PAGE and assay products detected by Western blotting and probing with Syrian hamster antibody 3F4. The CFCA was supplemented with glycogen for which +/-PK samples were taken. Samples treated with PK are in lane 3 (0.03125 mg/ml glycogen), lane 4 (0.0625 mg/ml glycogen), lane 5 (0.125 mg/ml glycogen), lane 6 (0.25 mg/ml glycogen), lane 7 (0.5 mg/ml glycogen), lane 8 (1 mg/ml), lane 9 (2 mg/ml), lane 10 (4 mg/ml), lane 11 (8 mg/ml), lane 12 (16 mg/ml) and lane 13 (32 mg/ml). The corresponding samples that were not treated with PK are in section B, lanes 14 to 24.

Verification of the presence of PrP^{Sc} was done by Western blotting after proteinase K digestion. As demonstrated in figure 4.1, proteinase K digests the N-terminus of PrP leaving behind an undigested, proteinase-resistant C-terminal domain. Full length PrP^{Sc} can be either di-, mono- or un-glycosylated and therefore Western blotting reveals three bands for each type of glycoform of PrP. Proteinase K treatment causes each of the three bands to have an increased electromobility following SDS PAGE, due to the reduction in molecular weight of the protein. In addition, different strains of mouse derived scrapie have different glycoform ratios that are maintained across multiple passages in mice (Collinge *et al.*, 1996). Glycoform ratios for four different TSE strains are summarised in table 4.1 demonstrating the differences in the percentages of PrP molecules that are either di-, mono- or un-glycosylated. Gycosylation profiles are believed to result as a consequence of the reaction between PrP^{C} and PrP^{Sc} and the selection by PrP^{Sc} to preferentially convert only certain glycoforms of PrP^{C} (Vorberg and Priola, 2002). Glycoform selection by PrP^{Sc} is also in part, determined by cell type and the differential expression of PrP glycoforms within that cell (DeArmond *et al.*, 1997) and also by, the subcellular compartment that conversion of PrP^{C} takes place (Jeffrey *et al.*, 2005).

The CFCA was originally designed with hamster derived scrapie strain 263K, which converted rHaPrP purified from cultured mouse fibroblast cells and radiolabelled with ^{35}S-methionine (Kocisko *et al.*, 1994). This was subsequently modified to use bacterially recombinant untagged PrP that can be purified to give high yields that have no cellular contamination, unlike previous methods that use cell culture derived PrP^{C}. In addition, the CFCA has been modified to be more physiological by removing the chaotrope guanidine hydrochloride from the conversion buffer. Typically other researchers have used the mouse scrapie strain 87V as a seed to catalyse the conversion of rMoPrP to a PK-resistant isoform. This strain of mouse scrapie is from a p7/p7 (108F/189V) mouse background and converts approximately 20 % of the rMoPrP monomers. When I used ME7, 79A and 22F strains of mouse scrapie I found that they converted approximately 18%, 3.5 % and 2.5 % of the rMo3F4PrP substrate, respectively.

I then supplemented the CFCA with different subcellular fractions, however any detrimental effects of the addition of cellular material was determined by the incubation of rMoPrP with LD9 cell homogenates. This was a mock CFCA experiment in the absence of any mouse scrapie seed and proteolytic digestion was observed (figure 4.3). Even at a 1/4000 dilution of LD9 homogenate, rMoPrP digestion was evident with complete digestion as low as a 1/250 dilution of the cell homogenate.

Subcellular fractions of TSE susceptible cell lines were added to the CFCA and the effect on conversion efficiency monitored. The ME7-seeded CFCA was supplemented with subcellular fractions from the ME7 susceptible cell line, LD9. Supplementing with LD9 fractions 1 to 5 (enriched for plasma membrane) caused an increase in the conversion efficiency of ME7 in the CFCA where fractions 2 and 3 were significantly different from the control ME7-seeded CFCA. The mouse scrapie strain ME7 converted approximately 18 % of the rMo3F4PrrP substrate into a PK-resistant isoform. When supplemented with LD9 fractions 2 and 3, there was an increase to 36.7 % and 33.9 % of rMo3F4PrP converted, respectively. From the LD9 organelle distribution bar chart in figure 3.8, fractions 2 and 3 are enriched for plasma membrane. The positive effect of plasma membrane on conversion efficiency was not surprising. This compartment of the cell has previously been suggested as the site of conversion *in vivo*, with many studies implicating plasma membrane in this process (Jeffrey *et al.*, 1994, Kazlauskaite *et al.*, 2002, Sanghera *et al.*, 2002, Paquet *et al.*, 2007). I rationalised that the increase in conversion efficiency of ME7 was because of a potential influx of specific co-factors into the CFCA by the addition of these particular fractions.

Mass spectrometric analysis of LD9 fraction 3 suggested that it was principally composed of cytoplasmic proteins, rather than plasma membrane proteins (table 4.2). The predominance of cytoplasmic proteins in LD9 fraction 3 may not be an accurate representation of the proteins present as plasma membrane proteins are particularly difficult to separate from the lipid bilayer due to strong hydrophobic and hydrophilic regions within the protein (Santoni *et al.*, 2000). In addition to difficulties in delipidation of plasma membrane bound proteins, solubilisation is greatly reduced

due to the inherent properties of these membrane-bound proteins. To improve the detection of these proteins, specific steps were included in the sample preparation to counteract these problems (Mirza *et al.*, 2007). Firstly, the low density subcellular fractions were treated with methanol to extract the proteins from the lipid bilayer. Secondly, proteins were centrifuged to concentrate the sample prior to resuspension in 4 M urea, 100 mM ammonium bicarbonate solution which was done to increase the solubility of plasma membrane proteins prior to tryptic digestion. Unfortunately, this did not appear to give a result that supported the annexin-II Western blot, which showed the enrichment of the plasma membrane in these fractions. However, I believe that the steps taken to increase plasma membrane extraction and solubilisation were not as successful as hoped. In addition, during subcellular fractionation the cytoplasmic proteins should be solubilised in the homogenisation buffer which theoretically should remain at the very top of the gradient. This was evident as there was an interface observed after ultra centrifugation between the homogenisation buffer and the OptiPrep™ gradient. The small volume of homogenisation buffer was consistently removed in the first fraction and therefore the constituents of the cytoplasm should only be present in fraction 1. An explanation for the presence of cytoplasmic proteins in fraction 3 could be the result of sample overloading causing disruptions to the gradient. Alternatively, the loss of plasma membrane proteins in the sample would give an artificially high reading for other proteins that were also present. In this case, the mass spectrometry would and did identify many peptides originating from cytoplasmic proteins.

If fraction 3 was enriched for plasma membrane then the effect on ME7 conversion in the CFCA could have been a generalised association between PrP^{C} and / or PrP^{Sc} with the lipid bilayer acting as a scaffold for conversion. Fractions 6 to 22, from the subcellular fractionation of the LD9 cell line, were enriched for organelles such as lysosomes, Golgi body, endoplasmic reticulum and mitochondria and gave no enhancement to ME7 conversion efficiency (figure 4.4). Fractions 7 to 13 were contaminated with proteolytic enzymes and therefore these fractions were diluted a further 1/200, prior to adding into the CFCA (figure 4.5). Any potential co-factors in these fractions were diluted along with the proteases which resulted in conversion similar to that of the CFCA positive control reaction.

The CFCA was repeated using the 79A strain of mouse scrapie and supplemented with subcellular organelles purified from the cell line SMB-PS, which is susceptible to 79A (figure 4.7). Supplementing the 79A CFCA with SMB-PS low density subcellular fractions 1 to 5, did not result in a significant increase in the conversion of rMo3F4PrP into a PK-resistant isoform. However, fractions 8 and 9 were significantly different than the control reaction and showed an increase in the conversion efficiency of 79A. The conversion percentage values in figure 4.8 for SMB-PS subcellular fractions 7 to 10 follow the normal distribution profile of Golgi body (see figure 3.9). The mouse derived scrapie strain 79A is very inefficient at converting rMo3F4PrP in the CFCA and only 3.5 % is converted to the PK-resistant isoform. However, in the presence of SMB-PS subcellular fractions enriched for Golgi body, there was a significant increase to 5.7 % of rMo3F4PrP being converted by 79A. The fractions 12, 13, 15, 17 and 19 gave significant reductions in conversion efficiency suggesting that there may be factors that inhibit the conversion process of rMo3F4PrP. The addition of fraction 22 to the 79A seeded CFCA resulted in a significant increase in conversion. This fraction represents the base of the OptiPrep™ 10-20 % gradient and as such will contain cellular debris that escaped the PNS spin as well as any dense organelles that have sedimented. It is therefore difficult to ascertain the contents of this fraction. To assess this, I could have used a different gradient that extends to 25 % or 30 % OptiPrep™, which would separate out the constituents of fraction 22 from the 10-20 % gradient.

To determine strain specificity of LD9 plasma membrane enriched subcellular fractions, they were tested in the CFCA seeded by 79A, which was unknown to infect LD9 cells. The LD9 fractions 4 and 5 increased conversion of rMo3F4PrP into a PK-resistant isoform, however this was not significant (figure 4.10). Therefore, the observed effect of LD9 subcellular fractions enriched for plasma membrane may not be strain specific because the enhancement is regardless of cell line susceptibility. To understand this result it was hypothesised that the presence of plasma membrane in the CFCA presented an increase in surface area thereby increasing the number of interactions between rMo3F4PrP and the mouse scrapie seed.

To determine whether the increases in conversion efficiency observed for two different strains of mouse scrapie were not just cell line specific, the CFCA was used with a different cell line. The CFCA seeded with ME7 was supplemented with the corresponding SMB-PS subcellular fractions enriched for plasma membrane. SMB-PS cells are not susceptible to infection by ME7; however SMB-PS low density subcellular fractions significantly enhanced the amount of conversion over the control experiment (figure 4.12). This re-enforced the hypothesis that the presence of plasma membrane in the CFCA was an enhancement caused by an increase in the surface area. An experiment to answer this was to create artificial lipid membranes composed of cholesterol and sphingolipid. These membranes have previously been demonstrated to interact strongly with PrP^C (Sanghera *et al.*, 2002, Critchley *et al.*, 2004). These membranes do not contain any contaminants such as proteins or carbohydrates that are present in cellular membranes. Unfortunately, time and financial constraints prevented the purchase of these lipids; future experiments would incorporate this as a control experiment to determine the role of a lipid bilayer in conversion.

I therefore rationalised that glycogen, a high molecular weight polymer, may also behave as a non-specific scaffold within the CFCA and provide comparative data. Firstly, it was proposed that glycogen was an important polysaccharide scaffold that was incorporated into amyloid fibrils *in vivo* (Dumpitak *et al.*, 2005). Panza and co-workers also demonstrated that the fibrilisation of rSHaPrP into amyloid fibrils was accelerated when in the presence of glycogen (2008). The assay used was similar to the CFCA, as the conversion buffer used low concentrations of detergent and salts (Stöhr *et al.*, 2007). Therefore, serial dilutions of glycogen were added to an ME7 seeded CFCA to determine any potential effects glycogen may have on ME7 conversion efficiency. Results initially appeared to indicate that at concentrations of approximately 0.0625 mg/ml to 0.25 mg/ml glycogen, ME7 conversion was inhibited. As the concentration of glycogen increased to the maximum of 4 mg/ml there was a steady increase in PrP conversion resulting in a net increase over the conversion efficiency of the positive control. To validate this result, an experiment was setup to analyse the effects of a broad range of glycogen concentrations (0.03125 mg/ml to 32 mg/ml glycogen) would have on conversion efficiency in the

CFCA. Unfortunately, on further repeats, variable and inconsistent results were achieved and this may require future examination to clarify the role of glycogen in conversion.

It is possible that a competing reaction, such as fibrilisation of rMo3F4PrP was occurring during incubation of the CFCA. Previous studies have demonstrated that glycogen accelerates and enhances the fibrilisation pathway of rPrP and hence it is possible that this is occurring in conjunction with conversion in the CFCA. This was suggested by observations in figure 4.16 panel A (lane 3, 6 and 10) where there is an apparent doubling in the amount of rMoPrP converted to a PK-resistant isoform. However, this appeared to be happening stochastically, regardless of glycogen concentration. This result was replicated and not in the same pattern, in the duplicate set of assays setup at the same time as those shown in figure 4.16. If conversion of rMoPrP by ME7 was the only reaction then you would expect to see either a gradual change in conversion efficiencies with glycogen concentration; or no effect on conversion efficiency at all. The fibrilisation process appears to be a random process with subtle changes in the reaction mixture and/or environment responsible for this reaction to occur. Therefore, these experiments were stopped based on the assumption that fibrilisation occurs by an uncontrollable process and was responsible for the prevention of measuring the effect glycogen had on rMo3F4PrP in the CFCA.

To summarise, the CFCA provided the means to study the effect of subcellular fractions from TSE susceptible cell lines on the conversion of rMo3F4PrP in the presence of a mouse scrapie seed. Low density subcellular fractions from the fibroblastic cell line LD9, provided a nonspecific enhancement of rMo3F4PrP conversion when in the presence of either ME7 or 79A. The strain 79A does not infect the LD9 cell line and therefore this cell line should not contain any strain specific co-factors, if the original hypothesis is correct. On the other hand, Golgi body enriched fractions from the 79A susceptible cell line SMB-PS, enhanced conversion of rMo3F4PrP to a PK-resistant isoform when in the presence of the mouse scrapie strain 79A. Unfortunately, these fractions were not tested in the CFCA experiment seeded by the ME7 strain of mouse scrapie due to shortages of infectious material.

5. Proteomic determination of molecules co-purifying with PrP^{Sc} in scrapie associated fibrils from different strains of mouse-passaged scrapie

5.1 Introduction

Chapter 4 described the identification of subcellular fractions from TSE susceptible cell lines that enhanced the conversion efficiency of recombinant prion protein seeded with PrP^{Sc} from mouse adapted scrapie by means of the CFCA. Fractions enriched for plasma membrane from two cell lines increased conversion efficiency seeded by the mouse scrapie strain, ME7. The specific cell lines used were an ME7 susceptible cell line (fibroblastic cell line, LD9) and a non-ME7 susceptible cell line (microglial cell line, SMB-PS).

PrP^{C} is a conserved GPI anchored sialoglycoprotein that is constitutively expressed in all mammalian cells of the nervous system (Oesch *et al.*, 1985, Stahl *et al.*, 1987). Its secondary structure is composed predominately of α-helices and during prion disease there is a conformational change in the structure of PrP^{C} to an isoform that is rich in β-pleated sheet, PrP^{Sc} (Caughey *et al.*, 1991*a*). This change in structure results in PrP^{Sc} being insoluble and partially resistant to protease digestion. The disease associated isoform PrP^{Sc} is hypothesised to be the principle component of the infectious agent in TSEs and is reported to be responsible for the neurodegenerative outcome of the infection (Aguzzi *et al.*, 2007). However, the molecular basis of the process by which PrP^{C} is converted to PrP^{Sc} is still unknown. It is known that PrP^{C} is required for disease because $PrP^{0/0}$ mice are resistant to prion infection (Bueler *et al.*, 1993). Accumulating evidence suggests that there are interactions between PrP and other molecules that are necessary for the conversion of PrP^{C} to PrP^{Sc} to take place (Shyng *et al.*, 1994, Telling *et al.*, 1995, DebBurman *et al.*, 1997, Wong *et al.*, 2001). It is assumed that PrP^{Sc} is the catalyst which imposes its conformation onto nascent PrP^{C} causing the disease associated structural changes. Additional proteins or molecules in conversion could act as chaperones to assist in the refolding of PrP^{C} (Jin *et al.*, 2000, Sarnataro *et al.*, 2004). Alternatively, these accessory molecules could form a scaffold that allows for the correct interaction between PrP^{C} and PrP^{Sc} (Alper *et al.*, 1967, Priola and Caughey, 1994, Adler *et al.*, 2003, Deleault *et al.*, 2003). Therefore, there is the possibility that many accessory molecules or co-factors exist and they could differ depending on the prion strain. Different strains are reported to differ by protein conformation and their structural properties; therefore

this is likely to influence or be influenced by any interaction with a co-factor (Safar *et al.*, 1998).

During the conversion process, PrP^C is conformationally altered to the structure of PrP^{Sc} and is likely to become bound to PrP^{Sc} during polymerisation of the amyloid fibrils, which are often observed in TSE infected brains (DeArmond *et al.*, 1985). Since PrP^C and PrP^{Sc} are believed to interact during conversion, any co-factors that mediate, direct or aid this interaction in any way may become integrated into the fibril. Therefore, characterisation of the constituents of the fibril may help to shed light on the identities of the co-factors involved.

A variety of molecules have already been reported to interact with either PrP^C and/or PrP^{Sc} and the majority of these have been identified through affinity binding experiments, such as cross-linking and co-immunoprecipitation with PrP^C (for a review, see Aguzzi *et al.*, 2008). In general, these experiments have only been applied to PrP^C to understand and predict the function of PrP^C. In addition to characterising PrP^C function, the identification of interaction partners may give insights into co-factors that are necessary for PrP^{Sc} propagation.

The experimental observation that there are co-factors necessary for prion conversion was initially published in 1995 by Telling and co-workers (Telling *et al.*, 1995). The co-factor was referred to as protein X and its involvement was invoked to explain data on the transmission of human prions to transgenic mice expressing mouse, human or a mouse-human chimeric PrP. Results suggested that the binding site of protein X to PrP^C was putatively located in the carboxyl terminus after experiments revealed that amino acid substitution at positions 167, 171, 214 and 218 prevented PrP^{Sc} formation (Perrier *et al.* 2002). However, the identity of protein X is still unknown, although many co-factors have been suggested.

One of the factors suggested to be involved in prion conversion is an unknown cellular receptor for PrP^C that is responsible for the internalisation of PrP^C and PrP^{Sc} into the cell, *via* clathrin-coated pits (Shyng *et al.*, 1994, Shyng *et al.*, 1995, Reiger *et al.*, 1997). A second molecular subtype that is known to associate with PrP^C and is suggested to play an important role in conversion and prion formation is nucleic

acids. Experiments on the binding of nucleic acids to PrP^C were shown to cause a conformational change in the protein to the β-sheet rich isoform. (Cordeiro *et al.*, 2001). Since these experiments, it has been proposed that RNA molecules specifically stimulate PrP^{Sc} formation *in vitro* (Deleault *et al.*, 2003, Supattapone, 2004). Another set of molecules that bind PrP^C and are implicated in PrP^{Sc} formation are glycosaminoglycans (GAGs), such as heparan sulphate and pentosan polysulphate (Priola and Caughey, 1994, Wong *et al.*, 2001). Interestingly, these same GAGs have inhibitory properties in scrapie-infected cells and animals (Adjou *et al.*, 2003). The conflicting data from this study would suggest that extracellular GAGs may sequester PrP^C from intracellular GAGs, thus preventing the correct interaction between PrP^C and PrP^{Sc}.

In this chapter, I outline work undertaken to identify protein species that make up SAF. The principle component of TSE-associated amyloid fibrils is PrP^{Sc}, however it was hypothesised that co-factors that are necessary for PrP conversion may become associated with amyloid fibrils during the conversion process. Comparison of SAF preparations from different strains of mouse scrapie may also reveal differences in fibril composition, which could indicate strain specific proteins.

As discussed in chapter 4, LD9 low density subcellular fractions enhanced the conversion efficiency of mouse scrapie in the CFCA. Mass spectrometry of a subcellular fraction enriched for LD9 plasma membrane provided a list of protein identifications with which to compare (Table 4.2). Mass spectrometric analysis of mouse scrapie associated fibrils isolated from TSE infected mouse brains was hypothesised to reveal the presence of plasma membrane derived proteins with which to compare against LD9 subcellular fraction 3. The identity of non-PrP proteins associated with mouse scrapie would provide a list of potential interaction partners that are relevant to PrP conversion.

Mass spectrometry is a technique that is used to identify both individual proteins contained within single bands isolated from SDS PAGE gels or to identify the proteins present within more complex samples. Samples for mass spectrometric analysis were pre-treated with trypsin, which acted at specific locations along the peptide backbone. Trypsin is a serine protease that hydrolyses the peptide backbone

at the carboxyl side of lysine or arginine unless a proline is the next amino acid in the peptide chain. Tryptic peptides were desalted and concentrated before separation using high pressure liquid chromatography (HPLC) and eluted into an electrospray ion source. Electrospray ionisation (ESI) nebulised the HPLC elute into highly charged droplets, which were sprayed into the mass spectrometer. In this case, tandem MS/MS was used, which comprised of a quadrupole mass analyser that measured the mass-to-charge (*m/z*) ratio of the ionised peptides. Ions of a particular *m/z* ratio are selected before entering a collision cell filled with helium. Collision of the ions with the collision gas causes fragmentation of the ions and the fragment ions are analysed by time-of-flight measurement in a ToF MS instrument. The Q-ToF MS/MS system gives high resolution and accuracy of peptide masses when compared against other MS instruments. ESI-MS/MS was used to provide a tandem mass spectra that were submitted to MASCOT (version 2.2) and compared against the IPI mouse database of peptides from known murine proteins.

5.2 Silver stain detection of the proteinaceous constituents of scrapie associated fibrils

The preparation of scrapie associated fibrils makes use of relatively crude techniques that separate fibrils on the basis of insolubility and density. After homogenisation of brain material, detergent extraction of insoluble material results in a pellet enriched for insoluble constituents, which is resuspended in dH_2O and centrifuged through a 20 % sucrose cushion. This step separates molecular species by density, such that proteins of a high density will pass through the sucrose cushion, whereas low density proteins will remain in the solution above the sucrose cushion. Amyloid fibrils are aggregates of PrP^{Sc} and have a high molecular density and therefore were found in the pellet. However, other protein species that co-purify with PrP^{Sc} may be co-factors that are necessary for conversion and/or prion formation (DebBurman *et al.*, 1997, Saborio *et al.*, 1999). It has also been suggested that different strains of TSE will have different co-factors that aid in strain differentiation (Toyama *et al.*, 2007). To analyse the differences in proteinaceous species for different strains of TSE, SAF preparations of mouse adapted scrapie were mixed with modified Laemmli sample buffer (MLSB) (4 M urea, 5 % (v/v) glycerol, 5 % (w/v) SDS, 5 % (v/v) β-mercaptoethanol, 65 mM Tris (pH 6.8)) prior to separation by SDS PAGE and

stained with silver nitrate solution following the protocol as described in chapter 2 (section 2.1.2.3). The MLSB solution was used because of the insoluble nature of SAF preparations and this buffer is designed to solubilise more insoluble proteins as well as reduce streaking of aggregated protein through the gel. The mouse adapted scrapie strains ME7, 79A and 22F were analysed using this method.

Figure 5.1 shows a silver stained gel of very few differences in protein species between ME7, 79A and 22F SAF preparations. It does, however, show that there are differences in the amount of different proteins in each SAF preparation when comparing the same concentration of SAF preparation separated on the gel. Concentration of PrP^{Sc} was done by Western blotting SAF preparations against a serial dilution of $rMoPrP^{WT}$ of known concentration and using the anti-PrP antibody AG4 (data not shown). Comparison of lane 2 (250 ng ME7), lane 6 (250 ng 79A) and lane 10 (250 ng 22F) revealed there are differences in the amounts of proteins detected between the molecular weight markers 17 kDa and 6 kDa.

Due to the very few protein bands and differences in silver stained profiles of SAF after PK treatment, it was decided that further proteomic analysis by cutting out individual bands from such a SDS PAGE gel would not be advantageous. Instead, proteinaceous constituents of SAF preparations were analysed directly by mass spectrometry without pre-separation by SDS PAGE and then visualisation by silver staining.

5.3 Mass spectrometry of SAF preparations from uninfected mouse brains

Preparation of SAF using the method as described in chapter 2 (section 2.1.2.15) results in an enrichment of amyloid fibrils. However, there will be 'contamination' from other proteins that have similar properties to SAF, such as insolubility and/or high molecular weight, but which are not physically associated with SAF *in vivo*. To identify and discard these proteins from future proteomic analyses, the SAF protocol was applied to uninfected wild type and PrP-null ($PrP^{0/0}$) mouse brains. The same number of brains (four mouse brains) from wild type and $PrP^{0/0}$ mice were used which was also the same number of brains used in analyses of mouse scrapie infected brain.

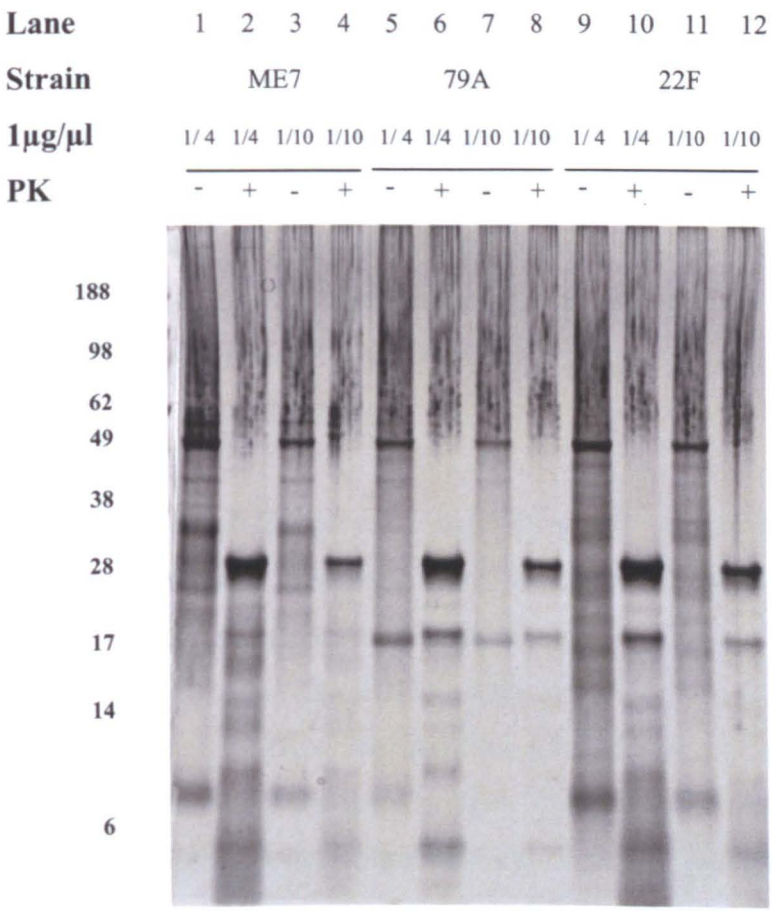

Figure 5.1: Preparations of PrP^{Sc} and associated proteins from ME7, 79A and 22F infected mouse brains were visualised by silver staining.

Scrapie associated fibrils were isolated from ME7, 79A and 22F infected mouse brains and SAF preparations were made up to 1 µg/µl (section 2.1.2.15) prior to treated with and without PK. SAF were diluted to either 250 ng (1/4) or 100 ng (1/10) and separated by SDS PAGE. Silver staining of the SDS PAGE gel was done to detect separated protein species. Molecular weight markers are in kDa.

Mass spectrometry of mock-SAF preparations from uninfected wild type mouse brains revealed five significant protein identifications, based on a minimum of two distinct peptides being identified by a MASCOT search of the IPI murine database. The results of this search are shown in table 5.1. SAF preparations from uninfected $PrP^{0/0}$ mice also had five significant protein identifications of which three were novel compared to the mock-SAF preparations of wild type mice (Table 5.1). This experiment was repeated three times from three separate SAF preparations, each on four uninfected wild type or $PrP^{0/0}$ mouse brains. Proteins that were detected in the wild type mouse brains after a mock-SAF preparation included calcium/calmodulin dependent protein kinase, ferritin (light chain), versican core protein and myelin associated oligodendrocyte basic protein isoform 1. Mock-SAF preparations on $PrP^{0/0}$ mice contained calcium/calmodulin dependent protein kinase and myelin associated oligodendrocyte basic protein isoform 1 again, the proteins histone (H1.2) and myomesin-2 were also identified.

Calcium/calmodulin dependent protein kinases (CamKII) are serine/threonine protein kinases located in synaptic junctions. They are important kinases involved in the induction of synaptic plasticity, long term memory and learning (Shulman and Hanson, 1993, Lisman, 1994). CamKII is a high molecular weight complex (500-600 kDa) composed of 10 to 12 oligomers that form a holoenzyme. This protein is highly abundant, making up 2 % of total brain protein. Therefore the presence of CamKII in SAF preparations is possibly due to the high abundance of this protein coupled with its high molecular weight.

Other proteins identified were ferritin and versican core protein. Ferritin is a large globular protein composed of 24 subunits (450 kDa total), the function of which is to store iron ions in the cell. Versican is a large chondroiton sulphate proteoglycan with a molecular mass of >1000 kDa (Zimmermann and Ruoslahti 1990). The presence of these proteins in SAF preparations is also likely to be down to their high molecular weights. Myomesin-2 has a molecular weight of 185 kDa and is located in striated muscle cells. The SAF preparation is from mouse brains and this identification could either represent contamination of the SAF preparation or a false positive from the

Protein ID	Gene ID	Subcellular Location	WT Peptide Hits	Null Peptide Hits
Ca^{2+}/Cal dependent protein kinase (α type)	CamK2a	Cell junction	6	4
Ca^{2+}/Cal dependent protein kinase (β type)	CamK2b	Cell junction	5	0
Ferritin (light chain 1)	Ftl1	Cytoplasm	6	0
Histone (H1.2)	Hist1h1c	Nucleus	0	2
Versican core protein	Vcan	Extracellular	2	0
Myomesin-2	Myom2	Cytoskeleton	0	2
Myelin associated oligodendrocyte basic protein isoform 1	Mobp	Cytoplasm	2	2
Vomeronasal-1 receptor	V1rh5	Plasma membrane	0	2

Table 5.1: MASCOT searches of data generated by means of mass spectrometry resulted in the identification of peptides from proteins associated with the mock-SAF preparations of uninfected mouse brains.

This table outlines the identifications of proteins associated with a mock-SAF preparation on mouse brains from WT and $PrP^{0/0}$ mouse brains. Four brains (for both WT and $PrP^{0/0}$) were homogenised prior to detergent extraction and differential centrifugation to precipitate protein species. Precipitated proteins were reduced and alkylated in 6 M guanidine hydrochloride prior to tryptic digestion and separation of sample by HPLC for which the elute was analysed by tandem MS/MS. Peptide hits represent best data from three replicate experiments

mass spectrometry approach. Myelin associated oligodendrocyte basic protein is an abundant protein that is constitutively expressed in oligodendrocytes in the CNS (Holz *et al.*, 2000). The presence of this protein in the SAF preparations is likely to be by chance due to its high abundance in the brain. Vomeronasal-1 receptors are G-protein coupled receptors that are present on the surface of vomeronasal sensory neurons and are involved in pheromone and odorant binding (Grus *et al.*, 2007). The vomeronasal receptor has a molecular weight of 42 kDa and its occurrence in the mock SAF preparation is difficult to interpret.

In summary, these experiments have provided a background list of proteins that appear to be isolated by the techniques employed in SAF preparations, even in the absence of TSE disease in mice. This therefore, allows such proteins to be discounted from real results of the analyses of SAF preparations.

5.4 Mass Spectrometry of SAF preparations

Scrapie associated fibrils were isolated from the brains of infected mouse brains for proteomic analyses. SAF preparations are known to be principally composed of amyloid fibrils of PrP^{Sc}, however several authors have reported the presence of a polysaccharide scaffold and proteoglycans (Snow *et al.*, 1989, Appel *et al.*, 1999, Dumpitak *et al.*, 2005). SAF were prepared from the brains of mice infected with 79A, ME7 and 22F from which 5 µl (equivalent to 5 µg) of pre-sonicated fibrils were resuspended in 95 µl of 6 M guanidine hydrochloride. Denaturation in guanidine is necessary to cause significant denaturation of the fibril and expose any co-factors associated internally. Reduction and carboxymethylation of the disulphide bond in this buffer will also allow for as many cleavage sites in the amyloid fibril to be targeted for tryptic digestion. SAF samples were precipitated and resuspended in a 4 M urea based buffer to aid solubility and digestion with trypsin at 37 °C and the peptides analysed by MS/MS.

For every protein identified by the MASCOT search, a minimum of two peptide hits were required to give a significant detection score. Table 5.2 lists the number of peptide hits identified by mass spectrometry.

Protein ID	Gene ID	Subcellular Location	Number of Peptide Hits		
			ME7	79A	22F
Actin, cytoplasmic 1	Actb	Cytoskeleton	8	13	4
Tubulin beta-2A chain	Tubb2a	Cytoskeleton	0	5	0
Tubulin beta-2B chain	Tubb2b	Cytoskeleton	10	11	2
Tubulin beta-2C chain	Tubb2c	Cytoskeleton	10	12	0
Tubulin beta-4 chain	Tubb4	Cytoskeleton	0	0	6
Tubulin beta-5 chain	Tubb5	Cytoskeleton	0	2	2
Tubulin alpha-1A	Tuba1a	Cytoskeleton	5	8	3
Tubulin alpha-1B	Tuba1b	Cytoskeleton	0	8	0
Na^+/K^+ transporting ATPase subunit α-3	ATP1a3	Plasma membrane	5	9	4
Na^+/K^+ transporting ATPase subunit α-2	ATP1a2	Plasma membrane	5	0	0
Guanine nucleotide binding protein subunit-α	Gnao1	Plasma membrane	4	5	3
Creatine kinase B type	Ckb	Cytoplasm	4	5	3
GAPDH isoform 1	Gapdh	Cytoplasm	3	5	3
Apolipoprotein E precursor	Apoe	Plasma membrane/secreted	9	3	0
Prolow density lipoprotein receptor precursor	Lrp1	Plasma membrane	0	3	0
2',3'-cyclic nucleotide 3'-phosphodiesterase isoform	Cnp1	Plasma membrane	0	2	0
Heat shock cognate 71 kDa protein	Hspa8	Cytoplasm	3	3	0
Synapsin-1 isoform 1b	Syn1	Plasma membrane/Golgi body	0	3	0
Alpha enolase	Eno1	Cytoplasm/plasma membrane	2	2	0
Vesicle fusing ATPase	Nsf	Cytoplasm/Golgi body	2	0	0
Disks large homolog 4	Dlg4	Plasma membrane	0	0	2

Dynamin-1	Dnm1	Clathrin pits	0	2	0
TBC1 domain family, member 10b	Tbc1db10b	Cytoplasm	2	0	0
Prion protein	PrP	Plasma membrane	6	5	3

Table 5.2: Proteomic determination of molecules co-purifying with PrP^{Sc} in scrapie associated fibrils from ME7, 79A and 22F mouse passaged scrapie.

This table lists the identification of proteins associated with a SAF preparation on mouse brains infected with ME7, 79A and 22F. Four brains (for all three strains of mouse scrapie) were homogenised prior to detergent extraction and differential centrifugation to precipitate protein species. Precipitated proteins were reduced and alkylated in 6 M guanidine hydrochloride prior to tryptic digestion and separation of sample by HPLC for which the elute was analysed by tandem MS/MS. Peptide hits represent best data from three replicate experiments.

A MASCOT search of the IPI murine database identified multiple subunits of tubulin and actin in SAF preparations from ME7, 79A and 22F infected mouse brains. These proteins are cytoskeletal and therefore are abundant and have a high molecular weight. In addition to cytoskeletal proteins, many plasma membrane bound proteins were also identified and included proteins such as Na^+/K^+ transporting ATPase and guanine nucleotide binding protein. The subunits from these two proteins were detected in all three SAF preparations suggesting that they are not necessarily strain specific co-factors. However, the presence of these plasma membrane proteins may indicate that the location of conversion of PrP^C to PrP^{Sc} is on the plasma membrane. Other plasma membrane bound proteins that were detected were apolipoprotein E and alpha-enolase (also found in the cytoplasm) in ME7 and 79A SAF preparations, 2',3'-cyclic nucleotide 3'-phosphodiesterase isoform, prolow density lipoprotein receptor and synapsin-1 (also found in the Golgi body), dynamin-1 in only the 79A SAF preparation and finally disks large homolg 4 in only the 22F SAF preparation.

In addition to plasma membrane bound proteins there were some cytoplasmic based proteins detected. These included creatine kinase B and GAPDH in all three SAF preparations, heat shock cognate 71 kDa protein in the ME7 and 79A preparations and finally, TBC1 domain family member 10b in the ME7 SAF preparation. The protein vesicle fusing ATPase was detected in the ME7 SAF preparation and is reported to be cytoplasmic, however it is also found in the Golgi body.

Further analysis of these proteins detected by MS/MS in the literature has indicated that some of these proteins have previously been correlated to either PrP^C function or associated with PrP^{Sc} (Spielhaupter and Schätzl, 2001, Magalhães *et al.*, 2002, Skinner *et al.*, 2006, Petrakis *et al.*, 2008). The results of proteomic analysis of PrP interaction partners from cross-linking experiments with the β4 subunit of nicotinic acetycholine have suggested that a multiprotein complex is found on the plasma membrane of neurons (Petrakis *et al.*, 2008). This complex was reported to include other proteins identified in the current study, including Na^+/K^+ ATPase, 2',3'-cyclic nucleotide 3'-phosphodiesterase, β-actin, creatine kinase and synapsin-1.

5.5 Mass spectrometry of SAF preparations pre-treated with PK

The analysis of tryptic peptides of SAF preparations from three strains of mouse scrapie revealed a selection of candidate proteins that could be prion co-factors (table 5.2). This list is relatively large and a possible method to refine the list was to exclude proteins that are not specifically attached to the amyloid fibril, but rather co-purify by associating to the fibril. Amyloid fibrils are aggregates of proteins which will have many potential interaction sites for the non-specific binding of proteins, present in the local vicinity of the aggregate or which are exposed to the fibril during purification. To exclude these proteins, SAF preparations were pre-treated with PK, which digested non-specific proteins into peptides that were subsequently not identified by mass spectrometry techniques. This is because the peptide search parameters are set to peptides that are generated by tryptic digestion rather than generated by another proteolytic enzyme. PrP^{Sc} is partially resistant to PK digestion and the C-terminus of PrP, along with other protein species, survived PK digestion as judged by separation by SDS PAGE and stained with silver nitrate solution (figure 5.1).

The sample preparation protocol in chapter 2 (section 2.1.2.6 and 2.1.2.7) for mass spectrometry analysis of SAF was followed, with the following alterations. Pre-sonicated SAF preparations were incubated with 60 μg/μl of PK at 37 °C for one hour and the reaction was stopped by the addition of pefabloc to a final concentration of 25 mM. Digested SAF preparations were precipitated in acetone to concentrate protein and to separate the protein from PK and pefabloc. Acetone precipitation was incorporated after PK digestion because it was believed that this organic solvent limited the amount of PK peptides that would be precipitated. Acetone is not as hydrophobic as other solvents and therefore small peptides would be less prone to precipitation as they would if absolute ethanol or chloroform was used. The pellet was resuspended in 6 M guanidine hydrochloride as per the standard protocol adopted for mass spectrometry of SAF preparations.

The results of the proteomic analyses of SAF preparations pre-treated with PK include only a very few significant protein identifications and are given in table 5.3.

Protein ID	Gene ID	Subcellular Location	Number of Peptide Hits		
			ME7	79A	22F
Myelin-associated oligodendrocyte basic protein	Mobp	Cytoplasm	3	0	0
Prolow-density lipoprotein	Lrp1	Plasma membrane	2	0	0
Ferritin heavy chain	Fth1	Cytoplasm	0	0	2
Ferritin light chain 1	Ftl1	Cytoplasm	0	0	2
Shugoshin-like 2	Sgol2	Nucleus	0	0	2
Dmx-like 2	Dmxl2	Plasma membrane	0	2	0

Table 5.3: Identification of peptides detected by mass spectrometric analysis of SAF preparations pre-treated with PK from mouse brains infected with three different mouse scrapie strains.

This table lists the identification of proteins associated with a SAF preparation pre-treated with PK, on mouse brains infected with ME7, 79A and 22F. Four brains (for all three strains of mouse scrapie) were homogenised and treated with PK prior to detergent extraction and differential centrifugation to precipitate protein species. Precipitated proteins were reduced and alkylated in 6 M guanidine hydrochloride prior to tryptic digestion and separation of sample by HPLC for which the elute was analysed by tandem MS/MS. Peptide hits represent best data from three replicate experiments

In this table, proteins such as ferritin and myelin associated oligodendrocyte basic protein were included even though they were identified in the SAF preparations of uninfected mouse brains (table 5.1). However, some proteins were identified specifically in preparations from different strains; these are, prolow-density lipoprotein in ME7 SAF preparations, Dmx-like 2 protein in 79A preparations and shugoshin-like 2 protein in 22F preparations. Prolow-density lipoprotein and Dmx-like 2 protein are plasma membrane proteins, however shugoshin-like 2 is a nuclear protein that would appear, initially, to have little relevance to PrP conversion or TSE disease.

5.6 Validation of proteins detected by mass spectrometry by Western blotting

The proteomic determination of proteins associated with SAF preparations by mass spectrometry provided a list of protein identifications. However, to confirm the presence of these proteins in the sample, a second experiment to validate mass spectrometry results was required. Identification of proteins was therefore done by Western blotting with antibodies directed against a selection of proteins identified in SAF preparations. Primary antibodies for Na^+/K^+ transporting ATPase, apolipoprotein E and GAPDH were obtained based on antibody availability.

Figure 5.2 shows Western blots of SAF preparations from the brains of mice infected with ME7, 79A and 22F, along side negative control mock-SAF preparations from both uninfected wildtype and $PrP^{0/0}$ mouse brains. Apolipoprotein E and GAPDH were found to be present in all three SAF preparations whereas Na^+/K^+ transporting ATPase was detected only in ME7 and 79A SAF preparations. Western blotting of apolipoprotein and GAPDH in 22F showed only a faint band representing each of these proteins when compared against the more intense bands on the Western blot for ME7 and 79A SAF preparations. Preparation of 22F fibrils was hindered by what appeared to be co-purifying proteases leading to degradation of all proteinaceous material in the sample. This observation was made when comparisons of 22F SAF preparations were done by Western blotting with 8H4, 24 hours after isolation from mouse brains. Immediately after isolation from infected mouse brains, Western blot fibrils produced the corresponding full length di-, mono-, and unglycosylated bands of PrP^{Sc}. However, after only 24 hours, these proteins became truncated,

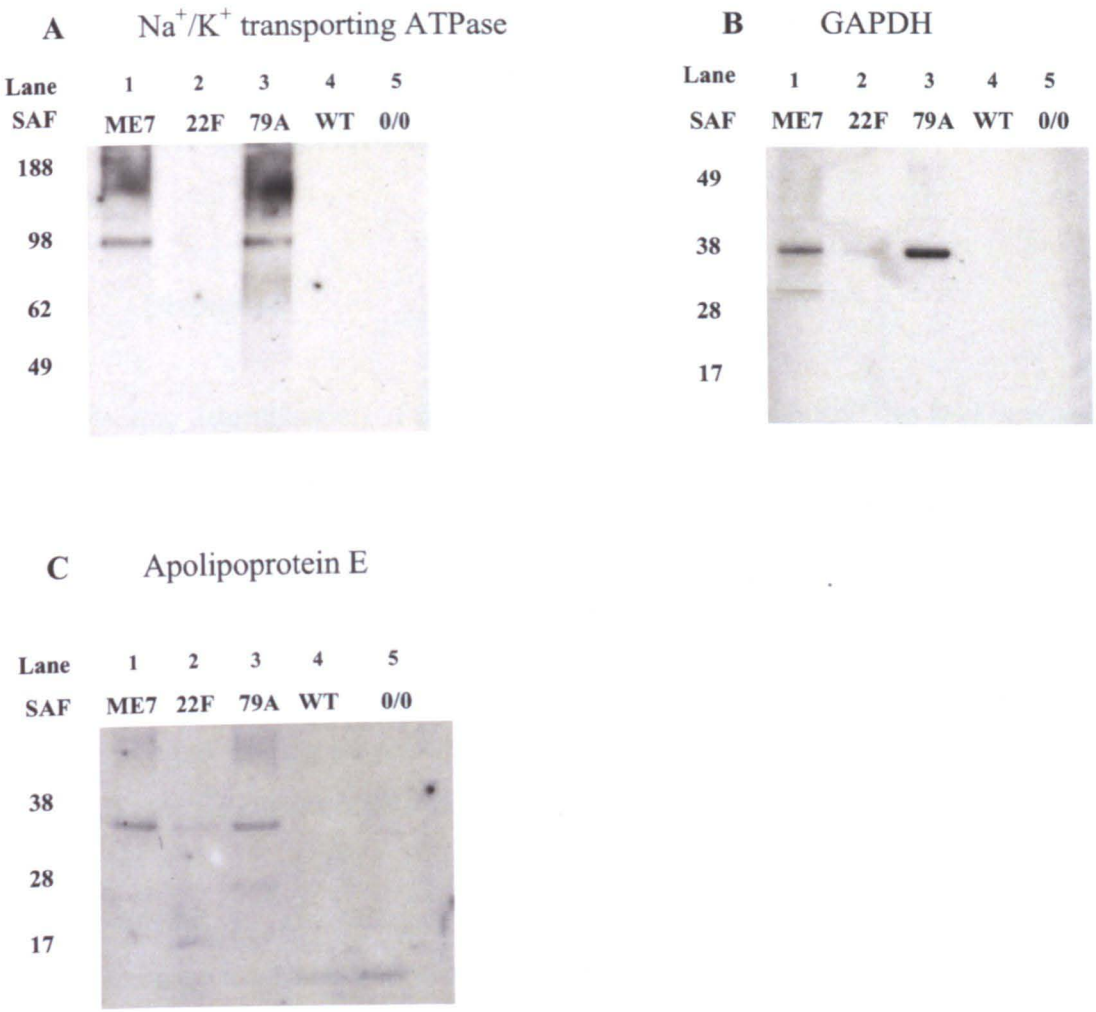

Figure 5.2: Western blot analysis of mouse scrapie associated fibrils for proteins previously identified by mass spectrometry.

0.25 µg/µl pre-sonicated SAF from an ME7 (lane 1), 22F (lane 2) and 79A (lane 3) SAF preparation was loaded onto a 12-well 4-12% Bis-Tris SDS PAGE and protein species were separated at 180 V for 45 minutes. The SDS PAGE gel was blotted onto PVDF membrane and probed with the primary antibody for (A.) Na^+/K^+ transporting ATPase at 1:3000, (B.) GAPDH at 1:32,000 or (C.) Apolipoprotein E at 1:1000. The secondary antibodies applied to the blot were (A.) anti-rabbit HRP at 1:3000, (B.) anti-rabbit HRP at 1:3000 (C.) anti-rat HRP at 1:3000. In lane 4 and lane 5 there was 0.25 µg/µl of SAF preparation material from uninfected wild type (WT) and $PrP^{0/0}$ (0/0) mouse brains respectively. Molecular weight markers are in kDa.

characterised by a loss in molecular weight and the presence of a 4th band on the Western blot that was assumed to be truncated unglycosylated PrP^{Sc} (data not shown). As a control experiment, SAF preparations from uninfected wild type and $PrP^{0/0}$ mouse brains were also Western blotted for these three proteins, with neither Na^+/K^+ transporting ATPase, GAPDH or apolipoprotein E being detected in these samples.

5.7 Discussion

Proteomic determination of molecules that co-purify with PrP^{Sc} in SAF preparations was primarily done to identify plasma membrane derived molecules that may be involved in prion conversion. In chapter 4, LD9 low density subcellular fractions enhanced conversion efficiency of ME7 and 79A in the CFCA (figure 4.4 and 4.9 respectively). If there are molecules in the plasma membrane that are prion co-factors then it is likely that during conversion of PrP^C to PrP^{Sc}, these co-factors will become incorporated into the amyloid fibril during polymerisation and aid in the retention of strain specific attributes following infection *in vivo*.

To attempt to characterise non-PrP constituents of SAF preparations, SAF preparations from ME7, 79A and 22F infected mouse brains were separated by SDS PAGE followed by visualisation by silver staining (figure 5.1). SAF preparations were either treated or not treated with PK prior to separation by SDS PAGE. Pre-treatment with PK will degrade any proteins that either co-purify with SAF preparations or are non-specifically attached to the surface of the fibril. However, even though I hypothesised that different TSE strains would contain different molecular constituents, silver staining of PK treated SAF preparations of three different strains of mouse scrapie did not highlight any obvious differences in their silver staining profile. Mass spectrometry was therefore used to analyse SAF preparations from mice infected with different strains of mouse scrapie.

Preparation of SAF by detergent extraction and differential centrifugation produces an enrichment of PrP^{Sc}; however there will be contamination from other proteins. These contaminants will either have similar properties to SAF, such as a high molecular weight and/or insolubility, or will be associated with PrP^{Sc} non-

specifically. To account for proteins that may co-purify with PrP^{Sc}, the SAF preparation protocol was applied to uninfected wild type and $PrP^{0/0}$ mouse brains (table 5.1). Proteins that were purified in these preparations were subsequently excluded from future results of SAF preparations that were carried out on mouse scrapie infected mouse brains. These list of proteins included CamKII, a serine/threonine protein kinase located in synaptic junctions. Not only is this protein very abundant but it also has a molecular weight of 500-600 kDa, making this protein a good example of the type of protein that will be isolated from the brain using the SAF preparation protocol. Other proteins isolated from brain using the SAF protocol included proteins such as ferritin and versican core protein which are 450 kDa and >1000 kDa respectively. Ferritin is also known to oligomerise which will cause further increases in molecular weight (Hasan *et al.*, 2006) and has previously been shown to contaminate SAF preparations (Walker *et al.*, 1996).

SAF preparations from ME7, 79A and 22F infected mouse brains were analysed by mass spectrometry and peptide MS/MS data was searched against the IPI mouse database of known murine proteins using the MASCOT search engine. Proteins that were identified in the uninfected SAF preparation and listed in table 5.1, were excluded from table 5.2. In all SAF preparations various actin and tubulin isoforms were identified which are high molecular weight cytoskeletal proteins. Although these proteins may be adhering to PrP^{Sc} non-specifically they cannot be discounted yet as they may provide a scaffold that aids in misfolding and amyloid fibril morphology.

Mass spectrometry of tryptic peptides from ME7, 79A and 22F SAF preparations was used to identify the co-purifying proteinaceous constituents from these three different strains of mouse scrapie. As expected, PrP was detected in all three SAF preparations validating the success of the SAF protocol and also the mass spectrometric identifications. Two of the more significant protein identifications were for two subunits of the Na^+/K^+ transporting ATPase. This sodium pump distributes Na^+ and K^+ ions across the plasma membrane which determines the resting potential for several important secondary functions. This plasma membrane bound enzyme transports two potassium ions inwards for every three sodium ions it transports to the extracellular matrix. It is an important enzyme found in all cells,

most notably in neurons where it is responsible for the resting potential necessary for transmitting synaptic impulses (Blanco and Mercer, 1998). Mutations and defects in this protein have been reported to be associated with neurodegenerative disorders. Work published by Palladino and colleagues observed that mutations in the *Drosophila* α-subunit of Na^+/K^+ transporting ATPase resulted in severe neuronal damage and a marked reduction in lifespan (2003). Previous work by the same group had indicated that inhibition of the Na^+/K^+ transporting ATPase caused vacuolation similar to that seen in the spongiform of TSE infections (Calandriello *et al.*, 1995). The authors of this publication hypothesised that Na^+/K^+ transporting ATPase was targeted by the infectious agent and thus caused the characteristic spongiosis of TSE diseases. Although this is a tenuous link and probably unlikely, it can be hypothesised that PrP^C may interact with Na^+/K^+ transporting ATPase on the plasma membrane of neurones. The loss of this enzyme by incorporation into amyloid fibrils may play a part in spongiosis of the grey matter of TSE infected brains. This hypothesis is supported by the recent publication by Petrakis and colleagues, where PrP^C was shown to interact with the β4 subunit of nicotinic acetycholine (nAChR). Further study of this interaction revealed that PrP^C may be a member of a multiprotein complex incorporating nAChR and Na^+/K^+ transporting ATPase (Petrakis *et al.*, 2008). Other proteins included in this complex included the proteins 2',3'-cyclic nucleotide 3'-phosphodiesterase and synapsin-1, which were previously shown to interact with PrP^C (Petrakis and Sklaviadis, 2006). These two proteins were also detected in SAF preparations as indicated in table 5.2.

The protein 2',3'-cyclic nucleotide 3'-phosphodiesterase (CNP1) is a membrane bound enzyme involved in the synthesis of the myelin sheath that surrounds the axon of neurons (Kursula *et al.*, 2008). However, the identity of this enzyme is unknown, although it was reported that CNP1 is associated with microtubules and may act as an anchor for tubulin (Bifulco *et al.*, 2002). Deregulation in CNP1 is believed to play an important pathogenic role in demyelinating diseases of the brain, such as multiple sclerosis (Rösener *et al.*, 1997). A putative role for CNP1 in PrP^C cell biology may be to provide an anchor point between the previously mentioned multiprotein complex and the cytoskeleton.

Synapsin-1 is a plasma membrane bound protein involved in the regulation of neurotransmitter release at the synaptic junction (De Camilli *et al.*, 1990). Previous reports have shown that synapsin-1 specifically interacts with PrP at the presynaptic junction, suggesting a role for PrP^{C} in the regulation or recycling of synaptic vesicles (Spielhaupter *et al.*, 2001). In another report, PrP^{Sc} was demonstrated to co-localise with synapsin-1 and other synaptic proteins at the presynapse, indicating synaptic transport as a possible route of PrP^{Sc} spread throughout the brain (Kovács *et al.*, 2005).

The literature was surveyed for indicators that the remainder of the protein identifications made by mass spectrometric analysis of SAF preparations may associate with PrP. The identification of dynamin-1 in the 79A SAF preparation is interesting since dynamin-1 has previously been reported to play an important role in the internalisation of PrP^{C} (Magalhães *et al.*, 2002). In this study, PrP was shown to be dependent on dynamin-1 mediated internalisation into the endosomal pathway for degradation or recycling back to the plasma membrane. The remainder of protein identifications made by mass spectrometric analysis had no previously reported links to PrP^{C} or PrP^{Sc}. However this does not rule out these proteins as co-factors but instead necessitates a more in-depth analysis of their structure and function to determine any potential involvement with PrP.

The generation of an extensive list of proteins identities associated with SAF preparation makes analysis of strain specific markers difficult. To further process this list down to more specific interactions between fibrils and potential co-factors, treatment of SAF with PK prior to tryptic digestion was carried out. It was envisaged that this process would degrade all proteins that are loosely attached to the surface of the fibril. If co-factors are present in the amyloid fibril then they are as likely to be present internally as well as externally. It was hypothesised that these proteins will be buried away from the activity of PK but once resuspended in 6 M guanidine hydrochloride for reduction and alkylation of the disulphide bridge, potential co-factors will become revealed and susceptible to tryptic digestion and detection by mass spectrometry.

MASCOT searches on the identification of peptides from PK-treated SAF preparations generated two proteins that were previously unidentified in SAF preparations. The proteins shugoshin-like 2 and Dmx-like 2 were detected in 22F and 79A SAF preparations, respectively. Shugoshin-like 2 is located in the nucleus of the cell and is an important protein associated with the protection of centromere cohesion prior to meiosis (Kitajima *et al.*, 2006). The function of this protein makes it an unlikely candidate of a prion co-factor. On the other hand, the Dmx-like 2 (Dmxl2) protein is suggested to be a scaffold protein for MADD and RAB3GA. These are located in the plasma membrane of synaptic vesicles and the synapse junction (Munton *et al.*, 2007). However, the functional identity of Dmxl2 is only by similarity and not through experimental data. The two proteins that Dmxl2 is reported to interact with, MADD and RAB3GA, play significant roles in survival and death through MAP kinase activation and caspase-mediated cell death. PrP is hypothesised to play a role in cell signalling and cell survival, making an interaction with proteins in the MAP kinase pathway a possibility for PrP function. Whether or not these proteins are necessary for prion conversion is unknown and further analysis into possible interaction partners of PrP in the MAP kinase pathway may be a favourable place to start. Follow up experiments on determining the relevance of these proteins are discussed in chapter 7.

Mass spectrometric analysis of ME7 SAF preparation that was pre-treated with PK again revealed peptides for the protein prolow-density lipoprotein receptor (Lrp1). This protein was originally detected in the 79A SAF preparation that was not pre-treated with PK which suggests that this marker is not strain specific (table 5.2). This protein is a multifunctional plasma membrane receptor involved in the endocytosis of many different types of extracellular proteins (Herz *et al.*, 1992). One of the more interesting functions was the suggestion that Lrp1 removes protease inhibitors from the extracellular matrix (Strickland *et al.*, 1990, Kristensen *et al.*, 1990). In addition to these observations, the cytoplasmic tail of Lrp1 is reported to interact with apolipoprotein E, another protein identified in 79A SAF preparations (Chen *et al.*, 1990).

Support for these findings has come from two publications published recently in proteomic journals. Petrakis and colleagues used LC-MS/MS techniques, which were

similar to my methods, to identify a series of proteins that co-purify with natural scrapie isolated from ovine brain (2009). In this study, proteins such as calcium/calmodulin-dependent protein kinase-II (CamKII/A), ferritin, versican and ubiquitin were identified. These proteins were also detected in my SAF preparations, however, I also detected these proteins in mock-SAF preparations of uninfected mouse brain. Nevertheless, Petrakis and colleagues did detect some novel proteins, including brain link protein (BRAL1), desmoglein1 (DSG1) and plakoglobin (JUP) all of which have been suggested to be involved in prion propagation and therefore could be used as a target for therapeutics. A separate study on the proteomic analysis of SAF preparations from scrapie infected hamster brain showed similar results to that by Petrakis and my own research (Giorgi *et al.*, 2009). Interestingly, in this study, proteins such as apolipoprotein E, GAPDH and tubulin were also found to be associated with SAF preparations.

The analysis of mouse scrapie strains by mass spectrometry has raised questions about some of the various proteins identified and their potential roles in PrP conversion. Some are not likely to be strain specific and may instead indicate the site of conversion where these proteins were accidently incorporated, rather than playing an important role such as strain differentiation. Ideally, recombinant protein of each of the potential co-factor candidates would be acquired and used to supplement the CFCA to analyse the effect on the conversion of rMo3F4PrP to a PK-resistant isoform. Unfortunately, proteins such as Na^+/K^+ transporting ATPase are multi-domain proteins that span the membrane several times. This is almost impossible to over-express and purify using models such as bacteria. In addition, time and financial constraints prevented further analysis into recombinant proteins and the supplementation into the CFCA and other PrP misfolding assays.

6. Development of protein misfolding assays and the addition of cell-derived conversion enhancing factors to the oligomerisation assay

6.1 Introduction

In chapter 4, results from the subcellular fractionation of TSE susceptible cell lines showed that plasma membrane-enriched fractions increase conversion efficiency of rPrP in an ME7-seeded CFCA. In addition, plasma membrane fractions prepared from cells that are not susceptible to ME7 infection, SMB-PS cells, also increased conversion efficiency of PrP seeded by ME7 PrP^{Sc}. The mechanisms by which plasma membrane fractions enhance PrP conversion are not clear, but the constituents of the plasma membrane fractions may aid conversion by providing a 'surface' which can enhance PrP misfolding in general, rather than TSE-specific conversion. The interaction between the rPrP substrate and plasma membrane fractions could be investigated further by use of PrP misfolding assays that do not incorporate a PrP^{Sc} seed. I hypothesised that an alternative *in vitro* assay, such as an oligomerisation assay, would provide an understanding on how PrP refolding was affected when in the presence of plasma membrane-enriched fractions. This chapter details the optimisation and validation of an *in vitro* oligomerisation assay that involved the refolding of rPrP to β-sheet rich oligomers in the absence of any PrP^{Sc} seed.

The *in vitro* refolding of rPrP into an infectious entity has been proposed as a means to effectively demonstrate the protein only hypothesis. Over the past few years, the seedless refolding of rPrP into a form which causes disease in animals has been published by several scientific groups (Legname *et al.*, 2004, Legname *et al.*, 2005, Castilla *et al.*, 2006, Simoneau *et al.*, 2007). However, these publications have met criticism due to either low infectivity titres of the newly generated synthetic prion or have not faithfully passed on strain properties onto nascent PrP^{C}. To acquire the structural conformation associated with each strain of TSE requires the imprinting of the conformation from the infectious agent in the first instance and then segregating the original seed from the newly created PrP^{Sc}, prior to *in vivo* infection studies. In addition, it has been demonstrated that PrP^{Sc} potentially interacts with several interaction partners *in vivo*, which may play important roles in the make-up of the infectious agent and aiding in the differentiation of strains (Toyama *et al.*, 2007). More specifically, recent studies have indicated the roles of polyanions, lipids and

glycogen as structural scaffold molecules that may play roles in the formation of distinct PrP^{Sc} conformations and fibril morphology.

In vitro PrP-refolding assays in the absence of a PrP^{Sc} seed may also provide detailed information on the folding landscape of PrP, as well as clues about intermediate species between PrP^{C} and the PrP^{Sc} isoform found in amyloid fibrils. Critical observations in the brains of some vCJD and GSS infected humans have shown that neurodegeneration has occurred in the absence of detectable amyloid fibrils (Budka *et al.*, 1995, Budka *et al.*, 1997). In addition, pathological examinations of certain lines of transgenic mice infected with GSS have indicated that even in the presence of amyloid fibrils, there was no neurodegeneration (Piccardo *et al.*, 2007). These observations raised key questions about the nature of the infectious agent and the role of mature amyloid fibrils in disease. In other protein misfolding disorders, such as Alzheimer's disease, the neurotoxic agent has been suggested to be smaller, soluble oligomers composed of a few subunits of Aβ rather than a mature polymeric fibril of aggregated protein (Lue *et al.*, 1999, McLean *et al.*, 1999). In fact, the higher order aggregation of protein is suggested instead, to be a protective measure during which neurotoxic oligomers are sequestered into inert fibrils. Therefore investigations of how PrP misfolds and the mechanisms that control such a process may reveal a better understanding as to what structures PrP can form and their relationship to neurotoxicity.

The *in vitro* refolding of recombinant PrP has been demonstrated in many publications and a variety of different methods have been used to cause the refolding of either full length or truncated recombinant PrP, to β-sheet rich isoforms (Zhang *et al.*, 1997, Lu *et al.*, 2001, Sokolowski *et al.*, 2003, Torrent *et al.*, 2003, Tahiri-Alaoui *et al.*, 2004, Bocharova *et al.*, 2005, Rezaei *et al.*, 2005, Martins *et al.*, 2006, Redecke *et al.*, 2006). The two known isoforms of PrP, *in vitro*, that are β-sheet rich are referred to as oligomers and fibrils. Oligomers are smaller in size than fibrils and consist of only a few subunits of PrP. In contrast, the fibrilisation pathway forms mature fibrils of PrP consisting of many subunits. Fibrils are generally more resistant to proteolytic digestion and have a higher binding affinity to thioflavin-T, a chemical used to detect protein fibrils.

Oligomerisation of unfolded, truncated, recombinant human prion protein (trHuPrP) with a methionine at residue 129 (Met129) proceeded at a faster rate than trHuPrP with a valine at residue 129 (Val129) (Tahiri-Alaoui *et al.*, 2004). It was observed that trHuPrP(Val129) had a higher propensity to form α-helical rich monomers rather than β-sheet rich oligomers. This correlates with *in vivo* data indicating that humans homozygous for Met129 are more susceptible to vCJD than those who are homozygous for Val129 or Met/Val heterozygotes (Collinge *et al.*, 1991, Palmer *et al.*, 1991). Further work with these two polymorphic variants demonstrated that the trHuPrP(Val129), not trHuPrP(Met129) had a higher propensity to form fibrils than trHuPrP(Met129) when spontaneous or seeded fibrilisation was initiated (Baskakov et al., 2005). These publications therefore suggest that refolding of rPrP into oligomeric isoforms may be more physiologically relevant than rPrP induced into the fibrilisation pathway. This work has been supported by investigations into the neurotoxicity of oligomers *in vitro* and *in vivo* (Simoneau *et al.*, 2007). In this work, oligomers and fibrils were made from full length rMoPrP by incubation of α-monomeric PrP in an acidic buffer at 45 °C (Rezaei *et al.*, 2005, Eghiaian *et al.*, 2007). *In vitro* cultures of mouse cortical neurons were separately exposed to β-oligomers and fibrils and, interestingly, only the β-oligomers caused toxicity. The β-oligomers and fibrils were then intracerebrally injected into C57BL/6 $PrP^{+/+}$ and $PrP^{0/0}$ mice whereupon neurodegeneration was observed in both mouse lines injected with β-oligomers. Fibril preparations did not cause the same extent of neurodegeneration. Taken together, these publications would suggest that the *in vitro* oligomerisation pathway is more indicative of the misfolding of PrP into neurotoxic species *in vivo* during disease. Based on this data, this was the assay I chose for the oligomerisation of rPrP.

The oligomerisation of trHuPrP, as previously demonstrated, provided the basis of a method to optimise and set-up an *in vitro* refolding assay that could be used in conjunction with the CFCA to understand the role of co-factors in PrP misfolding. Although Tahiri-Alaoui's study used N-terminally truncated protein, for the current study the use of truncated variants of PrP was not ideal as the absence of the PrP N-terminus (1-89) may inhibit the interaction between PrP and potential co-factors. In addition, this project was principally dealing with strains of mouse derived scrapie as a basis to understand the role of co-factors in strain variation. Therefore, full length

rMoPrP was the desired substrate for all assays, including the CFCA and the oligomerisation assay.

Initially this chapter describes the development of an oligomerisation assay that involves the conversion of full length α-monomeric rMoPrP to β-sheet rich oligomers. The assay should be reproducible, and provide kinetic or thermodynamic data on the oligomerisation pathway such that variations to this pathway caused by the addition of putative co-factors could be quantified. Several methods were researched to find an assay that was experimentally robust and physiologically relevant.

At the outset, the main aim of this project was to determine the subcellular localisation of strain specific co-factors, their identities and how they interact with PrP^{C} and PrP^{Sc}. Chapter 3 describes the subcellular fractionation of TSE susceptible cell lines into samples enriched for different compartments of the cell. In chapter 4, plasma membrane-enriched fractions from LD9 cells were shown to enhance the conversion efficiency of recombinant PrP seeded with PrP^{Sc} from two strains of scrapie, ME7 and 79A, in the CFCA. However, this enhancement of conversion was not strain specific which was an unexpected result since the cell line used was susceptible to the ME7 strain of mouse scrapie, but not to 79A. To determine the interaction between plasma membrane and rMoPrP and whether the addition of plasma membrane made rMoPrP more susceptible to generic misfolding, a protein misfolding assay was developed and optimised to investigate the effect of plasma membrane-enriched fractions on PrP misfolding (see chapter 6). In this chapter, I also describe the use of the oligomerisation assay to analyse the effect plasma membrane enhanced fractions from the LD9 cell line, on the refolding of rMoPrP to oligomeric isoforms.

6.2 Calibration of size exclusion chromatography column

The oligomerisation assay involves the analysis of the misfolding of rPrP to a β-oligomer isoform. However, it is difficult to detect PrP oligomers against a background of PrP monomers without prior separation of these two isoforms. To do this size exclusion chromatography (SEC) column was utilised which, when under high pressure, separated different solubilised molecular species by their molecular weight. A SEC column contains a column of densely packed gel filtration beads that are porous and of a very precise size. Under high pressure from the HPLC, the sample will be forced into the column, whereupon smaller proteins move in and out of the pores in the SEC beads and thereby take longer to pass through the column than proteins of a higher molecular weight. Proteins that elute from the column can be monitored by absorbance of UV at 280 nm (amino acid tryptophan), 220 nm (peptide bond).

The optimisation and validation of the refolding of rPrP to a β-oligomer isoform in this chapter used oligomer quantitation based on two different SEC columns. The first column used was the TSKgel G3000SW (Tosoh Bioscience) which was 600 mm in length and contains particles with a diameter of 10 μm and 250 Å pores. This column had a separation limit of 10 kDa to 500 kDa for globular proteins. Calibration of this column was done by monitoring the elution of molecular weight standards including thyroglobulin (660 kDa), γ-globulin (150 kDa), ovalbumin (45 kDa), ribonuclease A (13.7 kDa), p-aminobenzoic acid (137 Da). A graph of elution volume verses molecular weight for these standard proteins is shown in figure 6.1 panel A.

The second column was used to further separate higher molecular weight species from each other. This column was a TSKgel G4000SWxl (Tosoh Bioscience) and was 300 mm in length containing gel filtration particles with a diameter of 8 μm and 450 Å pores. This column had a separation limit of 20 kDa to 7000 kDa for globular proteins. Calibration of this column was done by monitoring the elution of the molecular weight standards including thyroglobulin (660 kDa), apoferritin (443 kDa), γ-globulin (150 kDa) and p-aminobenzoic acid (137 Da). A graph of elution

A TSKgel G3000SW

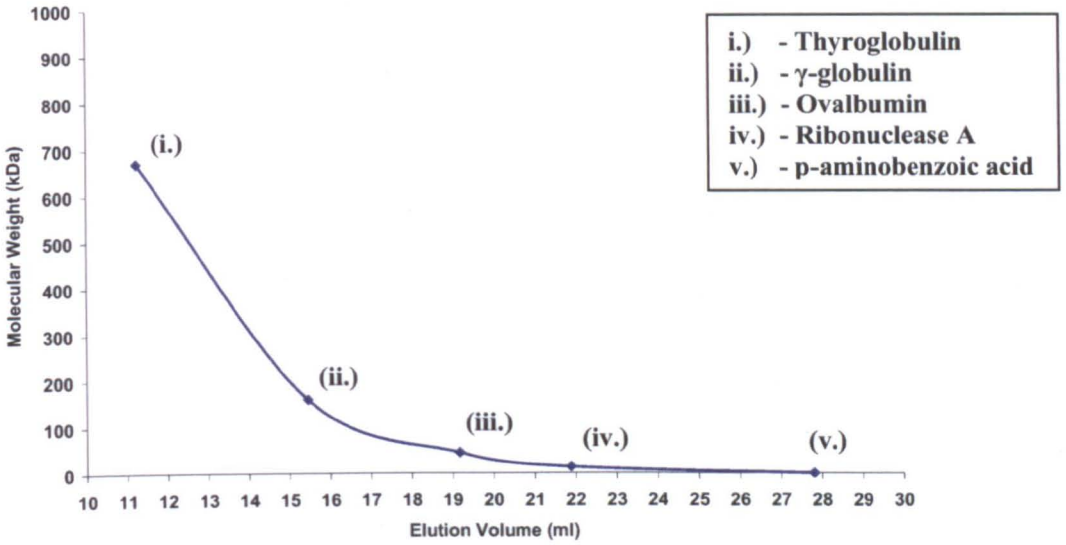

B TSKgel G4000SWxl

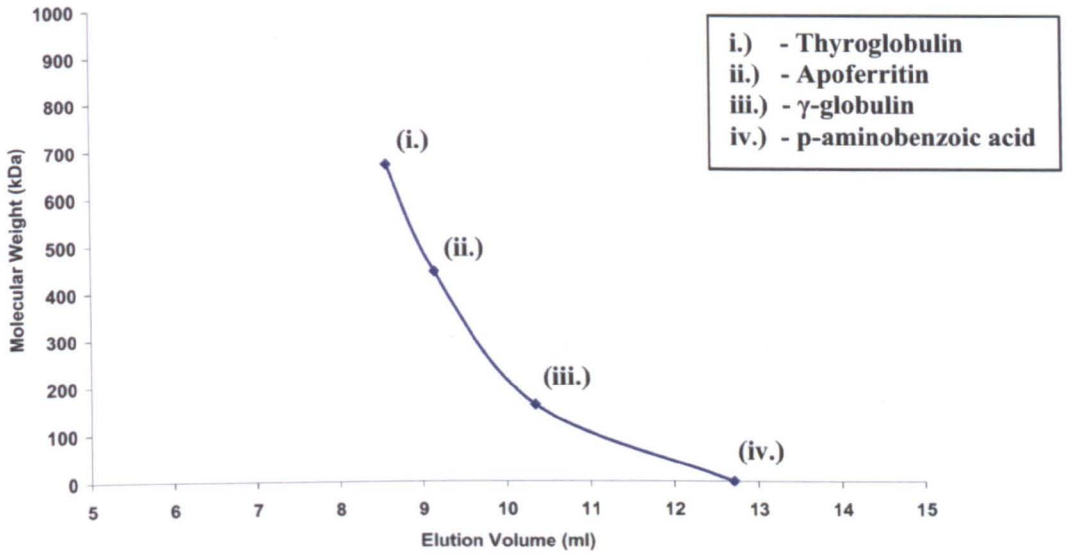

Figure 6.1: Size exclusion HPLC analysis of protein standard mixture as monitored by UV 280 nm.

Protein standards for the calibration of the TSKgel G3000SW and TSKgel G4000SWxl SEC columns were re-suspended in column running buffer (0.1 M sodium phosphate, 0.1 M sodium sulphate (pH 7)) and 10 µl injected onto the SEC column) column attached to an ÄKTA Purifier HPLC instrument for each analysis. The eluate was monitored by absorbance at UV 280 nm.

volume verses molecular weight for these standard proteins is shown in figure 6.1 panel B.

6.3 Oligomerisation of denatured recombinant mouse PrP

The aim of this project was to identify the subcellular localisation of co-factors that stimulated the conversion of PrP^{C} to PrP^{Sc} using mouse scrapie as a model. I wanted to elucidate whether subcellular fractions from TSE susceptible cell lines that were identified to influence conversion efficiencies in the CFCA also affected non-seeded PrP misfolding. The oligomerisation of recombinant PrP offered a methodology to analyse the interaction of potential co-factors with PrP during misfolding to a β-sheet rich isoform.

During optimisation of oligomerisation assays, full length $rMoPrP^{WT}$ (23-231) with the sequence from the s7 allele of *Prnp* was used. Recombinant $MoPrP^{WT}$ was over-expressed and purified as described in chapter 2 (sections 2.1.2.11 to 2.1.2.14) with several alterations as per the published protocol (Tahiri-Alaoui *et al.*, 2004). Following concentration of purified $rMoPrP^{WT}$ to 1 mg/ml, samples were lyophilised for 12 hours and the lyophilised protein was re-suspended in oligomerisation buffer (6 M guanidine hydrochloride, 50 mM tris-HCl, pH 7.2) to a concentration of 10 mg/ml. Oligomerisation of denatured rMoPrP was carried out by placing 100 µl samples into dialysis cellulose tubing with a 3.5 kDa molecular weight cut-off and placed into 2 litres of dialysis buffer (5 M urea, 20 mM sodium acetate, 200 mM sodium chloride (pH 3.7)). 10 µl samples were extracted at sequential time points for analysis by means of size exclusion chromatography. The column used was a TSKgel G3000SW that was connected to an ÄKTA HPLC to monitor UV absorbance at 280 nm and equilibrated with the running buffer (1 M urea, 200 mM sodium chloride, 20 mM sodium acetate (pH 3.7)) at a flow rate of 1 ml/min. Figure 6.2 shows the oligomerisation time course of $rMoPrP^{WT}$ as determined by SEC analysis.

The time course of refolding of $rMoPrP^{WT}$ when dialysed against 5 M urea, 0.2 M sodium chloride buffer (pH 3.7), $rMoPrP^{WT}$ refolds into nonspecific aggregates

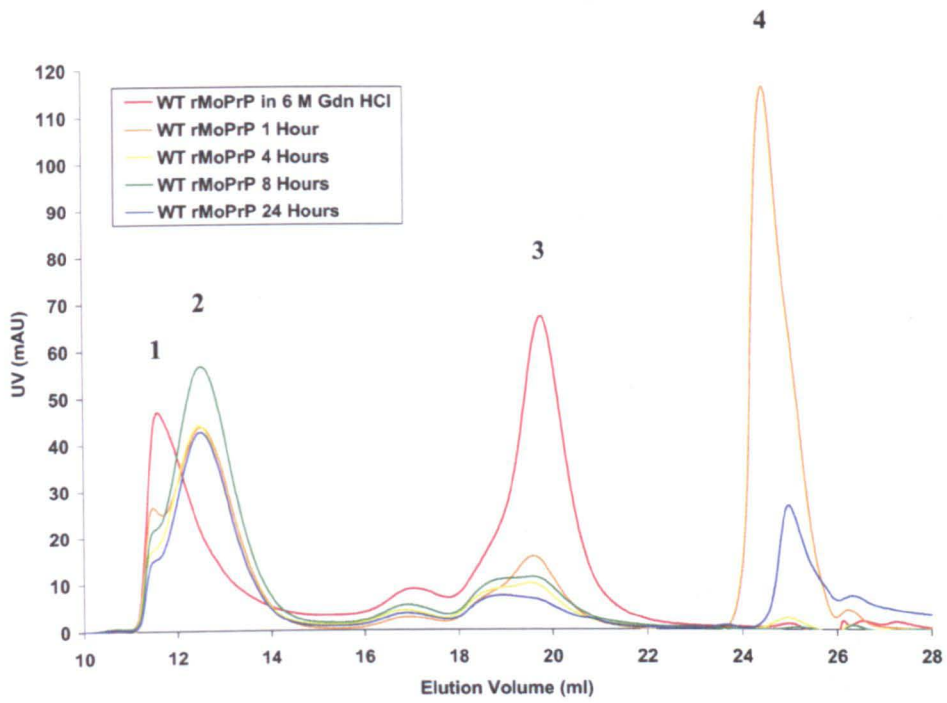

Figure 6.2: Size exclusion HPLC analysis of rMoPrP^{WT} (10 mg/ml), applied to a 7.5 x 300 mm G3000SW column, monitored at UV 280 nm.

The SEC profiles are a time course of the refolding of full length rMoPrP from a denatured state in 6 M guanidine hydrochloride, 50 mM tris-HCl (pH 7.2), into oligomers by dialysis against 5 M urea, 20 mM sodium acetate, 200 mM sodium chloride (pH 3.7). From a reaction volume of 250 µl, 10 µl aliquots were taken at 1, 4, 8 and 24 hours and aliquots were analysed by means of SEC. Chromatogram peaks are labelled 1 to 4 and represent the four different isoforms of PrP as described in section 6.3.

(peak 1), β-oligomers (peak 2) and monomeric PrP (peak 3) as separated by size exclusion chromatography (SEC) (figure 6.2). I know that peak 1 is caused by unspecified aggregates because this peak is present on the edge of the column void volume and therefore any protein that elutes at this point is very large. In addition to the first three peaks, there is a fourth peak in the chromatogram between 24 ml and 26 ml (peak 4). The identity of the protein representing this peak in the UV 280 nm was unknown and therefore further analysis was done. From this point on peak numbers 1 to 4 will be used to annotate each isoform of $rMoPrP^{WT}$ detected. To determine the different molecular isoforms of rMoPrP and their secondary structures, a 10 µl sample of α-monomeric $rMoPrP^{WT}$ was injected onto the TSK G3000SW SEC column equilibrated with the oligomerisation buffer (5 M urea, 20 mM sodium acetate, 200 mM sodium chloride (pH 3.7) (figure 6.3 section A). This buffer was chosen as the SEC running buffer since peak 4 was only present when the protein was dialysed against this buffer. Samples of peaks 1, 3 and 4 were taken for separation by SDS PAGE gel and visualisation by silver nitrate (figure 6.3 panel B). The silver stained SDS PAGE gel demonstrates that all peaks in the chromatogram in figure 6.2 are proteinaceous and appear to be rPrP as determined by molecular weight markers.

Samples of peaks 1, 3 and 4 were also taken for assessment of secondary structure by circular dichroism (figure 6.4). The CD analysis of peak 4 revealed the spectra of a protein that is partially folded into an α-helical conformation, however this spectra is missing a minima at 208 nm which, in conjunction with a minima at 222 nm, would be indicative of a fully folded α-helical protein (figure 6.4 panel A). The CD spectra of peak 3 shows that the presence of 5 M urea in the SEC column running buffer has partially unfolded $rMoPrP^{WT}$, causing the shift in the CD spectra. CD analysis of peak 3 showed a protein with a structure that was difficult to interpret (figure 6.4 panel B). However, it was assumed from figure 6.2 that peak 3 represents denatured rMoPrP. Peak 1 is an unspecified aggregation of PrP, however, the CD spectra would suggest that there is some partial structure (figure 6.4 panel C). The minima at 216 nm shows that there is some β-sheet present in this isoform.

A

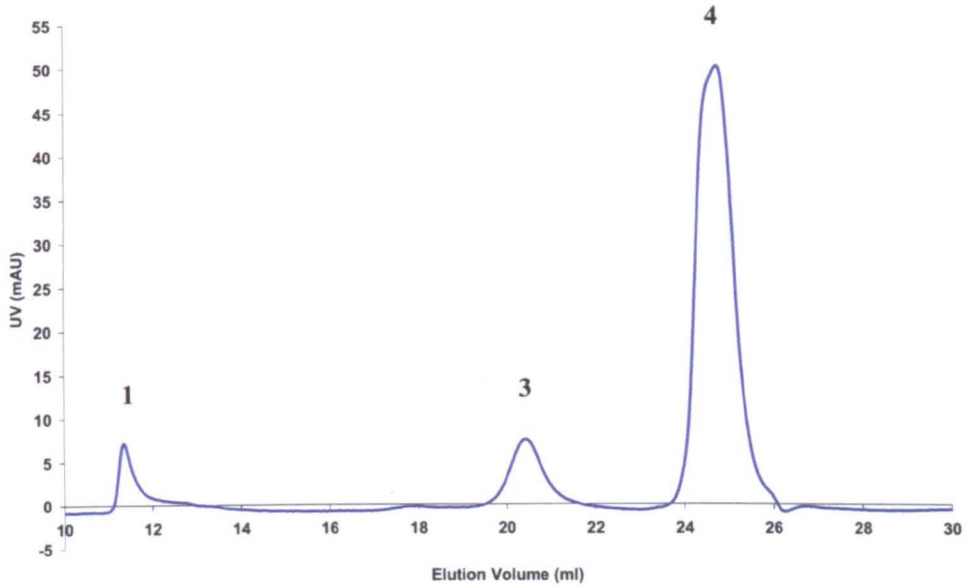

B

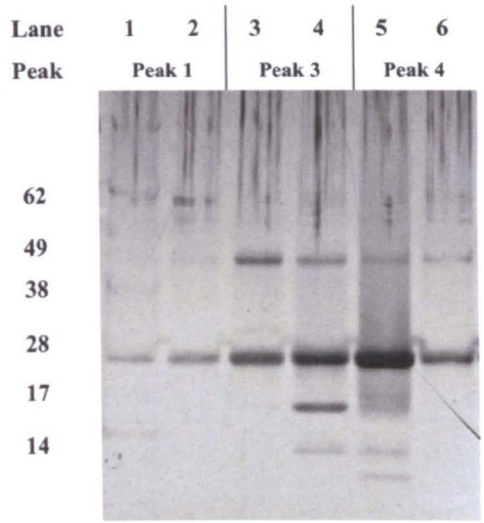

Figure 6.3: Analysis of rMoPrP^{WT} (0.6 mg/ml) separated by a 7.5 x 300 mm G3000SW column monitored at UV 280 nm.

(A) A 10 µl sample of α-monomeric rMoPrP^{WT} was injected onto the TSK G3000SW SEC column equilibrated with the oligomerisation buffer (5 M urea, 20 mM sodium acetate, 200 mM sodium chloride (pH 3.7). (B) Two samples encompassing the eluate from peaks 1, 3 and 4 were taken for analysis by separation on an SDS PAGE gel and stained with silver nitrate, which showed that peaks in the chromatogram are proteinaceous and were determined to be rMoPrP based on molecular weight (kDa).

A **Partially folded rMoPrP (Peak 4)** **B** **Unfolded rMoPrP (Peak 3)**

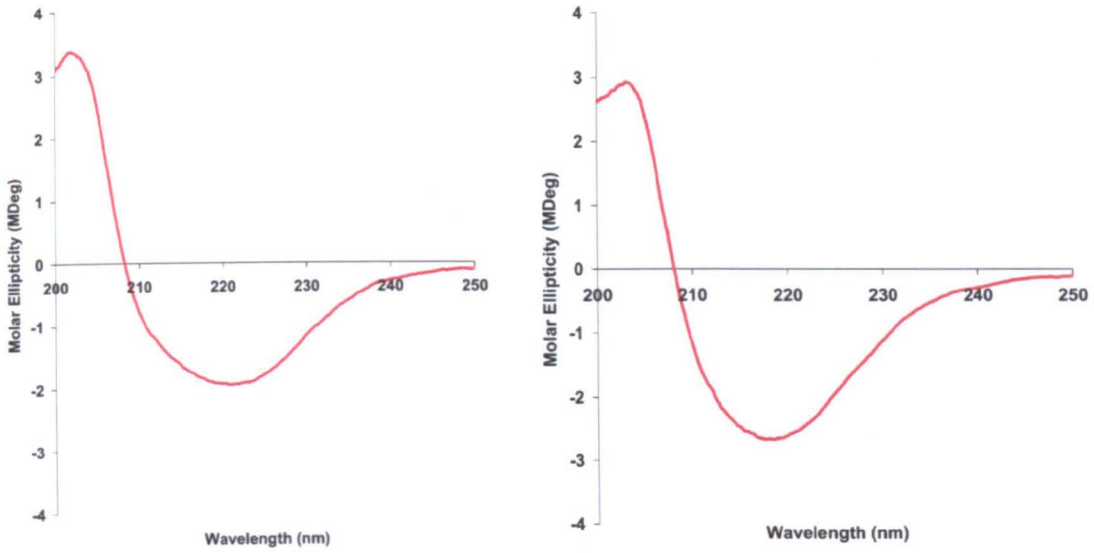

C **Unspecified aggregates of rMoPrP (Peak 1)**

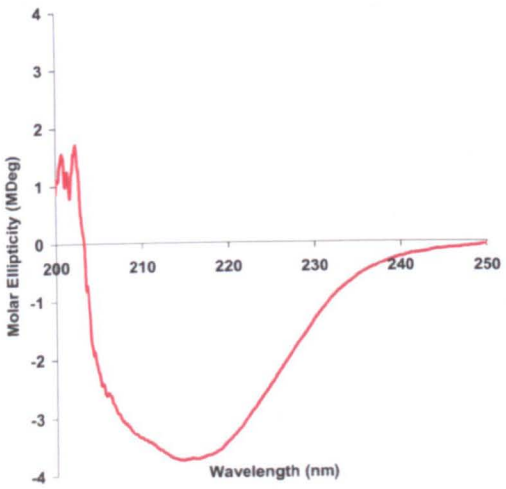

Figure 6.4: Characterisation of prion isoforms by circular dichroism.

The *in vitro* refolding of denatured rMoPrP^{WT} in the oligomerisation assay with far-UV circular dichroism spectra for (A) partially folded monomeric rMoPrP^{WT} (peak 4), (B) unfolded rMoPrP^{WT} (peak 3) and (C) unspecified aggregations of rMoPrP^{WT} (peak 1). The spectra were recorded using a 0.5 mm path length cell and data points from a blank run of just the SEC column buffer (1 M urea, 200 mM sodium chloride and 20 mM sodium acetate (pH 3.4)) removed from experimental CD spectra.

The rMoPrP^{WT} starting sample is in a denatured state in 6 M guanidine hydrochloride prior to dialysis against the oligomerisation buffer. When denatured rMoPrP^{WT} was assessed by SEC, rMoPrP partially misfolds while on the SEC column, into unspecified aggregates (peak 1) due to the change in chaotrope concentration (from 6 M guanidine hydrochloride to 1 M urea). This explains the abundance of PrP in peak 1 at the start of this time course. However, during the time course, denatured rMoPrP is dialysed against a 5 M urea based buffer, which causes the desired refolding of denatured rMoPrP into a stable β-sheet oligomer prior to separation by SEC.

The full length rMoPrP species used in this study has shown to be successfully oligomerised into a β-oligomeric isoform that was rich in β-sheet with a molecular weight similar to 10-12 subunits of rMoPrP. The studies by Tahiri-Alaoui and co-workers had demonstrated that the use of trHuPrP with either a methionine or valine at position 129 dramatically affected the oligomerisation rate and final amount of β-oligomer. To attempt to validate the current version of the assay, which used full length rMoPrP rather than trHuPrP, the oligomerisation of rMoPrP with a proline to leucine polymorphism at position 164 was investigated. The proline to leucine substitution at codon 168 in ovine PrP results in an increase in resistance to inoculation with experimental BSE of sheep expressing this protein variant (Goldman *et al.*, 2006). Previously, the P168L polymorphism had been made in a murine background, the equivalent codon in mice is 164 (rMoPrP^{P164L}, Kirby *et al.*, 2006). In this publication, it was also demonstrated that rMoPrP^{P164L} was resistant to conversion in the CFCA by the mouse scrapie strain 87V. This study therefore showed that the P164L polymorphism, in murine PrP, maintained phenotypic integrity.

Figure 6.5 shows the investigation into the oligomerisation of rMoPrP^{P164L} and that the polymorphism at this position altered the progression of oligomerisation of rMoPrP. In comparison with rMoPrP^{WT} there was a slower build up of the oligomer and unspecified aggregate, apparently by greater initial folding of the denatured protein to the α-monomer (figure 6.5). As the time course proceeded there was a notable loss of protein, which can be explained by the accumulation of protein aggregates not detected by SEC as a result of the relatively low concentration of urea in the HPLC running buffer.

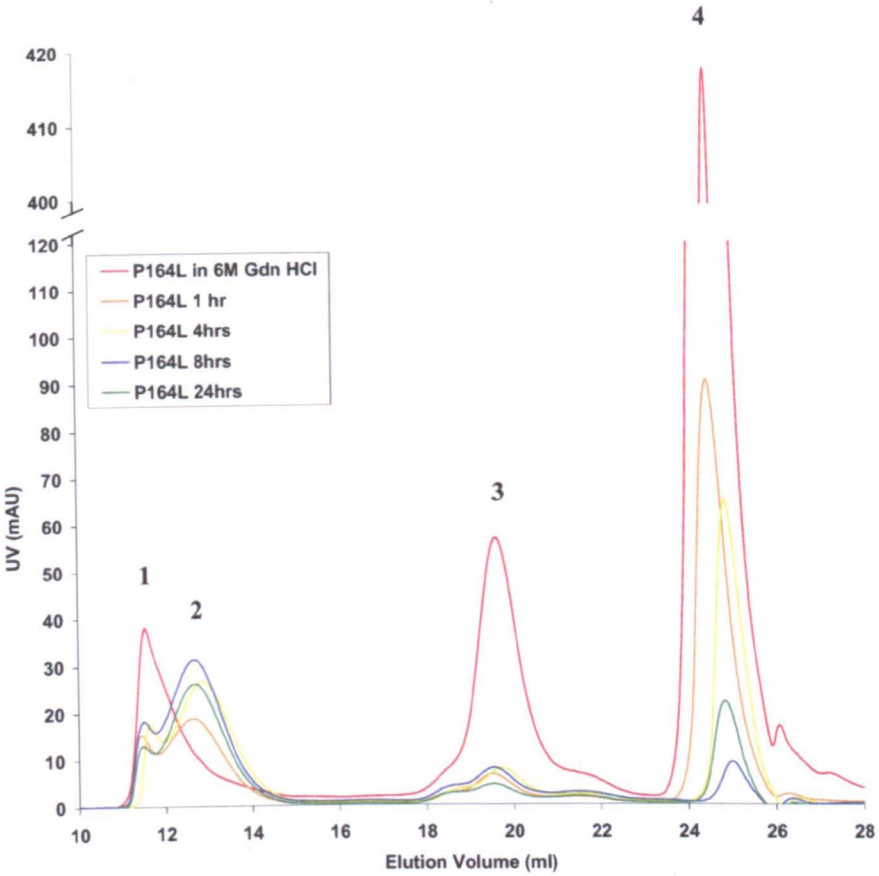

Figure 6.5: Size exclusion HPLC analysis of rMoPrP^{P164L} (10 mg/ml), applied to a 7.5 x 300 mm G3000SW column, monitored at UV 280 nm.

The SEC profiles are a time course of the refolding of full length rMoPrP with a leucine at residue 164 from a denatured state in 6 M guanidine hydrochloride, 50 mM tris-HCl (pH 7.2) into oligomers by dialysis against 20 mM sodium acetate (pH 3.7). From a reaction volume of 250 µl, 10 µl aliquots was removed at 1, 4, 8 and 24 hours and injected onto the SEC column. Denatured monomeric rMoPrP^{WT} elute between 19 and 21 ml (peak 3), partially folded monomeric rMoPrP^{WT} elute between 24 and 26 ml (peak 4), oligomeric rMoPrP^{WT} elute between 12 and 14 ml (peak 2) and unspecified aggregates of rMoPrP^{WT} elute between 11 and 12 ml (peak 1). Chromatogram peaks are labelled 1 to 4 and represent the four different isoforms of PrP as described in section 6.3.

The oligomerisation assay was adapted from the publication in 2004 by Tahiri-Alaoui and co-workers, however it had some deficiencies when the method was used with full length rMoPrP^{WT} rather than trHuPrP. Firstly, the starting rMoPrP was denatured, into an unfolded state, by 6 M guanidine hydrochloride and this may not represent the state of PrP^{C} *in vivo* during the initial stages of conversion. The presence of high concentrations of denaturant may also have an adverse affect on the structure of co-factor(s) and any potential interaction it may have with rMoPrP. Secondly, the magnitude of unspecified aggregates in this assay made it difficult to accurately measure oligomerisation rates and the percentage of total rMoPrP refolded to the β-oligomer. During the setup of this oligomerisation assay it was observed that the amount of unspecified aggregate appeared to be random, with varying amounts of the soluble portion of unspecified aggregates represented in the SEC chromatogram. If the effect of co-factors on PrP misfolding is subtle, then interpretation of oligomerisation rates may be difficult with random aggregation also occurring *in vitro*. Alternatively, if the addition of co-factors to the assay destabilises rMoPrP then it may be more susceptible to aggregation when in the presence of aggregation processes *in vitro*.

6.4 Heat induced oligomerisation of recombinant ovine PrP variants

In section 6.3 I outlined work aimed at developing a method of PrP oligomerisation in a buffer containing modest levels of denaturant and at a reduced pH. I found this method unsuitable and sought an alternative approach. Taking these factors into account, I decided that a different oligomerisation assay was needed, in particular an assay that used full length mammalian rPrP and would be physiologically relevant.

Various other misfolding methods have been published and a particularly attractive method uses heat to induce oligomerisation of PrP (Rezaei *et al.*, 2005). In this publication, full length α-monomeric OvPrP oligomerised by thermal refolding at 45 °C under acidic conditions. Although this assay appeared to be similar to the work by Tahiri-Alaoui and co-workers, these reaction conditions resulted in the oligomerisation of rOvPrP into two distinct oligomeric species. The oligomers have measured sizes of a 12-mer and a 36-mer. They were soluble, displayed partial resistance to proteolytic digestion and also a capacity to bind thioflavine T. The

oligomeric PrP was neurotoxic to mouse cortical neurons *in vitro* and exhibited higher intrinsic levels of neurotoxicity *in vivo* when compared to fibrils (Simoneau *et al.*, 2007).

Since work to develop the denaturant-based assay was problematic, partially confounded by the use of different length and PrP species to that used in published work, initial attempts to adopt a heat-induced oligomerisation method made use of the same protein used in the publication by Rezaei et al, full length recombinant sheep PrP. In 2002, Rezaei's group had presented data on differences in the unfolding intermediates of different ovine PrP variants leading to the correlation between genotypic susceptibility of sheep carrying different PrP variants and the kinetic energy required to unfold each of the corresponding proteins *in vitro*. Sheep carrying the prion protein variants ARR and AHQ tend to be resistant to classical scrapie, whilst those carrying the VRQ and ARQ prion protein variants tend to be susceptible. Rezaei demonstrated that VRQ and ARQ proteins have a higher thermal stability than ARR and AHQ, which were associated with resistance to infection. The stability of ovine PrP is likely to be associated with susceptibility to scrapie and incubation time before clinical onset (Rezaei *et al.*, 2000, Rezaei *et al.*, 2002). However, this publication did not investigate differences in the oligomerisation of different rOvPrP variants.

I expressed recombinant OvPrP with the amino acid sequence A136-R154-R171 ($rOvPrP^{ARR}$) in 1B392 *E.coli* from the modified pTrcHisB vector and purified as outlined previously (chapter 2, sections 2.1.2.10 and 2.1.2.11) with some alterations. Inclusion bodies were re-suspended in 10 ml/g IMAC buffer A (9 M urea, 0.1 M sodium phosphate, 0.01 M tris-HCl (pH 8)). The suspension was repeatedly vortexed and stirred continuously to aid protein solubilisation. Solubilised inclusion bodies were centrifuged as described previously in chapter 2, to remove the insoluble fraction. The supernatant was mixed with 5 % (v/v) Ni-NTA resin (Qiagen) that had previously been equilibrated with IMAC buffer A and incubated at 4 °C for 120 minutes revolving on a tube rotator (Stuart Scientific). The homogeneous mixture was poured into a 10 ml disposable polypropylene column (Qiagen) and the loading run through collected. The Ni-NTA column was washed with 5 column volumes of IMAC buffer A and bound protein species were eluted with IMAC buffer B (500

mM imidazole, 0.02 M MOPS (pH 7)) and eluate collected in 2 ml fractions. I made these changes to mimic experimental conditions described by Rezeai and colleagues (2000).

Samples were resolved using SDS-PAGE and proteins visualised by staining with Instant Blue Coomassie. Recombinant $OvPrP^{ARR}$ containing fractions were desalted using a PD-10 desalting column (GE Healthcare) equilibrated with 20 mM sodium citrate (pH 3.4). The eluate was collected in 500 µl fractions and then analysed by UV spectroscopy at 280 nm to determine protein concentration. Full length $rOvPrP^{ARR}$ at a concentration of 1.75 mg/ml were incubated at 45 °C and 10 µl samples taken every 15 minutes for the duration of the time course. Samples were separated by a 300 x 7.8 nm TSKG4000SWxl gel filtration HPLC column equilibrated with 20 mM sodium citrate (pH 3.4) at a flow rate of 1 ml/min. The eluate was monitored by UV absorbance at 280 nm for which the data was plotted against elution volume (ml) for each of the samples taken throughout the time course.

A representative oligomerisation time course of $rOvPrP^{ARR}$ as separated by SEC chromatography and analysed by UV 280 nm is shown in figure 6.6 and shows that the starting α-monomeric $rOvPrP^{ARR}$ multimerises into two distinct oligomeric isoforms. Comparison of elution volumes against the calibration profile for the TSKG4000SWxl column indicated that the oligomers were consistent with the previously published sizes of a 12-mer and a 36-mer of $rOvPrP^{ARR}$. The small peak in UV absorbance at an elution volume of 5.5 ml is an unspecified aggregation of $rOvPrP^{ARR}$ and is ignored from analysis from this point onwards. The identity of this PrP isoform is known as the elution volume is at the edge off the column void volume and therefore has a very large molecular weight. From four repeats, integration of the area under each of the peaks representing the three isoforms of $rOvPrP^{ARR}$ allowed for further analysis into the refolding rate of oligomerisation for the $rOvPrP^{ARR}$ (figure 6.7). From figure 6.7 it can be seen that, although initially there is an equal amount of refolding from α-monomer to the 12-mer and 36-mer β-oligomer isoforms, it is assumed that the reaction proceeds from α-monomer refolding to 12-mer and then the 36-mer β-oligomer isoform. This data is in line with that published previously and suggests that 12-meric β-oligomers seed the formation

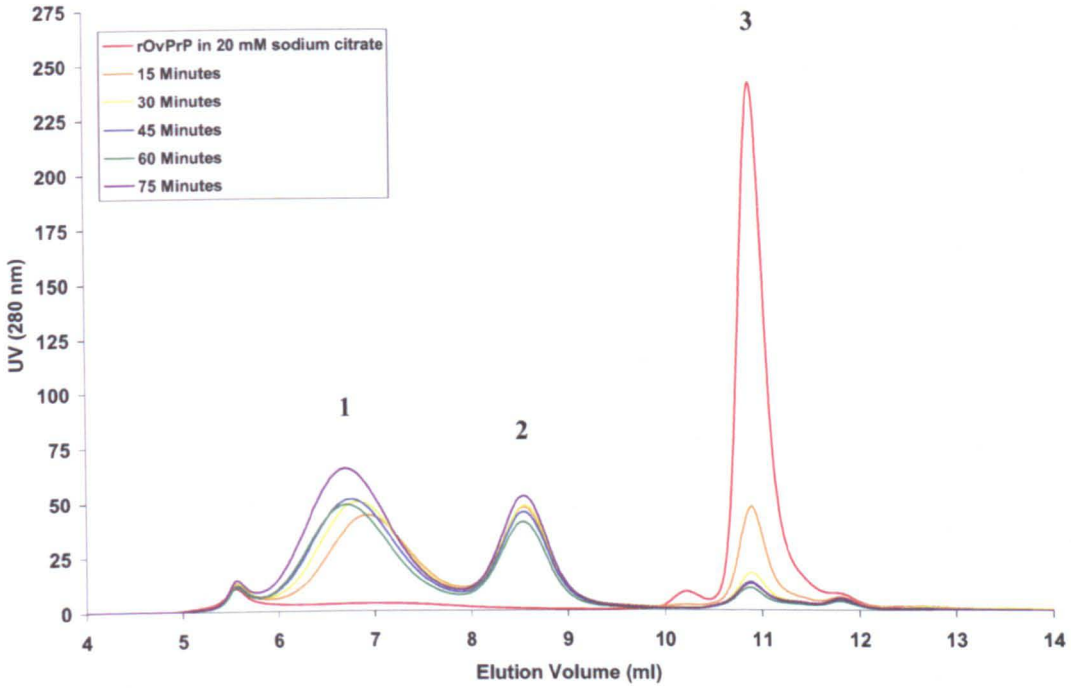

Figure 6.6: Size exclusion HPLC analysis of rOvPrP^{ARR} (1.75 mg/ml), applied to a 7.5 x 300 mm G4000SWxl column, monitored at UV 280 nm.

The SEC analyses from a time course of the refolding of full length rOvPrP^{ARR} variant from the native α-monomeric state in 20 mM sodium citrate (pH 3.7) into two distinct soluble oligomers by incubation at 45°C. From a reaction volume of 100 µl, 10 µl aliquots were removed at 15, 30, 45, 60 and 75 minutes and injected onto the SEC column. Monomers elute between 10.5 and 11.5 ml (peak 3), the 12-mer oligomer elutes between 8 and 9 ml (peak 2) and the 36-mer oligomer elutes between 6 and 8 ml (peak 1). The oligomers have an apparent mass of approximately 360 kDa and 1080 kDa for the 12-mer and the 36-mer respectively, as based on calibration by globular protein size standards.

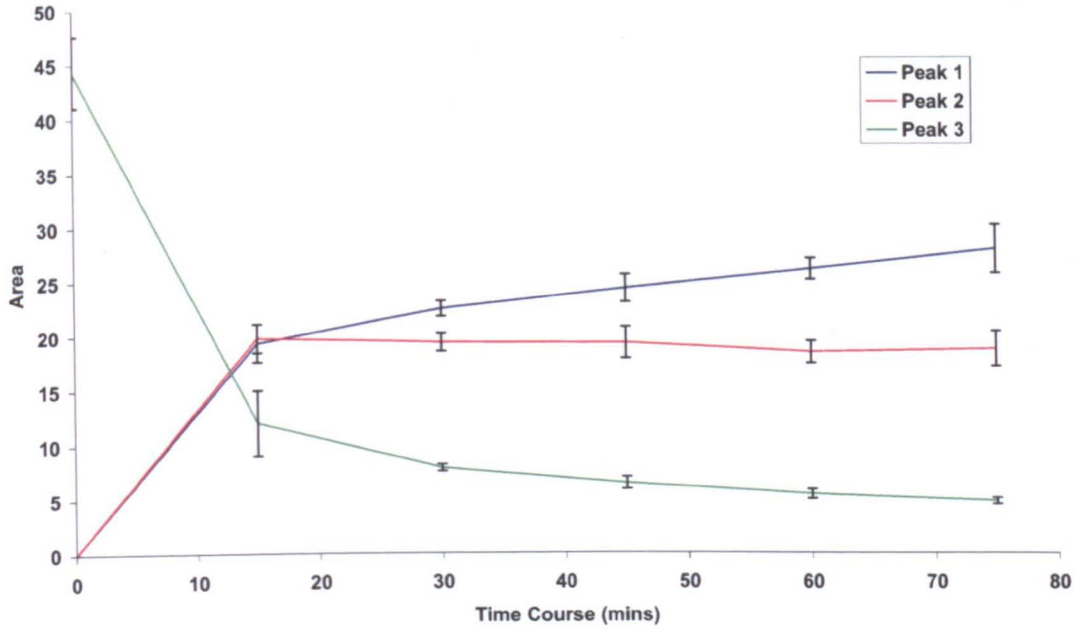

Figure 6.7: Semi-quantitative measure of the proportion of rOvPrP^{ARR} isoforms by integration of the area under each peak.

Evaluation of the area under each chromatogram profile was carried out using the integration facility on the AKTA HPLC Unicorn 4.1.1 operating system. Blue line represents 36-mer oligomer (peak 1), the red line represents the 12-mer oligomer (peak 2) and the green line represents the α-monomer (peak 3). Results showed that monomeric rOvPrP^{ARR} refolded into a 12-mer oligomer which seeded the formation of the 36-mer oligomer.

of the 36-mer β-oligomer (Rezaei *et al.*, 2005).

Although the above results suggested that the heat-induced oligomerisation assay could provide a means of quantifying the rates of oligomerisation, I next wanted to assess whether variations in experimental conditions could produce different results. To do this I analysed the rates of heat-induced oligomerisation of an alternate ovine PrP variant with the amino acid sequence, V136-R154-Q171 (rOvPrP^{VRQ}). The same experimental protocol, including protein expression, purification and final concentration was used to allow results to be compared directly. The results from oligomerisation of rOvPrP^{VRQ} are presented in figure 6.8 a representative chromatogram and figure 6.9, which represents the average of four repeats.

Figure 6.8 shows the time course of the oligomerisation of α-monomeric rOvPrP^{VRQ} to β-oligomer isoforms by thermal refolding, which has a similar rate of oligomerisation to rOvPrP^{ARR} as illustrated in figure 6.6. Further analysis of the area under each UV 280 nm peak using integration suggested that there were subtle differences in the kinetics of oligomerisation of rOvPrP^{ARR} and rOvPrP^{VRQ} (figure 6.7 and 6.9, respectively). Firstly, there was a slower rate of oligomerisation from α-monomeric rOvPrP^{VRQ} to the low molecular weight β-oligomer. Secondly, less 36-mer oligomer had formed than 12-mer oligomer after 15 minutes in the rOvPrP^{VRQ} oligomerisation when compared against rOvPrP^{ARR}, at the same time point. After 15 minutes the reaction appeared to have gone largely to completion and there appeared to be no further seeding of the rOvPrP^{VRQ} 36-mer oligomer by the 12-mer oligomers.

The differences observed in the oligomerisation of rOvPrP variants demonstrated that subtle sequence changes in the sequence of PrP alter conformational plasticity during thermal misfolding. The propensity of rOvPrP^{ARR} to oligomerise when compared against rOvPrP^{VRQ} seemed counter-intuitive when disease susceptibility *in vivo* would dictate that an increase in misfolding potential would be associated with increased susceptibility to disease. However, I hypothesised that the 12-mer oligomer may have a higher capacity for neurotoxicity which in the case of rOvPrP^{VRQ}, was the most prevalent β-oligomer formed. Alternatively, it could be that these assays measure propensity to misfold generally, rather than disease-specifically (see figure

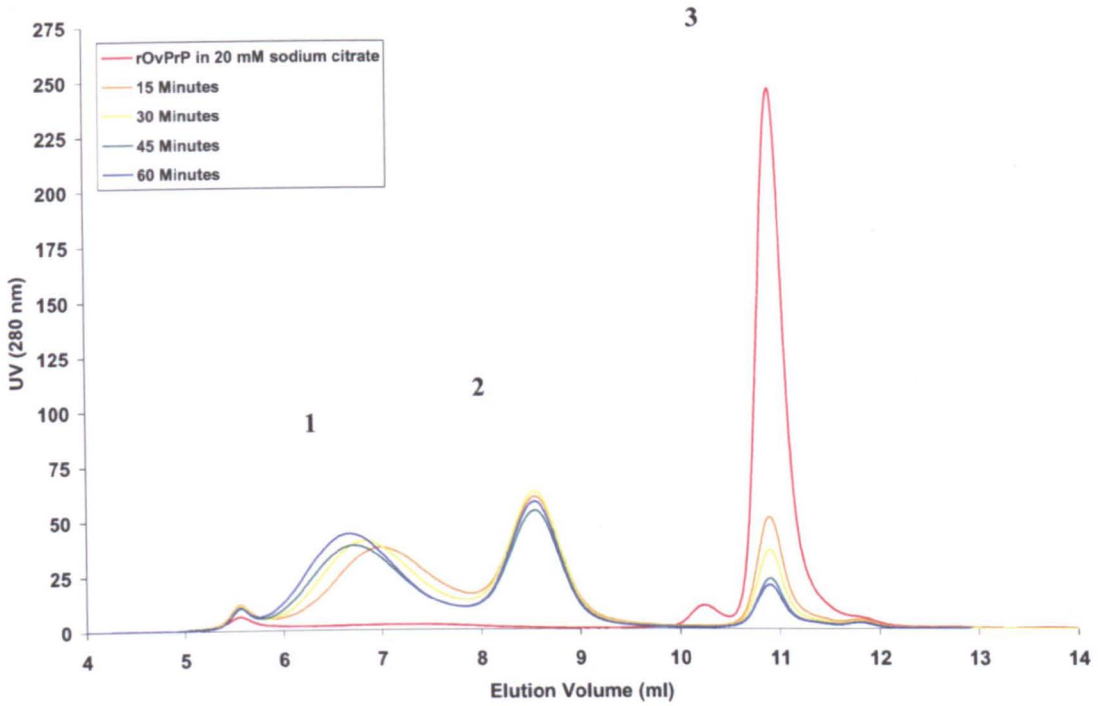

Figure 6.8: Size exclusion HPLC analysis of rOvPrP^{VRQ} (1.75 mg/ml), applied to a 7.5 x 300 mm G4000SWxl column, monitored at UV 280 nm.

The SEC profiles are a time course of the refolding of full length VRQ rOvPrP variant from the native α-monomeric state in 20 mM sodium citrate (pH 3.7) into two distinct soluble oligomers by incubation at 45°C. From a reaction volume of 100 µl, 10 µl aliquots were removed at 15, 30, 45 and 60 minutes and injected onto the SEC column. Monomers elute between 10.5 and 11.5 ml (peak 3), the 12-mer oligomer elutes between 8 and 9 ml (peak 2) and the 36-mer oligomer elutes between 6 and 8 ml (peak 1). The oligomers have an apparent mass of approximately 360 kDa and 1080 kDa for the 12-mer and the 36-mer respectively, as based on calibration by globular protein size standards.

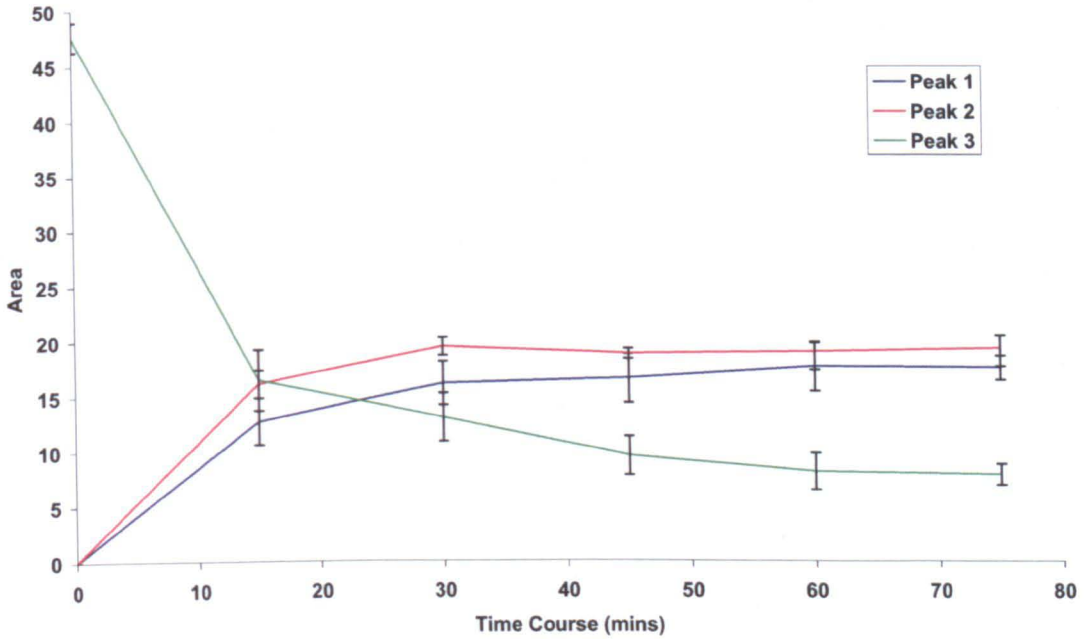

Figure 6.9: Semi-quantitative measure of the proportion of rOvPrP^{VRQ} isoforms by integration of the area under each peak.

Evaluation of the area under each chromatogram profile was carried out using the integration facility on the AKTA HPLC Unicorn 4.1.1 operating system. Blue line represents 36-mer oligomer (peak 1), the red line represents the 12-mer oligomer (peak 2) and the green line represents the α-monomer (peak 3). Results showed that monomeric rOvPrP^{VRQ} refolds equally into 12-mer and 36-mer oligomers.

7.1). To elucidate, future work could incorporate other rOvPrP variants to be analysed or their propensity to refold *in vitro*.

These experiments on the oligomerisation of rOvPrP variants demonstrated that the thermal refolding of rOvPrP in the presence of an acidic buffer formed the basis of an assay that was sensitive, quantitative and reproducible. Therefore, I next applied the oligomerisation assay to rMoPrP variants with a view of determining the kinetics of oligomerisation.

6.5 Heat induced oligomerisation of recombinant mouse PrP

Vendrely and co-workers demonstrated that, like ovine PrP, full length rMoPrP^{WT} also formed two distinct oligomeric isoforms by thermal refolding (2005). However, the experimental kinetics of refolding of α-monomeric rMoPrP^{WT} to β-oligomers was not the same as observed for rOvPrP in Rezaei's or my investigations (section 6.4, Rezaei *et al.*, 2005). Thermal refolding of α-monomeric rMoPrP^{WT} to the 12-mer and 36-mer appeared not to follow a three stage reaction from monomer to 12-mer to 36-mer. Instead α-monomeric rMoPrP^{WT} refolded equally into 12-mer and 36-mer oligomers. In addition the rMoPrP^{WT} 36-mer appeared to have a more α-helical secondary structure and was considerably less stable than the 36-mer β-oligomer of rOvPrP^{ARR}. I therefore used the oligomerisation assay to analyse the oligomerisation of rMoPrP.

The expression, purification and oligomerisation of rMoPrP with the amino acid sequence from the s7 allele (rMoPrP^{WT}), was performed as described for rOvPrP in section 6.3. Recombinant MoPrP^{WT}, at a concentration of 2 mg/ml in a 20 mM sodium citrate (pH 3.4) buffer was heated to 45 °C and aliquots were removed for analysis by size exclusion chromatography. Typical results of such an experiment are shown in figure 6.10 which shows that thermal refolding from the native α-monomeric isoform of rMoPrP^{WT} produces two distinct oligomeric species, a 12-mer and a 36-mer. The experiment was repeated three times and the areas under the respective peaks were integrated and averaged. A plot of the relative proportions of each of the species against time is shown in figure 6.11 from which it can be seen that after only 15 minutes there is ~ 45 % α-monomer left with the remaining

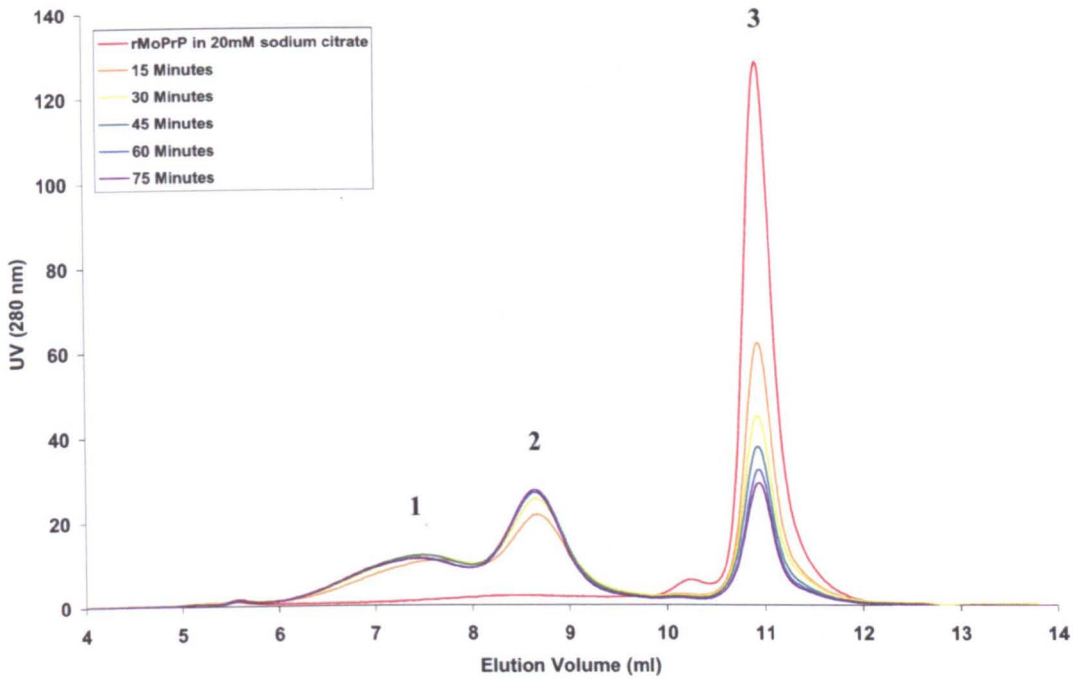

Figure 6.10: Size exclusion HPLC analysis of rMoPrP^{WT} (2 mg/ml), applied to a 7.5 x 300 mm G4000SWxl column, monitored at UV 280 nm.

SEC analyses from a time course of the refolding of full length rMoPrP^{WT} in the native α-monomeric state in 20 mM sodium citrate (pH 3.7) into two distinct soluble oligomers by incubation at 45 °C. From a reaction volume of 100 µl, 10 µl aliquots were removed at 15, 30, 45, 60 and 75 minutes and injected onto the SEC column. Monomers (peak 3) elute between 10.5 and 11.5 ml, the 12-mer oligomer (peak 2) elutes between 8 and 9 ml and the 36-mer oligomer (peak 1) elutes between 6 and 8 ml. The oligomers have an apparent mass of approximately 360 kDa and 1080 kDa for the 12-mer and the 36-mer respectively, as based on calibration by globular protein size standards.

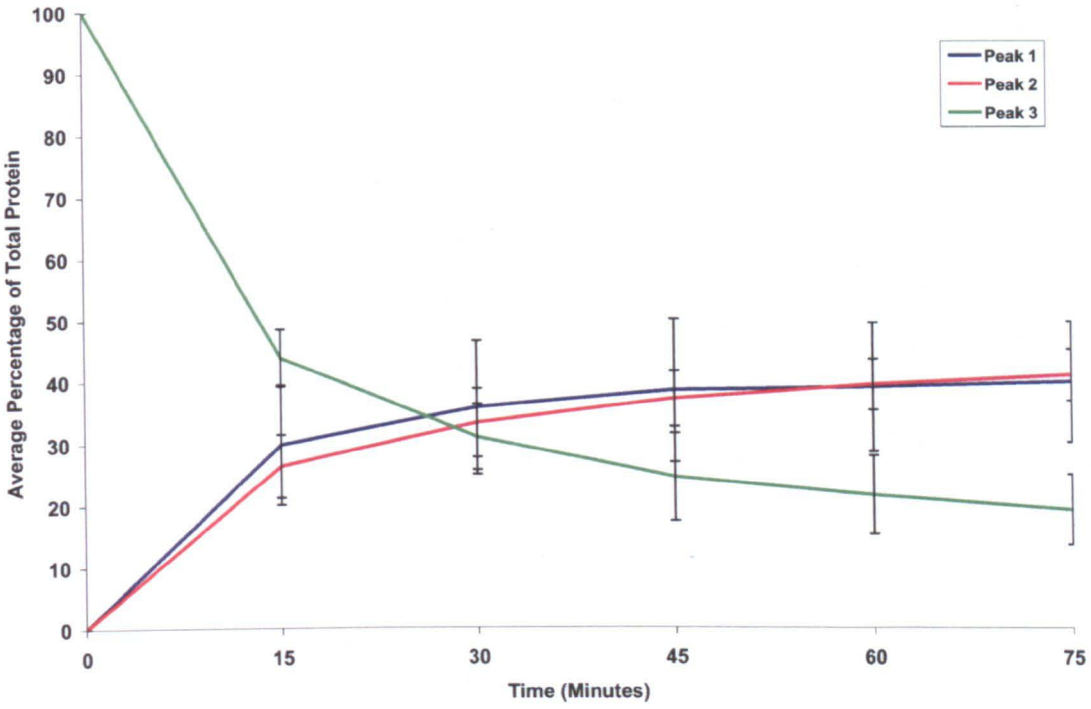

Figure 6.11: Semi-quantitative measure of the proportion of rMoPrP^{WT} isoforms by integration of the area under each peak.

The refolding of full length rMoPrP^{WT} variant from the native α-monomeric state in 20 mM sodium citrate (pH 3.7) into two distinct soluble oligomers by incubation at 45 °C. Evaluation of the area under each chromatogram profile was carried out using the integration facility on the ÄKTA HPLC Unicorn 4.1.1 operating system. Blue line represents 36-mer oligomer (peak 1), the red line represents the 12-mer oligomer (peak 2) and the green line represents the α-monomer (peak 3). Results show that the there is a steady refolding of monomeric rMoPrP^{WT} to 12-mer and 36-mer oligomers.

refolded into 12-mer (~ 25 %) and 36-mer. (~ 30 %). This figure also shows that after 15 minutes there was a slow progression from $rMoPrP^{WT}$ α-monomer to both 12-mer and 36-mer oligomers which steadily proceeded throughout the time course.

The oligomerisation of $rMoPrP^{WT}$ suggested that the heat-induced oligomerisation assay could also provide a means of quantifying the rates of rMoPrP oligomerisation. Therefore, I wanted to assess whether variants of rMoPrP could produce different results. To do this I analysed the rate of heat-induced oligomerisation of the alternate murine PrP variant with the P164L polymorphism ($rMoPrP^{P164L}$). This rMoPrP variant was chosen to compare on the basis that differences were detected in the denaturant-induced oligomerisation of $rMoPrP^{WT}$ and $rMoPrP^{P164L}$ in section 6.3. The same experimental protocol, including protein expression, purification and final concentration was used to allow results to be compared directly. The results from oligomerisation of $rMoPrP^{P164L}$ are presented in figure 6.12 (representative chromatograms) and figure 6.13, which represents the average of three repeats.

In comparison, the thermal refolding of $rMoPrP^{P164L}$ was remarkably different to oligomerisation of $rMoPrP^{WT}$ (compare data in figures 6.10 and 6.12) A typical SEC chromatogram from the oligomerisation time course is presented in figure 6.12. It can be clearly seen that there was an immediate and almost complete loss of α-monomeric $rMoPrP^{P164L}$ by the time the first sample was taken at 15 minutes and instead both 12-mer and 36-mer oligomeric species were formed. At each time point thereafter there was a noticeable reduction in the peak representing the 36-mer oligomer and a steady increase in the 12-mer oligomer. Further analysis of the area under each UV 280 nm peak by integration suggested that there were differences in the kinetics of oligomerisation of $rMoPrP^{WT}$ and $rMoPrP^{P154L}$ (figure 6.13). After 15 minutes there was only ~ 10 % α-monomeric rMoPrP and the majority had refolded into the 36-mer oligomer (~ 60 %) with the remaining ~ 25 % in the 12-meric isoform. As the time course progressed there was a slow reduction in the 36-mer, presumably as it broke down into a 12-mer oligomers. This assay therefore provides a means to study the addition of subcellular fractions to the oligomerisation of rMoPrP

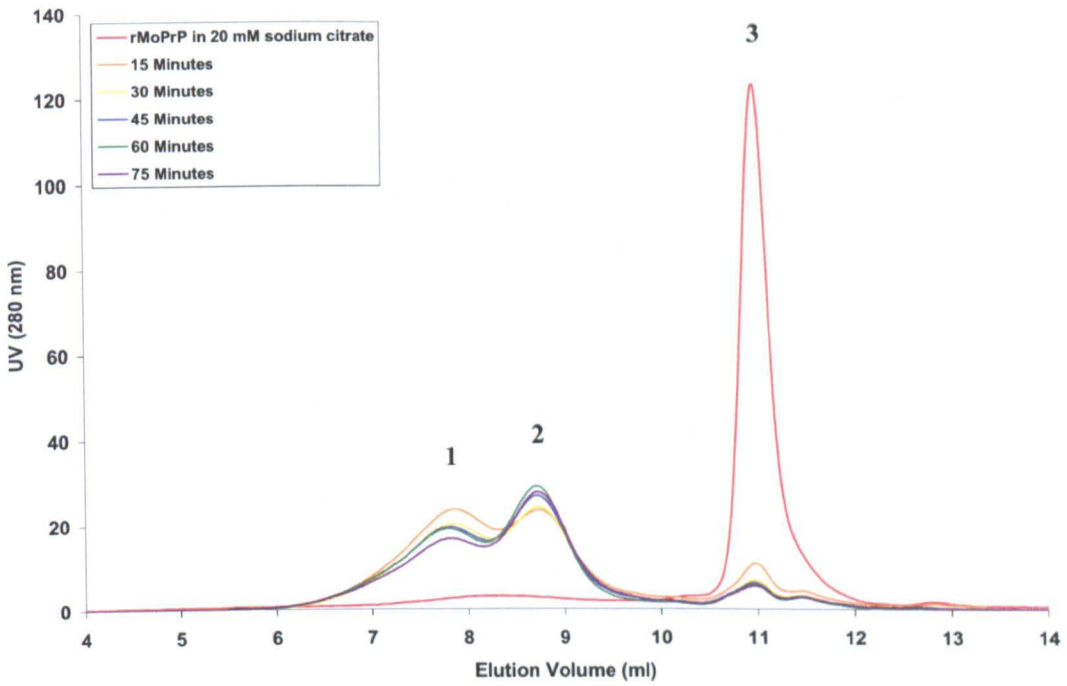

Figure 6.12 Size exclusion HPLC analysis of rMoPrP^{P164L} (2 mg/ml), applied to a 7.5 x 300 mm G4000SWxl column, monitored at UV 280 nm.

The SEC profiles are a time course of the refolding of the full length rMoPrP variant with the P164L polymorphism from the native α-monomeric state in 20 mM sodium citrate (pH 3.7) into two distinct soluble oligomers by incubation at 45 °C. From a reaction volume of 100 µl, 10 µl aliquots were removed at 15, 30, 45, 60 and 75 minutes and injected onto the SEC column. Monomers (peak 3) elute between 10.5 and 11.5 ml, the 12-mer oligomer (peak 2) elutes between 8 and 9 ml and the 36-mer oligomer (peak 1) elutes between 6 and 8 ml. The oligomers have an apparent mass of approximately ~ 360 kDa and ~ 1080 kDa for the 12-mer and the 36-mer respectively, as based on calibration by globular protein size standards.

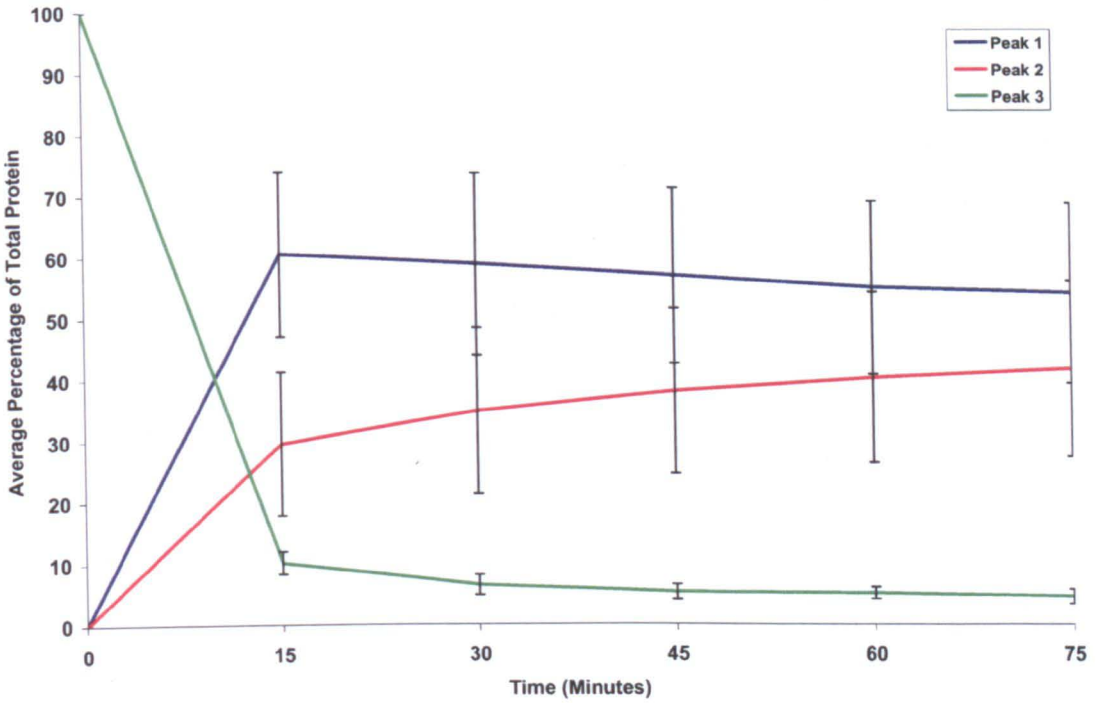

Figure 6.13: Semi-quantitative measure of the proportion of rMoPrP^{P164L} isoforms by integration of the area under each peak.

The refolding of full length P164L rMoPrP variant from the native α-monomeric state in 20 mM sodium citrate (pH 3.7) into two distinct soluble oligomers by incubation at 45 °C. Evaluation of the area under each chromatogram profile was carried out using the integration facility on the ÄKTA HPLC Unicorn 4.1.1 operating system. Blue line represents 36-mer oligomer, the red line represents the 12-mer oligomer and the green line represents the α-monomer. Results show that monomeric rMoPrP^{P164L} refolds rapidly into 12-mer and 36-mer oligomers, however the 36-mer oligomer dissociates, presumnbaly back to 12-mer and/or monomer.

6.6 Addition of subcellular fractions to the oligomerisation assay

Plasma membrane-enriched fractions from the LD9 cell line enhanced the conversion efficiency of ME7 and 79A in the CFCA (see chapter 4). It is likely that plasma membrane-enriched fractions contain generic co-factors as evidenced by the increased conversion efficiency of ME7 and 79A in the CFCA when in the presence of these fractions. However, it is also possible that generalised co-factors for all strains are present on the plasma membrane of LD9 cells and it is instead something else that is required, such as a specific cellular location, which provides strain specificity. Therefore, I wanted to assess whether the plasma membrane from LD9 cells also enhanced non-seeded conversion of $rMoPrP^{WT}$.

To replicate, in the oligomerisation assay, the exact ratio of rMoPrP and subcellular fraction present in each CFCA would not be possible due to the restrictions in protein concentration that are required for the successful oligomerisation of rMoPrP. Therefore, 50 % of the sample volume for oligomerisation was made up of the subcellular fraction. This required a doubling in the concentration of the rMoPrP stock to 4 mg/ml to give a final rMoPrP concentration of 2 mg/ml. The oligomerisation of rMoPrP was carried out as described previously (section 6.5) with samples taken at 15 minute intervals throughout the time course. Comparisons were made between the effect of a plasma membrane enriched fraction and that of a mitochondrial enriched fraction on the oligomerisation of full length rMoPrP.

The expression, purification and oligomerisation of full length rMoPrP with the amino acid sequence from the s7 allele (wild type) were performed as described in section 6.5. Full length wild type rMoPrP ($rMoPrP^{WT}$) at a concentration of 2 mg/ml in a 20 mM sodium citrate (pH 3.4) buffer was heated to 45 °C which caused thermal refolding from the native α-monomeric isoform to two distinct oligomeric species, a 12-mer and a 36-mer (figure 6.14). This figure is a typical chromatogram of the oligomerisation of $rMoPrP^{WT}$ as described previously in chapter 6 (figure 6.10), however there is a small degree of unspecified aggregates eluting at 5.5 ml.

Next, an equivalent oligomerisation assay was performed, by use of rMoPrP, but in the presence of a plasma membrane enriched fraction (fraction 3) from the LD9 cell

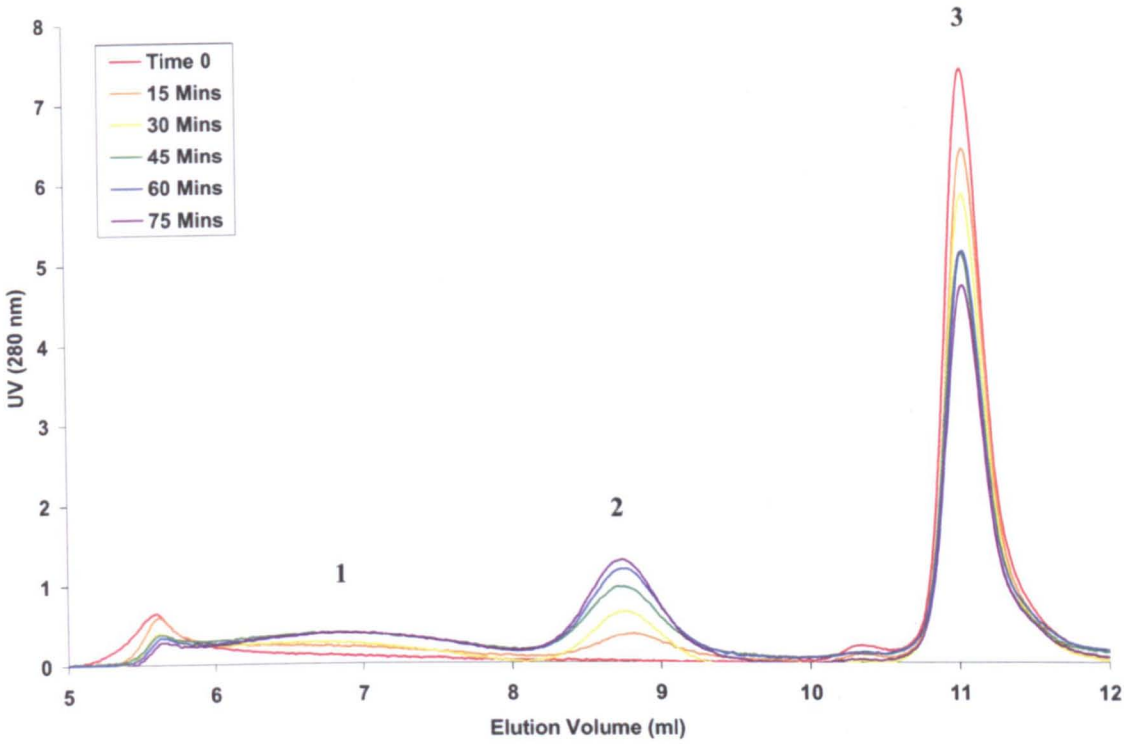

Figure 6.14: Size exclusion HPLC analysis of rMoPrP^{WT} (2 mg/ml), applied to a 7.5 x 300 mm G4000SWxl column, monitored at UV 280 nm.

SEC analyses from a time course of the refolding of full length rMoPrP^{WT} in the native α-monomeric state in 20 mM sodium citrate (pH 3.7) into two distinct soluble oligomers by incubation at 45°C. From a reaction volume of 100 µl, 10 µl aliquots were removed at 15, 30, 45, 60 and 75 minutes and injected onto the SEC column. Monomers elute between 10.5 and 11.5 ml (peak 3), the 12-mer oligomer elutes between 8 and 9 ml (peak 2) and the 36-mer oligomer elutes between 6 and 8 ml (peak 1). The oligomers have an apparent mass of approximately 360 kDa and 1080 kDa for the 12-mer and the 36-mer respectively, as based on calibration by globular protein size standards.

line. A typical result from these experiments is shown in figure 6.15. The presence of plasma membrane in the oligomerisation assay appeared to inhibit the oligomerisation of rMoPrP. Instead, α-monomeric $rMoPrP^{WT}$ appeared to form two completely different isoforms, as assessed by SEC. There is a peak (peak 2) that elutes at approximately 9 ml which is consistent with a smaller oligomeric isoform of approximately 8 subunits of $rMoPrP^{WT}$. The second novel isoform of $rMoPrP^{WT}$ to be observed was peak 4, which was represented by a shoulder (between 11 ml and 11.5 ml) off peak 3 and it is not immediately clear what conformation of $rMoPrP^{WT}$ this peak represents.

Circular dichroism was performed to determine the secondary structure of this shoulder in the chromatogram (peak 4 in figure 6.15) by collecting 500 µl fractions using the fraction collector attached to the ÄKTA purifier FPLC. Representative CD spectra for peak 4 is shown in figure 6.16 and show a largely unstructured conformation for this isoform of $rMoPrP^{WT}$. The CD spectra is rather weak and this is possibly due to either contamination of various salts in the sample originating from OptiPrep™ and/or the homogenisation buffer, or dilution of the protein sample post-SEC. Nevertheless, analysis of peak 4 by CD has revealed a lack of structure. However, there is a resemblance to a typical β-sheet spectra and therefore I cannot discount that the $rMoPrP^{WT}$ here is only partially unstructured.

The subcellular fractions are composed of precipitated cellular material resuspended in the oligomerisation buffer and therefore should only contain minute amounts of OptiPrep™ and/or homogenisation buffer. To control for those factors, the oligomerisation assay was supplemented with a different fraction that was enriched for a different organelle and had previously shown to have no effect in the CFCA. Fraction 18 was enriched for mitochondria and did not contain the plasma membrane marker annexin-II as determined by Western blotting (see figure 3.6), and was therefore an appropriate sample for comparison. Resuspended cellular material from fraction 18 was added to the oligomerisation assay and the effect on the thermal refolding of full length $rMoPrP^{WT}$ was monitored. Full length $rMoPrP^{WT}$ at a concentration of 2 mg/ml in 20 mM sodium citrate (pH 3.4) was heated to 45 °C from which 10 µl samples were taken at 15 minute intervals and analysed by HPLC-SEC. The eluate was monitored by UV 280 nm and for each of the different time

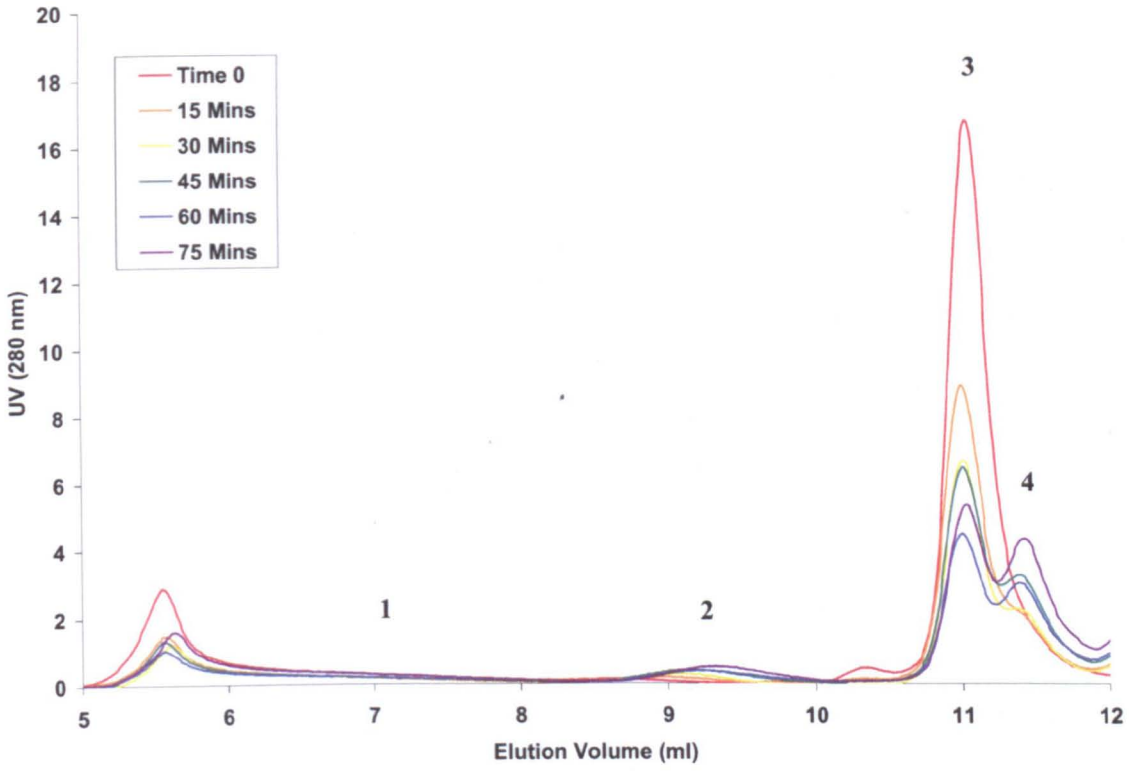

Figure 6.15: Size exclusion HPLC analysis of rMoPrP^{WT} (2 mg/ml) supplemented with an LD9 plasma membrane-enriched subcellular fraction and applied to a 7.5 x 300 mm G4000SWxl column, monitored at UV 280 nm.

SEC analyses from a time course of the refolding of full length rMoPrP^{WT} in the native α-monomeric state in 20 mM sodium citrate (pH 3.7) into two distinct soluble oligomers by incubation at 45 °C. To this reaction a 1:1 (v/v) ratio of fraction 3 from a subcellular fractionation of LD9 cells was added. From a reaction volume of 100 µl, 10 µl aliquots were removed at 15, 30, 45, 60 and 75 minutes and injected onto the SEC column. Monomers elute between 10.5 and 11.5 ml (peak 3), an oligomer of ~ 8 subunits elutes between 9 and 9.5 ml (peak 2) and an unknown isoform of PrP elutes between 11.5 and 12 ml (peak 4). The peak at 5.5 ml represents the unspecified aggregation of PrP and there is the absence of the 36-mer oligomer (peak 1) in this chromatogram. The oligomer has an apparent mass of approximately 240 kDa as based on calibration by globular protein size standards.

A rMoPrP^{WT} (Peak 4)

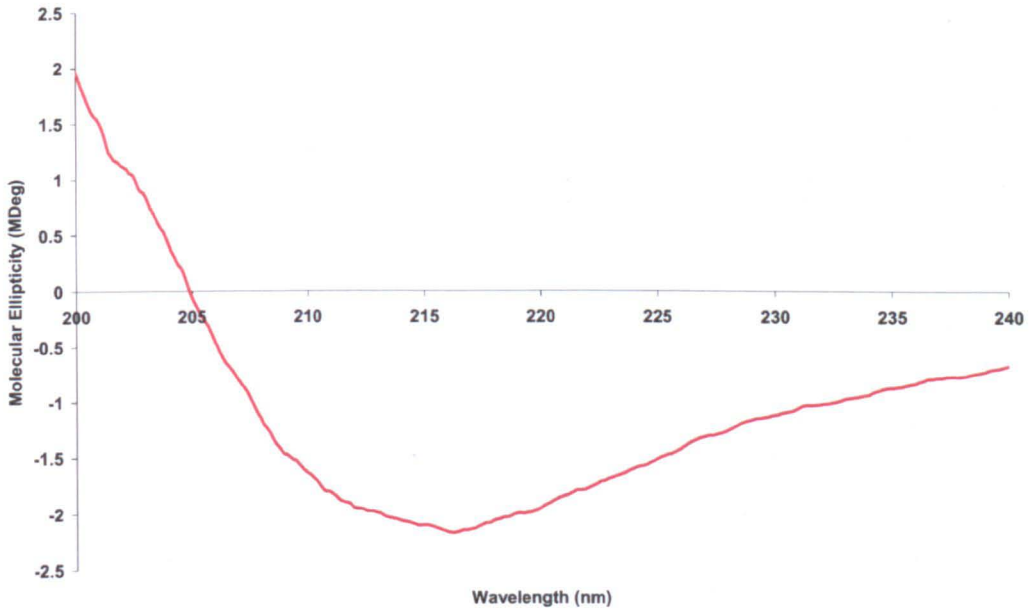

Figure 6.16: Characterisation of prion isoforms by circular dichroism.

The *in vitro* oligomerisation of rMoPrP into two novel isoforms in the presence of low density subcellular fractions from a TSE susceptible cell line. Far-UV circular dichroism spectra for peak 4 from figure 6.15. The spectra were recorded in a 0.5 mm path length cell and analysed against SEC column buffer (20 mM sodium citrate (pH 3.4)). Spectra shows that there is a minima at 216 nm which is indicative of a protein with a secondary structure consisting of β-sheet.

points the data was plotted. A typical result from these experiments is shown in figure 6.17. The mitochondrial enriched fraction did not have any discernable effect on the thermal refolding of $rMoPrP^{WT}$. As demonstrated in figure 6.17, α-monomeric $rMoPrP^{WT}$ refolded into two oligomeric isoforms with elution times that are similar to those seen in the chromatogram of $rMoPrP^{WT}$ in isolation (see figure 6.14). There is a slight shoulder to the peak representing α-monomeric however this is of low intensity and may be the result of a nonspecific interaction between mitochondrial plasma membrane and $rMoPrP^{WT}$.

6.7 Discussion

The misfolding of recombinant PrP *in vitro* has previously been published with multiple different methods and refolding pathways proposed (Jackson *et al.*, 1999, Baskakov *et al.*, 2002, Sokolowski et al., 2003, Tahiri-Alaoui *et al.*, 2003, Rezaei *et al.*, 2005, Martins *et al.*, 2006). A method to produce PrP oligomers, proposed by Baskakov in 2002 and again in 2003 by Tahiri-Alaoui, was suggested to be indicative of PrP misfolding *in vivo* and that the oligomers produced were energetically stable and did not mature into amyloid fibrils *in vitro*. The experimental protocol used rPrP denatured in 6 M guanidine hydrochloride, which after dialysis into an acidic buffer of less denaturant, refolded into a β-sheet rich oligomer. An acidic pH was necessary for the refolding to the β-oligomer as a neutral pH caused the fibrilisation of rPrP. The acidic pH is believed to be physiologically relevant, as it was previously proposed that prion conversion may occur in the endocytic pathway of the cell (Borchelt *et al.*, 1992). Unfortunately, this assay was designed with a truncated and therefore His-tagged, recombinant variant of HuPrP. The N-terminal His-tag is composed of 6 histidines, which was required for purification by Ni-IMAC chromatography. The presence of a His-tag reduces the physiologically relevancy of these experiments and, if used in the current study, may prevent association between rPrP and co-factors. In addition the removal of the N-terminal region may also have a negative impact on prion co-factor interaction due to a potential loss of co-factor binding site(s). When this assay was attempted using denatured full length rMoPrP without a His-tag, oligomerisation was largely successful and the differences in refolding between polymorphic variants were observed (figures 6.2 and 6.5). However, certain details of this assay prevented accurate analysis of the rate of

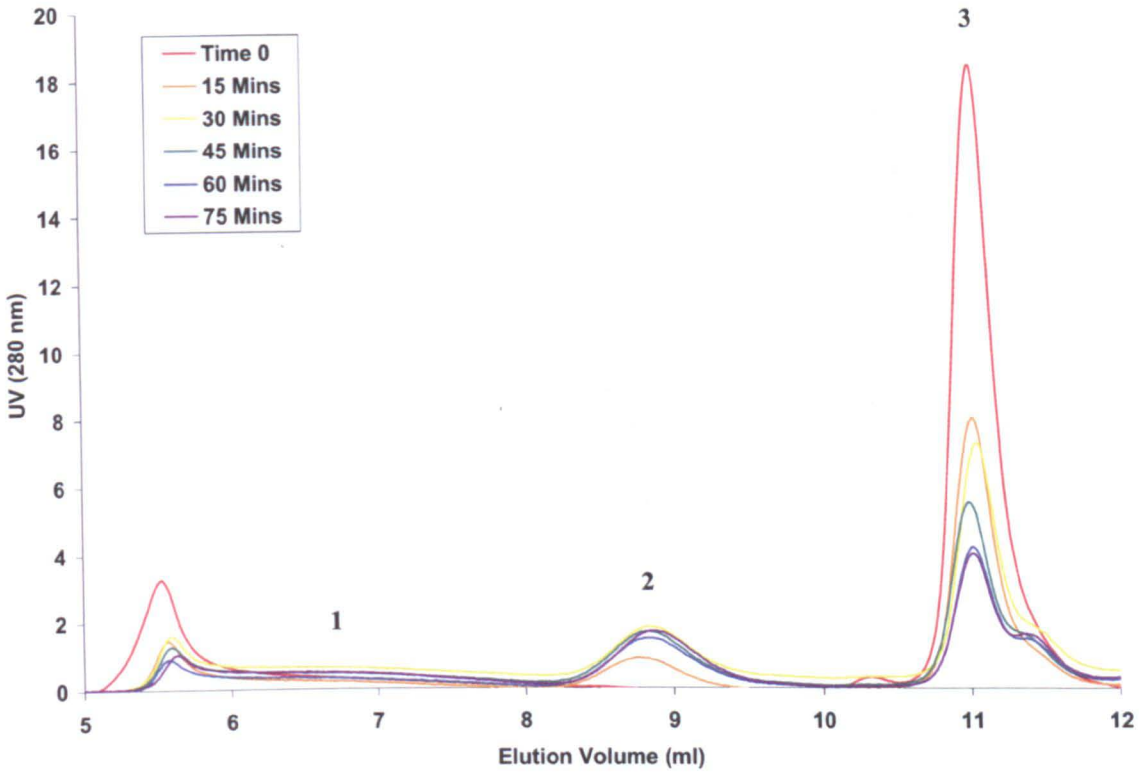

Figure 6.17: Size exclusion HPLC analysis of rMoPrP^{WT} (2 mg/ml) supplemented with an LD9 mitochondrial enriched subcellular fraction and applied to a 7.5 x 300 mm G4000SWxl column, monitored at UV 280 nm.

SEC analyses from a time course of the refolding of full length rMoPrP^{WT} in the native α-monomeric state in 20 mM sodium citrate (pH 3.7) into two distinct soluble oligomers by incubation at 45 °C. To this reaction a 1:1 (v/v) ratio of fraction 18 from a subcellular fractionation of LD9 cells was added. From a reaction volume of 100 µl, 10 µl aliquots were removed at 15, 30, 45, 60 and 75 minutes and injected onto the SEC column. Monomers elute between 10.5 and 11.5 ml (peak 3), the 12-mer oligomer elutes between 8 and 9 ml (peak 2) and the 36-mer oligomer elutes between 6 and 8 ml (peak 1). The oligomers have an apparent mass of approximately 360 kDa and 1080 kDa for the 12-mer and the 36-mer respectively, as based on calibration by globular protein size standards.

oligomerisation due to the presence of an overbearing amount of unspecified aggregates, as determined by SEC. These aggregates of rMoPrP were caused by the sudden shift from a buffer with a high molar concentration of chemical denaturant to a buffer that had a much lower concentration of denaturant. The formation of aggregates was not controllable and thus could not be accounted for when determining rate calculations. In addition, during the time course of oligomerisation there appeared to be a large loss of total protein from the system, as determined by integration of SEC chromatograms. It was decided, therefore that this assay would not provide an accurate and quantitative assay for the analysis of rPrP refolding in the presence of potential prion conversion co-factors.

The second refolding assay investigated involved the thermal refolding of full length rOvPrP to two distinct oligomers in the presence of an acidic buffer (Rezaei *et al.*, 2005). Rezaei and colleagues had previously observed that incubating α-monomeric rOvPrP in 20 mM sodium citrate buffer (pH 3.4) at 45 °C allowed quantitative measures of oligomerisation rates by time course SEC analyses. Reaction kinetics suggested that the α-monomer refolded sequentially into a 12-mer β-oligomer, which with time, formed a 36-mer β-oligomer. Both oligomers were shown to be soluble, stable, and rich in β-sheet and displayed a slight resistance to protease degradation. The β-oligomeric isoforms of PrP have previously been hypothesised to play a role in neurotoxicity by disrupting cellular homeostasis (Moreira *et al.*, 2002, Lashuel *et al.*, 2002). Neurotoxicity was subsequently demonstrated by observations made on the *in vivo* and *in vitro* effects of the β-oligomers formed using the Rezaei methodology (Simoneau *et al.*, 2007). In this publication, subcortical injection of β-oligomers into a panel of mice resulted in more neurodegeneration than when compared against matured fibrils of the same recombinant protein. It was also shown that neuronal cultures were susceptible to cell death when exposed to β-oligomer preparations but not to mature fibril preparations. These experiments suggest that the oligomerisation assay and the methodology for refolding rPrP into the β-oligomer conformation was biologically significant.

The oligomerisation of rOvPrP by thermal refolding of the α-monomer has previously been shown to result in the production of two distinct β-oligomeric isoforms. However, differences in rates of oligomerisation between different

polymorphic variants of ovine PrP have not been investigated. There are three major polymorphic residues in ovine PrP at positions 136, 154 and 171. Sheep carrying different protein variants are either susceptible (PrP^{VRQ}) or resistant (PrP^{ARR}) to TSE disease. In chapter 1, table 1.2 is a list of the 16 polymorphic variants in sheep and their susceptibilities to scrapie infection. The oligomerisation of the ARR and VRQ polymorphic variants of rOvPrP revealed subtle differences in kinetic properties (figure 6.6 to figure 6.9). The α-monomer of $rOvPrP^{ARR}$ formed β-oligomers more rapidly than the $rOvPrP^{VRQ}$ variant. In addition, the $rOvPrP^{VRQ}$ formed more 12-mer oligomers than 36-mer oligomers which in the case of the $rOvPrP^{ARR}$ variant formed approximately equal measures of 12-mer and 36-mer. This data would suggest that $rOvPrP^{VRQ}$ protein is kinetically less efficient at misfolding into the oligomeric isoform and therefore the equilibrium was shifted in favour of the 12-mer under these experimental conditions.

A previous publication by Rezaei and co-workers had suggested that there was a correlation between conformational stability and disease susceptibility (Rezaei *et al.*, 2002). Allelomorphs such as the disease susceptible VRQ were thermodynamically more stable and exhibited less conformational plasticity than allelomorphs that are associated with resistance to disease. My results supported their observations outlined in this chapter where $rOvPrP^{VRQ}$ was slightly slower to oligomerise than the $rOvPrP^{ARR}$ variant (figures 6.6 to 6.9).

The investigations of thermal refolding of rOvPrP variants had shown that this assay was stable and reproducible in the laboratory and therefore the oligomerisation of rMoPrP was attempted. It was essential to be able to alter the assay to make use of murine rPrP for several reasons. Firstly, the main aim of this project was to investigate co-factors that are associated with the conversion of murine PrP by mouse scrapie PrP^{Sc} and in the interest of consistency the oligomerisation assay needed to use murine rPrP. Secondly, the subcellular fractions that enhanced conversion of rMoPrP in the CFCA were of murine origin and to avoid species incompatibility, rMoPrP was again used in the oligomerisation assay. Work published by Vendrely and co-workers demonstrated that rMoPrP could be oligomerised into two distinct β-oligomers using the methodology outlined by Rezaei and colleagues (Rezaei *et al.*, 2005, Vendrely *et al.*, 2005). However, the reaction

kinetics were observed to be different to those of ovine PrP and the sequential formation of monomer to 12-mer to 36-mer was not observed. Instead, the 12-mer and 36-mer appeared to form concomitantly and although the 12-mer was rich in β-sheet, as assessed by FTIR spectroscopy, the 36-mer was an unstable isoform composed predominantly of α-helices. These observations are peculiar and it was suggested that the 36-mer oligomer formed under a different reaction scheme to that of the 12-mer oligomer. The importance and relevance of these observations are unknown at present.

The oligomerisation of $rMoPrP^{WT}$ was compared against the oligomerisation of a polymorphic variant, in which residue 164 was changed from a proline to a leucine (figure 6.10 and 6.12). This change in amino acid has previously been associated with resistance of PrP to conversion *in vitro* and resistance of sheep to TSE disease *in vivo*, as previously described in this chapter (Goldmann et al., 2006, Kirby et al., 2006). The thermal refolding of $rMoPrP^{WT}$ revealed that α-monomeric $rMoPrP^{WT}$ oligomerises into a 12-mer and 36-mer oligomer, as determined by SEC (figure 6.10). The oligomerisation followed a similar reaction scheme to that published by Vendrely and co-workers where α-monomeric $rMoPrP^{WT}$ refolded equally into a 12-mer oligomer and a 36-mer oligomer. However, $rMoPrP^{P164L}$ oligomerised significantly more rapidly than $rMoPrP^{WT}$ with a sudden and dramatic loss of α-monomer within 15 minutes. In addition, it was also demonstrated that $rMoPrP^{P164L}$ initially formed more 36-mer oligomers than 12-mer oligomers. The 36-mer oligomers were shown to be lost with time presumably by breaking down and refolding into 12-mer β-oligomers.

To understand this result and explain it in relation to observations *in vivo* and *in vitro*, it has been observed that the P164L polymorphism and other polymorphic variations at this residue, reduces the structural stability of rMoPrP (Dr Andrew Gill, unpublished data). This loss of stability caused the quick refolding of the α-monomer to the 36-mer oligomer in the oligomerisation assay as shown in figure 6.12. Furthermore, it can be hypothesised that its association with resistance to conversion *in vivo* is acutely linked to its reduced structural stability. If PrP *in vivo* has this particular polymorphism it could be possible that proteins that are structurally less stable may misfold into a non-disease specific isoform more readily. These

misfolded isoforms would be recognised by cellular quality control machinery and therefore cleared more rapidly, thereby reducing the amount of PrP available for conversion *in vivo*. This may seem counter-intuitive, however if it is not in the α-monomeric form then firstly, it may not be present at the correct cellular location for conversion by PrP^{Sc} and secondly, may be conformationally incompatible for conversion. This mechanism of resistance may be similar to that of the polymorphic variants of OvPrP and their effect on susceptibility to scrapie infection, as observed earlier in this chapter (section 6.4).

The thermal refolding of rMoPrP in the presence of an acidic buffer to two distinct oligomeric isoforms, as assessed by SEC, was demonstrated to be a stable and reproducible assay for studying the refolding characteristics of rMoPrP. With a working oligomerisation assay I then went on and analysed the effect of low density subcellular fractions on the oligomerisation of $rMoPrP^{WT}$.

Previously the subcellular fractionation of a TSE susceptible cell line had provided an insight into factors that enhance the conversion of rMoPrP into a PK-resistant β-sheet rich isoform that is very similar to PrP^{Sc} (chapter 4). These fractions contained plasma membrane and were observed to enhance conversion in a nonspecific manner. The cell line that was fractionated to provide samples was the fibroblastic LD9 cell line and this is susceptible to various strains of mouse scrapie, including ME7, 22L and RML (Mahal et al., 2007). However, low density subcellular fractions enhanced the conversion efficiency of the mouse scrapie strains ME7 and 79A. If these fractions did not contain specific co-factors then it is reasonable to suggest that the plasma membrane was interacting with the rMoPrP substrate in a general way. It was hypothesised that plasma membrane caused a conformational change in the α-monomeric conformation of rMoPrP that induced efficient conversion to a PK-resistant isoform in the CFCA. If the presence of plasma membrane destabilised the conformation of the rMoPrP substrate then this would match previous publications that have demonstrated that a loss of thermodynamic stability increases the propensity of rPrP for conversion (Harrison *et al.*, 1999, Vanik and Surewicz, 2002).

The subcellular fractionation of the LD9 cell line into fractions by ultracentrifugational separation, supplied samples enriched for different organelles as

determined by Western blotting for specific markers. Western blotting for the plasma membrane marker annexin-II showed that fraction 3 was the most highly enriched fraction for plasma membrane and was subsequently used to supplement the oligomerisation assay. Methanol precipitation of this fraction followed by centrifugation and re-suspension of the pellet in 20 mM sodium citrate (pH3.4) to give a final concentration of 2 mg/ml rMoPrP and, to control for this experiment, a sample of the same aliquot of rMoPrP was diluted 1:1 with just 20 mM sodium citrate (pH 3.4) and heated to 45 °C as per the oligomerisation protocol described previously in this chapter (section 6.5). Recombinant mouse PrP in the absence of any subcellular fraction refolds from the α-monomer conformation into a 12-mer and 36-mer oligomer as separated by HPLC-SEC and analysed by UV absorbance at 280 nm (figure 6.14). When compared against the thermal refolding of rMoPrP in the presence of fraction 3 there was an inhibitory effect caused by this plasma membrane enriched fraction (figure 6.15). Instead of forming two oligomeric isoforms, there was instead two novel isoforms formed, which were of smaller size. Firstly there was an oligomer of approximately 8 subunits and the second novel isoform was observed to elute just after α-monomeric rMoPrP and circular dichroism suggested that it had a degree of β-sheet secondary structure in it. This change in conformation would explain the difference in elution time as size exclusion chromatography elutes proteins by size rather than actual molecular weight. The increase in β-sheet in the structure of this isoform has probably caused the size to become smaller by tightening the structure. Alternatively, low density subcellular fractions may contain cellular proteases that have truncated rMoPrP, which would also result in a peak that has a later elution volume. Further structural analysis of the isoforms eluted from these oligomerisation assays would need to be performed prior to verification of the secondary structure; however this was not carried out due to lack of time.

To verify that the effect observed in figure 6.15 was specifically related to the plasma membrane and not any artificial contaminants from OptiPrep™ or the homogenisation buffer used to homogenise and fractionate the LD9 cell line, the oligomerisation assay was supplemented with a non-plasma membrane enriched fraction. Fraction 18 represented a sample that was predominantly made up of mitochondria and which had no discernible plasma membrane present, as determined by Western blotting for those relevant subcellular markers. As can be seen in figure

6.17, the addition of fraction 18 to the oligomerisation assay did not have the same inhibitory effect as observed for fraction 3. The amount of 36-mer oligomer was not as great as that seen in the un-supplemented oligomerisation assay however this was deemed insignificant. These small effects on thermal refolding could be due to an nonspecific interaction with the mitochondrial membrane or other mitochondrial proteins present in this fraction. However, there is a definite progression from α-monomer to 12-mer and 36-mer which is not what was observed when fraction 3 was added to the assay.

The observation that the thermal refolding of rMoPrP was disrupted by the presence of plasma membrane has consequences for *in vitro* assays in general but also on the way that we view mechanisms of how rMoPrP reacts to refolding conditions in the cell. The CFCA was previously used to demonstrate the enhancing effects of plasma membrane on conversion seeded by two different stains of mouse scrapie however this would appear to not be in accord with the decrease in oligomeric species. This may have highlighted that the CFCA is a one step process that immediately converts rMoPrP into a PrP^{Sc} like isoform rather than including an intermediate species such as an oligomer. This would explain the differences observed on the effect of plasma membrane in the CFCA and oligomerisation assay. Alternatively, the results may have demonstrated that PrP refolds into oligomeric species and amyloid fibrils in different parts of the cell, both of which contribute to neurodegeneration but by different pathways. These results have highlighted the difficulties in understanding the *in vivo* conversion process using *in vitro* methods.

To try to understand the interaction between PrP and subcellular fractions further, ongoing work in the laboratory has made use of an alternative *in vitro* misfolding assay. Based on the protocol described previously by Bocharova and colleagues the pathway of PrP misfolding, leading to amyloid fibrils has been investigated (2005). In this assay, recombinant $MoPrP^{WT}$, in a partially denaturing buffer, was induced to fibrilise by shaking at 37 °C for 24 hours and fibrilisation monitored by increase in thioflavin-T (ThT) fluorescence. This work was carried out by a research assistant in the laboratory (Miss Sonya Agarwal) but made use of subcellular fractions from LD9 cells that I had previously produced. Typical results from the fibrilisation are shown in figure 6.18 from four different subcellular fractions of LD9 cells, and each panel

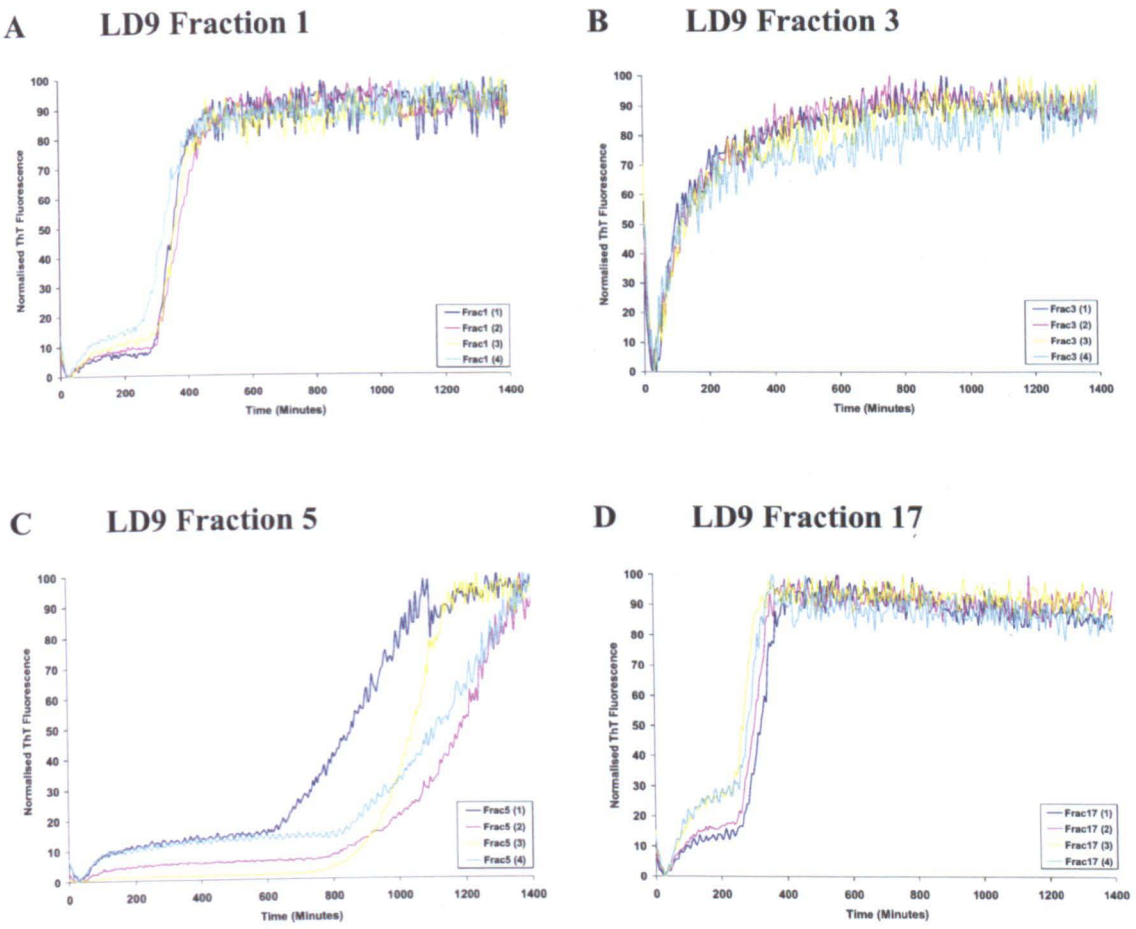

Figure 6.18: Analysis of rMoPrP^{WT} (1 mg/ml) supplemented with LD9 subcellular fractions 1, 3, 5 and 17 by thioflavin-T fluorescence.

Fibrilisation reaction contains 5.2 µM rMoPrP mixed with (A) LD9 subcellular fraction 1, (B) LD9 subcellular fraction 3, (C) LD9 subcellular fraction 5 and (D) LD9 subcellular fraction 17, in a reaction volume of 160 µl of fibrilisation buffer (2 M guanidine hydrochloride, 0.05 M MES, 0.01 M thiourea, rMoPrP^{WT}, 0.01 mM thioflavin-T) with three Teflon balls per well and incubated at 37 °C, shaking at 900 rpm. Each experiment was repeated four times and data normalised to produce data between 0-100 % ThT fluorescence and plotted on the same graph. A noticeable dip in fluorescence immediately after the assay has been initiated is present in all traces and is particularly pronounced in panel B, since no fibrilisation occurs in these samples.

represents several repeat assays. In each case, ThT fluorescence has been normalised to give between 0-100 %. When $rMoPrP^{WT}$ was shaken in the presence of fraction 1 (top) or fraction 17 (bottom) of the fractionation gradient, fibrilisation proceeded with short lag times, as evidenced by sigmoidal increase in ThT fluorescence at ~ 300 minutes. When in the presence of a LD9 plasma membrane enriched subcellular fraction (fraction 3), fibrilisation of $rMoPrP^{WT}$ was inhibited as defined by the absence of the sigmoidal curve for ThT fluorescence (figure 6.18 panel B). Instead, ThT fluorescence remained similar to background levels, although because the data has been normalised to fit the maximum fluorescence to 100 %, the graph appears to show an increase in fluorescence at early time points. With fraction 5 the fibrilisation of $rMoPrP^{WT}$ occurs with a dramatically increased lag time and in some replicate assays fibrilisation is not complete in the time scale of the experiment. This work is ongoing in the laboratory and represents initial findings; however these observations appear to support previously discussed experimental results where the interaction of LD9 plasma membrane with rMoPrP possibly causes stabilisation of the conformation which is not conducive for oligomerisation or fibrilisation, but is conducive for conversion in the CFCA.

To conclude, the low density subcellular fractions from the subcellular fractionation of the LD9 cell line have given different effects depending on whether the *in vitro* assay used is unseeded, or seeded with mouse-adapted scrapie.

7. General discussion

7.1 Discussion

Prions are self propagating infectious proteins that act autocatalytically, typically propagating a phenotypic change in the host. In 1982, Prusiner coined the term prion to describe a proteinaceous agent that was both pathogenic and transmissible in the absence of a pathogen specific nucleic acid (Prusiner, 1982). The prion protein is the principal component of this novel pathogen and causes disease by propagation of its unnatural conformation onto host PrP^{C}. Different conformations of PrP^{Sc} appear to be specific to different TSE strains and this is believed to form the molecular basis for the different phenotypic properties of different strains (Bessen *et al.*, 1995). However, PrP^{Sc} conformation may not be the only critical factor in strain differentiation since the multiplicity of different TSE strains would require a discrete conformation of PrP^{Sc} to encode each set of phenotypes. To account for the putative diversity of PrP^{Sc} conformers it has been suggested that prion co-factors play an important role in aiding PrP^{C} conversion efficiency and dictating strain properties. Co-factors could play a variety of roles in prion conversion, including a chaperone function to reduce the energy required to refold PrP^{C}, provision of a molecular scaffold to bring all the necessary molecules together or to specifically sequester PrP^{C} and PrP^{Sc} in the correct subcellular domain and environmental conditions for conversion. This project involved the investigation into the subcellular localisation of potential prion co-factors that stimulate prion protein conversion.

7.2 A method for the extraction and isolation of subcellular organelles of two TSE susceptible cell lines was developed

To date, TSE susceptible cell lines have provided an important role in the analysis of the molecular mechanisms that govern cell susceptibility to infection and the mechanisms behind the spread of the infectious agent. The number of cell lines that are susceptible to infection *ex vivo* is limited and there are a number of strains that are yet to be demonstrably infectious to cell cultures (Vilette, 2007). These observations strengthen the possible role of strain specific factors in prion conversion because different cells may have differential expression of different proteins, which may have an effect on conversion efficiency.

Chapter 3 describes the development of a fractionation protocol for the isolation of subcellular organelles from two different cell lines. The SMB-PS and LD9 cell lines are susceptible to different strains of mouse scrapie and were used in experiments aimed at determining the subcellular localisation of potential conversion enhancing co-factors. Cell lines were cultured to confluence and gently homogenised to release intact internal organelles prior to ultracentrifugation through a density gradient. Monoclonal antibodies that recognised organelle specific protein markers were used to analyse organelle distribution throughout the gradient (figure 3.6 and 3.8).

The subcellular fractionation protocol allowed for the isolation and extraction of subcellular organelles from the LD9 and SMB-PS cell lines. A density gradient of 10-20 % proved to effectively separate plasma membrane, lysosomes, Golgi body, endoplasmic reticulum and mitochondria to a degree that showed that there was enrichment for each of these organelles in distinct fractions.

Understanding the cellular trafficking of PrP^{C} is critical to aid understanding of the pathogenic conversion to PrP^{Sc} and ultimately cell death. There is evidence to suggest that PrP^{Sc} accumulates in lysosomes (Mayer *et al.*, 1992, Grigoriev *et al.*, 1999), endosomes (Jeffrey *et al.*, 2009), endoplasmic reticulum (Béranger *et al.*, 2002) and the plasma membrane (Caughey and Raymond, 1991*a*, Jeffrey *et al.*, 1992, Jeffrey *et al.*, 1994, Paquet *et al.*, 2007) of neuronal and glial cells, implicating these areas as sites for conversion. In addition to these observations, *in vitro* pulse chase experiments have shown that internal PrP^{Sc} is N-terminally truncated thereby suggesting that PrP^{C} to PrP^{Sc} conversion takes place at the plasma membrane prior to internalisation and digestion (Caughey and Raymond, 1991).

If prion conversion takes place at the plasma membrane then internalisation and 'infection' of the cell has been proposed to happen via clathrin-coated pits (Peters *et al.*, 2003, Sunyach *et al.*, 2003, Sarnataro *et al.*, 2009). The presence of PrP^{Sc} internally in the endocytic pathway can therefore be explained as an event that occurs post-initial contact. To support this statement, a recent study demonstrated that PrP^{Sc}, as well as, PrP^{C}, is also internalised via clathrin coated-pits (Jeffrey *et al.*, 2009). Therefore these observations suggest that the plasma membrane plays an important pathological role in prion conversion. However, different strains of scrapie have been

shown to infect different cell types causing strain specific pathological changes, possibly via differences in the site of conversion and/or PrP^{Sc} processing (Gonzalez *et al.*, 2003, McGovern and Jeffrey, 2007). Alternatively, it has been suggested that conversion and uptake of PrP^{Sc} occurs independently of PrP^{Sc} variation and instead it is the presence of plasma membrane co-factors and the micro-environment that are key (Greil *et al.*, 2008). The conflicting observations on the site of conversion serve to highlight the difficulty in understanding cellular infection by prions. It is likely that a number of entry points into the cell exist, which may or may not be strain dependent, however the site of the first prion multiplication site is strongly suggested to be at the plasma membrane. This therefore was a primary objective to analyse for the presence of co-factors. However, the cellular internalisation of PrP^{Sc} is suggestive of other sites of prion conversion and therefore other implicated organelles cannot be discounted as sites of prion conversion and strain specific co-factors.

7.3 Four different strains of mouse scrapie were used successfully in the CFCA which highlighted differential conversion efficiencies

Historically, the CFCA has been used with the mouse adapted scrapie strain, 87V, which converts approximately 20 % of the rMo3F4PrP substrate into PrP^{res}. However, this was not the only strain of mouse scrapie that has been tested in the CFCA. Other TSE strains successfully used in the CFCA include, ME7, 79A, 22F, 301V (mouse adapted BSE) and 263K (hamster adapted scrapie). In this project, the CFCA was therefore extended to include experiments seeded with the four mouse adapted scrapie strains, 87V, ME7, 79A and 22F, which showed that there were differences in the conversion efficiencies for each of the four different strains of mouse scrapie. For ME7, 79A or 22F seeded CFCA the approximate percentage of substrate converted to PrP^{res} was 18 %, 3.5 % and 2.5 % of the rMo3F4PrP substrate, respectively. Low conversion efficiency rates had implications for the reliability of results due to small differences in replicates resulting in large standard errors during analysis.

The inability of mouse scrapie to convert 100 % of the substrate is not limited by time but could instead be due to either inadequate assay buffer conditions, or a deficiency of prion co-factors that are necessary for efficient conversion. Another

explanation for differences in conversion efficiencies between different strains of mouse scrapie is that fibril morphology could influence the number of free ends available to convert nascent PrP^{C} to PrP^{Sc}. This theory has been applied to the PMCA assay to explain amplification of the protease-resistant product by multiple rounds of sonication. Cyclic sonication breaks up the fibrils, presenting new fibril ends for further nascent PrP molecules to be converted to the protease-resistant isoform.

7.4 The CFCA was supplemented with subcellular fractions from TSE susceptible cell lines to identify strain specific organelles that enhance conversion

Using the protocol described in chapter 3, subcellular fractions were prepared and organelle distributions assessed by Western blotting and densitometric analysis. Subcellular fractions from both the SMB-PS and LD9 cell lines were tested in the CFCA as shown in chapter 4. Analysis of the effect of subcellular fractions on the conversion efficiency showed that fractions enriched for plasma membrane from LD9 cells enhanced conversion in the CFCA seeded with both ME7 or 79A. This cell line is susceptible to ME7 infection but not to the 79A strain of mouse scrapie. This would suggest a physical rather than biochemical reason for enhancement of conversion by the presence of plasma membrane from this cell line. This could be through the increase in surface area and the plasma membrane proteins providing a point with which to anchor substrate and seed together. Conversely, when the CFCA was done with fractions enriched for SMB-PS plasma membrane, no enhancement of conversion efficiency was evident. This cell line is susceptible to 79A infection but not ME7 infection. Instead subcellular fractions enriched for Golgi body enhanced 79A conversion in the CFCA. Unfortunately, the supplementation of an ME7 seeded CFCA with Golgi body enriched fractions from the SMB-PS cell was not done, due to lack of time and resources.

These data suggest the action of prion co-factors thus implying that LD9 cells have the co-factors on the surface and that strain tropism is governed by other additional factors. Other factors could include PrP expression levels, PrP trafficking, prion co-factor expression levels and environmental conditions that are necessary to generate a long term infection. This is true for the SMB-PS cell line which presumably may

require endocytosis and retrograde transport of PrP^{Sc} to the Golgi body for conversion of PrP^{C}. Another implication is that different cell types may have different locations of conversion, thereby explaining discrepancies in these results.

7.5 A variety of different proteins were detected in SAF preparations from ME7, 79A and 22F mouse scrapie by mass spectrometry

Chapter 5 describes the mass spectrometric analysis of SAF preparations from ME7, 79A and 22F infected mouse brains. Mass spectrometric analysis was done in the hope of identifying proteins that are either located in the plasma membrane or the Golgi body, the two areas implicated in strain specific prion conversion. Preparation of SAF material was done by detergent extraction and differential centrifugation (Hope *et al.*, 1986). This method is effective at partially purifying the infectious agent, however, other proteins not associated with disease will be co-purified. To account for these proteins and to exclude them from future experimental analysis, SAF preparations on uninfected wild type and $PrP^{0/0}$ brains were done. As expected, the proteins present within these control SAF preparations were either highly abundant or high molecular weight proteins. Mass spectrometric analysis of ME7, 79A and 22F SAF preparations, after removal of proteins also identified in control preparations, showed a number of proteins that appear to be specifically associated with mouse scrapie fibrils. One of the more interesting proteins identified was the plasma membrane protein, Na^{+}/K^{+} transporting ATPase. This protein was detected in all three strains of SAF and has previously been reported to be associated with neurodegenerative disorders (Calandriello *et al.*, 1995, Palladino *et al.*, 2003). Although this protein cannot be considered to be a strain specific co-factor, it has been hypothesised that PrP^{C} may interact with Na^{+}/K^{+} transporting ATPase on the plasma membrane of neurones (Petrakis *et al.*, 2008). Recent findings support a physiological interaction of Na^{+}/K^{+} transporting ATPase with PrP^{C}, where it was shown that these two proteins may be a member of a multiprotein complex incorporating the β4 subunit of nicotinic acetycholine (Petrakis and Sklaviadis, 2006, Petrakis *et al.*, 2008). Other proteins detected in this complex included 2',3'-cyclic nucleotide 3'-phosphodiesterase (CNP1) and synapsin-1, which were also detected by mass spectrometry in my SAF preparations (table 5.2). The detection of Na^{+}/K^{+} transporting ATPase, CNP1 and synapsin-1 may well be through nonspecific

interactions with PrP^{Sc} due to the possible proximity between the hypothetical multiprotein complex and the site of prion conversion. Conversely, the presence of these proteins may point to a key role of these proteins in facilitating prion conversion, potentially through localising PrP^{C} on the plasma membrane in a topology amenable for interaction with PrP^{Sc}. Crucially, the other protein members of the functional complex may become amalgamated into the growing fibril because they originally provided a site of interaction.

SAF preparations were pre-treated with proteinase K to digest any externally attached molecules to leave proteins that are integrated into the fibrils and therefore protected from proteolytic degredation. This reduced the number of tryptic peptide present after digestion and only single proteins were identified for each strain of mouse scrapie. Firstly, the prolow-density lipoprotein was detected in the ME7 SAF preparation, which is a multifunctional plasma membrane receptor involved in the endocytosis of many different types of extracellular proteins (Herz *et al.*, 1992). Whether this protein has any involvement in PrP^{C} cell biology is still to be elucidated, however its role in the endocytosis of metabolic products through clathrin-coated pits localises this protein to the same cellular location in which PrP^{Sc} entry has been suggested (Goldstein *et al.*, 1985). The Dmxl2 protein was the single positive identification made in the PK treated 79A SAF preparation. Dmxl2 is a synaptic membrane protein that is hypothesised to be involved in MAP kinase activation and caspase-mediated cell death (Munton *et al.*, 2007). One of the proposed functions of PrP^{C} is to mediate cell signalling and cell survival through signal transduction mechanisms. Therefore the identification of Dmxl2 in SAF preparations may perhaps implicate PrP^{C} with proteins in the MAP kinase pathway. However, this does not discount Dmxl2 as a strain specific co-factor as it is highly likely that a prion co-factor will either be localised in the same region as PrP^{C} or alternatively, the function of the prion co-factor will be associated with the function of PrP^{C}.

The infectious agent is hypothesised to be primarily composed of a misfolded host protein, PrP. However, analysis of PrP^{Sc} fibrils found in the brains of TSE infected animals has demonstrated that there are other molecules that co-purify with PrP^{Sc}. The presence of these co-prions may be explained, firstly, by a nonspecific

interaction caused by the nature of aggregated protein to cause protein precipitation, secondly, co-prions are not strain specific but are necessary for fibril morphology, thirdly, these molecules are instead an integral part of conversion and also aid in strain variation or finally, co-prions aid in conversion but are only present in the fibril indirectly and do not influence fibril morphology.

A long term aim in the TSE field is to prove the prion hypothesis by synthesising infectious prions *in vitro* from defined constituents. Legname and colleagues produced synthetic fibrils from recombinant PrP that caused a prion like disease in transgenic mice that over-express the same PrP construct (Legname *et al.*, 2004, Legname *et al.*, 2005). Even though these results appear, at face value, to prove the protein-only hypothesis they were generally met with scepticism. Firstly, the transgenic mice that over-express PrP were known to produce a spontaneous TSE-like disease in old age (Westaway et al., 1994, Chiesa *et al.*, 1998). Therefore the synthetic prions may not be completely responsible for disease and instead may seed misfolded PrP that is already present in these mice. Secondly, infectivity titres of these recombinant derived prions were an order of magnitude less than *bona fide* prions when disease was transmitted to wild type mice in a second passage.

Since these experiments were published, a different group have shown that the *de novo* generation of infectivity was possible using the PMCA methodology (Castilla *et al.*, 2005). The PMCA technique involves the combination of brain homogenates from infected and uninfected animals. Serial amplification cycles of sonication and dilution with normal brain homogenate amplifies protease-resistant protein and also appears to amplify infectivity. However, the molecular composition of the infectious agent could not be determined due to the complexity of the brain homogenate material used in these initial PMCA reactions. Further to this, the PMCA technique was optimised to use partially purified constituents, limiting the presence of potential co-factors included in the assay (Deleault *et al.*, 2005). By use of the simpified assay, it was observed that the addition of polyanionic accessory molecules amplified PrP^{res} *in vitro* and was both infectious and transmissible (Deleault *et al.*, 2007). The polyanionic molecules tested included nucleic acids and sulphated glycans such as heparan sulphate proteoglycan. It was subsequently demonstrated that PrP^{res} formation could be initiated spontaneously in the PMCA assay by mixing just

purified PrP^C and an accessory poly(A) RNA nucleic acid (Deleault *et al.*, 2007). The role of polyanions in PrP^{Sc} formation is unclear, however it has been shown that sulphated glycans co-localise with PrP^{Sc} *in vivo* and are suggested to be receptors for PrP^{Sc} on the surface of the cell (Snow *et al.*, 1989, Wong *et al.*, 2001, Hijazi *et al.*, 2005, Horonchik *et al.*, 2005). Therefore, the role of a polyanion could either be as a co-factor or a cellular receptor that is necessary for entry into the cell. Alternatively, polyanions could behave like a scaffold molecule that facilitates the polymerisation of the fibril. My results may indicate that the inclusion of a plasma membrane-enriched fraction may also similarly behave like a scaffold.

If it is plausible that the infectious agent is composed of PrP and other host-derived components, then it is possible that these non-PrP molecules may be involved in the conversion process. Certainly it has been suggested that the 37 kDa/67 kDa laminin receptor is needed for prion propagation in neuronal cells (Leucht *et al.*, 2003). Its role in conversion is still to be determined, but it has been suggested that it is a receptor for PrP^{Sc} and this interaction is necessary for cellular entry and the subsequent trafficking of PrP (Gauczynski *et al.*, 2006, Nikles *et al.*, 2008).

7.6 Different variants of rPrP have different thermal refolding rates in an oligomerisation assay

To further understand the enhancement of seeded conversion in the CFCA from low density subcellular fractions, these subcellular fractions were used to supplement an oligomerisation assay. This assay involved the heat refolding of α-monomeric rMoPrP at an acidic pH into two oligomeric isoforms, a 12-mer and a 36-mer. The oligomerisation of recombinant PrP *in vitro* is suggested to replicate *in vivo* mechanisms where PrP^C refolds into a neurotoxic oligomer prior to maturation into the amyloid fibril (Chiesa *et al.*, 2003, Nazor *et al.*, 2005).

The refolding of recombinant PrP was trialled extensively to find an assay that was as physiologically relevant to cellular conditions as possible. The method previously described by Rezaei and co-workers incorporated an increase in temperature and an acidic pH to refold recombinant PrP to two oligomeric isoforms (Rezaei *et al.*, 2005). Preliminary development of this assay was done with different variants of rOvPrP,

$rOvPrP^{ARR}$ and $rOvPrP^{VRQ}$. These two variants are associated with resistance and susceptibility to scrapie *in vivo*, respectively. Results, described in chapter 6, indicated that there is an inverse correlation between the propensity to oligomerise in the oligomerisation assay and disease susceptibility *in vivo*. This correlation is supported by the literature and shows that ovine PrP variants associated with susceptibility to conversion are thermodynamically more stable and therefore less likely to misfold into isoforms such as oligomers (Rezaei *et al.*, 2002).

The oligomerisation of $rMoPrP^{WT}$ was compared against a polymorphic variant, in which residue 164 was changed from a proline to a leucine (Figure 6.10 and figure 6.12). This polymorphism is associated with resistance to scrapie in sheep (Goldmann *et al.*, 2006). The P164L polymorphism caused rMoPrP to oligomerise at a faster rate with a higher propensity to form more 36-mer oligomers than 12-mer oligomers when compared against $rMoPrP^{WT}$. It was hypothesised that the P164L polymorphism reduced the structural stability of $rMoPrP^{P164L}$ and this explained the observations made on the oligomerisation of these two rMoPrP variants.

The oligomerisation assay was chosen as an alternative assay to the CFCA, over other assays such as the fibrilisation of rPrP, to analyse the effect of polymorphic variations in PrP for several reasons. Firstly, the oligomerisation of denatured rPrP has been shown to reflect *in vivo* observations such as the propensity of rPrP with a methionine at codon 129 to misfold into β-sheet rich oligomers when compared against rPrP with a valine at codon 129 (Tahiri-Alaoui *et al.*, 2004). The higher susceptibility of this PrP variant to misfold, correlates with the increased susceptibility of individuals to sCJD and vCJD. The fibrilisation of the same denatured proteins showed that rPrP with a valine at codon 129 had a higher propensity to form fibrils (Baskakov *et al.*, 2005).

Secondly, the oligomerisation of rPrP by thermal refolding has previously shown to produce oligomers that are neurotoxic to both *ex vivo* cultured neurones and to a panel of mice after subcortical injection (Simoneau *et al.*, 2007). Finally, the incorporation of size exclusion chromatography to separate different isoforms of rPrP allows for the quantitative analysis and comparison of different rPrP variants during an oligomerisation time course.

7.7 Low density subcellular fractions reduced the refolding rate of rMoPrP *in vitro*

The oligomerisation assay was used to analyse the effect of plasma membrane-enriched fractions on the refolding rate of rMoPrP *in vitro*. The refolding of rMoPrP into oligomeric isoforms was inhibited when in the presence of plasma membrane-enriched fractions from the subcellular fractionation of the LD9 cell line. These fractions were previously shown specifically to enhance the seeded conversion of rMo3F4PrP into PrP^{res} (figure 4.4 panel A). However, figure 6.15 shows that instead of refolding into two distinct oligomers, a smaller β-oligomer of PrP and a β-monomer form under these oligomerisation conditions. A control oligomerisation assay that was supplemented with a fraction enriched for mitochondria rather than plasma membrane was carried out and results showed this fraction had no discernible effect on the oligomerisation of rMoPrP (figure 6.17).

The thermal refolding of rMoPrP into oligomeric isoforms was inhibited by the presence of a LD9 low density subcellular fractions and this result has consequences on understanding how PrP reacts in the CFCA. LD9 plasma membrane-enriched fractions conversely enhanced conversion in the CFCA seeded by ME7 and 79A mouse scrapie, thus indicating that a different *in vitro* refolding mechanism than when compared to the oligomerisation assay. This suggests that the CFCA requires the substrate to be α-monomeric, whereas the oligomerisation of rPrP may require a substrate that is partially unfolded. The addition of low density subcellular fractions to the oligomerisation assay reduces the amount of α-monomer possibly by unfolding and subsequent misfolding into the β-monomer isoform. This reduction in α-monomeric substrate by the presence of plasma membrane would reduce the availability of $rMoPrP^{WT}$ for oligomerisation but possibly put the protein into a conformation more amenable to conversion in the CFCA, thereby explaining the apparent contradictory results.

Further to this the addition of plasma membrane fractions on the *in vitro* fibrilisation of rMoPrP showed that, when in the presence of a LD9 plasma membrane-enriched subcellular fraction, fibrilisation of $rMoPrP^{WT}$ was inhibited (figure 6.18 panel B). Control experiments with LD9 subcellular fractions 1 and 17 showed no effect on the

fibrilisation of $rMoPrP^{WT}$ whilst fraction 5 increased lag times for fibrilisation (figure 6.18 panels A, C and D). The interaction of LD9 plasma membrane with rMoPrP possibly causes a stabilisation of α-monomeric $rMoPrP^{WT}$, which is not conducive for oligomerisation or fibrilisation, but is for the seeded conversion in the CFCA. In figure 7.1, a hypothesised reaction pathway is shown, which illustrates the effect of plasma membrane-enriched fractions have on the stability of rPrP and the influence these fractions have on seeded conversion and unseeded refolding.

7.8 Summary

I developed a method for the extraction and isolation of subcellular organelles of two TSE susceptible cell lines, LD9 fibroblasts and SMB-PS microglial cells. Subcellular organelles were used initially to supplement the CFCA which showed that LD9 low density subcellular fractions enhanced the conversion efficiency of ME7 and 79A mouse scrapie in the CFCA. The LD9 cell line is susceptible to only ME7 and not 79A thus highlighting that the plasma membrane-enriched fractions may either offer a scaffold that co-localises PrP^{C} and PrP^{Sc}, or that the plasma membrane is a universal subcellular localisation for prion conversion. However, the conversion efficiency of ME7 and 79A was not enhanced by low density subcellular fractions from the SMB-PS cell line. This cell line is differentially susceptible when compared to the LD9 cell line and is susceptible to 79A but not ME7. This result shows that there is a cell line specific enhancement associated with the plasma membrane fractions of LD9 cells. To complement this result, Golgi body enriched fractions from the SMB-PS cell line enhanced 79A conversion efficiency in the CFCA thus suggesting a potential site for conversion in this cell line. To determine and identify potential prion co-factors, proteins that co-purified with PrP^{Sc} in SAF preparations were identified by mass spectrometry. A list of plasma membrane derived proteins was identified, of which a few have been previously identified to be associated in TSE disease. In addition, mass spectrometry was used to identify different protein constituents in three different strains of mouse scrapie which may represent strain specific co-factors and aid in strain variation.

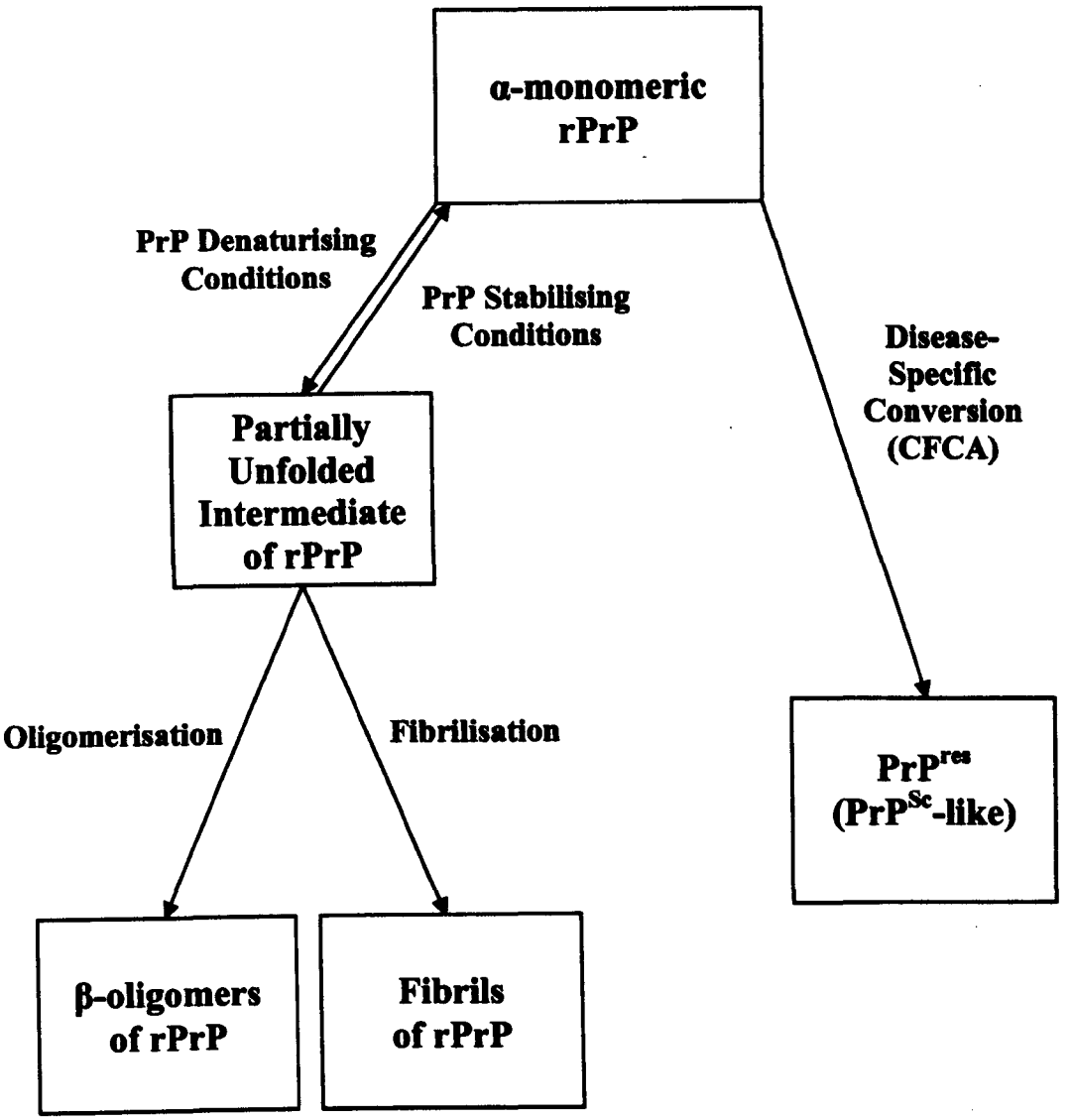

Figure 7.1: Possible *in vitro* misfolding pathways of rPrP

Monomeric rPrP in either a partially denatured or α-helical conformation is an important factor for the successful misfolding of rPrP *in vitro*. Partially denaturising conditions such as an acidic pH or the presence of a chaotrope are conducive for the oligomerisation or fibrilisation of rPrP, respectively. However, when these assays are supplemented with a plasma membrane-enriched subcellular fraction, there is a stabilisation of rPrP conformation back to a folded state thus preventing refolding into oligomers or fibrils. On the other side, the CFCA involves the disease-specific conversion of rPrP to PrP^{res} and when this assay is supplemented with a plasma membrane-enriched subcellular fraction, the conversion of α-monomeric rPrP is enhanced. However, it is likely that plasma membrane proteins preset in these subcellular fractions play an important role in strain specificity.

To further our understanding of the effect of low density subcellular fractions on the recombinant PrP substrate, an oligomerisation assay that involved the thermal refolding or rPrP into oligomeric isoforms was used. This assay had previously been used to identify different oligomerisation rates of rOvPrP variants which confer either susceptibility or resistance to sheep carrying the respective proteins, to scrapie. In addition, this assay also enabled the differentiation of rMoPrP variants that differed by the amino acid expressed at codon 164, which is also related to disease and resistance to conversion. The oligomerisation and fibrilisation assays were used to monitor the effects of plasma membrane-enriched fractions on the refolding of rMoPrP. These subcellular fractions appeared to specifically inhibit the refolding of monomeric rMoPrP to oligomeric and fibril isoforms. This result indicates that there are different mechanisms of rMoPrP refolding in the three assays used and that potentially the oligomerisation and fibrilisation assays are a generic misfolding of PrP rather than the specific seeding in the CFCA.

7.8.1 Possible future Work

From this study it can be seen that there are many unanswered questions concerning the specificity of conversion enhancing factors.

1. Further validation of the proteins identified by mass spectrometry to facilitate our understanding of the role these molecules play in prion conversion. This could be done by several methods include, co-immunoprecipitation to validate interactions, knockout of proteins identified in mice (dependent on viability) and finally, the identification and use of specific inhibitors that prevent the function of each of the proteins identified.

2. Proteinaceous constituents of SAF could be purified *ex vivo* or made into recombinant proteins, over-expressed and purified for the addition to the CFCA and the oligomerisation assay. Proteins such as Na^+/K^+ ATPase, synapsin-1, prolow density lipoprotein, Dmxl-2 and CNP1 have been shown to be integral parts of the amyloid fibril, as detected by tandem

MS/MS, and their activity on PrP during conversion or thermal refolding may show potential prion co-factor activity.

3. Application of systems biology models to further understand how each of the proteins identified by mass spectrometry interact with each other and to elucidate commonalities and differences in different strains of mouse scrapie.

4. The 79A-seeded CFCA showed that the Golgi body enriched fractions from the SMB-PS cell line increased 79A conversion efficiency. It would be useful to determine whether these fractions also increased ME7 conversion efficiency to determine whether the effect was strain or cell-line specific.

5. To further fractionate plasma membrane and Golgi body-enriched fractions to attempt to isolate the molecules that enhance conversion in the CFCA. This could be done, firstly, by the application of different OptiPrep™ gradients to sub-fractionate specific organelles and, secondly, by size exclusion chromatography to separate different molecules by their molecular weight.

6. To further define the different PrP isoforms in the oligomerisation assay when including or excluding low density subcellular fractions. Properties such as secondary structure could be analysed by circular dichroism or FT-IR and resistance to protease digestion could be measured by Western blotting after incubation with PK.

7. To diversify CFCA experiments to include subcellular fractions from other TSE susceptible cell lines and seed these assays with other mouse scrapie strains. To elucidate whether plasma membrane fractions from the LD9 cell line enhances conversion with other stains of mouse scrapie. In addition, it would also be useful to see if other TSE susceptible cell lines have different localisations of conversion enhancing factors and what effect these factors have on the oligomerisation of rPrP.

8. Appendix

A SMB-PS

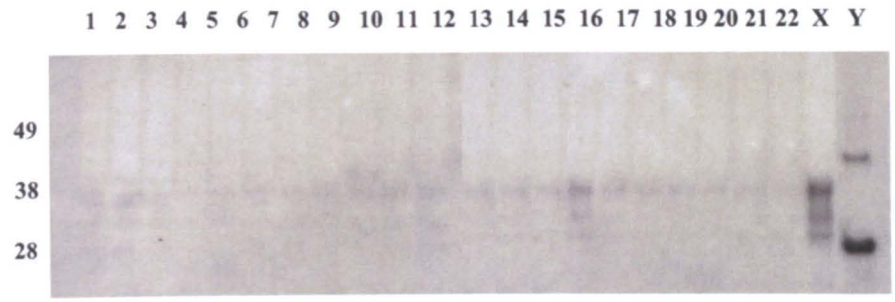

B LD9

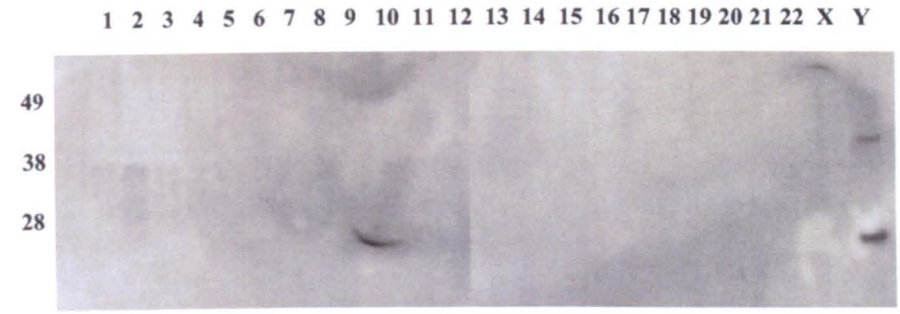

Appendix 1: Western blot analysis of SMB-PS and LD9 subcellular fractionation for endogenous PrP^C.

Subcellular fractions (1-22) were prepared as outlined in section 3.6 for (A.) SMB-PS cell line and (B.) LD9 cell line. Fractions were separated by SDS PAGE and assessed by Western blotting using the anti-PrP antibody 8H4 to show the distribution of PrP throughout each cell line. Lanes indicted as X and Y are of cell homogenate and 20 ng $rMoPrP^{WT}$, respectively. SMB-PS and LD9 subcellular fractionation shows that PrP^C is detected at very low concentrations throughout the subcellular fractionation as determined by the 27 kDa band of $rMoPrP^{WT}$ in lane Y. Molecular weight (kDa) is shown on the left hand side of each Western blot.

9. Bibliography

Adjou, K. T., Simoneau, S., Sales, N., Lamoury, F., Dormont, D., Papy-Garcia, D., Barritault, D., Deslys, J. P. and Lasmezas, C. I. (2003). A novel generation of heparan sulfate mimetics for the treatment of prion diseases. *J Gen Virol* **84**, 2595-603.

Adler, V., Zeiler, B., Kryukov, V., Kascsak, R., Rubenstein, R. and Grossman, A. (2003). Small, highly structured RNAs participate in the conversion of human recombinant PrP(Sen) to PrP(Res) in vitro. *J Mol Biol* **332**, 47-57.

Aguzzi, A., Sigurdson, C. and Heikenwaelder, M. (2008). Molecular mechanisms of prion pathogenesis. *Annu Rev Pathol* **3**, 11-40.

Aguzzi, A., Sigurdson, C. and Heikenwalder, M. (2007). Molecular Mechanisms of Prion Pathogenesis. *Annu Rev Pathol.*

Alper, T., Cramp, W. A., Haig, D. A. and Clarke, M. C. (1967). Does the agent of scrapie replicate without nucleic acid? *Nature* **214**, 764-6.

Alper, T., Haig, D. A. and Clarke, M. C. (1966). The exceptionally small size of the scrapie agent. *Biochem Biophys Res Commun* **22**, 278-84.

Angers, R. C., Browning, S. R., Seward, T. S., Sigurdson, C. J., Miller, M. W., Hoover, E. A. and Telling, G. C. (2006). Prions in skeletal muscles of deer with chronic wasting disease. *Science* **311**, 1117.

Appel, T. R., Dumpitak, C., Matthiesen, U. and Riesner, D. (1999). Prion rods contain an inert polysaccharide scaffold. *Biol Chem* **380**, 1295-306.

Atarashi, R., Nishida, N., Shigematsu, K., Goto, S., Kondo, T., Sakaguchi, S. and Katamine, S. (2003). Deletion of N-terminal residues 23-88 from prion protein (PrP) abrogates the potential to rescue PrP-deficient mice from PrP-like protein/doppel-induced Neurodegeneration. *J Biol Chem* **278**, 28944-9.

Atarashi, R., Wilham, J. M., Christensen, L., Hughson, A. G., Moore, R. A., Johnson, L. M., Onwubiko, H. A., Priola, S. A. and Caughey, B. (2008). Simplified ultrasensitive prion detection by recombinant PrP conversion with shaking. *Nat Methods* **5**, 211-2.

Barwise, J. L. and Walker, J. H. (1996). Annexins II, IV, V and VI relocate in response to rises in intracellular calcium in human foreskin fibroblasts. *J Cell Sci* **109 (Pt 1)**, 247-55.

Baskakov, I., Disterer, P., Breydo, L., Shaw, M., Gill, A., James, W. and Tahiri-Alaoui, A. (2005). The presence of valine at residue 129 in human prion protein accelerates amyloid formation. *FEBS Lett* **579**, 2589-96.

Baskakov, I. V. and Bocharova, O. V. (2005). In vitro conversion of mammalian prion protein into amyloid fibrils displays unusual features. *Biochemistry* **44**, 2339-48.

Baskakov, I. V., Legname, G., Baldwin, M. A., Prusiner, S. B. and Cohen, F. E. (2002). Pathway complexity of prion protein assembly into amyloid. *J Biol Chem* **277**, 21140-8.

Baskakov, I. V., Legname, G., Prusiner, S. B. and Cohen, F. E. (2001). Folding of prion protein to its native alpha-helical conformation is under kinetic control. *J Biol Chem* **276**, 19687-90.

Baylis, M. and Goldmann, W. (2004). The genetics of scrapie in sheep and goats. *Curr Mol Med* **4**, 385-96.

Behrens, A. and Aguzzi, A. (2002). Small is not beautiful: antagonizing functions for the prion protein PrP(C) and its homologue Dpl. *Trends Neurosci* **25**, 150-4.

Benestad, S. L., Arsac, J. N., Goldmann, W. and Noremark, M. (2008). Atypical/Nor98 scrapie: properties of the agent, genetics, and epidemiology. *Vet Res* **39**, 19.

Benestad, S. L., Sarradin, P., Thu, B., Schonheit, J., Tranulis, M. A. and Bratberg, B. (2003). Cases of scrapie with unusual features in Norway and designation of a new type, Nor98. *Vet Rec* **153**, 202-8.

Ben-Zaken, O., Tzaban, S., Tal, Y., Horonchik, L., Esko, J. D., Vlodavsky, I. and Taraboulos, A. (2003). Cellular heparan sulfate participates in the metabolism of prions. *J Biol Chem* **278**, 40041-9.

Beranger, F., Mange, A., Goud, B. and Lehmann, S. (2002). Stimulation of PrP(C) retrograde transport toward the endoplasmic reticulum increases accumulation of PrP(Sc) in prion-infected cells. *J Biol Chem* **277**, 38972-7.

Beranger, F., Mange, A., Solassol, J. and Lehmann, S. (2001). Cell culture models of transmissible spongiform encephalopathies. *Biochem Biophys Res Commun* **289**, 311-6.

Bessen, R. A., Kocisko, D. A., Raymond, G. J., Nandan, S., Lansbury, P. T. and Caughey, B. (1995). Non-genetic propagation of strain-specific properties of scrapie prion protein. *Nature* **375**, 698-700.

Bessen, R. A. and Marsh, R. F. (1992). Biochemical and physical properties of the prion protein from two strains of the transmissible mink encephalopathy agent. *J Virol* **66**, 2096-101.

Bessen, R. A. and Marsh, R. F. (1994). Distinct PrP properties suggest the molecular basis of strain variation in transmissible mink encephalopathy. *J Virol* **68**, 7859-68.

Biacabe, A. G., Laplanche, J. L., Ryder, S. and Baron, T. (2004). Distinct molecular phenotypes in bovine prion diseases. *EMBO Rep* **5**, 110-5.

Bifulco, M., Laezza, C., Stingo, S. and Wolff, J. (2002). 2',3'-Cyclic nucleotide 3'-phosphodiesterase: a membrane-bound, microtubule-associated protein and membrane anchor for tubulin. *Proc Natl Acad Sci U S A* **99**, 1807-12.

Birkett, C. R., Hennion, R. M., Bembridge, D. A., Clarke, M. C., Chree, A., Bruce, M. E. and Bostock, C. J. (2001). Scrapie strains maintain biological phenotypes on propagation in a cell line in culture. *Embo J* **20**, 3351-8.

Blanco, G. and Mercer, R. W. (1998). Isozymes of the Na-K-ATPase: heterogeneity in structure, diversity in function. *Am J Physiol* **275**, F633-50.

Bolton, D. C., McKinley, M. P. and Prusiner, S. B. (1982). Identification of a protein that purifies with the scrapie prion. *Science* **218**, 1309-11.

Borchelt, D. R., Taraboulos, A. and Prusiner, S. B. (1992). Evidence for synthesis of scrapie prion proteins in the endocytic pathway. *J Biol Chem* **267**, 16188-99.

Bossers, A., Belt, P., Raymond, G. J., Caughey, B., de Vries, R. and Smits, M. A. (1997). Scrapie susceptibility-linked polymorphisms modulate the in vitro conversion of sheep prion protein to protease-resistant forms. *Proc Natl Acad Sci U S A* **94**, 4931-6.

Bossers, A., de Vries, R. and Smits, M. A. (2000). Susceptibility of sheep for scrapie as assessed by in vitro conversion of nine naturally occurring variants of PrP. *J Virol* **74**, 1407-14.

Brown, D. R., Clive, C. and Haswell, S. J. (2001). Antioxidant activity related to copper binding of native prion protein. *J Neurochem* **76**, 69-76.

Brown, D. R., Schulz-Schaeffer, W. J., Schmidt, B. and Kretzschmar, H. A. (1997). Prion protein-deficient cells show altered response to oxidative stress due to decreased SOD-1 activity. *Exp Neurol* **146**, 104-12.

Brown, P., Cervenakova, L., Boellaard, J. W., Stavrou, D., Goldfarb, L. G. and Gajdusek, D. C. (1994). Identification of a PRNP gene mutation in Jakob's original Creutzfeldt-Jakob disease family. *Lancet* **344**, 130-1.

Bruce, M., Chree, A., McConnell, I., Foster, J., Pearson, G. and Fraser, H. (1994). Transmission of bovine spongiform encephalopathy and scrapie to mice: strain variation and the species barrier. *Philos Trans R Soc Lond B Biol Sci* **343**, 405-11.

Bruce, M. E. (1993). Scrapie strain variation and mutation. *Br Med Bull* **49**, 822-38.

Bruce, M. E. and Fraser, H. (1991). Scrapie strain variation and its implications. *Curr Top Microbiol Immunol* **172**, 125-38.

Bruce, M. E., McBride, P. A. and Farquhar, C. F. (1989). Precise targeting of the pathology of the sialoglycoprotein, PrP, and vacuolar degeneration in mouse scrapie. *Neurosci Lett* **102**, 1-6.

Bruce, M. E., McConnell, I., Fraser, H. and Dickinson, A. G. (1991). The disease characteristics of different strains of scrapie in Sinc congenic mouse lines: implications for the nature of the agent and host control of pathogenesis. *J Gen Virol* **72 (Pt 3)**, 595-603.

Bruce, M. E., Will, R. G., Ironside, J. W., McConnell, I., Drummond, D., Suttie, A., McCardle, L., Chree, A., Hope, J., Birkett, C. et al. (1997). Transmissions to mice indicate that 'new variant' CJD is caused by the BSE agent. *Nature* **389**, 498-501.

Bucciantini, M., Giannoni, E., Chiti, F., Baroni, F., Formigli, L., Zurdo, J., Taddei, N., Ramponi, G., Dobson, C. M. and Stefani, M. (2002). Inherent toxicity of aggregates implies a common mechanism for protein misfolding diseases. *Nature* **416**, 507-11.

Budka, H. (1997). The human prion diseases: from neuropathology to pathobiology and molecular genetics. Final report of an EU concerted action. *Neuropathol Appl Neurobiol* **23**, 416-22.

Budka, H. (2003). Neuropathology of prion diseases. *Br Med Bull* **66**, 121-30.

Budka, H., Aguzzi, A., Brown, P., Brucher, J. M., Bugiani, O., Gullotta, F., Haltia, M., Hauw, J. J., Ironside, J. W., Jellinger, K. et al. (1995). Neuropathological diagnostic criteria for Creutzfeldt-Jakob disease (CJD) and other human spongiform encephalopathies (prion diseases). *Brain Pathol* **5**, 459-66.

Bueler, H., Aguzzi, A., Sailer, A., Greiner, R. A., Autenried, P., Aguet, M. and Weissmann, C. (1993). Mice devoid of PrP are resistant to scrapie. *Cell* **73**, 1339-47.

Calandriello, L., Curini, R., Pennisi, E. M. and Palladini, G. (1995). Spongy state (status spongiosus) and inhibition of Na,K-ATPase: a pathogenetic theory. *Med Hypotheses* **44**, 173-8.

Campana, V., Sarnataro, D. and Zurzolo, C. (2005). The highways and byways of prion protein trafficking. *Trends Cell Biol* **15**, 102-11.

Carlson, G. A., Kingsbury, D. T., Goodman, P. A., Coleman, S., Marshall, S. T., DeArmond, S., Westaway, D. and Prusiner, S. B. (1986). Linkage of prion protein and scrapie incubation time genes. *Cell* **46**, 503-11.

Carp, R. I. and Callahan, S. M. (1991). Variation in the characteristics of 10 mouse-passaged scrapie lines derived from five scrapie-positive sheep. *J Gen Virol* **72 (Pt 2)**, 293-8.

Casalone, C., Zanusso, G., Acutis, P., Ferrari, S., Capucci, L., Tagliavini, F., Monaco, S. and Caramelli, M. (2004). Identification of a second bovine amyloidotic spongiform encephalopathy: molecular similarities with sporadic Creutzfeldt-Jakob disease. *Proc Natl Acad Sci U S A* **101**, 3065-70.

Castilla, J., Gonzalez-Romero, D., Saa, P., Morales, R., De Castro, J. and Soto, C. (2008). Crossing the species barrier by PrP(Sc) replication in vitro generates unique infectious prions. *Cell* **134**, 757-68.

Castilla, J., Saa, P., Hetz, C. and Soto, C. (2005). In vitro generation of infectious scrapie prions. *Cell* **121**, 195-206.

Caughey, B. (2003). Prion protein conversions: insight into mechanisms, TSE transmission barriers and strains. *Br Med Bull* **66**, 109-20.

Caughey, B. and Lansbury, P. T. (2003). Protofibrils, pores, fibrils, and neurodegeneration: separating the responsible protein aggregates from the innocent bystanders. *Annu Rev Neurosci* **26**, 267-98.

Caughey, B. and Raymond, G. J. (1991). The scrapie-associated form of PrP is made from a cell surface precursor that is both protease- and phospholipase-sensitive. *J Biol Chem* **266**, 18217-23.

Caughey, B., Raymond, G. J., Ernst, D. and Race, R. E. (1991). N-terminal truncation of the scrapie-associated form of PrP by lysosomal protease(s): implications regarding the site of conversion of PrP to the protease-resistant state. *J Virol* **65**, 6597-603.

Caughey, B. W., Dong, A., Bhat, K. S., Ernst, D., Hayes, S. F. and Caughey, W. S. (1991). Secondary structure analysis of the scrapie-associated protein PrP 27-30 in water by infrared spectroscopy. *Biochemistry* **30**, 7672-80.

Chandler, R. L. (1961). Encephalopathy in mice produced by inoculation with scrapie brain material. *Lancet* **1**, 1378-9.

Chen, W. J., Goldstein, J. L. and Brown, M. S. (1990). NPXY, a sequence often found in cytoplasmic tails, is required for coated pit-mediated internalization of the low density lipoprotein receptor. *J Biol Chem* **265**, 3116-23.

Chessler, S. D. and Byers, P. H. (1993). BiP binds type I procollagen pro alpha chains with mutations in the carboxyl-terminal propeptide synthesized by cells from patients with osteogenesis imperfecta. *J Biol Chem* **268**, 18226-33.

Chien, P., Weissman, J. S. and DePace, A. H. (2004). Emerging principles of conformation-based prion inheritance. *Annu Rev Biochem* **73**, 617-56.

Chiesa, R. and Harris, D. A. (2000). Nerve growth factor-induced differentiation does not alter the biochemical properties of a mutant prion protein expressed in PC12 cells. *J Neurochem* **75**, 72-80.

Chiesa, R., Piccardo, P., Ghetti, B. and Harris, D. A. (1998). Neurological illness in transgenic mice expressing a prion protein with an insertional mutation. *Neuron* **21**, 1339-51.

Chiesa, R., Piccardo, P., Quaglio, E., Drisaldi, B., Si-Hoe, S. L., Takao, M., Ghetti, B. and Harris, D. A. (2003). Molecular distinction between pathogenic and infectious properties of the prion protein. *J Virol* **77**, 7611-22.

Clarke, M. C. and Haig, D. A. (1970). Evidence for the multiplication of scrapie agent in cell culture. *Nature* **225**, 100-1.

Clarke, M. C. and Millson, G. C. (1976). Infection of a cell line of mouse L fibroblasts with scrapie agent. *Nature* **261**, 144-5.

Collinge, J. (1999). Variant Creutzfeldt-Jakob disease. *Lancet* **354**, 317-23.

Collinge, J. (2001). Prion diseases of humans and animals: their causes and molecular basis. *Annu Rev Neurosci* **24**, 519-50.

Collinge, J., Palmer, M. S. and Dryden, A. J. (1991). Genetic predisposition to iatrogenic Creutzfeldt-Jakob disease. *Lancet* **337**, 1441-2.

Collinge, J., Sidle, K. C., Meads, J., Ironside, J. and Hill, A. F. (1996). Molecular analysis of prion strain variation and the aetiology of 'new variant' CJD. *Nature* **383**, 685-90.

Cordeiro, Y., Machado, F., Juliano, L., Juliano, M. A., Brentani, R. R., Foguel, D. and Silva, J. L. (2001). DNA converts cellular prion protein into the beta-sheet conformation and inhibits prion peptide aggregation. *J Biol Chem* **276**, 49400-9.

Courageot, M. P., Daude, N., Nonno, R., Paquet, S., Di Bari, M. A., Le Dur, A., Chapuis, J., Hill, A. F., Agrimi, U., Laude, H. et al. (2008). A cell line infectible by prion strains from different species. *J Gen Virol* **89**, 341-7.

Coustou, V., Deleu, C., Saupe, S. and Begueret, J. (1997). The protein product of the het-s heterokaryon incompatibility gene of the fungus Podospora anserina behaves as a prion analog. *Proc Natl Acad Sci U S A* **94**, 9773-8.

Critchley, P., Kazlauskaite, J., Eason, R. and Pinheiro, T. J. (2004). Binding of prion proteins to lipid membranes. *Biochem Biophys Res Commun* **313**, 559-67.

De Camilli, P., Benfenati, F., Valtorta, F. and Greengard, P. (1990). The synapsins. *Annu Rev Cell Biol* **6**, 433-60.

De Duve, C. and Wattiaux, R. (1966). Functions of lysosomes. *Annu Rev Physiol* **28**, 435-92.

DeArmond, S. J., McKinley, M. P., Barry, R. A., Braunfeld, M. B., McColloch, J. R. and Prusiner, S. B. (1985). Identification of prion amyloid filaments in scrapie-infected brain. *Cell* **41**, 221-35.

DeArmond, S. J., Mobley, W. C., DeMott, D. L., Barry, R. A., Beckstead, J. H. and Prusiner, S. B. (1987). Changes in the localization of brain prion proteins during scrapie infection. *Neurology* **37**, 1271-80.

DeArmond, S. J., Sanchez, H., Yehiely, F., Qiu, Y., Ninchak-Casey, A., Daggett, V., Camerino, A. P., Cayetano, J., Rogers, M., Groth, D. et al. (1997). Selective neuronal targeting in prion disease. *Neuron* **19**, 1337-48.

DebBurman, S. K., Raymond, G. J., Caughey, B. and Lindquist, S. (1997). Chaperone-supervised conversion of prion protein to its protease-resistant form. *Proc Natl Acad Sci U S A* **94**, 13938-43.

Deleault, N. R., Geoghegan, J. C., Nishina, K., Kascsak, R., Williamson, R. A. and Supattapone, S. (2005). Protease-resistant prion protein amplification reconstituted with partially purified substrates and synthetic polyanions. *J Biol Chem* **280**, 26873-9.

Deleault, N. R., Harris, B. T., Rees, J. R. and Supattapone, S. (2007). Formation of native prions from minimal components in vitro. *Proc Natl Acad Sci U S A* **104**, 9741-6.

Deleault, N. R., Lucassen, R. W. and Supattapone, S. (2003). RNA molecules stimulate prion protein conversion. *Nature* **425**, 717-20.

Deneka, M. and van der Sluijs, P. (2002). 'Rab'ing up endosomal membrane transport. *Nat Cell Biol* **4**, E33-5.

Derkatch, I. L., Chernoff, Y. O., Kushnirov, V. V., Inge-Vechtomov, S. G. and Liebman, S. W. (1996). Genesis and variability of [PSI] prion factors in Saccharomyces cerevisiae. *Genetics* **144**, 1375-86.

Dickinson, A. G. and Meikle, V. M. (1971). Host-genotype and agent effects in scrapie incubation: change in allelic interaction with different strains of agent. *Mol Gen Genet* **112**, 73-9.

Dickinson, A. G., Meikle, V. M. and Fraser, H. (1968). Identification of a gene which controls the incubation period of some strains of scrapie agent in mice. *J Comp Pathol* **78**, 293-9.

Dickinson, A. G., Stamp, J. T., Renwick, C. C. and Rennie, J. C. (1968). Some factors controlling the incidence of scrapie in Cheviot sheep injected with a Cheviot-passaged scrapie agent. *J Comp Pathol* **78**, 313-21.

Djukic, M., Mildner, A., Schmidt, H., Czesnik, D., Bruck, W., Priller, J., Nau, R. and Prinz, M. (2006). Circulating monocytes engraft in the brain, differentiate into microglia and contribute to the pathology following meningitis in mice. *Brain* **129**, 2394-403.

Dlakic, W. M., Grigg, E. and Bessen, R. A. (2007). Prion infection of muscle cells in vitro. *J Virol* **81**, 4615-24.

Dumpitak, C., Beekes, M., Weinmann, N., Metzger, S., Winklhofer, K. F., Tatzelt, J. and Riesner, D. (2005). The polysaccharide scaffold of PrP 27-30 is a common compound of natural prions and consists of alpha-linked polyglucose. *Biol Chem* **386**, 1149-55.

Eberhard, D. A., Brown, M. D. and VandenBerg, S. R. (1994). Alterations of annexin expression in pathological neuronal and glial reactions. Immunohistochemical localization of annexins I, II (p36 and p11 subunits), IV, and VI in the human hippocampus. *Am J Pathol* **145**, 640-9.

Eghiaian, F., Daubenfeld, T., Quenet, Y., van Audenhaege, M., Bouin, A. P., van der Rest, G., Grosclaude, J. and Rezaei, H. (2007). Diversity in prion protein oligomerization pathways results from domain expansion as revealed by hydrogen/deuterium exchange and disulfide linkage. *Proc Natl Acad Sci U S A* **104**, 7414-9.

Eiden, M., Palm, G. J., Hinrichs, W., Matthey, U., Zahn, R. and Groschup, M. H. (2006). Synergistic and strain-specific effects of bovine spongiform encephalopathy and scrapie prions in the cell-free conversion of recombinant prion protein. *J Gen Virol* **87**, 3753-61.

Follet, J., Lemaire-Vieille, C., Blanquet-Grossard, F., Podevin-Dimster, V., Lehmann, S., Chauvin, J. P., Decavel, J. P., Varea, R., Grassi, J., Fontes, M. et al. (2002). PrP expression and replication by Schwann cells: implications in prion spreading. *J Virol* **76**, 2434-9.

Foster, J. D., Parnham, D., Chong, A., Goldmann, W. and Hunter, N. (2001). Clinical signs, histopathology and genetics of experimental transmission of BSE and natural scrapie to sheep and goats. *Vet Rec* **148**, 165-71.

Fournier, J. G., Escaig-Haye, F., Billette de Villemeur, T. and Robain, O. (1995). Ultrastructural localization of cellular prion protein (PrPc) in synaptic boutons of normal hamster hippocampus. *C R Acad Sci III* **318**, 339-44.

Fraser, H. (1993). Diversity in the neuropathology of scrapie-like diseases in animals. *Br Med Bull* **49**, 792-809.

Fraser, H. and Dickinson, A. G. (1968). The sequential development of the brain lesion of scrapie in three strains of mice. *J Comp Pathol* **78**, 301-11.

Gambetti, P., Kong, Q., Zou, W., Parchi, P. and Chen, S. G. (2003). Sporadic and familial CJD: classification and characterisation. *Br Med Bull* **66**, 213-39.

Gauczynski, S., Nikles, D., El-Gogo, S., Papy-Garcia, D., Rey, C., Alban, S., Barritault, D., Lasmezas, C. I. and Weiss, S. (2006). The 37-kDa/67-kDa laminin receptor acts as a receptor for infectious prions and is inhibited by polysulfated glycanes. *J Infect Dis* **194**, 702-9.

Gauczynski, S., Peyrin, J. M., Haik, S., Leucht, C., Hundt, C., Rieger, R., Krasemann, S., Deslys, J. P., Dormont, D., Lasmezas, C. I. et al. (2001). The 37-kDa/67-kDa laminin receptor acts as the cell-surface receptor for the cellular prion protein. *Embo J* **20**, 5863-75.

Ghetti, B., Piccardo, P., Spillantini, M. G., Ichimiya, Y., Porro, M., Perini, F., Kitamoto, T., Tateishi, J., Seiler, C., Frangione, B. et al. (1996). Vascular variant of prion protein cerebral amyloidosis with tau-positive neurofibrillary tangles: the phenotype of the stop codon 145 mutation in PRNP. *Proc Natl Acad Sci U S A* **93**, 744-8.

Giorgi, A., Di Francesco, L., Principe, S., Mignogna, G., Sennels, L., Mancone, C., Alonzi, T., Sbriccoli, M., De Pascalis, A., Rappsilber, J. et al. (2009). Proteomic profiling of PrP27-30-enriched preparations extracted from the brain of hamsters with experimental scrapie. *Proteomics* **9**, 3802-14.

Goldmann, W., Houston, F., Stewart, P., Perucchini, M., Foster, J. and Hunter, N. (2006). Ovine prion protein variant A(136)R(154)L(168)Q(171) increases resistance to experimental challenge with bovine spongiform encephalopathy agent. *J Gen Virol* **87**, 3741-5.

Goldmann, W., Hunter, N., Benson, G., Foster, J. D. and Hope, J. (1991). Different scrapie-associated fibril proteins (PrP) are encoded by lines of sheep selected for different alleles of the Sip gene. *J Gen Virol* **72 (Pt 10)**, 2411-7.

Goldmann, W., Hunter, N., Smith, G., Foster, J. and Hope, J. (1994). PrP genotype and agent effects in scrapie: change in allelic interaction with different isolates of agent in sheep, a natural host of scrapie. *J Gen Virol* **75 (Pt 5)**, 989-95.

Goldstein, J. L., Brown, M. S., Anderson, R. G., Russell, D. W. and Schneider, W. J. (1985). Receptor-mediated endocytosis: concepts emerging from the LDL receptor system. *Annu Rev Cell Biol* **1**, 1-39.

Gonzalez, L., Martin, S. and Jeffrey, M. (2003). Distinct profiles of PrP(d) immunoreactivity in the brain of scrapie- and BSE-infected sheep: implications for differential cell targeting and PrP processing. *J Gen Virol* **84**, 1339-50.

Graham, J. M. and Rickwood, D. (1996) Subcellular Fractionation: A Practical Approach. In *The Practical Approach Series*, 1st edn, pp. 1-29. Edited by D. Rickwood and B.D. Hames. Oxford: Oxford University Press.

Gregori, L., McCombie, N., Palmer, D., Birch, P., Sowemimo-Coker, S. O., Giulivi, A. and Rohwer, R. G. (2004). Effectiveness of leucoreduction for removal of infectivity of transmissible spongiform encephalopathies from blood. *Lancet* **364**, 529-31.

Greil, C. S., Vorberg, I. M., Ward, A. E., Meade-White, K. D., Harris, D. A. and Priola, S. A. (2008). Acute cellular uptake of abnormal prion protein is cell type and scrapie-strain independent. *Virology* **379**, 284-93.

Griffith, J. S. (1967). Self-replication and scrapie. *Nature* **215**, 1043-4.

Grigoriev, V., Escaig-Haye, F., Streichenberger, N., Kopp, N., Langeveld, J., Brown, P. and Fournier, J. G. (1999). Submicroscopic immunodetection of PrP in the brain of a patient with a new-variant of Creutzfeldt-Jakob disease. *Neurosci Lett* **264**, 57-60.

Gruenberg, J. (2001). The endocytic pathway: a mosaic of domains. *Nat Rev Mol Cell Biol* **2**, 721-30.

Gruetter, R. (2003). Glycogen: the forgotten cerebral energy store. *J Neurosci Res* **74**, 179-83.

Grus, W. E., Shi, P. and Zhang, J. (2007). Largest vertebrate vomeronasal type 1 receptor gene repertoire in the semiaquatic platypus. *Mol Biol Evol* **24**, 2153-7.

Hadlow, W. J. (1959). Myopathies of livestock. *Lab Invest* **8**, 1478-98.

Haire, L. F., Whyte, S. M., Vasisht, N., Gill, A. C., Verma, C., Dodson, E. J., Dodson, G. G. and Bayley, P. M. (2004). The crystal structure of the globular domain of sheep prion protein. *J Mol Biol* **336**, 1175-83.

Hanson, R. P., Eckroade, R. J., Marsh, R. F., Zu Rhein, G. M., Kanitz, C. L. and Gustafson, D. P. (1971). Susceptibility of mink to sheep scrapie. *Science* **172**, 859-61.

Harris, D. A. (2003). Trafficking, turnover and membrane topology of PrP. *Br Med Bull* **66**, 71-85.

Harrison, P. M., Chan, H. S., Prusiner, S. B. and Cohen, F. E. (1999). Thermodynamics of model prions and its implications for the problem of prion protein folding. *J Mol Biol* **286**, 593-606.

Hasan, M. R., Koikawa, S., Kotani, S., Miyamoto, S. and Nakagawa, H. (2006). Ferritin forms dynamic oligomers to associate with microtubules in vivo: implication for the role of microtubules in iron metabolism. *Exp Cell Res* **312**, 1950-60.

Herms, J., Tings, T., Gall, S., Madlung, A., Giese, A., Siebert, H., Schurmann, P., Windl, O., Brose, N. and Kretzschmar, H. (1999). Evidence of presynaptic location and function of the prion protein. *J Neurosci* **19**, 8866-75.

Herz, J., Clouthier, D. E. and Hammer, R. E. (1992). LDL receptor-related protein internalizes and degrades uPA-PAI-1 complexes and is essential for embryo implantation. *Cell* **71**, 411-21.

Hijazi, N., Kariv-Inbal, Z., Gasset, M. and Gabizon, R. (2005). PrPSc incorporation to cells requires endogenous glycosaminoglycan expression. *J Biol Chem* **280**, 17057-61.

Hill, A. F. and Collinge, J. (2003). Subclinical prion infection. *Trends Microbiol* **11**, 578-84.

Holz, A., Bielekova, B., Martin, R. and Oldstone, M. B. (2000). Myelin-associated oligodendrocytic basic protein: identification of an encephalitogenic epitope and association with multiple sclerosis. *J Immunol* **164**, 1103-9.

Hope, J., Morton, L. J., Farquhar, C. F., Multhaup, G., Beyreuther, K. and Kimberlin, R. H. (1986). The major polypeptide of scrapie-associated fibrils (SAF) has the same size, charge distribution and N-terminal protein sequence as predicted for the normal brain protein (PrP). *Embo J* **5**, 2591-7.

Horiuchi, H., Lippe, R., McBride, H. M., Rubino, M., Woodman, P., Stenmark, H., Rybin, V., Wilm, M., Ashman, K., Mann, M. et al. (1997). A novel Rab5 GDP/GTP exchange factor complexed to Rabaptin-5 links nucleotide exchange to effector recruitment and function. *Cell* **90**, 1149-59.

Horiuchi, M., Priola, S. A., Chabry, J. and Caughey, B. (2000). Interactions between heterologous forms of prion protein: binding, inhibition of conversion, and species barriers. *Proc Natl Acad Sci U S A* **97**, 5836-41.

Hornemann, S., Schorn, C. and Wuthrich, K. (2004). NMR structure of the bovine prion protein isolated from healthy calf brains. *EMBO Rep* **5**, 1159-64.

Horonchik, L., Tzaban, S., Ben-Zaken, O., Yedidia, Y., Rouvinski, A., Papy-Garcia, D., Barritault, D., Vlodavsky, I. and Taraboulos, A. (2005). Heparan sulfate is a cellular receptor for purified infectious prions. *J Biol Chem* **280**, 17062-7.

Horwich, A. L. and Weissman, J. S. (1997). Deadly conformations--protein misfolding in prion disease. *Cell* **89**, 499-510.

Houston, F., Foster, J. D., Chong, A., Hunter, N. and Bostock, C. J. (2000). Transmission of BSE by blood transfusion in sheep. *Lancet* **356**, 999-1000.

Houston, F., McCutcheon, S., Goldmann, W., Chong, A., Foster, J., Siso, S., Gonzalez, L., Jeffrey, M. and Hunter, N. (2008). Prion diseases are efficiently transmitted by blood transfusion in sheep. *Blood* **112**, 4739-45.

Howell, K. E., Gruenberg, J., Ito, A. and Palade, G. E. (1988). Immuno-isolation of subcellular components. *Prog Clin Biol Res* **270**, 77-90.

Howell, K. E., Schmid, R., Ugelstad, J. and Gruenberg, J. (1989). Immunoisolation using magnetic solid supports: subcellular fractionation for cell-free functional studies. *Methods Cell Biol* **31**, 265-92.

Hunter, N., Foster, J., Chong, A., McCutcheon, S., Parnham, D., Eaton, S., MacKenzie, C. and Houston, F. (2002). Transmission of prion diseases by blood transfusion. *J Gen Virol* **83**, 2897-905.

Iniguez, V., McKenzie, D., Mirwald, J. and Aiken, J. (2000). Strain-specific propagation of PrP(Sc) properties into baculovirus-expressed hamster PrP(C). *J Gen Virol* **81**, 2565-71.

Jackson, G. S., Hill, A. F., Joseph, C., Hosszu, L., Power, A., Waltho, J. P., Clarke, A. R. and Collinge, J. (1999). Multiple folding pathways for heterologously expressed human prion protein. *Biochim Biophys Acta* **1431**, 1-13.

Jeffrey, M., Goodsir, C. M., Bruce, M., McBride, P. A., Scott, J. R. and Halliday, W. G. (1994). Correlative light and electron microscopy studies of PrP localisation in 87V scrapie. *Brain Res* **656**, 329-43.

Jeffrey, M., Goodsir, C. M., Bruce, M. E., McBride, P. A., Scott, J. R. and Halliday, W. G. (1992). Infection specific prion protein (PrP) accumulates on neuronal plasmalemma in scrapie infected mice. *Neurosci Lett* **147**, 106-9.

Jeffrey, M., McGovern, G., Goodsir, C. M., Siso, S. and Gonzalez, L. (2009). Strain-associated variations in abnormal PrP trafficking of sheep scrapie. *Brain Pathol* **19**, 1-11.

Jewell, J. E., Conner, M. M., Wolfe, L. L., Miller, M. W. and Williams, E. S. (2005). Low frequency of PrP genotype 225SF among free-ranging mule deer (Odocoileus hemionus) with chronic wasting disease. *J Gen Virol* **86**, 2127-34.

Jin, T., Gu, Y., Zanusso, G., Sy, M., Kumar, A., Cohen, M., Gambetti, P. and Singh, N. (2000). The chaperone protein BiP binds to a mutant prion protein and mediates its degradation by the proteasome. *J Biol Chem* **275**, 38699-704.

Johnson, C., Johnson, J., Vanderloo, J. P., Keane, D., Aiken, J. M. and McKenzie, D. (2006). Prion protein polymorphisms in white-tailed deer influence susceptibility to chronic wasting disease. *J Gen Virol* **87**, 2109-14.

Jones, E. M. and Surewicz, W. K. (2005). Fibril conformation as the basis of species- and strain-dependent seeding specificity of mammalian prion amyloids. *Cell* **121**, 63-72.

Juling, K., Schwarzenbacher, H., Williams, J. L. and Fries, R. (2006). A major genetic component of BSE susceptibility. *BMC Biol* **4**, 33.

Kakimura, J., Kitamura, Y., Taniguchi, T., Shimohama, S. and Gebicke-Haerter, P. J. (2001). Bip/GRP78-induced production of cytokines and uptake of amyloid-beta(1-42) peptide in microglia. *Biochem Biophys Res Commun* **281**, 6-10.

Kaneko, K. (2002). [Prion disease and its therapeutic approaches: bovine spongiform encephalopathy (BSE) and variant CJD]. *Nippon Ronen Igakkai Zasshi* **39**, 489-93.

Kaneko, K., Vey, M., Scott, M., Pilkuhn, S., Cohen, F. E. and Prusiner, S. B. (1997). COOH-terminal sequence of the cellular prion protein directs subcellular trafficking and controls conversion into the scrapie isoform. *Proc Natl Acad Sci U S A* **94**, 2333-8.

Kanu, N., Imokawa, Y., Drechsel, D. N., Williamson, R. A., Birkett, C. R., Bostock, C. J. and Brockes, J. P. (2002). Transfer of scrapie prion infectivity by cell contact in culture. *Curr Biol* **12**, 523-30.

Kascsak, R. J., Rubenstein, R., Merz, P. A., Carp, R. I., Wisniewski, H. M. and Diringer, H. (1985). Biochemical differences among scrapie-associated fibrils support the biological diversity of scrapie agents. *J Gen Virol* **66 (Pt 8)**, 1715-22.

Kascsak, R. J., Rubenstein, R., Merz, P. A., Tonna-DeMasi, M., Fersko, R., Carp, R. I., Wisniewski, H. M. and Diringer, H. (1987). Mouse polyclonal and monoclonal antibody to scrapie-associated fibril proteins. *J Virol* **61**, 3688-93.

Kayed, R., Head, E., Thompson, J. L., McIntire, T. M., Milton, S. C., Cotman, C. W. and Glabe, C. G. (2003). Common structure of soluble amyloid oligomers implies common mechanism of pathogenesis. *Science* **300**, 486-9.

Kazlauskaite, J., Sanghera, N., Sylvester, I., Venien-Bryan, C. and Pinheiro, T. J. (2003). Structural changes of the prion protein in lipid membranes leading to aggregation and fibrillization. *Biochemistry* **42**, 3295-304.

Kimberlin, R. H. and Walker, C. A. (1978). Evidence that the transmission of one source of scrapie agent to hamsters involves separation of agent strains from a mixture. *J Gen Virol* **39**, 487-96.

Kirby, L., Birkett, C. R., Rudyk, H., Gilbert, I. H. and Hope, J. (2003). In vitro cell-free conversion of bacterial recombinant PrP to PrPres as a model for conversion. *J Gen Virol* **84**, 1013-20.

Kirby, L., Goldmann, W., Houston, F., Gill, A. C. and Manson, J. C. (2006). A novel, resistance-linked ovine PrP variant and its equivalent mouse variant modulate the in vitro cell-free conversion of rPrP to PrP(res). *J Gen Virol* **87**, 3747-51.

Kitajima, T. S., Sakuno, T., Ishiguro, K., Iemura, S., Natsume, T., Kawashima, S. A. and Watanabe, Y. (2006). Shugoshin collaborates with protein phosphatase 2A to protect cohesin. *Nature* **441**, 46-52.

Kitamoto, T. and Tateishi, J. (1994). Human prion diseases with variant prion protein. *Philos Trans R Soc Lond B Biol Sci* **343**, 391-8.

Klamt, F., Dal-Pizzol, F., Conte da Frota, M. J., Walz, R., Andrades, M. E., da Silva, E. G., Brentani, R. R., Izquierdo, I. and Fonseca Moreira, J. C. (2001). Imbalance of antioxidant defense in mice lacking cellular prion protein. *Free Radic Biol Med* **30**, 1137-44.

Knaus, K. J., Morillas, M., Swietnicki, W., Malone, M., Surewicz, W. K. and Yee, V. C. (2001). Crystal structure of the human prion protein reveals a mechanism for oligomerization. *Nat Struct Biol* **8**, 770-4.

Kocisko, D. A., Come, J. H., Priola, S. A., Chesebro, B., Raymond, G. J., Lansbury, P. T. and Caughey, B. (1994). Cell-free formation of protease-resistant prion protein. *Nature* **370**, 471-4.

Kocisko, D. A., Engel, A. L., Harbuck, K., Arnold, K. M., Olsen, E. A., Raymond, L. D., Vilette, D. and Caughey, B. (2005). Comparison of protease-resistant prion protein inhibitors in cell cultures infected with two strains of mouse and sheep scrapie. *Neurosci Lett* **388**, 106-11.

Kocisko, D. A., Priola, S. A., Raymond, G. J., Chesebro, B., Lansbury, P. T., Jr. and Caughey, B. (1995). Species specificity in the cell-free conversion of prion protein to protease-resistant forms: a model for the scrapie species barrier. *Proc Natl Acad Sci U S A* **92**, 3923-7.

Korth, C., Kaneko, K. and Prusiner, S. B. (2000). Expression of unglycosylated mutated prion protein facilitates PrP(Sc) formation in neuroblastoma cells infected with different prion strains. *J Gen Virol* **81**, 2555-63.

Kovacs, G. G., Preusser, M., Strohschneider, M. and Budka, H. (2005). Subcellular localization of disease-associated prion protein in the human brain. *Am J Pathol* **166**, 287-94.

Kristensen, T., Moestrup, S. K., Gliemann, J., Bendtsen, L., Sand, O. and Sottrup-Jensen, L. (1990). Evidence that the newly cloned low-density-lipoprotein receptor related protein (LRP) is the alpha 2-macroglobulin receptor. *FEBS Lett* **276**, 151-5.

Kuczius, T., Haist, I. and Groschup, M. H. (1998). Molecular analysis of bovine spongiform encephalopathy and scrapie strain variation. *J Infect Dis* **178**, 693-9.

Kursula, P. (2008). Structural properties of proteins specific to the myelin sheath. *Amino Acids* **34**, 175-85.

Kuwahara, C., Takeuchi, A. M., Nishimura, T., Haraguchi, K., Kubosaki, A., Matsumoto, Y., Saeki, K., Matsumoto, Y., Yokoyama, T., Itohara, S. et al. (1999). Prions prevent neuronal cell-line death. *Nature* **400**, 225-6.

Ladogana, A., Liu, Q., Xi, Y. G. and Pocchiari, M. (1995). Proteinase-resistant protein in human neuroblastoma cells infected with brain material from Creutzfeldt-Jakob patient. *Lancet* **345**, 594-5.

Lashuel, H. A., Hartley, D., Petre, B. M., Walz, T. and Lansbury, P. T., Jr. (2002). Neurodegenerative disease: amyloid pores from pathogenic mutations. *Nature* **418**, 291.

Laszlo, A., Moros, E. G., Davidson, T., Bradbury, M., Straube, W. and Roti Roti, J. (2005). The heat-shock factor is not activated in mammalian cells exposed to cellular phone frequency microwaves. *Radiat Res* **164**, 163-72.

Lee, K. S., Linden, R., Prado, M. A., Brentani, R. R. and Martins, V. R. (2003). Towards cellular receptors for prions. *Rev Med Virol* **13**, 399-408.

Legname, G., Baskakov, I. V., Nguyen, H. O., Riesner, D., Cohen, F. E., DeArmond, S. J. and Prusiner, S. B. (2004). Synthetic mammalian prions. *Science* **305**, 673-6.

Legname, G., Nguyen, H. O., Baskakov, I. V., Cohen, F. E., Dearmond, S. J. and Prusiner, S. B. (2005). Strain-specified characteristics of mouse synthetic prions. *Proc Natl Acad Sci U S A* **102**, 2168-73.

Lehmann, S. and Harris, D. A. (1996). Two mutant prion proteins expressed in cultured cells acquire biochemical properties reminiscent of the scrapie isoform. *Proc Natl Acad Sci U S A* **93**, 5610-4.

Leucht, C., Simoneau, S., Rey, C., Vana, K., Rieger, R., Lasmezas, C. I. and Weiss, S. (2003). The 37 kDa/67 kDa laminin receptor is required for PrP(Sc) propagation in scrapie-infected neuronal cells. *EMBO Rep* **4**, 290-5.

Lisman, J. (1994). The CaM kinase II hypothesis for the storage of synaptic memory. *Trends Neurosci* **17**, 406-12.

Lopez Garcia, F., Zahn, R., Riek, R. and Wuthrich, K. (2000). NMR structure of the bovine prion protein. *Proc Natl Acad Sci U S A* **97**, 8334-9.

Lu, B. Y. and Chang, J. Y. (2001). Isolation of isoforms of mouse prion protein with PrP(SC)-like structural properties. *Biochemistry* **40**, 13390-6.

Lue, L. F., Kuo, Y. M., Roher, A. E., Brachova, L., Shen, Y., Sue, L., Beach, T., Kurth, J. H., Rydel, R. E. and Rogers, J. (1999). Soluble amyloid beta peptide concentration as a predictor of synaptic change in Alzheimer's disease. *Am J Pathol* **155**, 853-62.

Maas, E., Geissen, M., Groschup, M. H., Rost, R., Onodera, T., Schatzl, H. and Vorberg, I. M. (2007). Scrapie infection of prion protein-deficient cell line upon ectopic expression of mutant prion proteins. *J Biol Chem* **282**, 18702-10.

Magalhaes, A. C., Baron, G. S., Lee, K. S., Steele-Mortimer, O., Dorward, D., Prado, M. A. and Caughey, B. (2005). Uptake and neuritic transport of scrapie prion protein coincident with infection of neuronal cells. *J Neurosci* **25**, 5207-16.

Magalhaes, A. C., Silva, J. A., Lee, K. S., Martins, V. R., Prado, V. F., Ferguson, S. S., Gomez, M. V., Brentani, R. R. and Prado, M. A. (2002). Endocytic intermediates involved with the intracellular trafficking of a fluorescent cellular prion protein. *J Biol Chem* **277**, 33311-8.

Mahal, S. P., Baker, C. A., Demczyk, C. A., Smith, E. W., Julius, C. and Weissmann, C. (2007). Prion strain discrimination in cell culture: the cell panel assay. *Proc Natl Acad Sci U S A* **104**, 20908-13.

Mallucci, G. R., White, M. D., Farmer, M., Dickinson, A., Khatun, H., Powell, A. D., Brandner, S., Jefferys, J. G. and Collinge, J. (2007). Targeting cellular prion protein reverses early cognitive deficits and neurophysiological dysfunction in prion-infected mice. *Neuron* **53**, 325-35.

Marijanovic, Z., Caputo, A., Campana, V. and Zurzolo, C. (2009). Identification of an intracellular site of prion conversion. *PLoS Pathog* **5**, e1000426.

Marsh, M., Schmid, S., Kern, H., Harms, E., Male, P., Mellman, I. and Helenius, A. (1987). Rapid analytical and preparative isolation of functional endosomes by free flow electrophoresis. *J Cell Biol* **104**, 875-86.

Marsh, R. F. and Hadlow, W. J. (1992). Transmissible mink encephalopathy. *Rev Sci Tech* **11**, 539-50.

Marsh, R. F. and Kimberlin, R. H. (1975) Comparison of scrapie and transmissible mink encephalopathy in hamsters. II. Clinical signs, pathology, and pathogenesis. *Journal of Infectious Diseases* **131**, 104-110.

Martins, S. M., Frosoni, D. J., Martinez, A. M., De Felice, F. G. and Ferreira, S. T. (2006). Formation of soluble oligomers and amyloid fibrils with physical properties of the scrapie isoform of the prion protein from the C-terminal domain of recombinant murine prion protein mPrP-(121-231). *J Biol Chem* **281**, 26121-8.

Maurin, M. and Raoult, D. (1999). Q fever. *Clin Microbiol Rev* **12**, 518-53.

Mayer, R. J., Landon, M., Laszlo, L., Lennox, G. and Lowe, J. (1992). Protein processing in lysosomes: the new therapeutic target in neurodegenerative disease. *Lancet* **340**, 156-9.

McGovern, G. and Jeffrey, M. (2007). Scrapie-specific pathology of sheep lymphoid tissues. *PLoS One* **2**, e1304.

McKinley, M. P., Meyer, R. K., Kenaga, L., Rahbar, F., Cotter, R., Serban, A. and Prusiner, S. B. (1991). Scrapie prion rod formation in vitro requires both detergent extraction and limited proteolysis. *J Virol* **65**, 1340-51.

McKinley, M. P., Taraboulos, A., Kenaga, L., Serban, D., Stieber, A., DeArmond, S. J., Prusiner, S. B. and Gonatas, N. (1991). Ultrastructural localization of scrapie prion proteins in cytoplasmic vesicles of infected cultured cells. *Lab Invest* **65**, 622-30.

McKintosh, E., Tabrizi, S. J. and Collinge, J. (2003). Prion diseases. *J Neurovirol* **9**, 183-93.

McLean, C. A., Cherny, R. A., Fraser, F. W., Fuller, S. J., Smith, M. J., Beyreuther, K., Bush, A. I. and Masters, C. L. (1999). Soluble pool of Abeta amyloid as a determinant of severity of neurodegeneration in Alzheimer's disease. *Ann Neurol* **46**, 860-6.

Meiner, Z., Gabizon, R. and Prusiner, S. B. (1997). Familial Creutzfeldt-Jakob disease. Codon 200 prion disease in Libyan Jews. *Medicine (Baltimore)* **76**, 227-37.

Milhavet, O., McMahon, H. E., Rachidi, W., Nishida, N., Katamine, S., Mange, A., Arlotto, M., Casanova, D., Riondel, J., Favier, A. et al. (2000). Prion infection impairs the cellular response to oxidative stress. *Proc Natl Acad Sci U S A* **97**, 13937-42.

Miller, M. W. and Williams, E. S. (2003). Prion disease: horizontal prion transmission in mule deer. *Nature* **425**, 35-6.

Mirza, S. P., Halligan, B. D., Greene, A. S. and Olivier, M. (2007). Improved method for the analysis of membrane proteins by mass spectrometry. *Physiol Genomics* **30**, 89-94.

Mo, H., Moore, R. C., Cohen, F. E., Westaway, D., Prusiner, S. B., Wright, P. E. and Dyson, H. J. (2001). Two different neurodegenerative diseases caused by proteins with similar structures. *Proc Natl Acad Sci U S A* **98**, 2352-7.

Moore, R. C., Hope, J., McBride, P. A., McConnell, I., Selfridge, J., Melton, D. W. and Manson, J. C. (1998). Mice with gene targetted prion protein alterations show that Prnp, Sinc and Prni are congruent. *Nat Genet* **18**, 118-25.

Moore, R. C., Lee, I. Y., Silverman, G. L., Harrison, P. M., Strome, R., Heinrich, C., Karunaratne, A., Pasternak, S. H., Chishti, M. A., Liang, Y. et al. (1999). Ataxia in prion protein (PrP)-deficient mice is associated with upregulation of the novel PrP-like protein doppel. *J Mol Biol* **292**, 797-817.

Moreira, P. I., Santos, M. S., Moreno, A., Rego, A. C. and Oliveira, C. (2002). Effect of amyloid beta-peptide on permeability transition pore: a comparative study. *J Neurosci Res* **69**, 257-67.

Mouillet-Richard, S., Ermonval, M., Chebassier, C., Laplanche, J. L., Lehmann, S., Launay, J. M. and Kellermann, O. (2000). Signal transduction through prion protein. *Science* **289**, 1925-8.

Munton, R. P., Tweedie-Cullen, R., Livingstone-Zatchej, M., Weinandy, F., Waidelich, M., Longo, D., Gehrig, P., Potthast, F., Rutishauser, D., Gerrits, B. et al. (2007). Qualitative and quantitative analyses of protein phosphorylation in naive and stimulated mouse synaptosomal preparations. *Mol Cell Proteomics* **6**, 283-93.

Naslavsky, N., Stein, R., Yanai, A., Friedlander, G. and Taraboulos, A. (1997). Characterization of detergent-insoluble complexes containing the cellular prion protein and its scrapie isoform. *J Biol Chem* **272**, 6324-31.

Nazor, K. E., Kuhn, F., Seward, T., Green, M., Zwald, D., Purro, M., Schmid, J., Biffiger, K., Power, A. M., Oesch, B. et al. (2005). Immunodetection of disease-associated mutant PrP, which accelerates disease in GSS transgenic mice. *Embo J* **24**, 2472-80.

Nikles, D., Vana, K., Gauczynski, S., Knetsch, H., Ludewigs, H. and Weiss, S. (2008). Subcellular localization of prion proteins and the 37 kDa/67 kDa laminin receptor fused to fluorescent proteins. *Biochim Biophys Acta* **1782**, 335-40.

Nishida, N., Harris, D. A., Vilette, D., Laude, H., Frobert, Y., Grassi, J., Casanova, D., Milhavet, O. and Lehmann, S. (2000). Successful transmission of three mouse-adapted scrapie strains to murine neuroblastoma cell lines overexpressing wild-type mouse prion protein. *J Virol* **74**, 320-5.

Oesch, B., Westaway, D., Walchli, M., McKinley, M. P., Kent, S. B., Aebersold, R., Barry, R. A., Tempst, P., Teplow, D. B., Hood, L. E. et al. (1985). A cellular gene encodes scrapie PrP 27-30 protein. *Cell* **40**, 735-46.

O'Rourke, K. I., Besser, T. E., Miller, M. W., Cline, T. F., Spraker, T. R., Jenny, A. L., Wild, M. A., Zebarth, G. L. and Williams, E. S. (1999). PrP genotypes of captive and free-ranging Rocky Mountain elk (Cervus elaphus nelsoni) with chronic wasting disease. *J Gen Virol* **80 (Pt 10)**, 2765-9.

Palladino, M. J., Bower, J. E., Kreber, R. and Ganetzky, B. (2003). Neural dysfunction and neurodegeneration in Drosophila Na+/K+ ATPase alpha subunit mutants. *J Neurosci* **23**, 1276-86.

Palmer, M. S. and Collinge, J. (1993). Mutations and polymorphisms in the prion protein gene. *Hum Mutat* **2**, 168-73.

Palmer, M. S., Dryden, A. J., Hughes, J. T. and Collinge, J. (1991). Homozygous prion protein genotype predisposes to sporadic Creutzfeldt-Jakob disease. *Nature* **352**, 340-2.

Panza, G., Stohr, J., Birkmann, E., Riesner, D., Willbold, D., Baba, O., Terashima, T. and Dumpitak, C. (2008). Aggregation and amyloid fibril formation of the prion protein is accelerated in the presence of glycogen. *Rejuvenation Res* **11**, 365-9.

Paquet, S., Daude, N., Courageot, M. P., Chapuis, J., Laude, H. and Vilette, D. (2007). PrPc does not mediate internalization of PrPSc but is required at an early stage for de novo prion infection of Rov cells. *J Virol* **81**, 10786-91.

Parchi, P., Castellani, R., Capellari, S., Ghetti, B., Young, K., Chen, S. G., Farlow, M., Dickson, D. W., Sima, A. A., Trojanowski, J. Q. et al. (1996). Molecular basis of phenotypic variability in sporadic Creutzfeldt-Jakob disease. *Ann Neurol* **39**, 767-78.

Pasquali, C., Fialka, I. and Huber, L. A. (1999). Subcellular fractionation, electromigration analysis and mapping of organelles. *J Chromatogr B Biomed Sci Appl* **722**, 89-102.

Patki, V., Virbasius, J., Lane, W. S., Toh, B. H., Shpetner, H. S. and Corvera, S. (1997). Identification of an early endosomal protein regulated by phosphatidylinositol 3-kinase. *Proc Natl Acad Sci U S A* **94**, 7326-30.

Pattison, I. H. and Jones, K. M. (1968). Modification of a strain of mouse-adapted scrapie by passage through rats. *Res Vet Sci* **9**, 408-10.

Pattison, I. H. and Millson, G. C. (1961). Scrapie produced experimentally in goats with special reference to the clinical syndrome. *J Comp Pathol* **71**, 101-9.

Pauly, P. C. and Harris, D. A. (1998). Copper stimulates endocytosis of the prion protein. *J Biol Chem* **273**, 33107-10.

Perrier, V., Kaneko, K., Safar, J., Vergara, J., Tremblay, P., DeArmond, S. J., Cohen, F. E., Prusiner, S. B. and Wallace, A. C. (2002). Dominant-negative inhibition of prion replication in transgenic mice. *Proc Natl Acad Sci U S A* **99**, 13079-84.

Peters, P. J., Mironov, A., Jr., Peretz, D., van Donselaar, E., Leclerc, E., Erpel, S., DeArmond, S. J., Burton, D. R., Williamson, R. A., Vey, M. et al. (2003). Trafficking of prion proteins through a caveolae-mediated endosomal pathway. *J Cell Biol* **162**, 703-17.

Petrakis, S., Irinopoulou, T., Panagiotidis, C. H., Engelstein, R., Lindstrom, J., Orr-Urtreger, A., Gabizon, R., Grigoriadis, N. and Sklaviadis, T. (2008). Cellular prion protein co-localizes with nAChR beta4 subunit in brain and gastrointestinal tract. *Eur J Neurosci* **27**, 612-20.

Petrakis, S., Malinowska, A., Dadlez, M. and Sklaviadis, T. (2009). Identification of proteins co-purifying with scrapie infectivity. *J Proteomics* **72**, 690-4.

Petrakis, S. and Sklaviadis, T. (2006). Identification of proteins with high affinity for refolded and native PrPC. *Proteomics* **6**, 6476-84.

Piccardo, P., Manson, J. C., King, D., Ghetti, B. and Barron, R. M. (2007). Accumulation of prion protein in the brain that is not associated with transmissible disease. *Proc Natl Acad Sci U S A* **104**, 4712-7.

Piening, N., Nonno, R., Di Bari, M., Walter, S., Windl, O., Agrimi, U., Kretzschmar, H. A. and Bertsch, U. (2006). Conversion efficiency of bank vole prion protein in vitro is determined by residues 155 and 170, but does not correlate with the high susceptibility of bank voles to sheep scrapie in vivo. *J Biol Chem* **281**, 9373-84.

Pimpinelli, F., Lehmann, S. and Maridonneau-Parini, I. (2005). The scrapie prion protein is present in flotillin-1-positive vesicles in central- but not peripheral-derived neuronal cell lines. *Eur J Neurosci* **21**, 2063-72.

Pocchiari, M., Puopolo, M., Croes, E. A., Budka, H., Gelpi, E., Collins, S., Lewis, V., Sutcliffe, T., Guilivi, A., Delasnerie-Laupretre, N. et al. (2004). Predictors of survival in sporadic Creutzfeldt-Jakob disease and other human transmissible spongiform encephalopathies. *Brain* **127**, 2348-59.

Polymenidou, M., Stoeck, K., Glatzel, M., Vey, M., Bellon, A. and Aguzzi, A. (2005). Coexistence of multiple PrPSc types in individuals with Creutzfeldt-Jakob disease. *Lancet Neurol* **4**, 805-14.

Priola, S. A. and Caughey, B. (1994). Inhibition of scrapie-associated PrP accumulation. Probing the role of glycosaminoglycans in amyloidogenesis. *Mol Neurobiol* **8**, 113-20.

Prusiner, S. B. (1982). Novel proteinaceous infectious particles cause scrapie. *Science* **216**, 136-44.

Prusiner, S. B. (1990). Novel structure and genetics of prions causing neurodegeneration in humans and animals. *Biologicals* **18**, 247-62.

Prusiner, S. B. (1997). Prion diseases and the BSE crisis. *Science* **278**, 245-51.

Prusiner, S. B. (1998). Prions. *Proc Natl Acad Sci U S A* **95**, 13363-83.

Prusiner, S. B. and DeArmond, S. J. (1987). Prions causing nervous system degeneration. *Lab Invest* **56**, 349-63.

Prusiner, S. B., Scott, M., Foster, D., Pan, K. M., Groth, D., Mirenda, C., Torchia, M., Yang, S. L., Serban, D., Carlson, G. A. et al. (1990). Transgenetic studies implicate interactions between homologous PrP isoforms in scrapie prion replication. *Cell* **63**, 673-86.

Race, R. E., Fadness, L. H. and Chesebro, B. (1987). Characterization of scrapie infection in mouse neuroblastoma cells. *J Gen Virol* **68 (Pt 5)**, 1391-9.

Rachidi, W., Vilette, D., Guiraud, P., Arlotto, M., Riondel, J., Laude, H., Lehmann, S. and Favier, A. (2003). Expression of prion protein increases cellular copper binding and antioxidant enzyme activities but not copper delivery. *J Biol Chem* **278**, 9064-72.

Raymond, G. J., Hope, J., Kocisko, D. A., Priola, S. A., Raymond, L. D., Bossers, A., Ironside, J., Will, R. G., Chen, S. G., Petersen, R. B. et al. (1997). Molecular assessment of the potential transmissibilities of BSE and scrapie to humans. *Nature* **388**, 285-8.

Raymond G. J., Bossers A., Raymond L.D., O'Rourke K.I., McHolland L.E., Bryant III, P.K., Miller M.W., Williams E.S., Smits M., and Caughey B. (2000). Evidence of a molecular barrier limiting susceptibility of humans, cattle and sheep to chronic wasting disease. *EMBO J* **19 (17)**, 4425-30.

Raymond, G. J., Olsen, E. A., Lee, K. S., Raymond, L. D., Bryant, P. K., 3rd, Baron, G. S., Caughey, W. S., Kocisko, D. A., McHolland, L. E., Favara, C. et al. (2006). Inhibition of protease-resistant prion protein formation in a transformed deer cell line infected with chronic wasting disease. *J Virol* **80**, 596-604.

Rezaei, H., Choiset, Y., Eghiaian, F., Treguer, E., Mentre, P., Debey, P., Grosclaude, J. and Haertle, T. (2002). Amyloidogenic unfolding intermediates differentiate sheep prion protein variants. *J Mol Biol* **322**, 799-814.

Rezaei, H., Eghiaian, F., Perez, J., Doublet, B., Choiset, Y., Haertle, T. and Grosclaude, J. (2005). Sequential generation of two structurally distinct ovine prion protein soluble oligomers displaying different biochemical reactivities. *J Mol Biol* **347**, 665-79.

Rezaei, H., Marc, D., Choiset, Y., Takahashi, M., Hui Bon Hoa, G., Haertle, T., Grosclaude, J. and Debey, P. (2000). High yield purification and physico-chemical properties of full-length recombinant allelic variants of sheep prion protein linked to scrapie susceptibility. *Eur J Biochem* **267**, 2833-9.

Rieger, R., Edenhofer, F., Lasmezas, C. I. and Weiss, S. (1997). The human 37-kDa laminin receptor precursor interacts with the prion protein in eukaryotic cells. *Nat Med* **3**, 1383-8.

Riek, R., Hornemann, S., Wider, G., Billeter, M., Glockshuber, R. and Wuthrich, K. (1996). NMR structure of the mouse prion protein domain PrP(121-321). *Nature* **382**, 180-2.

Riek, R., Hornemann, S., Wider, G., Glockshuber, R. and Wuthrich, K. (1997). NMR characterization of the full-length recombinant murine prion protein, mPrP(23-231). *FEBS Lett* **413**, 282-8.

Riesner, D., Kellings, K., Post, K., Wille, H., Serban, H., Groth, D., Baldwin, M. A. and Prusiner, S. B. (1996). Disruption of prion rods generates 10-nm spherical particles having high alpha-helical content and lacking scrapie infectivity. *J Virol* **70**, 1714-22.

Robinson, P. J. and Pinheiro, T. J. (2009). The Unfolding of the Prion Protein Sheds Light on the Mechanisms of Prion Susceptibility and Species Barrier. *Biochemistry*.

Rogers, M., Serban, D., Gyuris, T., Scott, M., Torchia, T. and Prusiner, S. B. (1991). Epitope mapping of the Syrian hamster prion protein utilizing chimeric and mutant genes in a vaccinia virus expression system. *J Immunol* **147**, 3568-74.

Rosener, M., Muraro, P. A., Riethmuller, A., Kalbus, M., Sappler, G., Thompson, R. J., Lichtenfels, R., Sommer, N., McFarland, H. F. and Martin, R. (1997). 2',3'-cyclic nucleotide 3'-phosphodiesterase: a novel candidate autoantigen in demyelinating diseases. *J Neuroimmunol* **75**, 28-34.

Roucou, X., Giannopoulos, P. N., Zhang, Y., Jodoin, J., Goodyer, C. G. and LeBlanc, A. (2005). Cellular prion protein inhibits proapoptotic Bax conformational change in human neurons and in breast carcinoma MCF-7 cells. *Cell Death Differ* **12**, 783-95.

Rubenstein, R., Carp, R. I. and Callahan, S. M. (1984). In vitro replication of scrapie agent in a neuronal model: infection of PC12 cells. *J Gen Virol* **65 (Pt 12)**, 2191-8.

Rudd, P. M., Wormald, M. R., Wing, D. R., Prusiner, S. B. and Dwek, R. A. (2001). Prion glycoprotein: structure, dynamics, and roles for the sugars. *Biochemistry* **40**, 3759-66.

Rutishauser, D., Mertz, K. D., Moos, R., Brunner, E., Rulicke, T., Calella, A. M. and Aguzzi, A. (2009). The comprehensive native interactome of a fully functional tagged prion protein. *PLoS One* **4**, e4446.

Rybicka, K. K. (1996). Glycosomes--the organelles of glycogen metabolism. *Tissue Cell* **28**, 253-65.

Saborio, G. P., Permanne, B. and Soto, C. (2001). Sensitive detection of pathological prion protein by cyclic amplification of protein misfolding. *Nature* **411**, 810-3.

Saborio, G. P., Soto, C., Kascsak, R. J., Levy, E., Kascsak, R., Harris, D. A. and Frangione, B. (1999). Cell-lysate conversion of prion protein into its protease-resistant isoform suggests the participation of a cellular chaperone. *Biochem Biophys Res Commun* **258**, 470-5.

Safar, J., Wille, H., Itri, V., Groth, D., Serban, H., Torchia, M., Cohen, F. E. and Prusiner, S. B. (1998). Eight prion strains have PrP(Sc) molecules with different conformations. *Nat Med* **4**, 1157-65.

Sales, N., Rodolfo, K., Hassig, R., Faucheux, B., Di Giamberardino, L. and Moya, K. L. (1998). Cellular prion protein localization in rodent and primate brain. *Eur J Neurosci* **10**, 2464-71.

Sanghera, N. and Pinheiro, T. J. (2002). Binding of prion protein to lipid membranes and implications for prion conversion. *J Mol Biol* **315**, 1241-56.

Santoni, V., Molloy, M. and Rabilloud, T. (2000). Membrane proteins and proteomics: un amour impossible? *Electrophoresis* **21**, 1054-70.

Sarnataro, D., Campana, V., Paladino, S., Stornaiuolo, M., Nitsch, L. and Zurzolo, C. (2004). PrP(C) association with lipid rafts in the early secretory pathway stabilizes its cellular conformation. *Mol Biol Cell* **15**, 4031-42.

Sarnataro, D., Caputo, A., Casanova, P., Puri, C., Paladino, S., Tivodar, S. S., Campana, V., Tacchetti, C. and Zurzolo, C. (2009). Lipid rafts and clathrin cooperate in the internalization of PrP in epithelial FRT cells. *PLoS One* **4**, e5829.

Schatzl, H. M., Laszlo, L., Holtzman, D. M., Tatzelt, J., DeArmond, S. J., Weiner, R. I., Mobley, W. C. and Prusiner, S. B. (1997). A hypothalamic neuronal cell line persistently infected with scrapie prions exhibits apoptosis. *J Virol* **71**, 8821-31.

Schulman, H. and Hanson, P. I. (1993). Multifunctional Ca2+/calmodulin-dependent protein kinase. *Neurochem Res* **18**, 65-77.

Shmerling, D., Hegyi, I., Fischer, M., Blattler, T., Brandner, S., Gotz, J., Rulicke, T., Flechsig, E., Cozzio, A., von Mering, C. et al. (1998). Expression of amino-terminally truncated PrP in the mouse leading to ataxia and specific cerebellar lesions. *Cell* **93**, 203-14.

Shyng, S. L., Heuser, J. E. and Harris, D. A. (1994). A glycolipid-anchored prion protein is endocytosed via clathrin-coated pits. *J Cell Biol* **125**, 1239-50.

Shyng, S. L., Moulder, K. L., Lesko, A. and Harris, D. A. (1995). The N-terminal domain of a glycolipid-anchored prion protein is essential for its endocytosis via clathrin-coated pits. *J Biol Chem* **270**, 14793-800.

Si, K., Lindquist, S. and Kandel, E. R. (2003). A neuronal isoform of the aplysia CPEB has prion-like properties. *Cell* **115**, 879-91.

Sigurdson, C. J. and Miller, M. W. (2003). Other animal prion diseases. *Br Med Bull* **66**, 199-212.

Silveira, J. R., Raymond, G. J., Hughson, A. G., Race, R. E., Sim, V. L., Hayes, S. F. and Caughey, B. (2005). The most infectious prion protein particles. *Nature* **437**, 257-61.

Simoneau, S., Rezaei, H., Sales, N., Kaiser-Schulz, G., Lefebvre-Roque, M., Vidal, C., Fournier, J. G., Comte, J., Wopfner, F., Grosclaude, J. et al. (2007). In vitro and in vivo neurotoxicity of prion protein oligomers. *PLoS Pathog* **3**, e125.

Skinner, P. J., Abbassi, H., Chesebro, B., Race, R. E., Reilly, C. and Haase, A. T. (2006). Gene expression alterations in brains of mice infected with three strains of scrapie. *BMC Genomics* **7**, 114.

Snow, A. D., Kisilevsky, R., Willmer, J., Prusiner, S. B. and DeArmond, S. J. (1989). Sulfated glycosaminoglycans in amyloid plaques of prion diseases. *Acta Neuropathol* **77**, 337-42.

Sokolowski, F., Modler, A. J., Masuch, R., Zirwer, D., Baier, M., Lutsch, G., Moss, D. A., Gast, K. and Naumann, D. (2003). Formation of critical oligomers is a key event during conformational transition of recombinant syrian hamster prion protein. *J Biol Chem* **278**, 40481-92.

Somerville, R. A., Chong, A., Mulqueen, O. U., Birkett, C. R., Wood, S. C. and Hope, J. (1997). Biochemical typing of scrapie strains. *Nature* **386**, 564.

Somerville, R. A., Hamilton, S. and Fernie, K. (2005). Transmissible spongiform encephalopathy strain, PrP genotype and brain region all affect the degree of glycosylation of PrPSc. *J Gen Virol* **86**, 241-6.

Spielhaupter, C. and Schatzl, H. M. (2001). PrPC directly interacts with proteins involved in signaling pathways. *J Biol Chem* **276**, 44604-12.

Stahl, N., Borchelt, D. R., Hsiao, K. and Prusiner, S. B. (1987). Scrapie prion protein contains a phosphatidylinositol glycolipid. *Cell* **51**, 229-40.

Stimson, E., Hope, J., Chong, A. and Burlingame, A. L. (1999). Site-specific characterization of the N-linked glycans of murine prion protein by high-performance liquid chromatography/electrospray mass spectrometry and exoglycosidase digestions. *Biochemistry* **38**, 4885-95.

Stohr, J., Weinmann, N., Wille, H., Kaimann, T., Nagel-Steger, L., Birkmann, E., Panza, G., Prusiner, S. B., Eigen, M. and Riesner, D. (2008). Mechanisms of prion protein assembly into amyloid. *Proc Natl Acad Sci U S A* **105**, 2409-14.

Strickland, D. K., Ashcom, J. D., Williams, S., Burgess, W. H., Migliorini, M. and Argraves, W. S. (1990). Sequence identity between the alpha 2-macroglobulin receptor and low density lipoprotein receptor-related protein suggests that this molecule is a multifunctional receptor. *J Biol Chem* **265**, 17401-4.

Swietnicki, W., Morillas, M., Chen, S. G., Gambetti, P. and Surewicz, W. K. (2000). Aggregation and fibrillization of the recombinant human prion protein huPrP90-231. *Biochemistry* **39**, 424-31.

Tahiri-Alaoui, A., Bouchard, M., Zurdo, J. and James, W. (2003). Competing intrachain interactions regulate the formation of beta-sheet fibrils in bovine PrP peptides. *Protein Sci* **12**, 600-8.

Tahiri-Alaoui, A., Gill, A. C., Disterer, P. and James, W. (2004). Methionine 129 variant of human prion protein oligomerizes more rapidly than the valine 129 variant: implications for disease susceptibility to Creutzfeldt-Jakob disease. *J Biol Chem* **279**, 31390-7.

Tanaka, M., Chien, P., Naber, N., Cooke, R. and Weissman, J. S. (2004). Conformational variations in an infectious protein determine prion strain differences. *Nature* **428**, 323-8.

Tanaka, M., Collins, S. R., Toyama, B. H. and Weissman, J. S. (2006). The physical basis of how prion conformations determine strain phenotypes. *Nature* **442**, 585-9.

Taraboulos, A., Jendroska, K., Serban, D., Yang, S. L., DeArmond, S. J. and Prusiner, S. B. (1992). Regional mapping of prion proteins in brain. *Proc Natl Acad Sci U S A* **89**, 7620-4.

Taraboulos, A., Serban, D. and Prusiner, S. B. (1990). Scrapie prion proteins accumulate in the cytoplasm of persistently infected cultured cells. *J Cell Biol* **110**, 2117-32.

Telling, G. C., Scott, M., Mastrianni, J., Gabizon, R., Torchia, M., Cohen, F. E., DeArmond, S. J. and Prusiner, S. B. (1995). Prion propagation in mice expressing human and chimeric PrP transgenes implicates the interaction of cellular PrP with another protein. *Cell* **83**, 79-90.

Tobler, I., Deboer, T. and Fischer, M. (1997). Sleep and sleep regulation in normal and prion protein-deficient mice. *J Neurosci* **17**, 1869-79.

Toyama, B. H., Kelly, M. J., Gross, J. D. and Weissman, J. S. (2007). The structural basis of yeast prion strain variants. *Nature* **449**, 233-7.

Tulp, A., Verwoerd, D. and Pieters, J. (1993). Application of an improved density gradient electrophoresis apparatus to the separation of proteins, cells and subcellular organelles. *Electrophoresis* **14**, 1295-301.

Tuzi, N. L., Cancellotti, E., Baybutt, H., Blackford, L., Bradford, B., Plinston, C., Coghill, A., Hart, P., Piccardo, P., Barron, R. M. et al. (2008). Host PrP glycosylation: a major factor determining the outcome of prion infection. *PLoS Biol* **6**, e100.

Tuzi, N. L., Gall, E., Melton, D. and Manson, J. C. (2002). Expression of doppel in the CNS of mice does not modulate transmissible spongiform encephalopathy disease. *J Gen Virol* **83**, 705-11.

van Rheede, T., Smolenaars, M. M., Madsen, O. and de Jong, W. W. (2003). Molecular evolution of the mammalian prion protein. *Mol Biol Evol* **20**, 111-21.

Vanik, D. L. and Surewicz, W. K. (2002). Disease-associated F198S mutation increases the propensity of the recombinant prion protein for conformational conversion to scrapie-like form. *J Biol Chem* **277**, 49065-70.

Vendrely, C., Valadie, H., Bednarova, L., Cardin, L., Pasdeloup, M., Cappadoro, J., Bednar, J., Rinaudo, M. and Jamin, M. (2005). Assembly of the full-length recombinant mouse prion protein I. Formation of soluble oligomers. *Biochim Biophys Acta* **1724**, 355-66.

Vey, M., Pilkuhn, S., Wille, H., Nixon, R., DeArmond, S. J., Smart, E. J., Anderson, R. G., Taraboulos, A. and Prusiner, S. B. (1996). Subcellular colocalization of the cellular and scrapie prion proteins in caveolae-like membranous domains. *Proc Natl Acad Sci U S A* **93**, 14945-9.

Vilette, D., Andreoletti, O., Archer, F., Madelaine, M. F., Vilotte, J. L., Lehmann, S. and Laude, H. (2001). Ex vivo propagation of infectious sheep scrapie agent in heterologous epithelial cells expressing ovine prion protein. *Proc Natl Acad Sci U S A* **98**, 4055-9.

Vorberg, I. and Priola, S. A. (2002). Molecular basis of scrapie strain glycoform variation. *J Biol Chem* **277**, 36775-81.

Vorberg, I., Raines, A., Story, B. and Priola, S. A. (2004). Susceptibility of common fibroblast cell lines to transmissible spongiform encephalopathy agents. *J Infect Dis* **189**, 431-9.

Walker, S. G., Dale, C. J. and Lyddiatt, A. (1996). Aqueous two-phase partition of complex protein feedstocks derived from brain tissue homogenates. *J Chromatogr B Biomed Appl* **680**, 91-6.

Weissmann, C. (1991). A 'unified theory' of prion propagation. *Nature* **352**, 679-83.

Weissmann, C. and Aguzzi, A. (1999). Perspectives: neurobiology. PrP's double causes trouble. *Science* **286**, 914-5.

Wells, G. A., Scott, A. C., Johnson, C. T., Gunning, R. F., Hancock, R. D., Jeffrey, M., Dawson, M. and Bradley, R. (1987). A novel progressive spongiform encephalopathy in cattle. *Vet Rec* **121**, 419-20.

Westaway, D., DeArmond, S. J., Cayetano-Canlas, J., Groth, D., Foster, D., Yang, S. L., Torchia, M., Carlson, G. A. and Prusiner, S. B. (1994). Degeneration of skeletal muscle, peripheral nerves, and the central nervous system in transgenic mice overexpressing wild-type prion proteins. *Cell* **76**, 117-29.

Wetzel, R., Shivaprasad, S. and Williams, A. D. (2007). Plasticity of amyloid fibrils. *Biochemistry* **46**, 1-10.

Wickner, R. B. (1994). [URE3] as an altered URE2 protein: evidence for a prion analog in Saccharomyces cerevisiae. *Science* **264**, 566-9.

Wickner, R. B., Edskes, H. K., Shewmaker, F. and Nakayashiki, T. (2007). Prions of fungi: inherited structures and biological roles. *Nat Rev Microbiol* **5**, 611-8.

Will, R. G., Ironside J. W, Zeidler M., Estibeiro K., Cousens S. N., Smith P. G., Alperovitch A., Poser S., Pocchiari M. and Hofman A. (1996) A new variant of Creutzfeldt-Jacob disease in the UK. *The Lancet* **347**, 921-925

Williams, E. S. and Miller, M. W. (2002). Chronic wasting disease in deer and elk in North America. *Rev Sci Tech* **21**, 305-16.

Wilson, J. M., de Hoop, M., Zorzi, N., Toh, B. H., Dotti, C. G. and Parton, R. G. (2000). EEA1, a tethering protein of the early sorting endosome, shows a polarized distribution in hippocampal neurons, epithelial cells, and fibroblasts. *Mol Biol Cell* **11**, 2657-71.

Wong, B. S., Pan, T., Liu, T., Li, R., Petersen, R. B., Jones, I. M., Gambetti, P., Brown, D. R. and Sy, M. S. (2000). Prion disease: A loss of antioxidant function? *Biochem Biophys Res Commun* **275**, 249-52.

Wong, C., Xiong, L. W., Horiuchi, M., Raymond, L., Wehrly, K., Chesebro, B. and Caughey, B. (2001). Sulfated glycans and elevated temperature stimulate PrP(Sc)-dependent cell-free formation of protease-resistant prion protein. *Embo J* **20**, 377-86.

Wright, E. M., Humphreys, G. O. and Yarranton, G. T. (1986). Dual-origin plasmids containing an amplifiable ColE1 ori; temperature-controlled expression of cloned genes. *Gene* **49**, 311-21.

Xing, Y., Nakamura, A., Chiba, T., Kogishi, K., Matsushita, T., Li, F., Guo, Z., Hosokawa, M., Mori, M. and Higuchi, K. (2001). Transmission of mouse senile amyloidosis. *Lab Invest* **81**, 493-9.

Yang, M., Ellenberg, J., Bonifacino, J. S. and Weissman, A. M. (1997). The transmembrane domain of a carboxyl-terminal anchored protein determines localization to the endoplasmic reticulum. *J Biol Chem* **272**, 1970-5.

Zahn, R., Liu, A., Luhrs, T., Riek, R., von Schroetter, C., Lopez Garcia, F., Billeter, M., Calzolai, L., Wider, G. and Wuthrich, K. (2000). NMR solution structure of the human prion protein. *Proc Natl Acad Sci U S A* **97**, 145-50.

Zhang, H., Stockel, J., Mehlhorn, I., Groth, D., Baldwin, M. A., Prusiner, S. B., James, T. L. and Cohen, F. E. (1997). Physical studies of conformational plasticity in a recombinant prion protein. *Biochemistry* **36**, 3543-53.

Zhang, J., Kang, D. E., Xia, W., Okochi, M., Mori, H., Selkoe, D. J. and Koo, E. H. (1998). Subcellular distribution and turnover of presenilins in transfected cells. *J Biol Chem* **273**, 12436-42.

Zlotnik, I. and Rennie, J. C. (1963). Further observations on the experimental transmission of scrapie from sheep and goats to laboratory mice. *J Comp Pathol* **73**, 150-62.